

# **Decision Diagrams Based On-line Testing of Digital VLSI Circuits**

**Pradeep Kumar Biswal**



# Decision Diagrams Based On-line Testing of Digital VLSI Circuits

*Thesis submitted in partial fulfillment of the requirements  
for the degree of*

**Doctor of Philosophy**

*by*

**Pradeep Kumar Biswal**

*Under the supervision of*  
**Dr Santosh Biswas**



**Department of Computer Science and Engineering**

**Indian Institute of Technology Guwahati  
Guwahati 781039, India**

**July 12, 2017**



*“Bande Purushottamam”*

Dedicated at the holy feet of my Beloved Guru Sri Sri Thakur  
Anukulchandra and guiding star of my life Pujaniya Babaida.



# Declaration

I, Pradeep Kumar Biswal, confirm that:

- a. The work contained in this thesis is original and has been done by myself and the general supervision of my supervisor.
- b. The work has not been submitted to any other Institute for any degree or diploma.
- c. Whenever I have used materials (data, theoretical analysis, results) from other sources, I have given due credit to them by citing them in the text of the thesis and giving their details in the references.
- d. Whenever I have quoted written materials from other sources, I have put them under quotation marks and given due credit to the sources by citing them and giving required details in the references.

Place: IIT Guwahati

Date:

**Pradeep Kumar Biswal**

Research Scholar

Department of Computer Science and Engineering,  
Indian Institute of Technology Guwahati,  
Assam-781039, India



# Certificate

This is to certify that this thesis entitled “**Decision Diagrams Based On-line Testing of Digital VLSI Circuits**” submitted by **Pradeep Kumar Biswal**, to the Indian Institute of Technology Guwahati, for partial fulfillment of the award of the degree of Doctor of Philosophy, is a record of bona fide research work carried out by him under my supervision and guidance.

The thesis, in my opinion, is worthy of consideration for award of the degree of Doctor of Philosophy in accordance with the regulations of the institute. To the best of my knowledge, the results embodied in the thesis have not been submitted to any other university or institute for the award of any other degree or diploma.

Place : I.I.T. Guwahati, India

Date:

(Santosh Biswas)

Associate Professor,

Dept. of Computer Science and Engineering,

Indian Institute of Technology, Guwahati



# Acknowledgements

I wish to express my most sincere gratitude and appreciation to my supervisor, Dr. Santosh Biswas, for his support, help and guidance throughout the research. His continued support led me the right way to bring forth this thesis successfully. I would like to extend my appreciation to my doctoral committee members, Prof. Jatindra Kumar Deka, Prof. Hemangee K. Kapoor and Prof. Roy Paily Palathinkal for providing constructive suggestions related to my work. I wish to thank Prof. Diganta Goswami, Head of the Department of Computer Science and Engineering and other faculty members for their support and help. I would also like to acknowledge the efforts devoted by all the teachers starting from my school days.

I am grateful to a number of people of IIT Guwahati who, over the last few years, have helped me by providing valuable ideas and suggestions. They include Prof. Sukumar Nandi, Prof. Gautam Biswas (Director), Prof. Gautam Barua (former Director), Dr. Aryabartta Sahu and Dr. Arnab Sarkar. I would also like to take this opportunity to thank all my friends, only to name a few, Malaya, Badri, Vaibhav, Vivek, Sandip, Lalatendu, Shirshendu, Biswajit, Shounak, Basant, Mayank, Nandi, Debasish, Pratap, Shibananda, Ananda, Mrityunjay, Pradeep, Amrita, Rabindra, who directly and indirectly helped in finishing my thesis. I am thankful to all my near and dear Guru-bhais (disciples of Sri Sri Thakur Anukulchandra) for their moral support and love which helped me to overcome all the tough situations in my life.

Last but most important are my parents and other family members whose blessings and love made my path of success. I am grateful to my father, mother, uncle, aunt, brothers and sisters who have always supported me at every course of my life and offered me constant encouragement and inspiration.



# Abstract

The rapid increase in complexity of VLSI circuits with the advent of Deep Sub-Micron (DSM) technology causes development of faults during their normal operation. In other words, the probability of occurrence of faults in modern VLSI circuits after deployment is high, even though they were tested successfully after manufacturing. Such faults cannot be detected by off-line test or Built-In-Self-Test (BIST) techniques, thus, On-line Testing (OLT) is becoming an essential part in Design for Testability (DFT). Most of the existing works presented in the literature on OLT of digital circuits have emphasized on the followings:- non-intrusiveness, totally self-checking, low area overhead, high fault coverage, low detection latency, etc. However, in DSM era, several other factors need to be considered, namely flexibility, coverage for advanced fault models, scalability, handling asynchronous circuits, etc. Considering all these facts, the main objective of this thesis is to design and develop efficient OLT schemes for detection of faults on-the-fly in digital VLSI circuits. All the proposed algorithms for on-line tester design use Decision Diagrams (DDs) to improve the scalability of the schemes.

All the existing works on OLT have ignored the issue of minimization of tap points (i.e., measurement limitation) of the Circuit Under Test (CUT) by the on-line tester. Minimization of tap points reduces load on the CUT and this in turn lowers the area overhead of the tester, however, it compromises fault coverage and detection latency. As the first contribution of the thesis, we propose an Ordered Binary Decision Diagram (OBDD) based OLT scheme for digital circuits by considering “number of tap points” as a new design parameter to provide flexibility in the OLT perspective. Experimentally, it is seen that measurement limitation has minimal impact on fault coverage and detection latency but it reduces area overhead of the on-line tester significantly.

The OLT schemes reported in the literature are mainly targeted towards the traditional stuck-at fault model and only few of them are designed for bridging faults. However, most of these techniques have considered only non-feedback bridging faults, because feedback bridging faults may cause oscillations and detecting them on-line using logic testing is

difficult. It may be noted that, not all feedback bridging faults cause oscillations and even if some does, there are test patterns for which the fault effect can be manifested logically. In this contribution, we propose an OBDD based OLT scheme for both feedback and non-feedback bridging faults. Experimentally, we have seen that consideration of feedback bridging faults along with non-feedback ones, improves fault coverage with marginal increase in the area overhead compared to schemes only involving non-feedback faults.

The majority of works on OLT reported in the literature are at the gate level and these schemes take reasonable computational time and have limited scalability. The reason being these schemes work at bit level, leading to the state explosion problem. This issue can be addressed by developing OLT schemes at higher description levels of the circuits. In the third contribution, we propose a High Level Decision Diagram (HLDD) based OLT scheme at Register Transfer Level (RTL) model of circuits in order to improve the scalability. Experiments on different benchmark circuits show that the test generation time is greatly improved, thus, large circuits can be easily handled. Further, it achieves lower area overhead at similar fault coverage compared to OLT schemes at gate level.

Most of the OLT schemes are designed for synchronous circuits compared to asynchronous circuits. There are very few works that have been proposed for OLT of asynchronous circuits and most of them are based on the Mutex approach. The area overhead of these schemes are quit high because of Mutex blocks, which are the main components of the on-line tester. In the final contribution, we propose an OBDD based OLT scheme for Speed Independent asynchronous (SI) circuits, which has low area overhead. The scheme is applied to different SI benchmark circuits and it is found that the area overhead of the on-line tester is much less compared to that of the existing Mutex approach.

**Keywords:** On-line Testing (OLT), fault models, synchronous circuit, asynchronous circuit, circuit at Register Transfer Level (RTL), Binary Decision Diagram (BDD), High Level Decision Diagram (HLDD), fault coverage, fault detection latency, area overhead.

# Contents

<b>List of Figures</b>	<b>xiii</b>
<b>List of Tables</b>	<b>xvii</b>
<b>Nomenclature</b>	<b>xix</b>
<b>1 Introduction</b>	<b>1</b>
1.1 Introduction to OLT of digital VLSI circuits . . . . .	4
1.2 Introduction to decision diagrams and their applications in digital circuit testing	6
1.3 Motivations and Contributions of the thesis . . . . .	8
1.4 Organization of the thesis . . . . .	12
<b>2 Literature review: On-line Testing of Digital VLSI Circuits and Decision Diagrams</b>	<b>13</b>
2.1 Digital VLSI testing . . . . .	13
2.1.1 Structural vs. functional testing . . . . .	16
2.1.2 Fault models . . . . .	19
2.1.3 Test programming . . . . .	21
2.1.4 Comparison of ATE based testing, BIST and OLT . . . . .	22
2.2 Literature review: On-line testing of digital VLSI circuits . . . . .	24
2.2.1 Signature monitoring in FSMs . . . . .	25
2.2.2 Self-checking design using error detecting codes . . . . .	28
2.2.3 Duplication schemes for OLT . . . . .	32
2.2.4 On-line BIST . . . . .	34
2.2.5 Pros and cons of different OLT techniques . . . . .	35
2.3 Desired features of OLT schemes . . . . .	35
2.3.1 Measurement limitation based flexibility in OLT . . . . .	35
2.3.2 OLT schemes for advanced fault model . . . . .	37

# CONTENTS

---

2.3.3	OLT schemes for circuits at higher description level . . . . .	39
2.3.4	OLT schemes for asynchronous circuits . . . . .	42
2.4	Complexity of generation of exhaustive set of test patterns for OLT . . . . .	43
2.4.1	Decision Diagrams . . . . .	44
2.4.2	Testing of digital circuits using Decision Diagrams . . . . .	51
2.5	Conclusion . . . . .	53
<b>3</b>	<b>On-line Testing with Measurement Limitation</b>	<b>55</b>
3.1	Introduction . . . . .	55
3.2	FSA framework under measurement limitation: Circuit modeling and <i>FN</i> - detector design . . . . .	57
3.2.1	Circuit modeling under single stuck-at fault . . . . .	58
3.2.2	<i>FN</i> -detector design for FSA model of a circuit . . . . .	59
3.3	Efficient construction of <i>FN</i> -detector . . . . .	65
3.3.1	OBDD based procedure for exhaustive test pattern generation for the NSF block under full measurement . . . . .	68
3.3.2	OBDD based procedure for determination of <i>FD</i> -transitions under measurement limitation . . . . .	71
3.3.3	<i>FN</i> -detector design for Output Function block of the circuit . . . . .	73
3.4	Experimental evaluation . . . . .	76
3.4.1	Trade-offs in <i>FN</i> -detector design: detection latency, fault coverage, measurement limitation and area overhead . . . . .	77
3.5	Conclusion . . . . .	82
<b>4</b>	<b>On-line Testing for Feedback Bridging Faults</b>	<b>83</b>
4.1	Introduction . . . . .	83
4.2	Circuit modeling and <i>FN</i> -detector design using FSA framework . . . . .	84
4.2.1	Circuit modeling under bridging faults . . . . .	85
4.2.2	<i>FN</i> -detector construction from the FSA model of the CUT . . . . .	91
4.3	Efficient construction of <i>FN</i> -detector for bridging faults . . . . .	92
4.3.1	Partition of the CUT into sub-circuits using cones of influence . . . . .	93
4.3.2	OBDD based procedure for generation of exhaustive set of <i>FD</i> - transitions for non-feedback bridging faults . . . . .	96
4.3.3	OBDD based procedure for generation of exhaustive set of <i>FD</i> - transitions for feedback bridging faults . . . . .	98

4.3.4	OBDD based procedure for illustration of an oscillating feedback bridging fault . . . . .	105
4.4	Experimental evaluation . . . . .	106
4.4.1	Fault coverage analysis . . . . .	107
4.4.2	Area overhead analysis . . . . .	108
4.5	Conclusion . . . . .	112
<b>5</b>	<b>On-line Testing at Register Transfer Level</b>	<b>113</b>
5.1	Introduction . . . . .	113
5.2	High-Level Decision Diagram . . . . .	114
5.3	Circuit modeling at RTL: Normal and faulty conditions . . . . .	116
5.3.1	Circuit modeling using HLDD . . . . .	120
5.3.2	RTL fault model and circuit modeling under fault. . . . .	123
5.4	Generation of exhaustive set of <i>FD</i> -control-patterns and design of <i>FN</i> -detector	127
5.4.1	Design of <i>FN</i> -detector . . . . .	129
5.4.2	<i>FN</i> -detector design for combinational part of the RTL circuit . . . . .	132
5.5	Experimental evaluation . . . . .	134
5.5.1	Fault coverage analysis . . . . .	134
5.5.2	Area overhead analysis . . . . .	136
5.6	Conclusion . . . . .	137
<b>6</b>	<b>On-line Testing of Speed Independent Asynchronous Circuits</b>	<b>139</b>
6.1	Introduction . . . . .	139
6.2	SI circuit modeling using Signal Transition Graph and generation of <i>FD</i> -transitions . . . . .	140
6.2.1	Converting STG into State Graph model and generation of <i>FD</i> -transitions . . . . .	148
6.3	Design of <i>FN</i> -detector using <i>FD</i> -transitions . . . . .	152
6.3.1	Circuit synthesis for <i>FN</i> -detector . . . . .	157
6.4	Efficient generation of <i>FD</i> -transitions directly from circuit description using OBDD . . . . .	160
6.5	Experimental evaluation . . . . .	163
6.5.1	Mutex approach to testing [107] . . . . .	164
6.5.2	Comparison with the Mutex approach . . . . .	166
6.6	Conclusion . . . . .	167

## CONTENTS

---

<b>7</b>	<b>Conclusions and Future scope of work</b>	<b>169</b>
7.1	Summary of the work . . . . .	169
7.2	Future scope of work . . . . .	171

# List of Figures

2.1	A typical VLSI design and test flow . . . . .	15
2.2	Principle of digital testing . . . . .	16
2.3	A 32 bit ripple carry adder . . . . .	18
2.4	A 32 bit ripple carry adder with the DFT circuitry . . . . .	18
2.5	Basic steps in test program generation . . . . .	21
2.6	BIST scheme . . . . .	23
2.7	Basic architecture for signature monitoring . . . . .	28
2.8	Basic architecture for self-checking circuit . . . . .	29
2.9	Basic architecture for self-checking sequential circuit . . . . .	30
2.10	Basic architecture for duplication based OLT . . . . .	32
2.11	BDD for Boolean function $f = xy' + yz$ . . . . .	45
2.12	Reduction rules:(a) merging, (b) eliminate . . . . .	45
2.13	Combinational circuit and it's SSBDD representation . . . . .	48
2.14	HLDD representation of a data path segment of an RTL circuit . . . . .	49
2.15	Decision Diagram representation of a control part segment when current state is $S2$ . . . . .	50
2.16	$OBDD_{normal}$ : representing $f_N(a, b, c) = ab' + a'b + a'c$ . . . . .	52
2.17	$OBDD_{faulty}$ : representing $f_F(a, b, c) = a'c + ab'c$ . . . . .	52
2.18	$OBDD_{xor}$ : representing $OBDD_{normal}$ XOR $OBDD_{faulty}$ . . . . .	52
3.1	Basic architecture of a sequential circuit with on-line tester ( $FN$ -detector) . . . . .	57
3.2	A simple sequential circuit with a s-a-1 fault . . . . .	60
3.3	FSA model for the circuit of Figure 3.2 . . . . .	60
3.4	$FN$ -detector for the FSA model of the circuit with a s-a-1 fault (Figure 3.3) . . . . .	62
3.5	Input-output of the NSF block . . . . .	66
3.6	OBDD for the function $v_{02}^+$ (circuit shown in Figure 3.2) . . . . .	69
3.7	OBDD for the function $v_{12}^+$ (circuit shown in Figure 3.2) . . . . .	70
3.8	XOR of $v_{02}^+$ and $v_{12}^+$ OBDD (circuit shown in Figure 3.2) . . . . .	70

## LIST OF FIGURES

---

3.9	OBDD for $v_{02}^+$ after edges and nodes for $FD$ -transition $\langle 10, 1, d1 \rangle$ being eliminated for $I_m = \{v_3\}$ and $S_m = \{v_2\}$ . . . . .	73
3.10	The $FN$ -detector for $FD$ -transition $\tau_{16}$ under $I_m = \{\}$ , $S_m = \{v_1, v_2\}$ and NSF output $v_2^+$ . . . . .	74
3.11	Example of OF block . . . . .	75
3.12	$FN$ -detector for the OF block (Figure 3.11) where line $a$ is not tapped . . . . .	75
3.13	Detection latency for s1488 versus different combinations of measurement limitations of one and two input lines of the NSF . . . . .	79
3.14	Area overhead for s1488 versus different combinations of measurement limitations of one and two input lines of the NSF . . . . .	79
3.15	Fault coverage for s1488 versus different combinations of measurement limitations of one and two input lines of the NSF . . . . .	80
4.1	A simple sequential circuit. . . . .	87
4.2	Sequential circuit with AND-bridging between lines $e_1$ and $e_2$ . . . . .	87
4.3	AND-bridging fault . . . . .	89
4.4	FSA model for the circuit (of Figure 4.1) under normal and faulty condition . . . . .	90
4.5	$FD$ -transition $\tau_{12} = \langle 00, 1, 01 \rangle$ detects the given AND-bridging fault by driving 0 to line $e_2$ and checking $s$ - $a$ -0 fault at line $e_1$ . . . . .	91
4.6	$FN$ -detector for the FSA model of the circuit shown in Figure 4.4 . . . . .	93
4.7	NSF (normal condition) partitioned using cones of influence on its outputs. . . . .	98
4.8	NSF with faults ( $e_2$ dominates $e_1$ and $e_1$ dominates $e_2$ ) . . . . .	99
4.9	OBDDs for non-feedback bridging fault when $e_2$ dominates $e_1$ . . . . .	100
4.10	NSF with fault, partitioned into cones, when $f$ dominates $b$ . . . . .	102
4.11	OBDDs for feedback bridging fault when $f$ dominates $b$ . . . . .	103
4.12	NSF with fault, partitioned into cones when $b$ dominates $f$ . . . . .	105
4.13	NSF with fault causing oscillation, partitioned into cones when $f$ dominates $b$ . . . . .	106
5.1	Graphical representation of a HLDD model. . . . .	115
5.2	Data path of the GCD algorithm at RTL. . . . .	119
5.3	Partitioning the CUT into sub-parts based on cones of influence. . . . .	121
5.4	HLDD representing $V_1^+$ . . . . .	122
5.5	Multiplexer and its equivalent circuit at logic gate level . . . . .	124
5.6	HLDD representing $V_1^+$ under normal condition. . . . .	125
5.7	HLDD representing $V_1^+$ under fault $F_1$ . . . . .	126
5.8	HLDD representing $V_2^+$ under normal condition. . . . .	126

5.9	HLDD representing $V_2^+$ under fault $F_1$ . . . . .	126
5.10	Interconnection of the CUT and the $FN$ -detector. . . . .	129
5.11	State transition diagram for the $FN$ -detector. . . . .	130
5.12	Timing diagram of the CUT versus $FN$ -detector under fault $F_i$ . . . . .	131
5.13	Combinational part of the GCD circuit. . . . .	133
5.14	Partitioning of the combinational part using cones of influence. . . . .	133
5.15	State transition diagram for the $FN$ -detector of the combinational part. . . . .	134
6.1	Example of speed independent circuit as CUT. . . . .	142
6.2	Transistor diagram of dynamic C-element. . . . .	142
6.3	Signal Transition Graph of the sample circuit (Figure 6.1). . . . .	142
6.4	STG representation of stuck-on fault in $n1$ of C2 (Figure 6.1). . . . .	144
6.5	STG representation of stuck-on fault in $p1$ of C1 (Figure 6.1). . . . .	144
6.6	STG representation of stuck-on fault in $n2$ of C1 (Figure 6.1). . . . .	145
6.7	STG representation of s-a-0 fault in line-2 (Figure 6.1). . . . .	146
6.8	STG representation of s-a-0 fault in line-13 (Figure 6.1). . . . .	146
6.9	SG sub-model for the normal circuit (STG of Figure 6.3) . . . . .	150
6.10	SG sub-model for the circuit with $n1$ stuck-on fault in C2 (STG of Figure 6.4).150	150
6.11	SG sub-model for the circuit with $p1$ stuck-on fault in C1 (STGs of Figure 6.5).151	151
6.12	SG for detecting the $FD$ -transitions $\langle X'11, X'6 \rangle$ and $\langle X'13, X'8 \rangle$ . . . . .	155
6.13	SG for detecting the $FD$ -transitions—Sl. No. 1 and 2 of Table 6.2 . . . . .	155
6.14	SG for detecting the $FD$ -transition—Sl. No. 3 of Table 6.2 . . . . .	156
6.15	SG for detecting the $FD$ -transitions—Sl. No. 6 and 7 of Table 6.2 . . . . .	156
6.16	SG for detecting the $FD$ -transitions—Sl. No. 8 and 9 of Table 6.2 . . . . .	156
6.17	Screenshot showing the synthesis of on-line detector from SG using Petrify .	158
6.18	$FN$ -detector circuit for the SG shown in Figure 6.14 . . . . .	158
6.19	Normal OBDD for $Aout_{normal}$ . . . . .	161
6.20	Faulty OBDD for $Aout_{faulty}$ . . . . .	161
6.21	XOR OBDD for the normal and faulty OBDDs . . . . .	162
6.22	Circuit 1 . . . . .	164
6.23	Circuit 2 . . . . .	164
6.24	Circuit 3 . . . . .	165
6.25	Block diagram of the checker . . . . .	166
6.26	A part of the checker circuit [107] . . . . .	166



# List of Tables

2.1	Variants of VLSI testing . . . . .	17
2.2	The pros and cons of structural and functional testing . . . . .	20
2.3	Merits and demerits of ATE based off-line structural testing [2,17] . . . . .	25
2.4	Merits and demerits of BIST . . . . .	26
2.5	Merits and demerits of OLT . . . . .	26
2.6	Pros and Cons of different OLT techniques . . . . .	36
3.1	Area Overhead (AO) for different combinations of measurement limitations, resulting Detection Latency (DL), AO comparison with [12,36] and CPU time to generate <i>FD</i> -transitions* . . . . .	81
4.1	Fault coverage by the proposed method, comparison with the existing technique [13] and CPU time to generate <i>FD</i> -transitions * . . . . .	109
4.2	Area overhead for the proposed method and comparison with [13] . . . . .	111
5.1	FSM representation of the control part of the GCD algorithm . . . . .	118
5.2	RTL faults for <i>if</i> and <i>else</i> blocks . . . . .	123
5.3	Fault coverage and exhaustive test set generation time of the proposed method and comparison with existing methods [36] and [12] . . . . .	135
5.4	Area overhead of the proposed method and comparison with [36] and [12] . . . . .	136
6.1	A partial list of faults and their effects on STG . . . . .	147
6.2	<i>FD</i> -transitions . . . . .	152
6.3	Fault coverage, area overhead ratio and execution time for the <i>FN</i> -detector designed using the proposed approach . . . . .	164
6.4	Area ratio for the Mutex approach . . . . .	166



# Nomenclature

CUT	Circuit Under Test
FSA	Finite State Automata
BIST	Built In Self Test
ATE	Automatic Test Equipment
OLT	On-line Testing
FSM	Finite State Machine
ATPG	Automatic Test Pattern Generation
TSC	Totally Self-Checking
DD	Decision Diagram
BDD	Binary Decision Diagram
OBDD	Ordered Binary Decision Diagram
ROBDD	Reduced Ordered Binary Decision Diagram
ADDs	Algebraic Decision Diagrams
SSBDDs	Structurally Synthesized Binary Decision Diagrams
HLDD	High Level Decision Diagram
<i>FD</i> -transitions	Fault Detecting transitions
<i>FN</i> -detector	Fault versus Normal condition detector
SI circuits	Speed Independent asynchronous circuits
CSC	Complete State Coding
RTL	Register Transfer Level
CED	Concurrent Error Detection
CEDD	Concurrent Error Detection and Diagnosis
<i>FD</i> -control-patterns	Fault Detecting Control Patterns
DFT	Design For Testability
DSM	Deep Sub-Micron
s-a fault	stuck-at fault
s-a-0	stuck-at-0

## NOMENCLATURE

---

s-a-1	stuck-at-1
DAG	Directed Acyclic Graph
BFS	Breadth First Search
NSF	Next State Function block
OF	Output Function block
FF	Flip-Flop
DCs	David Cells
Mutex	Mutual Exclusion
DL	Detection Latency
AO	Area Overhead
FC	Fault Coverage
SG	State Graph
STG	Signal Transition Graph
NOC	Network-On-Chip
SOC	System-On-Chip

# Chapter 1

## Introduction

The complexity of digital VLSI circuits in recent years has increased in a very impressive manner. The sophistication of VLSI technology has reached a point where an effort is made to put a large number of devices on a single chip by decreasing the dimensions of the transistors and interconnection wires, from micrometers to nanometers. As the fabrication technology moves to lower sub-micron processes and engineers keep increasing the design complexity, testing encounters greater challenges [2, 17]. Since the defects occurring at the time of manufacturing are unavoidable, so some of the chips may be faulty. Therefore, testing is mandatory to isolate fault free chips from the defective ones. Typically, testing a digital circuit involves applying test vectors to the inputs of the circuit and comparing the outputs of the circuit with the expected responses (i.e., golden responses). The circuit is considered fault free if the responses match for all test vectors. Otherwise, it is considered faulty. The role of testing is to detect whenever any erroneous output is produced by the circuit and to separate out the faulty chips, followed by shipping only the normal ones to the customer.

Testing of digital VLSI circuits can be classified into three important classes as:- Automatic Test Equipment (ATE) based testing [79, 90], Built-In-Self-Test (BIST) [8, 33] and On-line Testing (OLT) [83, 84, 103]. ATE is a computer controlled equipment which is used to apply test patterns to the Circuit Under Test (CUT), compare the output responses obtained from the CUT with the stored responses for the fault free circuit and finally declare the CUT as fault free or faulty. In ATE based testing, the circuit is tested just after it's manufacturing. The main difficulties of ATE based testing in advanced semiconductor technology are at-speed and in-situ testings [17]. Further, the cost of ATE based testing is high because of the cost of its individual components [79, 90]. These difficulties are addressed by the BIST technique, where a part of on-chip circuitry is used to test the circuit itself (i.e., CUT). In BIST, a circuit is tested every time before it is powered on for operation. The

## 1 Introduction

---

basic BIST architecture comprises three additional on-chip hardware blocks along with the CUT—(i) pattern generator, (ii) response analyzer, and (iii) test controller. Though the BIST technique supports at-speed and in-situ testings but it incurs an on-chip hardware overhead as well as a greater design complexity [2, 17, 133].

These traditional off-line testing strategies (ATE based testing and BIST) cannot detect faults that develop on-the-fly during operation of the circuit. It has been observed that the probability of occurrence of such faults in the present day VLSI circuits designed using deep sub-micron technology is high [48, 87]. Immediate detection of faults that occur on-the-fly during operation of the circuit requires incorporation of a technique which will continuously observe the circuit's operation by checking whether the response follows its normal behavior. These techniques fall under the category of OLT [83, 84]. Therefore, OLT is becoming an indispensable part of testing. *OLT can be defined as the procedure to enable integrated circuits to verify the correctness of their functionality during normal operation by checking whether the response of the circuit conforms to its desired dynamic behavior.* Unlike off-line testing, OLT does not require any external test equipment or on-chip pattern generator for generating test inputs for the CUT. It requires an on-chip Design For Testability (DFT) circuitry to test the CUT for all the input patterns that would appear during normal operation [10, 84, 103]. In this thesis we look at OLT of digital VLSI circuits.

Since last two decades, a number of OLT techniques have been proposed for digital circuits, which can be broadly classified as—signature monitoring in Finite State Machines (FSMs) [22, 66, 67, 100, 115], self-checking design [34, 39, 84], partial replication [12, 13, 35, 36, 116] and on-line BIST [4, 7, 82, 113, 130]. The OLT techniques namely, signature monitoring and self checking design, require some special properties in the circuit structure, which lead to a change in the original structure of the circuit. So, these two OLT techniques are intrusive in nature. Since change in the original structure of the circuit is not desirable, so these techniques have limited applicability. Also, the OLT technique based on on-line BIST utilizes the idle times of the various parts of the circuit during operation to perform testing. Therefore, the efficiency of on-line BIST mainly depends on the amount of idle times available in the circuit modules. The present day circuits target to achieve pipelining and parallelism, which reduce the idle times of their modules (i.e, high utilization of their modules). So, on-line BIST cannot be considered as an efficient technique for OLT. In the case of partial replication technique, a minimized version of the CUT is designed and OLT is performed by cross-checking for similarity of output responses of the CUT and the replicated circuit. The partial replication technique is widely used in OLT because of the advantages such as simplicity in design [116], non-intrusiveness (minimal changes in original structure

---

of the CUT) [35, 36], flexibility in terms of trade-offs between area and power overheads of the on-line tester versus fault coverage and detection latency [12, 13], etc. However, it has been found that most of the OLT schemes developed based on the partial replication technique target the traditional single stuck-at (s-a) faults and attempt to tap as many lines as possible of the CUT [12, 35, 36]. Further, these schemes consider circuits modeled at gate level, so they are not scalable [12, 13, 35, 36]. In addition, these schemes are designed only for synchronous circuits and hence, cannot be directly applied to asynchronous circuits. The partial replication based OLT schemes for synchronous circuits involve generation of test patterns and design of an on-line tester as a synchronous circuit using straightforward FSM synthesis philosophy [12, 13]. In case of OLT of asynchronous circuits, the on-line tester must also be asynchronous. If the synchronous philosophy is applied for design of asynchronous on-line tester, then the FSM may have Complete State Coding (CSC) violations and liveness issues. Such an FSM cannot be synthesized as an asynchronous circuit [80].

Based on the above discussion it may be concluded that partial replication is considered to be the best option among all other OLT techniques however, it has some shortfalls. In this work, we aim to design partial replication based OLT schemes for digital VLSI circuits to overcome these drawbacks. The major contributions of the thesis are—(1) Introduction of “minimization of tap points” of the CUT or “measurement limitation” as a new parameter for OLT and design a flexible OLT scheme with the concept of tap point minimization. The scheme analyzes the effect of minimization of tap points on fault coverage, detection latency and area overhead. (2) Design of an OLT scheme for AND-OR bridging faults which covers both feedback and non-feedback bridging faults. The scheme first isolates the oscillating feedback bridging faults, then handles all non-feedback and non-oscillating feedback bridging faults. (3) Development of an OLT scheme for circuits at higher description level, e.g., Register Transfer Level (RTL). The scheme is capable of handling large sized circuits. (4) Development of an OLT scheme for Speed Independent asynchronous (SI) circuits.

This chapter is organized as follows. In Section 1.1, we present a brief discussion on OLT of digital VLSI circuits. Following that, a brief literature review on Decision Diagrams (DDs) and their applications in digital circuit testing are presented in Section 1.2. Finally, the motivations and contributions of the thesis in the area of OLT of digital VLSI circuit are discussed in Section 1.3.

### 1.1 Introduction to OLT of digital VLSI circuits

OLT techniques for digital VLSI circuits, reported in the literature, can be broadly classified into the following categories: a) Signature monitoring in FSMs, b) Self-checking design, c) Partial replication and d) On-line BIST.

Signature monitoring techniques for OLT basically work by studying the state sequences of the circuit FSM model during its operation [22, 66, 67, 100, 115]. Signatures are FSM state sequences traversed during execution. In these methods, signatures are analyzed concurrently with the execution of the circuit. This analysis targets to detect faults leading to illegal paths in the control flow graph, i.e., paths having transitions which do not exist in the FSM specification. To make the runtime signature of the fault-free circuit FSM different from the one with the fault, a signature invariant property is forced during FSM synthesis. To obtain an FSM with signature invariant property, the state assignment procedure may have to be modified to take into account the constraints related to such an invariant. In the worst case, when the FSM graph is well connected, a large number of new states are added to achieve the signature invariant property. Thus, this technique is an intrusive one. Further, the state explosion problem in FSM models makes the application of this scheme difficult for practical circuits; results reported in the OLT literature using these schemes are limited to circuits having typically about one hundred states.

The technique of self checking design involves encoding of the circuit outputs using some error detecting code and then checking the corresponding property of code invariance (e.g., parity,  $m$ -out-of- $n$  code, etc.) [20, 34, 39, 49, 53, 84, 128]. This technique ensures that erroneous outputs generated due to any fault will not be misinterpreted as correct ones. For a checker, a non-code word output is the error indication. Examples of some error detecting codes used for OLT are parity codes [34, 39],  $m$ -out-of- $n$  codes [20], berger-codes [78], etc. The area overhead for making circuits self checkable is usually not high. A number of design and synthesis constraints are however required by the coding technique based methodologies to control the scope of fault propagation. For example, the method reported in [53] necessitates that all inverters be pushed to the primary inputs and the one discussed in [34] mandates that there is no logic sharing inside the sub-circuits corresponding to outputs comprising a single parity group. Since these techniques require some special properties in the circuit structure, they require re-synthesis and re-design, which lead to a change in the original structure of the circuit. Therefore, self-checking design is accordingly termed as intrusive OLT methodology, which because of structural changes may affect the critical paths in the circuit leading to compromise in the operating speed of the design.

Drineas et al. [35, 36] have developed a method based on partial duplication, which

is non-intrusive, generic and flexible in terms of trade-offs regarding area overhead with respect to detection latency. This approach replicates only a part of the original circuit (i.e., CUT) that can detect all the targeted faults in that circuit. A complete set of test vectors is generated using any Automatic Test Pattern Generation (ATPG) algorithm on the next state logic of the CUT, considering the current state bits also as primary inputs. In [35], a subset of the test vectors are taken and synthesized into a “prediction logic” that generates the expected next state of the CUT when any input-present state combination matches with a test vector (of the subset used in the “prediction logic” design). The prediction logic outputs are compared with state flip-flop outputs of the CUT and in case of a mismatch, a fault indicator bit is set. The input-present state combinations which are not considered in the subset of test vectors are don’t cares and this results in the “prediction logic” circuit having lower area as compared to the CUT. The key idea of this method is based on the generation of complete set of test vectors using ATPG algorithms. Since ATPG algorithms generally reveal one test vector for a given fault, they are executed multiple number of times in order to generate a complete set of test vectors. In case of practical circuits, the use of ATPG algorithms may become extremely complex, as OLT requires the exhaustive set (or a large subset) of test vectors. Results have been illustrated in the papers [35, 36] for circuits up to 64 states and 3 inputs only. Recently, a number of partial replication based OLT schemes have been developed using Binary Decision Diagrams (BDDs) [9, 12, 13], which are scalable to handle circuits having about ten thousand gates and five hundred flip flops.

Design of circuits with additional on-chip logic, which can be used to test the circuit before it powers on, is called off-line BIST. Off-line BIST resources can be used for OLT [4, 7, 82, 113, 130, 131] during the idle times of the various circuit modules. The advantage is resource sharing for both on-line and off-line BIST. However, idle times are reducing in modern day circuits (because of pipelining and parallelism) and so these schemes are of limited utility.

All the above mentioned OLT techniques have emphasized on keeping the scheme as non-intrusive as possible, totally self-checking, low power and area overheads, high fault coverage (mainly single s-a faults), low detection latency, etc. However, in deep sub-micron era, several other factors need to be considered for OLT, which include,

- OLT schemes should provide flexibility in terms of trade-offs between area and power overheads of the on-line tester versus fault coverage and detection latency [12, 13].
- The on-line tester should cover advanced fault models [32, 73] (e.g., bridging faults, delay faults, etc.),

## 1.2 Introduction to decision diagrams and their applications in digital circuit testing

---

- Requirement for improvement of scalability of OLT schemes by switching to higher description levels [57, 58] (e.g. register transfer level, behavioral level, etc.) from gate level.
- OLT schemes should be developed for asynchronous circuits or circuits with multiple clocks [107, 109].

Based on the above discussion, it can be concluded that OLT techniques of digital circuits require research and experiments in the areas mentioned above.

## 1.2 Introduction to decision diagrams and their applications in digital circuit testing

Efficient ways of representing and manipulating Boolean functions of digital systems are important in testing [2, 17]. A variety of methods have been proposed and among them Decision Diagrams (DDs) have found widespread use as a concrete data structure for Boolean function representation and manipulation [110, 134].

One of the most primitive DDs is Binary Decision Diagram (BDD), which is a graphical representation of Shannon decomposition of a Boolean function [3, 64]. The idea of representing and manipulating Boolean functions as BDDs was introduced for the first time for circuit simulation in [64] and test generation in [3]. To elaborate, BDD is a directed acyclic graph in which every node represents a Boolean function. Every non-terminal node of a BDD is associated with one input variable of the Boolean function. There are two outgoing edges from the non-terminal nodes. If a non-terminal node represents a Boolean function  $f$  and is associated with the input variable  $x$ , then one outgoing edge points to the node which represents the function  $f|_{x=1}$ . On the other hand, the second edge points to the node which corresponds to the function  $f|_{x=0}$ . In a BDD, there are only two terminal nodes which represent the constant functions 1 and 0.

BDD has recently gained popularity as an efficient data structure for handling Boolean functions because of the extensions made by Bryant [16]. Bryant reduced the graph sizes by two simple rules—(i) if both the outgoing edges of a node point to the same child, then the parent node is eliminated and all of its incoming edges are redirected to the child, (ii) if any two nodes are roots of two isomorphic subgraphs, then one of them is deleted and all edges to that (deleted) node are redirected to the other retained node. The size of a BDD largely depends on variable ordering. BDDs that are constructed with a define variable ordering are called Ordered BDDs (OBDDs). Many algorithms for efficient variable

ordering have been proposed in the literature [5, 41, 52, 72]. Bryant proposed polynomial time algorithms (in size of the OBDDs) for manipulating them. In 1986, Bryant presented a special OBDD called Reduced OBDD (ROBDD), which is a canonical (unique) form of representation of a Boolean function [16]. This canonical property makes ROBDDs useful in performing different operations like equivalence checking between Boolean functions, validity of a Boolean function, satisfiability of a Boolean function, absence of redundant variables in a Boolean function, etc. [16]. For this reason, ROBDDs have found widespread use in VLSI CAD applications including testing of digital circuits [12, 13].

Testing of digital circuits using OBDD model can be accomplished by first representing all the output expressions using separate OBDDs under normal and faulty conditions. Then logical XOR operation is performed between the normal and faulty OBDDs and resulting XORed OBDD is constructed. Finally, the test patterns can be generated by applying “satisfy-all-1” operation on the XORed OBDD. In this way, OBDD model makes the test generation process simple and becomes an efficient data structure for digital circuit testing. However, the run time complexity of the CAD tools developed based on OBDD methodology may reach impractical limits typical for circuits with more than a thousand input and state bits [12, 13]. This is because of the fact that in such cases generation of OBDDs itself become complex [16].

Apart from BDD and its variants, different types of DDs have been proposed in past several years and they have strong impact in the area of formal verification and testing of digital systems. Some of them are, Algebraic Decision Diagrams (ADDs) [6], Structurally Synthesized BDDs (SSBDDs) [95, 96], High Level Decision Diagrams (HLDDs) [92, 93, 122, 124], etc. ADDs are the extended versions of BDDs which allow non-boolean values such as integers and real numbers to be associated to the terminal nodes [6]. ADDs are generally useful in verification and testing of arithmetic circuits by representing vectors of Boolean functions as word-level functions, e.g., integer or floating-point functions. SSBDDs are another special class of BDDs to represent the structural properties of the digital circuits in terms of signal paths [95, 96]. The SSBDDs were introduced to improve the efficiency of test generation methods for gate level structural faults without representing them explicitly. The main advantage of SSBDD based test generation methods is that they can be easily generalized for higher level DDs to handle digital circuits represented at higher abstraction levels [125]. These variants of DDs address the issue of complexity of ROBDDs.

Now-a-days, testing at gate level is a very complicated and time consuming problem because the circuit complexity has increased rapidly. Further, testing of such complex circuits using ROBDD model is difficult because generation of these DDs itself become too complex.

### 1.3 Motivations and Contributions of the thesis

---

Thus, researchers are interested to test the circuits at higher level like behavioral or Register Transfer Level (RTL). High Level Decision Diagrams (HLDDs) were first introduced to represent the digital systems at higher abstraction levels for the ease of fault simulation and diagnosis [122, 124]. The main advantage of HLDDs is that they allow generalization and extension of the gate level fault simulation and test generation algorithms to higher abstraction levels. For this reason, the variables in the form of Boolean values are extended to Boolean vectors or integers and the Boolean functions are extended to the data manipulation operations [96]. A series of works have been proposed by Raik et al., where they have used HLDD as an efficient model for generating test sets for circuits at RTL [91–93]. They have shown experimentally that the test generation time at RTL can be improved to a great extent using HLDDs. The main differences between HLDD model and BDD model are: (a) the terminal nodes in the HLDDs are labeled by some operations or functions whereas the terminal nodes in the BDDs are labeled with constants 0 and 1, (b) the non-terminal nodes in HLDDs are labeled by some control expressions whereas the non-terminal nodes in BDDs are labeled by some variables. Therefore, HLDDs are used to represent circuits at higher description level and BDDs are used to represent circuits at gate level.

### 1.3 Motivations and Contributions of the thesis

Based on the literature review on OLT of digital circuits (in Section 1.1) and application of DDs in circuit testing (in Section 1.2), the contributions of the thesis are presented in this section. In addition, motivations of the proposed works are also discussed.

- **Flexible OLT scheme design: An OBDD based approach to OLT of digital VLSI circuits with measurement limitation**

- Since the on-line tester circuit is fabricated on the same chip with the CUT, thus any point of the CUT can be tapped (measured) easily. This enables the measurement of any required digital parameter of the CUT by the tester. So all of the above mentioned OLT schemes have ignored the issue of tap points or measurement limitation [12, 13, 35, 36]. However, tapping of lines of any circuit results in increase of load (fan-outs) on the gates which drive the tap points. To handle the increased load extra buffers are required, which increase the area of the circuit. If the on-line tester is designed with high number of tapings in the CUT, it results in huge area overhead. So, minimization of tap points (i.e, measurement limitation) of the CUT by the tester is another parameter which needs to be studied from the OLT perspective.

- In this contribution, we design an OBDD based OLT scheme for digital circuits, targeting minimization of tap points. However, minimization of tap points also compromises fault coverage and detection latency. We have considered “number of tap points” as a new design parameter to provide flexibility in terms of trade-offs between area overhead versus fault coverage and detection latency. The scheme starts with generation of test patterns for all possible faults of the circuit under full measurement. Following that, the test patterns that can still detect faults under a given measurement condition are retained. Finally, the on-line tester is designed using these remaining test patterns. The procedure of generation of test patterns and determination of test patterns under measurement limitation are implemented using OBDDs.
  - Results on ISCAS’89 benchmark circuits illustrate that measurement limitation has minimal impact on fault coverage and detection latency but reduces the area overhead of the tester. Further, it was also found that for a given detection latency and fault coverage, area overhead of the proposed scheme is lower compared to other similar schemes reported in the literature.
- **OLT for advanced fault model: An OBDD based approach to OLT of digital VLSI circuits for feedback bridging faults**
    - In majority of the works on OLT of digital circuits, single s-a fault model is considered. However, in modern integration technology, single s-a fault model can capture only a small fraction of real defects [135] and as a remedy, advanced fault models such as bridging faults, transition faults, delay faults, etc., are now being considered. The number of OLT schemes for advanced fault models is few and most of them are based on the bridging fault model. Since feedback bridging faults may cause oscillations, so detecting them on-line is a difficult task in OLT. Most of the works on OLT of bridging fault model have considered only non-feedback bridging faults and ignored feedback bridging faults. As the existing schemes have directly dropped all the feedback bridging faults, thus these schemes compromise fault coverage significantly [13, 73]. However, not all feedback bridging faults create oscillations and even if some does, there are also test patterns for which the fault effect can be manifested logically. Thus, there is a need to study the importance of non-oscillating feedback bridging faults in OLT.
    - In this contribution, we design an OBDD based OLT scheme for bridging fault model. The proposed scheme considers both non-feedback and feedback bridging

faults. The major steps of the scheme are—(a) checking if a feedback bridging fault causes oscillations and filtering out oscillating feedback bridging faults, (b) generating exhaustive test patterns for non-feedback bridging faults and non-oscillating feedback bridging faults. All these steps are implemented using OBDDs which enable the proposed scheme to handle fairly complex circuits.

- Results on ISCAS'89 benchmarks illustrate that consideration of feedback bridging faults along with non-feedback ones improve fault coverage, however, increase in area overhead is marginal compared to schemes only involving non-feedback faults.

- **OLT for circuits at higher description level: A HLDD based approach to OLT of digital VLSI circuits at Register Transfer Level**

- Most of the OLT schemes reported in the literature are at the gate level and these techniques take reasonable computational time and are not scalable for larger circuits. The major reason being these schemes work at bit level, leading to the state explosion problem. This issue of scalability can be solved by developing OLT schemes for circuits at higher description levels, like RTL, behavioral level, etc. The number of OLT schemes at higher description level is less compared to gate level [43, 57, 58] and they have major issues such as high latency, intrusiveness, architecture dependency, etc. Thus, there is a need to develop efficient OLT schemes at RTL in order to overcome these issues.
- The partial replication based OLT schemes at gate level using OBDDs [12, 13] satisfy almost all efficient parameters of OLT, i.e., non-intrusiveness, architecture independence, low area and power overheads, low detection latency, etc. However, these schemes are not scalable to handle large circuits because they work at gate level and the test pattern generation time of these schemes are quite high even for moderate sized circuits. To retain the advantages of partial replication based schemes, in this contribution we aim at developing a partial replication based OLT scheme at RTL. However, unlike the use of BDD for gate level representation, in RTL we use HLDD. The CUT is partitioned into a number of sub-circuits and each sub-circuit is represented using different HLDDs under normal and faulty conditions. For each fault, Fault Detecting control patterns (*FD*-control-patterns) are generated from HLDD representations. Finally, on-line tester circuit is designed using *FD*-control-patterns and their faulty responses.
- The proposed scheme is applied to different HLSynth92 benchmark circuits and

it is shown that the test generation time is greatly improved using HLDDs, thus, large circuits can be easily handled. It also achieves comparable fault coverage and area overhead with respect to OLT schemes at gate level.

- **OLT for asynchronous circuits: An OBDD based approach to OLT of Speed Independent asynchronous circuits**

- Recently, VLSI community has grown interest in asynchronous circuits because they have no clock skew problem, have potentially lower power consumption, can be designed for average case performances rather than the worst case performances, and have higher degree of modularity. Testing of asynchronous circuits as compared to synchronous circuits is considered difficult due to the absence of the global clock. Also, OLT of such circuits is one of the challenging tasks. It is seen that most of the OLT schemes are designed for synchronous circuits compared to asynchronous circuits. There are very few works that have been proposed for OLT of asynchronous circuits [107, 109, 129] and are based on Mutex approach. However, these schemes have issues like high area overhead, protocol dependency, etc. Thus, there is a need to develop efficient OLT schemes for asynchronous circuits to overcome these problems.
- In this contribution, we propose an OBDD based OLT scheme for Speed Independent asynchronous (SI) circuits which is protocol independent and incurs low area overhead. We model the SI circuits along with their faults as Signal Transition Graphs (STGs) and then translate them into State Graphs (SGs), from which test patterns are determined. An efficient way of generation of the test patterns directly from the circuit description using OBDD, without need of the explicit SG model, is also discussed. Finally, we propose a new technique for on-line tester design which can be synthesized as an SI circuit. The tester is designed as SG model which is live and has Complete State Coding (CSC); these properties ensure its synthesizability as an SI circuit.
- The scheme is applied to different SI benchmark circuits and it is found that the area overhead for the on-line tester is much less compared to the existing Mutex approach. The scheme provides flexibility to trade-off area overhead by reducing fault coverage and detection latency depending upon the testability requirements. Such flexibility can not be achieved by the Mutex approach.

### 1.4 Organization of the thesis

The rest of the thesis is organized as follows.

**Chapter 2:** In this chapter, we present literature review on OLT of digital VLSI circuits, followed by DDs and their applications in circuit testing. The pros and cons of the reported OLT techniques are discussed and then motivations and contributions of the thesis are derived.

**Chapter 3:** In this chapter, we propose an OBDD based OLT scheme for digital VLSI circuits with measurement limitation in order to provide flexibility in the on-line tester design.

**Chapter 4:** In this chapter, we propose an OBDD based OLT scheme for advanced fault model-bridging faults, where both feedback and non-feedback bridging faults are considered.

**Chapter 5:** In this chapter, we propose a HLDD based OLT scheme for digital VLSI circuits at RTL in order to improve scalability.

**Chapter 6:** In this chapter, we propose an OBDD based OLT scheme for asynchronous circuits. The scheme is applicable to all types of SI circuits.

**Chapter 7:** In this chapter, we summarize the works done in this thesis and future scope is presented.

## Chapter 2

# Literature review: On-line Testing of Digital VLSI Circuits and Decision Diagrams

This chapter presents a literature review regarding On-line Testing (OLT) of digital circuits and application of Decision Diagrams (DDs) in testing. Section 2.1 starts with a brief introduction to digital VLSI testing and concludes with the motivation of OLT in the current era of deep sub-micron designs. Section 2.2 discusses different techniques of OLT for digital VLSI circuits and their pros and cons. The major issues of OLT are discussed in Section 2.3, which include flexibility in terms of trade-offs between area overhead versus fault coverage and detection latency, coverage for advanced fault models, scalability, applicability for asynchronous circuits, etc. This is followed by an overview of different types of DDs and their applications in modeling and testing of digital circuits, in Section 2.4. Finally, we conclude in Section 2.5

### 2.1 Digital VLSI testing

The challenge of testing digital systems has grown rapidly over the last two decades. As the fabrication technology moves to lower sub-micron processes and engineers keep increasing the design complexity, testing encounters greater challenges. The complexity of VLSI technology has reached a point where an effort is made to put millions of transistors on a single chip by decreasing the feature size. The reduction in feature size increases operation speed, allows design of complex circuits, provides high performance, etc., however, it also raises the probability of occurrence of defects in the integrated circuits. Since the defects occurring

## 2.1 Digital VLSI testing

---

during the process of manufacturing are unavoidable, so some of the circuits may be faulty. Hence, testing is mandatory to isolate fault free circuits from the defective ones [2, 17, 99]. Further, the advent of complex systems like Network-On-Chip (NOC) [40] and System-On-Chip (SOC) [132] make it mandatory to start considering testing early in the design process. This process of test planning include, but are not limited to, development of accurate fault models, examining testability at a higher level of design representation and embedding more effective test constructs prior to or during synthesis [81, 133].

Figure 2.1 illustrates a typical digital VLSI design and test flow. This starts with the development of the specifications for the system from the set of requirements, which includes functional characteristics ( i.e., input-output), operating characteristics (i.e., power, frequency, noise, etc.), environmental and physical characteristics (i.e., packaging, humidity, temperature, etc.) and other constraints like area, pin count, etc. This is followed by an architectural design to produce a system level structure of realizable blocks for the functional specifications. These blocks are then implemented at the Resister Transfer Level (RTL) using some hardware description language like Verilog or VHDL. The next step is called logic design, where the blocks are decomposed into logic gates maintaining operating characteristics and other constraints like area, pin count, etc. Lastly, at the physical design step, the logic gates are implemented using physical devices (e.g., transistors) and a chip layout is produced. Then the chip layout is converted into photo masks which are used in the fabrication process. Backtrack from an intermediary stage of the design and test flow may be required if the design constraints are not satisfied. It is unlikely that all fabricated chips would satisfy the desired specifications. Impurities and defects in materials, equipment malfunctions, etc. are some causes leading to the mismatches. The role of testing is to detect the mismatches, if any. As shown in Figure 2.1, the test phase starts in the form of planning even before the logic synthesis and hardware based testing is performed after the fabrication. Depending on the type of circuit and the nature of testing required, some additional circuitry, pin out, etc. need to be added with the original circuit so that hardware testing becomes efficient in terms of fault coverage, test time, etc. This additional design to enhance test is called Design For Testability (DFT). For example, if one time manufacturing test is the requirement, then scan based design may suffice; however, if OLT is required, then the design must be augmented with circuit monitors. Figure 2.2 illustrates the basic operations of digital testing. Binary test vectors are applied as inputs to the circuit and the responses are compared with the golden signature, which is the ideal response from a fault free circuit. Testing can be classified according to several criteria. Table 2.1 summarizes the most important attributes of various testing methods and the associated terminology. The

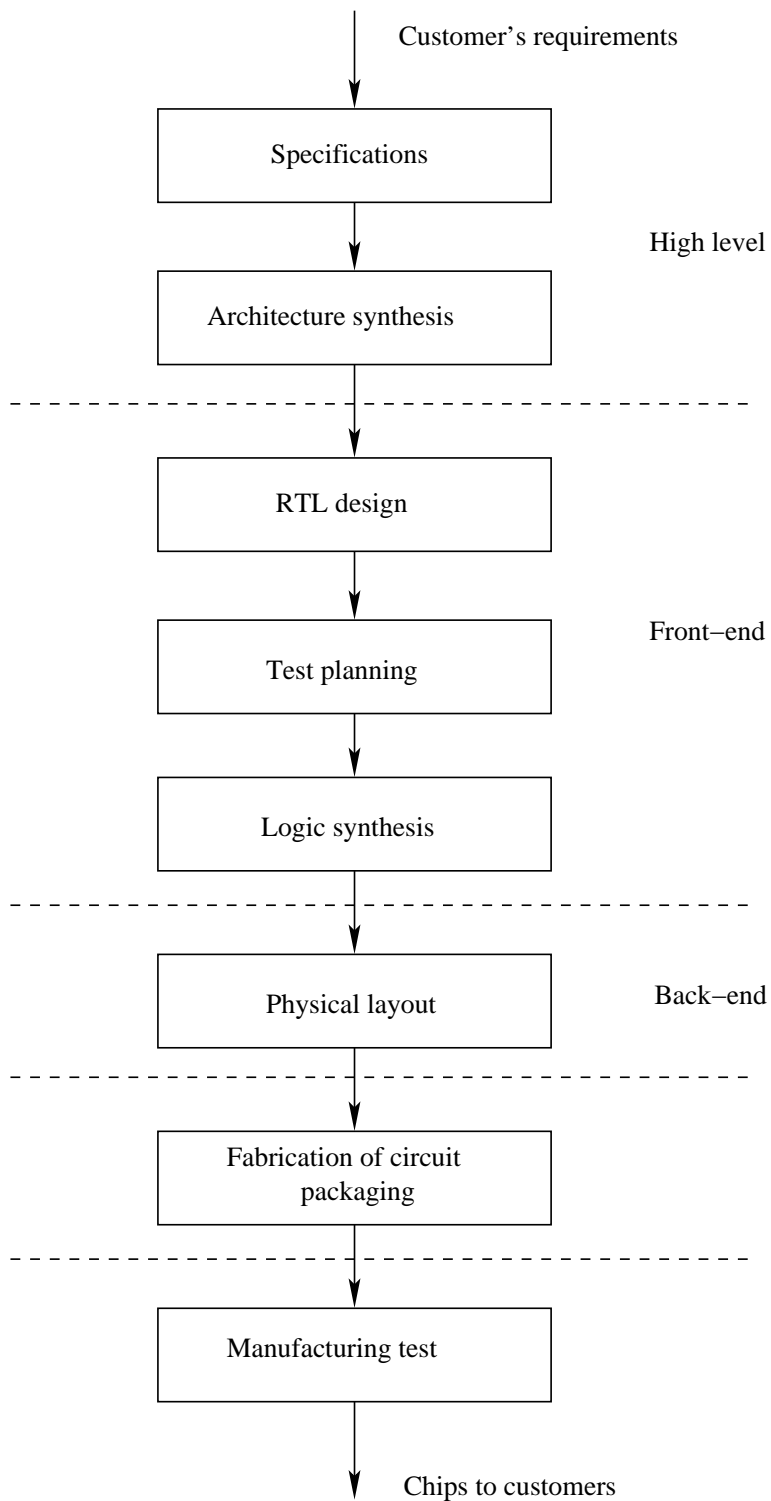


Figure 2.1: A typical VLSI design and test flow

## 2.1 Digital VLSI testing

---

items presented in bold letters in the table are related to OLT.

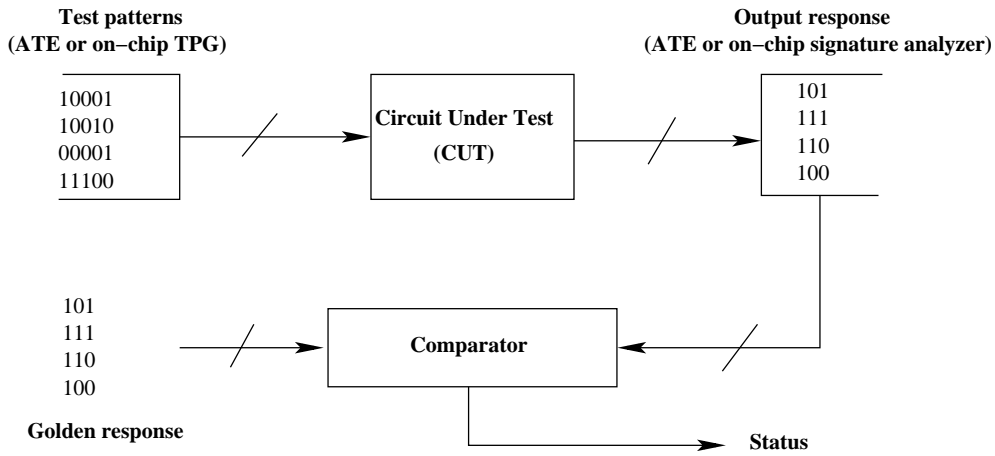


Figure 2.2: Principle of digital testing

### 2.1.1 Structural vs. functional testing

The tests used for verifying that the chip meets the input-output specifications are called functional testing. Typically they have low fault coverage. Further, test pattern generation for exhaustive functional testing may be quite expensive. The number of test vectors required for this is of the order of  $2^n$ , where  $n$  is the number of inputs. The situation becomes more complex if it has sequential elements in it [2,17]. For example, the 32-bit full adder shown in Figure 2.3 requires  $2^{33}$  vectors for exhaustive functional testing. Using structural knowledge of the system this complexity, however, can be reduced to a great extent. Structural testing, introduced by Eldred in [38], depends on the specific structure of the circuit involving gate types, interconnects, fault models, etc. One of the advantages of structural testing is the ability to develop efficient algorithms to generate the structural test vectors. For example, by using the information about the structure of the adder (shown in Figure 2.3) and adding a small amount of additional hardware, it can be tested with 8 test vectors only. The 32 bit adder with DFT circuitry is shown in Figure 2.4.

It may be noted that in this case, two—31 bit shift registers, and 31 number of 2 : 1 multiplexers comprise the additional DFT circuit. One shift register (called input register) provides inputs to the “carry input” bits of the individual adders during test and the other shift register (called output register) latches outputs from the “carry output” bits of the individual adders. In the modified 32 bit adder, the carry input to the  $i^{th}$  (full) adder is multiplexed with the  $i^{th}$  bit of the input shift register,  $1 \leq i \leq 31$ . During normal operation

Table 2.1: Variants of VLSI testing

Criterion	Attributes of testing method	Terminology
When is the test performed?	Concurrently with the normal system operation	<b>On-line/Concurrent testing</b>
	As a separate activity	Off-line testing
Where is the source of stimuli?	Inputs during operation	<b>On-line testing</b>
	Within the chip	Built-In-Self-Test (BIST)
	Applied by an external device	Automatic Test Equipment (ATE) based testing
What is tested?	Design errors	Design verification testing
	Fabrication errors	Manufacturing test
	Failure during operation	<b>On-line testing (OLT)</b>
Which physical object is being tested?	Wafer	Non packaged ICs level testing
	IC	Packaged level testing
	Board	Board level testing
	System	System level testing
How are the stimuli applied?	In a fixed predetermined order	Static Testing
	Depending on results	Adaptive testing
How fast are the stimuli applied?	Much slower than the normal speed of operation	DC (static) testing
	At normal speed of operation	<b>At-speed testing</b>
Who checks the results?	On-chip circuit	<b>Self-checking</b>
	External tester	External testing

## 2.1 Digital VLSI testing

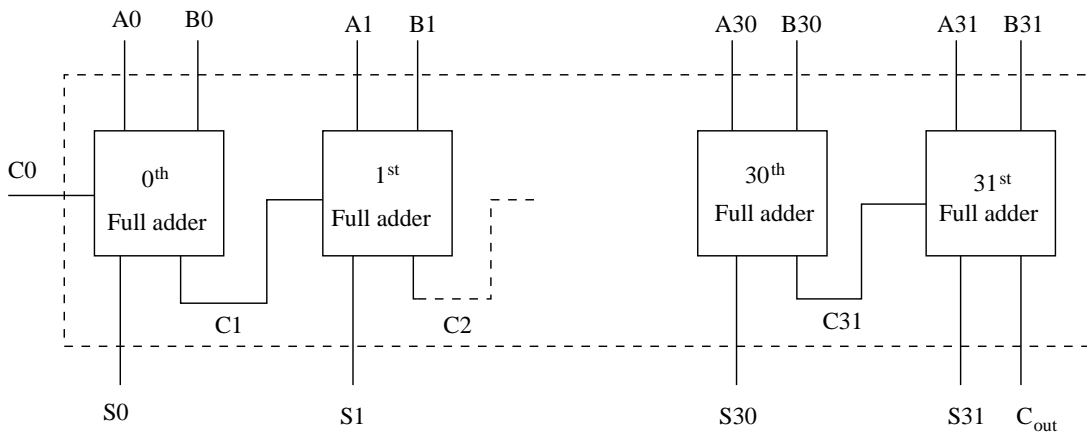


Figure 2.3: A 32 bit ripple carry adder

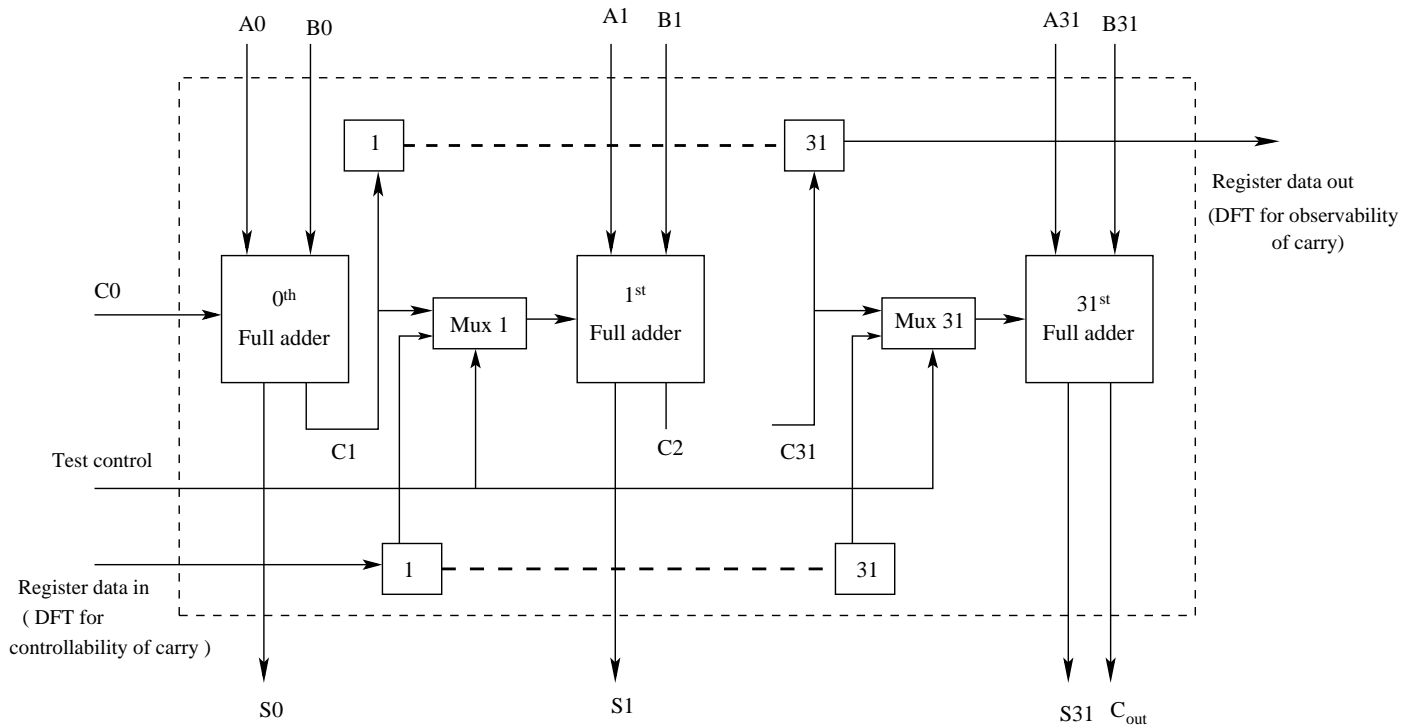


Figure 2.4: A 32 bit ripple carry adder with the DFT circuitry

of the 32 bit adder, the multiplexers connect the carry input of the  $i^{th}$  (full) adder to the carry output of the  $(i - 1)^{th}$  (full) adder,  $1 \leq i \leq 31$ . However, during test, the multiplexers connect the carry input of the  $i^{th}$  (full) adder to the output of the  $i^{th}$  bit of the input shift register,  $1 \leq i \leq 31$ . The values in the shift register are fed externally. It may be noted that by this DFT arrangement all the (full) adders can be controlled individually as direct access is provided to the carry inputs of the adders; inputs other than carry are already controllable. Hence, testing in this case would be for each (full) adder individually and that requires 8 test vectors as each of the 32 full adders can be tested in parallel. Correct operations of each of the full adders are determined by looking at the sum and the carry outputs. Sum outputs are already available externally and hence no DFT circuit is required to make them directly observable. For the carry outputs, however, another similar DFT arrangement is required to make them observable externally. This would require the output (31 bit parallel load and) shift register where the carry output bit of the  $(i - 1)^{th}$  adder is connected to the  $i^{th}$  input of the output shift register,  $1 \leq i \leq 31$ . Once the values of all the carry bits are latched in the register, which is done in parallel during test, they are shifted out sequentially. In this case a full adder is tested functionally and structural information is used at the cascade level. Thus, it may be stated that “structural testing is functional testing at a level lower than the basic input-output functionality of the system”. In the case of digital circuits, structural testing is “functional testing at the level of gates and flip-flops”. Structural test vectors aim to detect manufacturing faults and try to confirm the correctness of the device structures in the manufacturing process like wires, flip-flops and gates. The pros and cons of structural and functional testing are shown in Table 2.2.

### 2.1.2 Fault models

Central to the advantages of structural testing are the fault models. At the physical level an enormous number of different faults could be present and it is quite complex to analyze them at that level. Thus, physical level faults are grouped together with regard to their manifestation at the logic functionality of the circuit, which are termed as fault models [2, 17]. A fault model facilitates the identification of targets for testing and generation of input patterns to test the faults in the fault model. The most commonly used fault model is the single stuck-at (s-a) fault model [2, 17]. This is modeled by having a circuit net s-a logic 0 or 1 (i.e., s-a-1 or s-a-0). The number of s-a faults in a circuit is linear with respect to the number of nets in the circuit netlist; if there are  $n$  nets in a circuit, the number of single s-a faults is  $O(2n)$ .

With the arrival of deep sub-micron designs, it is found that the single s-a fault model

## 2.1 Digital VLSI testing

---

Table 2.2: The pros and cons of structural and functional testing

<b>Functional testing</b>	<b>Structural Testing</b>
Without fault models.	With fault models.
Manually generated design verification test patterns.	Automatic Test Pattern Generation (ATPG) algorithms available.
Slow and labor intensive.	Efficient and automated.
Fault coverage not known (need fault simulation).	Fault coverage is a quantified metric.
Long test length.	Short length of test patterns (efficient compaction algorithms available)
Fault coverage usually low	Fault coverage determined by the user
Useful in design verification.	Not very helpful in verification (Assumes correct design).

cannot capture more than a low fraction of physical defects [135]. As a result, advanced fault models are being advocated for. They include path-delay fault model [19], bridging fault model [104],  $n$ -Detect tests [88], etc.

**Delay faults:** Delay faults can be categorized into two types namely, delay to rise and delay to fall. Delay to rise faults occur when the time required for the voltage (corresponding to logic 0) to rise (to the voltage corresponding to logic 1), in a circuit net, is higher than a threshold. Likewise for the delay to fall fault. Under both such faults, the delay of critical paths may rise leading to violation of setup time requirements of the registers. In other words, the delay caused by these faults are such that the new signal value corresponding to the transition at the net under fault is not latched by the state register.

**Bridging faults:** A fault in a circuit that results due to unwanted shorts between the lines is called a bridging fault. For most DSM CMOS fabrication processes, a large percentage of malfunctions results due to such bridging faults [104]. The shorted lines are assumed to form AND and OR logic operation; so the model is called wired-OR or wired-AND bridging fault. There are two types of bridging faults—non-feedback and feedback. If there exists at-least one path between the shorted lines, then the bridging fault is called feedback, otherwise it is called non-feedback.

**$n$ -Detect:** The  $n$ -Detect approach uses traditional s-a fault model in conjunction with enhanced test pattern generation algorithms to detect the same fault multiple times. The model is based on the fact that random excitation and observation of a site by different test vectors may enable detection of defects related to that site that were missed by approaches where a single vector was used for testing.

### 2.1.3 Test programming

The test program development consists of two broad steps—(i) generation of test vectors and (ii) generation of the corresponding golden responses for a fault free circuit. Figure 2.5 shows the basic steps of a test program generation.

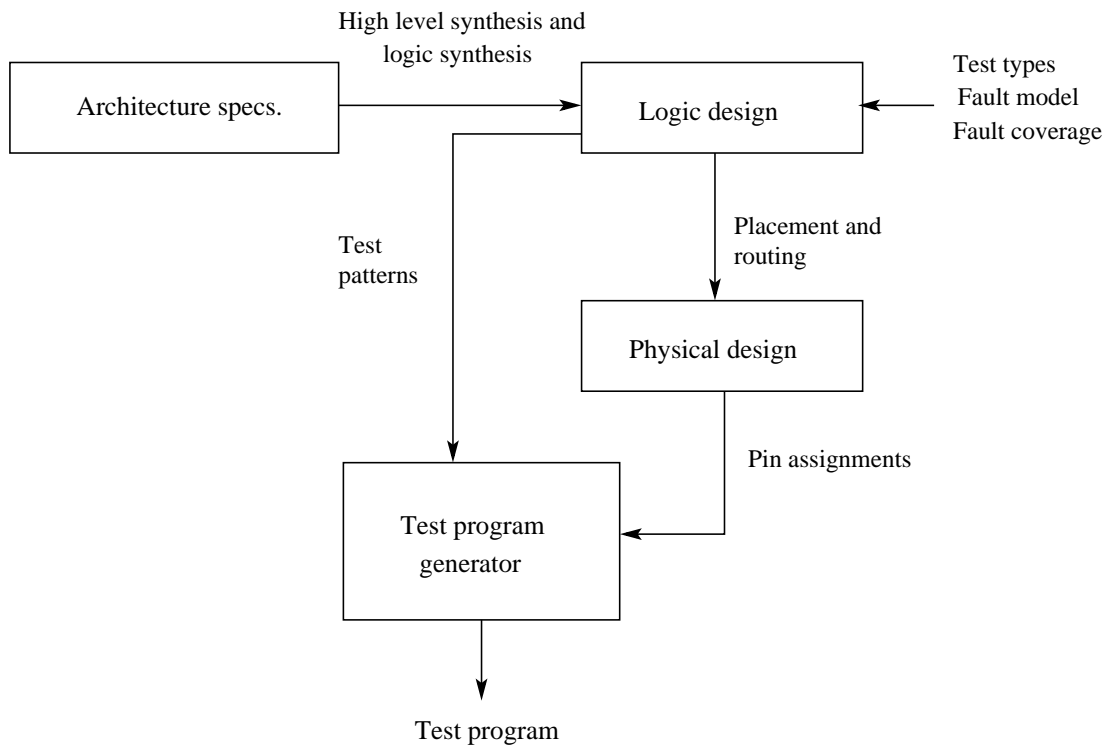


Figure 2.5: Basic steps in test program generation

#### Test pattern generation

It involves generation of a minimal subset of input patterns, such that all faults of the considered fault model are sensitized and their effects are propagated to the output. The process of test pattern generation can be divided into two distinct phases; 1) test generation and 2) test application.

For (1), appropriate circuit model (e.g., gate level model) and fault model (e.g., s-a fault model) are to be identified. Construction of a test pattern for a fault comprises determining an input pattern such that the output obtained from the circuit with the fault is different from that of the fault free circuit. As test patterns are to be generated for all faults, this approach can be computationally expensive, however, it is performed off-line and only once after the design stage. On the other hand, for (2), all test patterns are to be applied to

## 2.1 Digital VLSI testing

---

each integrated circuit manufactured which may be millions in number; thus, the test set generated must be efficient in terms of the time required for application to the circuits.

An overview of the algorithms used for test pattern generation is as follows. An ATPG algorithm basically comprises three steps:

- **Fault propagation:** Select a line from the point of occurrence of the fault to the Circuit Under Test (CUT) output that would be used to manifest the effect of the fault. The inputs of all the gates falling in that path other than the one through which the fault is to be propagated are to be driven to their non-controlling values; for example, if a two input OR gate, having inputs  $X$  and  $Y$ , is in the fault propagation path and input  $X$  is the line through which the fault is to be propagated to the output, then  $Y$  is to be set to 0; a dual of this step is applicable for an AND gate.
- **Fault sensitization:** Assume a value at the fault site that is opposite of the fault to be detected; in other words, if a s-a-1 is to be detected at net  $A$ , then assume a signal value 0 at  $A$ .
- **Line justification:** Determine if an input pattern exists such that the assumed value at net  $A$  is attained and the path from net  $A$  to the output is sensitized.

The same technique can be applied to a sequential circuit, but before that the sequential elements of the circuit are explicitly driven to a required state using scan based DFT circuitry [2, 17]. The well known ATPG algorithms are D-algorithm, PODEM and FAN [2, 17, 133].

### Output response analysis

ATPG algorithms also provide the expected output response from the fault free CUT (for a given test). The test data obtained from the CUT is compared with the expected response and consequently, the comparison mainly serves two purposes. First, it helps to accept or reject the CUT. Secondly, the mismatch of output due to fault can be used for “fault mode analysis” which provides diagnostic information for improving the design, fabrication and test flow for the subsequent design iterations.

#### 2.1.4 Comparison of ATE based testing, BIST and OLT

VLSI testing can be broadly classified into the following three major categories on the basis of the phase (manufacturing, startup or on-line) during which the test is performed:

1. **ATE based testing:** This involves testing the circuit using Automatic Test Equipment (ATE) just after manufacturing. In this class of testing, test patterns are applied to a circuit and outputs are compared with the expected fault free responses using off-chip equipments [79, 90, 127]. Generally speaking, there is a difficulty in at-speed testing because the operational speed of modern day VLSI circuits is higher than that of an ATE. Since testing of a circuit using ATE is performed once just after its manufacturing, thus, the faults that develop after deployment of the circuit cannot be detected. So ATE based testing is according termed as off-line testing. Further, the cost of ATE based testing is high because of the price of its individual components.
2. **Built-In-Self-Test (BIST):** Due to the steep increase in complexity of digital circuits, BIST has been realized in many designs to implement some of the test functions on-chip [8, 33, 42]. Compared to off-line testing, the advantage of BIST is that it enables reduction in the demands on the external ATE, thus enabling at-speed and in-situ testing. This permits the scheme to test circuits every time they are powered ON, even after they are deployed in the system. The basic BIST components are the Test Pattern Generator (TPG), the Test Response Evaluation (TRE) unit and the Test Controller (TC) [17]. At the circuit level, the inputs have to be preceded by a multiplexer to connect either to the normal (functional) inputs or the outputs of the test pattern generator. TPG, TRE and multiplexer are controlled by the TC. Figure 2.6 illustrates the basic architecture of a circuit with BIST.

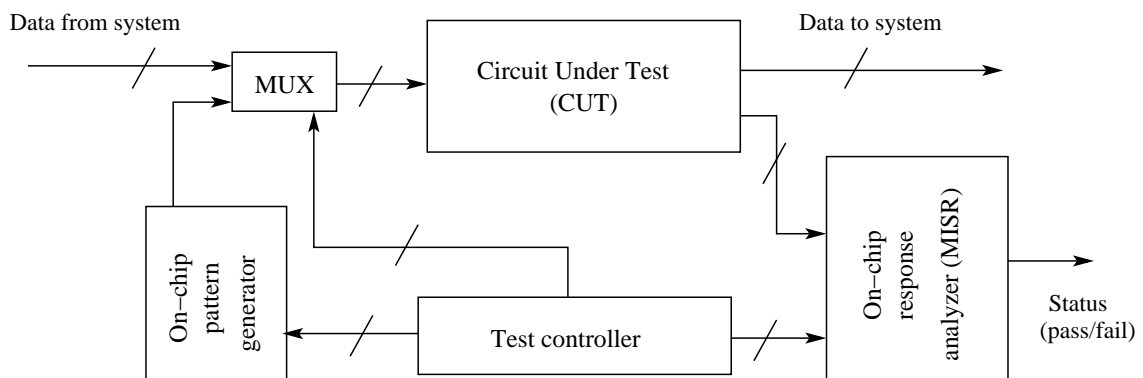


Figure 2.6: BIST scheme

### 3. On-line Testing (OLT):

It has been observed that as the scale of integration increases, the operation of the Integrated Circuits (ICs) are becoming increasingly susceptible to faults that are absent

## 2.2 Literature review: On-line testing of digital VLSI circuits

---

during fabrication or power up but develop on-the-fly [37, 84]. Off-line test strategies (like ATE based testing, BIST, etc.) need to withdraw the circuit from normal operation for testing, which may not be always permissible. Immediate detection of the faults that occur on-the-fly during operation of the circuit requires incorporation of a technique which will continuously observe its operation by checking whether the response follows its normal behavior. These techniques fall under the category of OLT [47, 83, 84, 89]. *OLT (also called concurrent testing) can be defined as a technique to monitor a circuit and detect the occurrence of a fault (from the fault model) within a finite time of its occurrence.* Unlike off-line testing (involving ATE based testing and BIST), where test vectors can be applied, either through external test equipments or on-chip pattern generators, OLT requires that the circuit contains some DFT circuitry to test itself for all the vectors that it encounters during its normal mode of operation. Thus, in OLT, neither can patterns be applied from a test circuit/pattern generator nor can the memory elements (registers) be separated from the core. In other words, unlike off-line testing, there is no “test mode” in OLT, where the circuit operation can be altered for testing. There are four primary parameters to be considered in the design of an OLT scheme:

- (a) Fault coverage: The fraction of all modeled faults that are detected; it is usually expressed in percentage.
- (b) Fault detection latency: The number of clock cycles that may be required for the detection of a fault after a deviation from the normal behaviour is observed for the first time.
- (c) Area overhead: The extra amount of on-chip hardware needed to perform OLT, i.e., area of the on-line tester circuit.
- (d) Power overhead: The extra power needed to perform OLT.

Tables 2.1.4, 2.1.4 and 2.1.4 compare these three major test paradigms to bring forth their advantages and disadvantages.

## 2.2 Literature review: On-line testing of digital VLSI circuits

In this section we provide a survey highlighting the works reported in the literature on OLT of digital circuits. Further, the pros and cons of each of the test methodologies are also

Table 2.3: Merits and demerits of ATE based off-line structural testing [2, 17]

Merits	Demerits
<ul style="list-style-type: none"> <li>• Low complexity of ATPG algorithms.</li> <li>• On-chip hardware overhead: 5 to 10% of core area.</li> <li>• Automated flow: Well-established CAD tool support for scan based DFT and ATPG.</li> </ul>	<ul style="list-style-type: none"> <li>• Difficulty in at-speed testing:               <ul style="list-style-type: none"> <li>– ATE speed is in MHz range while operational VLSI core speed may be several GHz.</li> </ul> </li> <li>• Converts sequential circuits to virtual combinational ones using scan chains.               <ul style="list-style-type: none"> <li>– Changes the core delay characteristics.</li> <li>– Requires a non-operational mode for testing: OLT is not supported.</li> </ul> </li> <li>• Dead load of test equipments               <ul style="list-style-type: none"> <li>– Difficulty in in-situ testing.</li> </ul> </li> </ul>

discussed. OLT techniques for digital VLSI circuits (both combinational and sequential), reported in literature, can be classified into the following main categories:

1. Signature monitoring in Finite State Machines (FSMs)
2. Self-checking design
3. Partial replication
4. On-line BIST

### 2.2.1 Signature monitoring in FSMs

Signature monitoring techniques for OLT basically work by studying the state sequences of the FSM model of a sequential circuit during its operation. Signatures are FSM state sequences traversed during execution. In these methods, signatures are analyzed concurrently with the execution of the circuit. This analysis targets to detect faults leading

## 2.2 Literature review: On-line testing of digital VLSI circuits

---

Table 2.4: Merits and demerits of BIST

Merits	Demerits
<ul style="list-style-type: none"> <li>• Reduced parasitics, loading, etc. due to absence of ATE, probes, packaging, etc.</li> <li>• Reduced test point access problem.</li> <li>• Startup, at-speed and in-situ testing supported.</li> </ul>	<ul style="list-style-type: none"> <li>• High on-chip hardware overhead when compared to ATE based testing.</li> <li>• On-chip BIST hardware design complexity               <ul style="list-style-type: none"> <li>– Signal application.</li> <li>– Signal tapping.</li> <li>– Test evaluation.</li> </ul> </li> <li>• Test of BIST hardware.</li> <li>• Cannot detect faults that develop on the fly.</li> <li>• CAD tools for automated BIST circuit design are rare or application specific.</li> <li>• On-chip power consumption</li> </ul>

Table 2.5: Merits and demerits of OLT

Merits	Demerits
<ul style="list-style-type: none"> <li>• All advantages of BIST holds.</li> <li>• On-line detection of faults is possible avoiding suspension of normal operation.</li> </ul>	<ul style="list-style-type: none"> <li>• Area and power overhead of the OLT circuit.</li> <li>• On-chip tester area overhead is higher compared to area requirements of BIST.</li> <li>• Testing of the OLT circuit.</li> <li>• No CAD tool for generating on-line test circuits is widely accepted or available commercially.</li> </ul>

to illegal paths in the control flow graph, i.e., paths having transitions which do not exist in the FSM specification. To ensure that the runtime signature of the fault free FSM is different from the one with fault, a *signature invariant property* is forced during FSM synthesis. The principle of signature monitoring for FSMs has been proposed in [66,67]. Figure 2.7 illustrates the basic architecture for OLT using the scheme of signature monitoring in FSMs. The main component of the monitor is a Multiple Input Shift Register (MISR), which generates a signature using the polynomial division of the codes of the state that is reached during normal operation. So the runtime signature represents a value of the path followed through the control-flow graph of the FSM. A primitive polynomial is used to perform division in order to reduce the fault masking (also called “aliasing”). The correct values of the signature are pre-computed from the specified FSM graph and are compared with the runtime signature at some special states called checking points. To ensure that the runtime signature of the normal circuit FSM is different from the faulty one, an invariant property is forced during FSM synthesis and can be stated as [67]:

**Signature invariance property:** The signature of the sequence of state codes obtained by polynomial division with the primitive divisor polynomial is invariant after each state in the graph, when any legal path is taken. Checking involves comparison of the runtime signature with the invariant reference signature when the current state corresponds to any selected check points. To obtain an FSM with signature invariance property the state assignment procedure is modified to take into account the constraints related to such an invariance. The approach has been proved to be feasible in [66,67] and several implementations based on this approach have been reported in [22,100,115].

The major advantage of the schemes based on signature monitoring is due to the fact that the area overhead incurred for OLT is extremely low (and almost negligible in cases of FSMs with large number of states); the results presented in [67] has reported that the area of the additional circuit required for OLT is about 1% to 5% of the CUT when the FSM is large. It is also discussed in [67] that detection latency may be high for some FSMs which can be remedied by increasing the number of checkpoints, however, incurring more area overhead. The hybrid signature monitoring scheme reported in [22] detects control flow errors caused by transient and intermittent faults. It is shown that the scheme has offered very high fault coverage with low detection latency and area overhead. In [115], a concurrent control flow error detection and recovery mechanism has been proposed using encoded signature monitoring technique. The scheme recovers from most of the control flow errors with relatively low performance overhead.

However, many times by default, signature invariance is not present. In that case, the

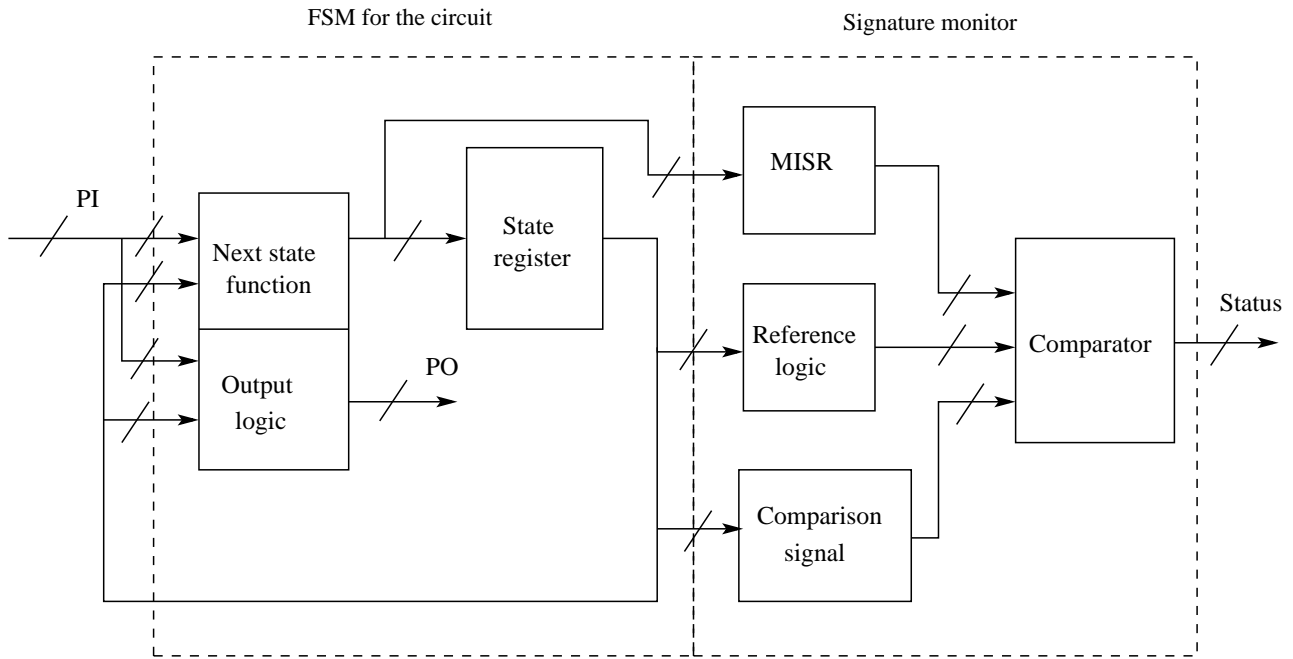


Figure 2.7: Basic architecture for signature monitoring

state assignment procedure of the FSM may have to be modified to take into account the constraints related to such an invariance. In other words, signature monitoring techniques for OLT require some special properties in the circuit structure, so they require re-synthesis and re-design, which lead to a change in the original structure of the circuit; they are accordingly termed as intrusive OLT methodologies. In the worst case, when the FSM graph is well connected, a large number of new states are added to achieve the signature invariant properly. Further, the state explosion problem in FSM makes the application of this scheme difficult for practical circuits; results reported in the OLT literature using these schemes are limited to circuits having typically about one hundred states.

### 2.2.2 Self-checking design using error detecting codes

The basic principle for self-checking design using error detecting codes is as follows. Let the Circuit Under Test (CUT) realize a Boolean function  $f$ . The OLT scheme contains another module called output characteristic predictor, which predicts some special characteristic of the CUT output  $f(i)$  for the input  $i$ , independently. Finally, the checker verifies whether the special characteristic of the output which is produced by the CUT in response to input  $i$  is same as the predicated one. If there is any mismatch found, then an error signal is produced. Some examples of the characteristic of  $f(i)$  (for self-checking using error detecting codes) are

parity of  $f(i)$ , 1's count in  $f(i)$ , etc. The basic self-checking design scheme discussed above is depicted in Figure 2.8.

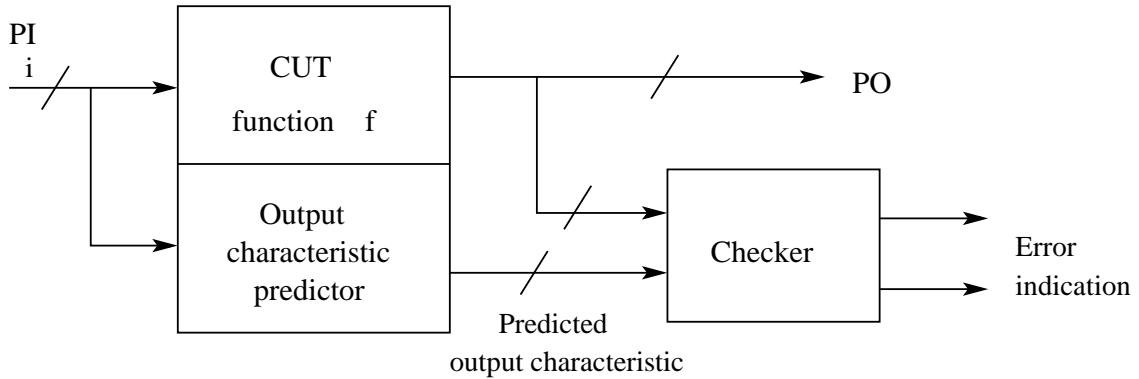


Figure 2.8: Basic architecture for self-checking circuit

The technique of OLT using self-checking circuits based on error detecting codes was motivated from the error detection and correction techniques used in communication. The CUT output (or information) bits are augmented with some additional bits, called check bits (using an additional logic), such that under normal condition of the CUT and the additional logic, the CUT output augmented with the check bits is a code word of the error detecting code chosen. The checker verifies whether the CUT output augmented with the check bits is a code word of the error detecting code chosen. The effect of a fault in the CUT leading to change in some output bit is called an *error*. The above mentioned technique can be easily used for sequential circuits [53, 118] where the CUT illustrated in Figure 2.8 is the next state function of the sequential circuit. The circuit corresponding to the output characteristic predictor feeds additional flip-flops (other than the ones in the original circuit). Thus, the outputs of circuit flip-flops augmented with that of the additional flip-flops is a code word of the error detecting code chosen. The checker taps the outputs of these flip-flops taken together. The basic self-checking design scheme for sequential circuits is depicted in Figure 2.9.

Before we move on to presenting the most important error detecting codes, we define some fundamental terms used in the context of self-checking circuits; they can be found in almost every publication addressing self-checking designs [14, 53].

**Self-testing circuit:** A circuit is self-testing, if for every fault in the specified fault model, there is an input that produces a non-code output.

**Fault-secure circuits:** A circuit is fault-secure, if an input can produce a non-code word or a correct code word. That is, they cannot be incorrect code words.

## 2.2 Literature review: On-line testing of digital VLSI circuits

**Totally Self-Checking (TSC):** A circuit is TSC with respect to all the modeled faults if and only if it is both self-testing and fault-secure.

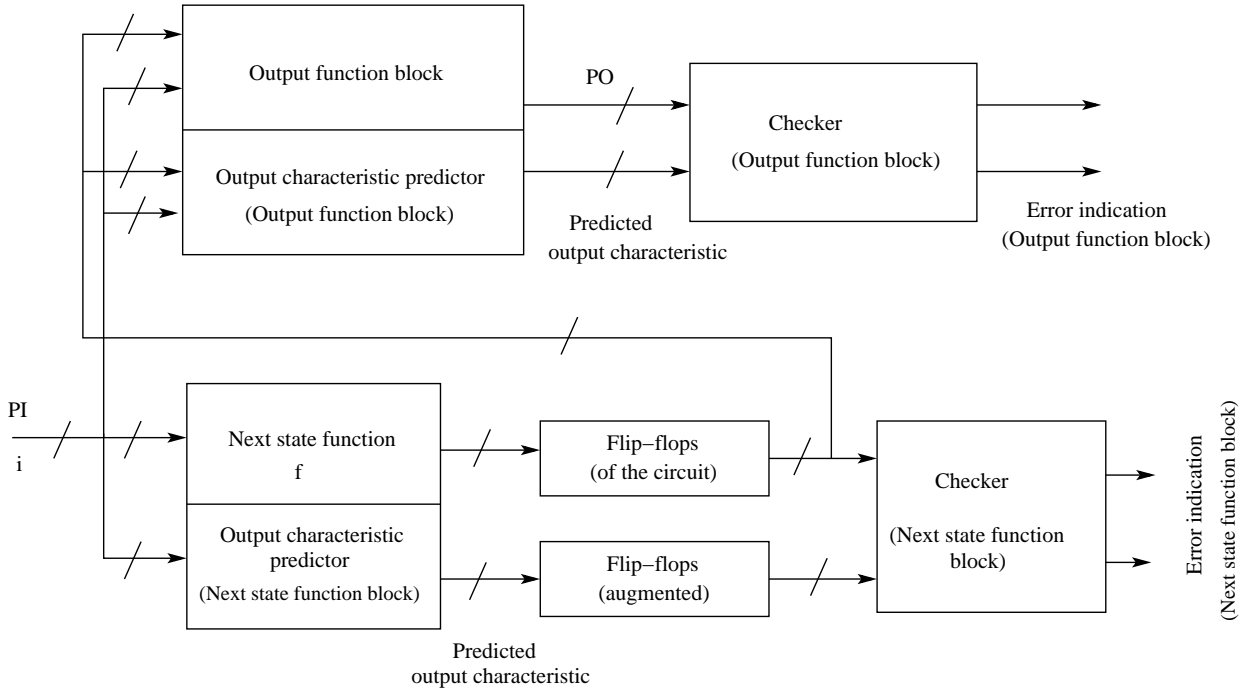


Figure 2.9: Basic architecture for self-checking sequential circuit

The totally self-checking property is the usual goal when designing a circuit having OLT capability. It guarantees that there are no redundant faults (self-testing) and that the erroneous outputs generated due to any fault will not be misinterpreted as correct ones (fault secure); the fault may be either in the CUT or the checker. A number of research papers have been published in the area of self-checking checker design using different codes [20, 34, 49, 53, 84, 86, 101, 102, 119, 128]. We now discuss some of the important coding techniques used in design of TSC circuits with pros and cons of each of them.

**Parity codes:** The most simple TSC circuit design is by using a single bit parity where a single check bit is added to the CUT output bits and it is calculated such that the parity of each code word is constant (odd or even). Such a parity code can detect all single or odd multiplicity errors. It is the cheapest possible error-detecting code since the check bit is only one. TSC circuit design using parity codes is reported in [84, 86]. It may be noted that if TSC circuits are designed using single bit parity codes, then all the faults that manifest themselves as even multiplicity errors cannot be detected. For such cases, circuits are synthesized specially such that all the faults in the modeled list manifest themselves as single or odd multiplicity errors. The technique presented in [34] has used single parity

bit for the entire circuit. To limit the scope of fault manifestation, each primary output is synthesized independently and so there is no sharing of logic gates among any pair of output bits. As a result, faults in any block can imply at most one output error. The single bit parity technique mandates no logic sharing among any two outputs. So it may result in high area overhead for some circuits. In order to reduce area overhead, the multiple-parity-group technique was introduced in [39,119] that allows logic sharing among some outputs. This technique partitions the primary outputs into different parity groups. It was shown that logic sharing can be allowed among the outputs that correspond to different parity groups and that would still result in faults changing only a single output bit. The outputs of the same parity group are verified using a TSC parity checker.

***m-out-of-n codes:*** An *m-out-of-n* code word has exactly *m* 1s out of total *n* bits. *m-out-of-n* code is an unordered code i.e., no two code words *x* and *y* are present such that *x* has 1 in every bit position where *y* has a 1. An example of *m-out-of-n* code for TSC circuit design can be found in [20]. Simple inspection of the results presented is enough to illustrate the complexity of checkers based on such unordered codes compared to a parity checker. They were not widely adopted since they are much more expensive to implement than parity based schemes.

**Berger codes:** A Berger code consists of an information part and a check part, which is the binary representation of the number of 1s in the information part. So, it is an unordered code. TCS circuits using this methodology can be found in [21,112]. Area overheads of the self-checking circuits designed using Berger codes are higher compared to ones designed using parity based schemes.

As a practical application, the residue code technique is used in [49] for design of self checking modulo multiplier, which is used in various cryptographic systems. In another work [128], D. P. Vasudevan and P. K. Lala have proposed a new approach for designing of self checking carry select adder of arbitrary size and the adder can detect both permanent and transient s-a faults on-line. The area overhead for making circuits totally self checkable is usually not high. A number of design and synthesis constraints are, however, required by the coding technique based methodologies to control the scope of fault propagation. For example, the method reported in [53] requires that all inverters be pushed to the primary inputs and for the scheme proposed in [34] there should be no logic sharing within a single parity group. Since these techniques require some special properties in the circuit structure, they require re-synthesis and re-design. So, OLT schemes based on design of TSC circuits using coding theory are intrusive in nature.

To address the issue of intrusiveness of coding theory based OLT schemes, weight based

codes are used [31], where a weight is assigned to each output (information) bit and the sum of weights of the output (information) bits, which have value 1, represent the check bits. Weight-based codes can distinguish between errors changing output bits from 1 to 0 and from 0 to 1, because both these errors result in a different weight. So they do not require any special synthesis constraints to restrict the fault manifestation. Further, such codes are positional ones, i.e., the check bits are a function of the erroneous bits as well as their positions in the output (which is determined by the individual weights assigned to the output bits). Thus, they can have high fault detection capabilities. The only drawback of using weight based codes is the high area overhead compared to Berger, parity or  $m$ -out-of- $n$  codes.

### 2.2.3 Duplication schemes for OLT

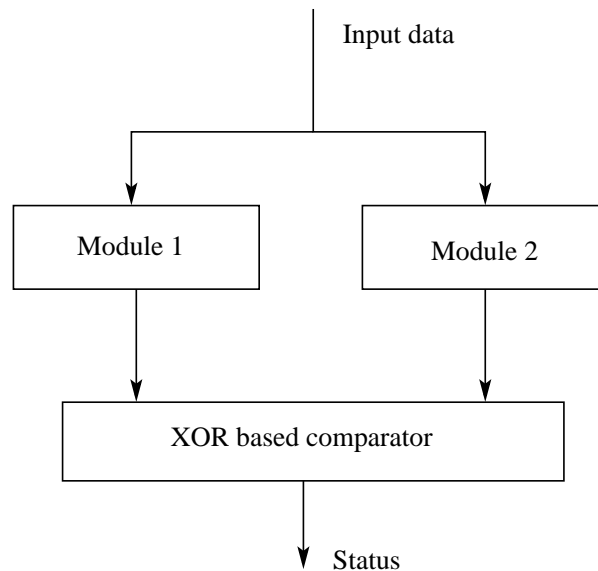


Figure 2.10: Basic architecture for duplication based OLT

One of the most straightforward way of designing systems with OLT capability is duplicating itself and crosschecking for similarity of the output responses. The basic duplication scheme is presented in Figure 2.10. Module 1 and Module 2 are functionally equivalent, that is, they operate identically (in the fault free case) and produce the same outputs when fed with the same inputs. If they are structurally equivalent as well (i.e., their gates and interconnections are identical), then the technique is called identical duplication. Otherwise, it is a diverse duplication technique. Duplication schemes are fault secure by their very nature. However, hardware overhead of more than 100% is introduced in the design if every module is physically duplicated [84]. In [76], Mitra et al. have compared identical and

diverse duplications with respect to their vulnerabilities to fault pairs; their simulation results are in favour of the diverse case. An interesting alternative to full hardware duplication is presented in [116], where Module 2 (Figure 2.10) is replaced by a minimized version of Module 1 (i.e, CUT), such that all targeted faults can be detected eventually. Further, the comparator is equipped with a (simple) test control unit that specifies if the checker must check or not, depending on the input word. So, it becomes a controllable comparator/checker. This technique is termed as “partial replication”. The main advantages of partial replication technique are due to its non-intrusiveness, low area overhead and flexibility in terms of trade-offs between area overhead versus fault coverage and detection latency.

A number of OLT schemes based on partial replication have been proposed by Drineas et al. [35,36], where a complete set of test vectors is obtained using standard Automatic Test Pattern Generation (ATPG) on the next state logic of the CUT, considering the current state bits also as inputs. Then a subset of the test vectors is taken and synthesized into a partially replicated circuit that generates the expected next state of the CUT when an input-present state combination matches with a test vector. The partially replicated circuit outputs are compared with state flip-flop outputs of the CUT and in case of a mismatch, a fault indicator bit is set. The input-present state combinations that are not considered in the test vector subset are treated as don't cares and this results in the partially replicated circuit having lower area when compared to the next state logic of the CUT. The efficiency of these schemes [35,36] strongly depends on the prior knowledge regarding the input patterns that the CUT is likely to receive. To elaborate, the patterns (test vectors) that occur frequently should be included in the subset for construction of the partially replicated tester and others that occur rarely may not be considered. Further, since ATPG algorithms generally reveal one test pattern for a given fault, they must be executed a multiple number of times to generate a complete (or large) set of test vectors. In case of practical circuits, the use of ATPG algorithms may become prohibitively complex, as OLT requires the exhaustive set (or a large subset) of test vectors. Since these schemes reported in [35,36] use standard ATPG algorithms for generation of test vectors, they are not scalable. Results have been reported for circuits up to 64 states and 3 inputs only.

Biswas et al. [10–12] have proposed a series of partial replication based OLT schemes for s-a faults. These techniques are non-intrusive in nature, flexible in terms of area overhead versus fault coverage and detection latency, and scalable up to circuits having ten thousand gates and five hundred flip flops. The complexity of generation of test patterns of the CUT is addressed by using Ordered Binary Decision Diagram (OBDD). The complete set of test patterns is generated from the OBDD representation of the CUT and on-line tester circuit

## 2.2 Literature review: On-line testing of digital VLSI circuits

---

is designed using a subset of these test patterns. The steps involved for generation of test patterns are—i) representing each output of the CUT using separate OBDDs under normal and faulty conditions, ii) performing XOR operation between normal and faulty OBDDs and constructing XORed OBDD, iii) applying “satisfy-all-1” on the XORed OBDD. Application of OBDD enables the proposed scheme to handle fairly complex circuits.

It is seen that most of the partial replication based OLT schemes reported in the literature work for single s-a faults [10–12,35,36]. However, in modern integration technology, single s-a fault model can capture only a small fraction of real defects and as a remedy, advanced fault models such as bridging faults, transition faults, delay faults, etc. are considered. Biswas et al. have extended the approach reported in [12] for bridging faults and delay faults in papers [13] and [9], respectively. However, in case of bridging faults the authors have considered only non-feedback bridging faults and ignored the feedback bridging faults as they create oscillations. Further, all the OLT schemes based on partial replication technique [9–13,35,36] consider the circuits modeled at gate level, hence these are scalable only up to certain extent. Also, these schemes are designed only for synchronous circuits, so they cannot be directly applied to asynchronous circuits. Another assumption is regarding the tapping of lines of the CUT by the on-line tester. All the existing works on on-line tester design tap as many lines as possible of the CUT because the on-line tester circuit is fabricated on the same chip with the CUT and any point of the CUT can be tapped easily. However, it is known that tapping of lines of any circuit results in increase of load (fanouts) on the gates which drive the tap points. To handle the increased load extra buffers are required, which increase the area of the circuit. So if the on-line tester is designed with more number of tapings in the CUT, it results in large area overhead.

### 2.2.4 On-line BIST

As discussed in Subsection 2.1.4, the scheme used for design of circuits with additional on-chip logic, which can be used to test the circuit every time before it starts up, is termed as off-line BIST. Off-line BIST resources can also be utilized for OLT [7, 82, 113, 130, 131]. This technique performs on-line BIST by utilizing the idle times of the various modules of the circuit during normal operation. Thus, this is the only technique that facilitates both on-line and off-line testing using the same on-chip resources. As the feasibility and efficiency of this scheme depends on the idle times of the circuit modules, it may not be applicable to modern day circuits. This is because, such circuits are designed to achieve parallelism and pipelining by reducing the idle times of the circuit modules.

### 2.2.5 Pros and cons of different OLT techniques

We have discussed four broad classes of OLT techniques with their advantages and disadvantages in Subsections 2.2.1, 2.2.2, 2.2.3 and 2.2.4. Table 2.6 shows the important pros and cons of these OLT techniques in brief. Based on the observations in Table 2.6, it can be stated that partial replication technique is the best among others. However, many issues still remain to be solved in partial replication based OLT schemes and some of the prominent ones are as follows:

- **Measurement limitation based flexibility:** The on-line testers should provide flexibility in terms of trade-offs between measurement limitation (reduction in number of tap points) versus area overhead, fault coverage and detection latency.
- **Coverage for advanced fault models:** Designing OLT schemes that support fault models appropriate for the latest VLSI design paradigm, e.g., bridging faults including feedback, delay faults, transition faults, etc.
- **Scalability:** The on-line tester design algorithms should be capable of handling large size circuits.
- **Handling asynchronous circuits:** Developing OLT schemes that are applicable for asynchronous circuits.

There are very few works that have been proposed to address these problems. In the next section, we review elaborately the existing works in these areas, following that, motivation of the thesis is discussed.

## 2.3 Desired features of OLT schemes

### 2.3.1 Measurement limitation based flexibility in OLT

In OLT, a tester circuit is designed using a subset of test patterns and it checks the response of the circuit against each of the patterns in the subset and detects if there is any deviation from the normal responses. The area and power overheads of an OLT scheme depend on the number of test patterns considered in the design of the on-line tester circuit. There are two possible approaches to reduce the area and power overheads of the on-line tester. First one is, by dropping some of the test patterns in the on-line tester design, however, it increases the fault detection latency. Second one is, by not considering some faults in the on-line tester design, however, it reduces the fault coverage. Similarly, the power overhead can be reduced

## 2.3 Desired features of OLT schemes

Table 2.6: Pros and Cons of different OLT techniques

OLT techniques	Pros	Cons
Signature monitoring in FSMs	Low area overhead	Intrusiveness
		State explosion problem in FSMs
		Applicable for small circuits
		High fault detection latency
Self-checking design	Low area overhead	Intrusiveness
		Low fault coverage
Partial replication	Simplicity in design,  Supports non-feedback bridging faults, Facilitates trade-offs between area overhead versus fault coverage and detection latency, Non-intrusiveness.	Area overhead is more than 100% (under full duplication)
		Maximum possible tap points (full measurement)
		Mainly applied for stuck-at faults
		Works at gate level, hence non-scalable
		Designed for synchronous circuits
On-line BIST	Provides both on-line and off-line testing with a single on-chip tester.	Depends on idle time of circuit modules
		High fault detection latency

by selecting test patterns such that the number of switchings between any two test patterns is less. Thus, flexibility in OLT schemes can be achieved through trade-offs between area and power overhead of the tester versus fault coverage and detection latency. The OLT schemes reported in [9, 12, 13] provide flexibility in terms of trade-offs between area overhead versus fault coverage and detection latency by selecting a subset of the test patterns. These works have shown that the area overhead can be lowered by considering a subset of test patterns for on-line tester construction. However, the subset is selected in a fashion such that for all faults, at-least one test pattern is present. It is also shown that the impact of lowering the test patterns is almost linear with the detection latency [9, 12, 13]. In [12], the authors have developed an OLT scheme using state based model for s-a faults and this scheme is extended

for non-feedback bridging faults and delay faults in [13] and [9], respectively.

The on-line tester circuit is placed on-chip with the Circuit Under Test (CUT). The tester taps certain lines of the CUT, whose values are used to determine whether any fault has developed in the CUT. Such tap points are analogous to sensors used in physical systems [62]. Unlike physical systems, where sensors cannot be placed at all desired locations, in case of circuits the on-line tester can tap any point of the CUT. So, all the above mentioned OLT schemes (Section 2.2.3) have emphasized on keeping the scheme as non-intrusive as possible, totally self-checking, low area overhead, high fault coverage, low detection latency, etc., but ignored the issue of tap points. However, tapping of lines of a CUT results in increase of load (fan-outs) on the gates which drive the tap points [63]. Such increase in load requires use of additional buffers that increase area overhead. So, if the concept of fault detection under measurement limitation (i.e., sensor placement limitation in case of physical system [85, 114]) is applied for OLT of circuits, we can minimize the tap points of the CUT and reduce the number of driving buffers. This will minimize the area overhead of the tester. However, minimization of tap points also compromise fault coverage and detection latency. So, number of tap points can be considered as a new design parameter to provide trade-offs between area overhead versus fault coverage and detection latency.

In this thesis, we develop a partial replication based OLT scheme for s-a faults with the concept of tap point reduction and analyze the affect of this reduction on fault coverage, detection latency and area overhead.

### 2.3.2 OLT schemes for advanced fault model

With the arrival of DSM designs it is observed that the single s-a fault model cannot capture more than a fraction of the real defects [135]. In view of this some initial efforts have been given for the design of circuits having OLT facility for advanced fault models. The number of such OLT schemes is few and most of them are based on the bridging fault model. Broadly speaking, if two normally distinct points (lines) are shorted together in a circuit, then the situation is called bridging fault. The shorted lines are assumed to form AND and OR logic operation; so the model is called wired-OR and wired-AND bridging fault. Bridging faults can be divided into two types (i) simple bridging fault or non-feedback bridging fault and (ii) feedback bridging fault. If there exist at-least one path between the two shorted lines, then the bridging fault is called feedback bridging fault, otherwise it is called non-feedback bridging fault. Now, we present a literature review on different OLT schemes for the bridging fault model.

OLT for bridging faults was first attempted in [73]. This scheme is based on self-

## 2.3 Desired features of OLT schemes

---

checking design, where the outputs are encoded with error detecting codes and presence of any bridging-fault would result in an output which is a non-code word. There are two major issues with the work, namely (i) inherently the methodology is intrusive and (ii) only non-feedback faults are considered. As already discussed, the basic idea of self-checking design comprises imposing some special structure in the circuit so that any fault (from the fault model considered) results in a non-code word as output, which leads its detection [53]. Further, the circuit would never produce a wrong codeword as output. To maintain the self-checking property, several design constraints are imposed during circuit synthesis making the scheme intrusive. Only non-feedback bridging faults are considered because in self checking design, effects of the faults need to be mapped to non-code words and if a fault causes oscillations such mappings are infeasible [73].

Biswas et al. in [13] have developed a partial replication based OLT scheme for bridging faults. Experimental results in this work illustrated an interesting fact that area overhead for OLT of bridging faults is not higher compared to that of s-a faults. The major reason is, a test pattern that detects a bridging fault also detects a s-a fault, but the reverse may not hold. So, while selecting the partial set of test patterns, only those which can detect some bridging fault are considered. Using this procedure, low detection latency and high fault coverage could be achieved for bridging faults, even at low area overheads. The tester inherently built for bridging faults also provided high fault coverage for s-a faults. However, again, only non-feedback bridging faults were considered in [13].

Das et al. in [32] attempted to test feedback bridging faults on-line in cluster based FPGAs. OLT is performed by comparing the outputs (for specific input test pattern sequence) of the FPGA block under test with golden response using an output response analyzer. For input cases, when the block under test does not cause oscillations, presence of fault can be easily tested by comparing responses. However, for other inputs there may be oscillations, to avoid which, an asynchronous circuit called Muller-C element is used in all the FPGA blocks. As Muller-C element is adaptable to delay variation, its presence helps in preventing the circuit to go into oscillation. Although the work was more of a proof of concept and tried on FPGA, it can be applied by suitable adaptation to ASIC based implementation as well. However, there are two main issues with this approach namely, intrusivity of the design and use of asynchronous elements. It may be noted that design of asynchronous testers for OLT of synchronous circuits is not desirable.

Based on the above literature review, in this thesis we propose a synchronous partial replication based OLT scheme for wired AND-OR bridging faults. The scheme first determines the bridging faults which do not lead to oscillations, i.e., all non-feedback and

some feedback bridging faults. Following that, exhaustive set of test patterns for these faults are generated. Also, it is checked if there are patterns, even in case of oscillating feedback bridging faults, which can detect these faults without oscillations. All these test patterns taken together are used to design the on-line tester, called *FN*-detector (Fault versus Normal condition detector).

### **2.3.3 OLT schemes for circuits at higher description level**

It has been observed that the partial replication based OLT schemes [9,12] at gate level satisfy almost all efficient parameters of OLT, i.e., non-intrusive, architecture independent, low area and power overheads, low detection latency, etc. However, these schemes are not scalable to handle large circuits because they work at gate level and the test pattern generation time of these schemes are quite high even for moderate sized circuits. So, testing at gate level becomes a complicated and time consuming task for complex circuits. To overcome this problem, researchers are interested to test the circuits at higher level of abstraction using high level fault models. However, testing at higher level is a challenging task due to lack of well accepted fault models, unlike at the gate level, where single s-a fault model is well accepted. But it is verified that there exists good correlation between high level fault models and gate level fault models [25,94], further gate level fault models have good correlation with physical defects. So, there exists indirect mapping between high level fault models and physical defects [133]. Since testing at lower levels (say gate level) using lower level fault models (say stuck-at-fault model) is scalable only up to certain extent (about 30K gates and 500 flip flops), so high level fault models are used to test the circuits at higher abstraction levels. In other words, even though gate level fault models are highly correlated to real defects, they are not scalable. This difficulty is addressed by developing high level fault models, testing of circuits using these fault models at higher abstraction levels and analyzing test quality by indirect mapping of faults versus physical defects [92,97,117].

Now we discuss some high level fault models which are based on behavioral or functional description of the circuit. These high level fault models are designed to provide good correlation with the gate level fault models. In [56], Anton Karputkin and Jaan Raik have proposed a set of behavioral fault models that target detection of stuck at faults in gate level implementations of the RTL designs. Experiments on a set of ITC'99 benchmarks show that the proposed fault models achieve high gate level stuck-at fault coverage (average of 86%). F. Coron et al. [25] proposed an RTL fault model which assumes that all the statements in the high level description are executed at least once and their fault effects are propagated to the primary outputs. This fault model captures the single stuck at bit faults on all assignment

## 2.3 Desired features of OLT schemes

---

statements based on a set of predefined rules. They have achieved a correlation coefficient about 77% between RTL and gate level fault coverages. The fault model at RTL presented in paper [59] is based on code validation techniques used in software testing. Results show that the RTL fault coverage obtained by using this fault model based methodology has a close match with the gate-level fault coverage. The mixed hierarchical functional fault models reported in paper [94] are designed to test sequential cores inside the Systems on a Chip (SoC). The fault models proposed in this paper, based on combination of hierarchical and functional fault models provide high fault coverage for sequential circuits. It is shown by experiments that these fault models cover more than 90% of gate-level stuck-at faults for testing of sequential cores.

Since last decade, a number of high level testing schemes have been proposed using different high level fault models. Among them the number of OLT schemes is very few compared to off-line mode of testing. Now, we start with some off-line testing schemes followed by existing OLT schemes at higher level. Pradip A. Thaker et al. [117] developed an RTL fault model and fault injection algorithm based on application of stratified sampling theory and stratum weight extraction techniques where the RTL fault coverage of a module tracks the gate-level fault coverage within error bounds predicted by the random sampling technique. An RTL Automatic Test Pattern Generation (ATPG) scheme [68] was proposed by Li et al., which is based on clustering of circuit states at higher description level, termed as behavioral phases. These phases represent the circuit functionality more explicitly, thus, simplifies the representation to ease the testing. A series of works have been proposed by Raimund Ubar et al. [92, 93], for generation of hierarchical test patterns for sequential circuits using HLDDs. Experimental results show that these schemes have achieved high fault coverage (average of 89% in [92] and average of 91% in [93]) and low test generation time for some benchmark circuits. Reinsalu et al. in [97, 98] have proposed a deductive method (based on bit coverage fault model) for RTL fault simulation using high level decision diagrams. Experimentally they have shown that good fault coverage (average of 90% in [98] and average of 86% in paper [97]) and shorter run-times are achieved with this method in comparison to gate level fault simulation. A new off-line testing scheme for RTL circuits has proposed by Mohammad Mirzaei et al. in [74]. This scheme introduces hybrid canonical data structure based on a decision diagram for generation of test patterns from the arithmetic model of a RTL circuit. Results illustrated that the scheme achieves high fault coverage (average of 93%) with very short processing time and minimum memory usage.

All the above testing schemes at RTL are purely based on off-line mode of testing and hence cannot detect the faults that develop during normal operation. There are very few

works on OLT of VLSI circuits at RTL. The first work in this direction [58] was presented by Ramesh Karri and Balakrishnan Iyer. This Concurrent Error Detection and Diagnosis (CEDD) technique is based on replication of model operations and the replicated operations are executed with the different functional units in the idle computation clock cycles. The outputs obtained from these functional units are compared and, thus, faulty units are detected. Although the technique has low area overhead but the main disadvantage of this scheme is that, it is difficult to find the idle computation clock cycles of functional units of a system; so it has long latency. Further, now-a-days systems are designed to achieve parallelism by keeping the functional units busy in all clock cycles. Since the scheme relays on execution of replicated operations with different functional units, thus this technique cannot be applied to the operations where there is no secondary functional units to execute the replicated operations [58].

In another work, Ramesh Karri and Kaijie Wu [57] developed an RTL Concurrent Error Detection (CED) technique based on algorithm level re-computing using allocation diversity and data diversity. In the case of allocation diversity technique, the operation-to-operator allocation in the normal computation and the re-computation cases are different, whereas in the data diversity technique, shift operands are applied to the re-computation. This time-redundancy-based CED scheme achieves high fault coverage with a very low area overhead. However, this scheme has high time overhead or fault detection latency because it performs normal computation and re-computation at different times and compares their results. O. Golubeva, M. Sonza Reorda and M. Violante [43] presented a behavioral RTL CED technique that deals with re-computation of the design operations with shifted operands. This scheme has been applied to two data dominated benchmark circuits; i.e., ELLIPF and DIFFEQ, where the fault coverage of functional units are found to be high.

From the above discussion we may state that the OLT schemes at higher abstraction level have the following issues– i) These schemes depend on idle time of different functional units of the CUT, so, they have high latency. ii) Since these schemes require some special properties in the circuit structure, they require re-synthesis and re-design of the original circuit. So, these OLT schemes are intrusive in nature. iii) These schemes are not architecture independent, since they always require secondary functional units for OLT. So, these schemes cannot be directly applied to all types of circuits.

To retain the advantages of partial replication based OLT schemes at gate level reported in [9, 12, 13], in this thesis we aim at developing a partial replication based OLT scheme at RTL. However, unlike the use of OBDD for gate level representation, in RTL we use High Level Decision Diagram (HLDD).

### 2.3.4 OLT schemes for asynchronous circuits

Most of the circuits used in VLSI designs are synchronous. Compared to synchronous circuits, asynchronous designs offer great advantages such as no clock skew problem, low power consumption and average case performances rather than worst case performances. Testing asynchronous circuits as compared to synchronous circuits is considered difficult due to the absence of the global clock [50]. Also, on-line testing of such circuits is one of the challenging tasks in deep sub-micron designs. The OLT schemes developed for synchronous circuits are not applicable to asynchronous circuits due to their different design principles. There are few works that have been proposed on OLT of asynchronous circuits [107, 109, 129]. Now we elaborate these works as follows.

Traditionally double redundancy methods were used for OLT of asynchronous designs [129]. In this scheme, two copies of the same circuit work in parallel and the on-line tester checks if they generate the same output. This scheme results in more than 100% area and power overheads. Further, both being the same circuit, they are susceptible to similar nature of failures. The schemes reported in [107, 109] basically work by checking if the output of the asynchronous circuit maintains a predefined protocol (i.e., there is no premature or late occurrence of transitions). The checker circuit is implemented using David Cells (DC), Mutual Exclusion (Mutex) elements, C-elements and logic gates. The checker circuit has two modes of operation—normal mode and self-test mode. In normal mode the checker is used to detect if there is any violation in the protocol being executed by the CUT. On the other hand, in self-test mode the checker is used to detect faults that may occur within the checker. Mutex elements (component of asynchronous arbiter) were used to grant exclusive access to the shared DCs between different modes of operation. The area overhead of the Mutex blocks is high, even compared to the original circuit. So, area overhead of the on-line tester in this case would be much higher than that of the original circuit and even the redundancy based methods. Further, this tester only checks the protocol and so fault coverage or detection latency cannot be guaranteed.

From the above discussion we aim at developing an efficient OLT scheme for asynchronous circuits which is protocol independent and incurs low area overhead. The proposed non-intrusive OLT scheme is easily applicable to all type of Speed Independent asynchronous (SI) circuits.

## 2.4 Complexity of generation of exhaustive set of test patterns for OLT

Unlike off-line testing where a single test pattern is enough for detecting a fault, OLT requires exhaustive set of test patterns [2, 17]. In OLT, first the exhaustive set of test patterns for each fault in the considered fault model is generated. Then the on-line tester circuit is constructed using these test patterns. The process of generation of exhaustive set of test patterns for a fault is quite involved. Generation of a single test pattern requires three steps—fault sensitization, fault propagation and line justification. If no input pattern exists (for a selected path) for fault propagation, then a backtrack is required by selecting another new path for fault propagation. The above three steps are repeatedly executed till no more new test patterns are determined. Also, for determination of each test pattern, multiple backtracks may be required. Further, it may be hard to determine whether no more new test patterns exist for a fault or the algorithm requires backtrack for a new path. It may be noted that the number of paths in a circuit net-list can be exponential in the number of its nets. Hence, there is a requirement of simplification techniques for generation of the exhaustive set of test patterns.

The simplification in the procedure of generation of exhaustive set of test patterns for a fault can be incorporated by representing the circuit outputs using Ordered Binary Decision Diagrams (OBDDs) and devising processing steps to work on these OBDD representations. To accomplish the exhaustive set of test pattern generation, an OBDD is constructed for each circuit output in both normal and faulty conditions. The normal and faulty OBDDs are XORed and the resulting XORed OBDD is constructed. The exhaustive set of test patterns is generated by applying the “satisfy-all-1” operation on the XORed OBDD. The operations on OBDDs was first proposed by Bryant in [16], where he has devised algorithms to perform Boolean operations using OBDD. The size of an OBDD depends mainly on variable ordering. Many algorithms for efficient variable ordering have been reported in the literature [5, 41, 52]. Reduced OBDD (ROBDD) is an OBDD where there is no redundant nodes as well as no isomorphic subgraphs. ROBDDs are compact and canonical representation of Boolean functions. This makes ROBDDs useful in various VLSI CAD applications, in particular, design, verification and testing of digital circuits [12, 13]. ROBDDs are suitable to represent digital circuits at logic gate level, however, they suffer from state explosion problem which limits their applications on large sized circuits.

To overcome the state explosion problem of ROBDDs, different types of Decision Diagrams (DDs) have been proposed mainly to represent large sized circuits at higher

level descriptions. Some of them are Algebraic Decision Diagrams (ADDs) [6], Structurally Synthesized BDDs (SSBDDs) [95, 96], High Level Decision Diagrams (HLDDs) [92, 93, 125], etc. ADDs are generally useful for representation, verification and testing of arithmetic circuits whereas SSBDDs are used to represent the structural properties of the digital circuits in terms of signal paths. HLDDs represent the digital system as a whole at higher levels like behavioral or RTL for the purpose of ease of fault simulation and diagnosis [96]. In the next subsection we discuss different types of DDs and their applications in representation of digital circuits at different level of abstractions.

### 2.4.1 Decision Diagrams

Decision Diagrams (DDs) are derived from Decision Trees (DTs) by reduction of nodes and edges, and are used to represent Boolean functions efficiently. The idea of representing Boolean functions using DDs was first introduced by Lee [64] and Akers [3] and they called these diagrams as Binary Decision Diagrams (BDDs). In the past several years, different types of DDs have been proposed for applications in digital circuit design, simulation and test. Now, we summarize a few of them.

#### Binary Decision Diagram (BDD)

BDD is a directed acyclic graph where a node represents a Boolean function. Every non-terminal node of a BDD is associated with one input variable of the Boolean function. Two outgoing edges are there from the non-terminal nodes. If a non-terminal node represents a Boolean function  $f$  and is associated with the input variable  $x$ , then one outgoing edge points to the node which represents the function  $f|_{x=1}$  (called Shannon cofactor of  $f$  with respect to  $x$ ). On the other hand, the second edge points to the node which corresponds to the function  $f|_{x=0}$  (called Shannon cofactor of  $f$  with respect to  $\bar{x}$ ). In a BDD, there are only two terminal nodes which represent the constant functions 1 and 0. Figure 2.11 illustrates the BDD representation of the Boolean function  $f = xy' + yz$ . The number of nodes in a BDD depends heavily on ordering of the input variables. An Ordered BDD (OBDD) is a BDD which has an ordering of input variables. The same figure (Figure 2.11) also illustrates the OBDD for representing of function  $f = xy' + yz$ , where ordering of variables is  $x \prec y \prec z$ .

In 1986, Bryant proposed Reduced OBDD (ROBDD) where the size of the BDD was reduced using two rules [16]. These two rules are:

- a) Merging of two non-terminal nodes: If any two nodes (non-terminals) are roots of two isomorphic subgraphs, then one of them is deleted and all edges to that (deleted) node

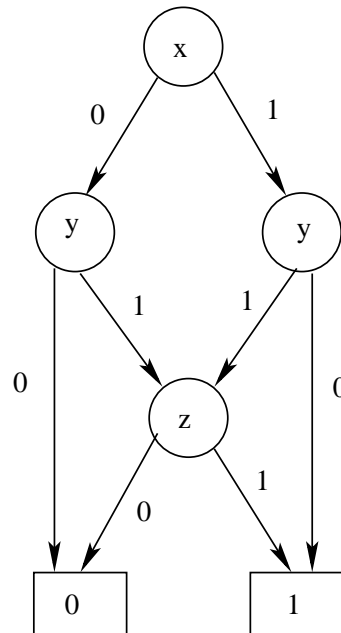
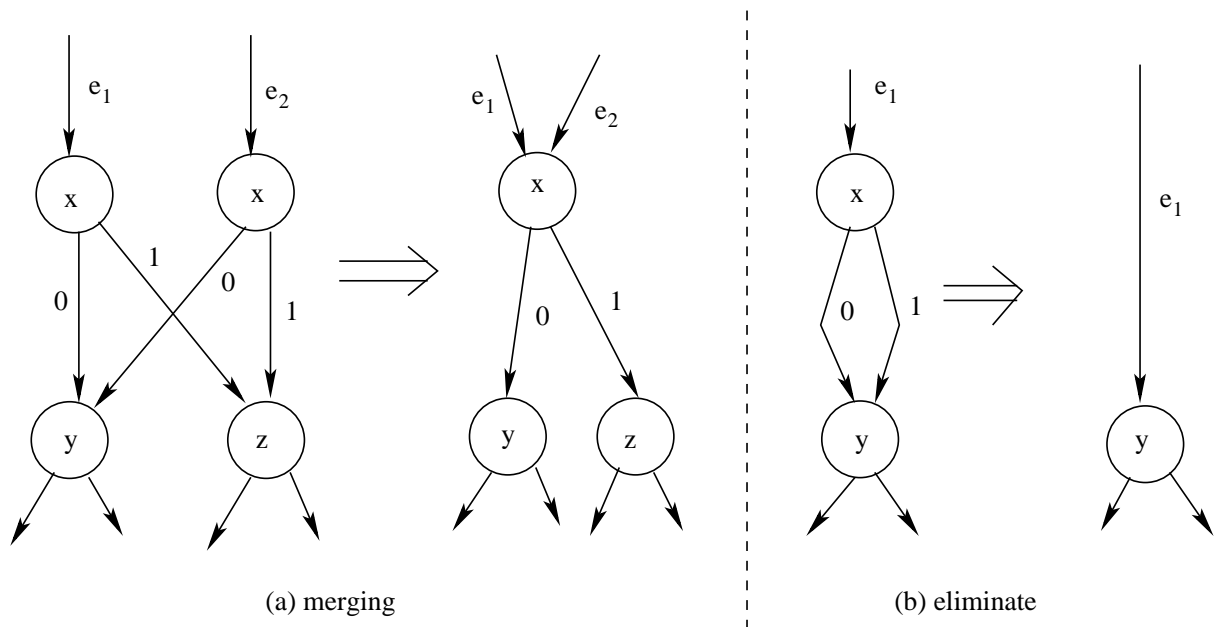


Figure 2.11: BDD for Boolean function  $f = xy' + yz$



(a) merging

(b) eliminate

Figure 2.12: Reduction rules:(a) merging, (b) eliminate

## 2.4 Complexity of generation of exhaustive set of test patterns for OLT

---

are redirected to the other retained node.

- b) Eliminate a non-terminal node: If both the outgoing edges of a node (non-terminal) point to the same child, then the parent node is eliminated and all of its incoming edges are redirected to the child. Such a node is called a redundant node.

Figure 2.12 represents the two reduction rules. Left side of the figure shows merging of two isomorphic subgraphs and right hand side of the figure shows elimination of a redundant node. We cannot apply any reduction rules to the BDD shown in Figure 2.11. Thus, this BDD is an ROBDD representing the function  $f = xy' + yz$ . The size of an ROBDD depends on the variable ordering. If the chosen variable ordering is a good one, then we get a compact representation for the given function, otherwise, the number of states in the ROBDD is large. Finding the optimal variable ordering of an ROBDD is a computationally expensive problem, but there exist several heuristics which usually generate a fairly good variable ordering [5, 41, 52].

ROBDDs provide compact and canonical representation of Boolean functions and support all the Boolean operations. The operations involve checking equivalence of Boolean functions, validity of a Boolean function, satisfiability of a Boolean function, absence of redundant variables in a Boolean function, etc. [51]. For this reason, ROBDDs have several applications in the area of design, verification and testing of digital circuits.

- *Equivalence of Boolean functions:* Instead of converting the functions to be compared into Sum of Product (SoP), Product of Sum (PoS), truth table or binary decision trees, we can construct ROBDDs using a common variable ordering. If the ROBDDs obtained are the same then the functions are equivalent.
- *Validity of Boolean function:* A Boolean function is valid if it returns TRUE for all possible variable assignments. This can be tested by noticing occurrence of terminal node 0 in the ROBDD. If there is no terminal node corresponding to 0 in the ROBDD then the function is valid, else not.
- *Satisfiability of Boolean function:* A Boolean function is satisfiable if it returns TRUE for some variable assignment. This can be tested by noticing occurrence of terminal node 1 in the ROBDD. If there is a terminal node corresponding to 1 in the ROBDD then function is satisfiable, else not.
- *Absence of Redundant Variable in a Boolean function:* In case there is a redundant variable in the function, it can be found out by constructing ROBDD of the function.

If the diagram does not have any occurrence of a particular variable, then the variable is redundant to the function.

### Structurally Synthesized Binary Decision Diagrams (SSBDDs)

SSBDDs are another special class of BDDs which are developed to represent structural aspects of digital circuits [95, 96]. SSBDDs are constructed directly from the the gate level topology of the circuits. SSBDDs were first introduced in [121, 122] as structural alternative graphs and became an efficient mathematical model to represent digital circuits. This model has several features in circuit modeling, simulation and test [54]. Firstly, the size of the SSBDD model is linear with respect to the circuit, while size of the ROBDD can be of exponential. Secondly, the SSBDD model retains circuit's structural property while other BDD models do not have such features. Finally, it also reduces the model complexity since the algorithms running on the SSBDD model treat different gates equivalently. Due to these advantages, the SSBDD model has been used in various CAD applications, such as fast generation of test patterns [121, 122], diagnosis of design errors in combinational circuits [55] and designing efficient algorithms for timing and fault simulation [123], etc.

Next we discuss how a SSBDD is generated directly from the gate level description of a digital circuit. First the circuit is partitioned into fanout free sub-circuits and each of them are modeled by different SSBDDs. Figure 2.13 shows a combinational circuit and it's SSBDD representation. The SSBDD represents the output of the circuit  $y = abc_1 + c_2d'$ , where  $a$ ,  $b$  and  $d$  are the input variables and  $c_1$  and  $c_2$  are the fanout branches of input  $c$  in the circuit. The SSBDD is a procedure of calculating the value of the output variable (here  $y$ ) for a given values of the node variables. This is performed by traversing the corresponding path in the SSBDD. If the value of a node variable is 1 (0) then the direction of the path is always towards the right (down) from the node. There are two terminal nodes in SSBDD which are labeled by Boolean constants 0 and 1. The terminal nodes are not shown in this figure and it is assumed that if there is no edge that goes down (right) from a node then terminal node 0 (1) is reached. The value of output variable  $y$  will be determined by the constant in the terminal node where the procedure stops. In this example, an input pattern 1110( $a, b, c, d$ ) is simulated and the path is traced through the node variables  $a$ ,  $b$  and  $c_1$  and stops at node variable  $c_1$ , which can be found in Figure 2.13(b). The path is stopped at node variable  $c_1$  because the value of variable  $c$  is 1 and there is no edge towards right from node variable  $c_1$ . Thus, this input pattern produces the value of  $y = 1$ . Similarly, for the input pattern 1001( $a, b, c, d$ ) the path is traversed through the node variables  $a$ ,  $b$ ,  $c_2$  and  $d'$ , and stops at node variable  $d'$ . At node variable  $c_2$ , the path is traced towards right for

## 2.4 Complexity of generation of exhaustive set of test patterns for OLT

the value of variable  $c = 0$  because this node contains complement of variable  $c$ . Finally, the path stops at node variable  $d'$  since no edge goes down from this node for the value of variable  $d = 1$ . Thus, the pattern results output  $y = 0$ .

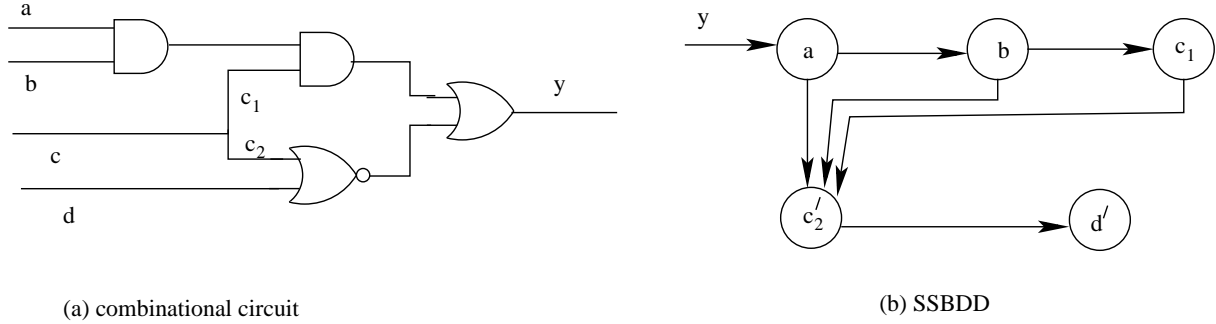


Figure 2.13: Combinational circuit and its SSBDD representation

### High Level Decision Diagrams

BDDs and SSBDDs are good in representing digital systems at logic gate level but, in case of complex systems, we often need to describe the systems at high levels, like behavioral, procedural or RTL. For this purpose High Level Decision Diagrams (HLDDs) were introduced to represent such systems at higher description levels [122,124]. Since the last decade, HLDDs have been used for high level and hierarchical test generation for complex digital circuits [91–93]. The main advantage of using HLDDs is to generalize and extend the gate level methods and algorithms of fault simulation and test generation to higher abstraction levels [96]. For this reason, the variables in the form of Boolean values are extended to Boolean vectors or integers and the Boolean functions are extended to data manipulation operations. HLDDs have also proven to be an efficient model for fault simulation and test generation at RTL as both data and control parts are handled in an uniform manner [92, 93]. When representing a digital circuit at higher level (say RTL) by HLDD model, in general case, a network of DDs rather than a single DD is required. Next, we discuss the representation of RTL circuits using HLDD model.

#### HLDD representation for RTL circuit

At RTL a circuit description is partitioned into two parts—data path and control part. The data path is viewed as an interconnection of modules, where there are different functional units, registers, multiplexers, etc. The control part of the circuit is viewed as an FSM and both the data path and the control part can be represented by different HLDDs.

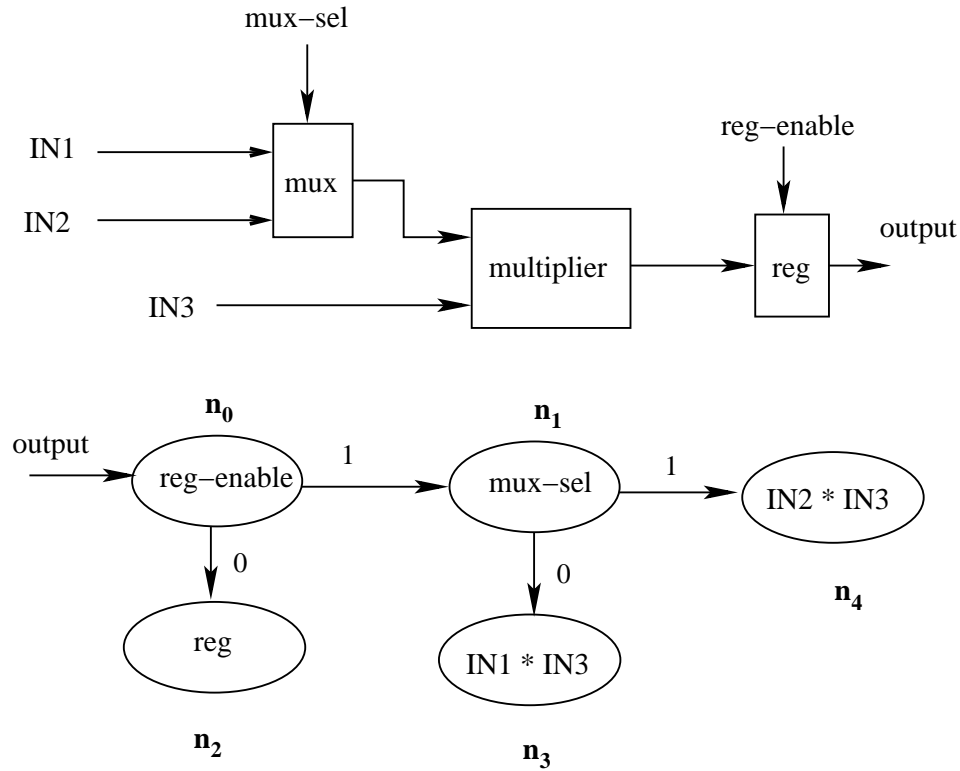


Figure 2.14: HLDD representation of a data path segment of an RTL circuit

The upper portion of Figure 2.14 shows an example of a data path of an RTL circuit. The circuit performs multiplication of two input numbers among three numbers and stores the product in the register (*reg*) and finally outputs the product. The first input i.e., *IN3* is directly applied to the multiplier whereas, the second input between *IN1* and *IN2* is selected by the multiplexer (*mux*). When the multiplexer selection line, i.e., *mux-sel* is 0(1), then *IN1*(*IN2*) is selected by the multiplexer and applied to the multiplier. The multiplication is performed (either  $IN1 * IN3$  or  $IN2 * IN3$ ) and the product is stored in the register when the register enable signal, i.e., *reg-enable* is high. The lower portion of Figure 2.14 shows the HLDD representation of the data path. The initial node  $n_0$  of the HLDD represents the *reg* and is associated with the expression *reg-enable*, i.e., enable signal of *reg*. Similarly, node  $n_1$  represents the *mux* and is associated with the expression *mux-sel*, i.e., selection line of *mux*. The content of the register remains unchanged as long as  $reg-enable=0$ ; this is modeled at terminal node  $n_2$ , labeled by constant assignment operation, which assigns the previous value of the register as output. Similarly, two multiplication operations  $IN1 * IN3$  and  $IN2 * IN3$  are carried out at the terminal nodes  $n_3$  and  $n_4$ , respectively. Thus, in the data path HLDD model, the non-terminal nodes are labeled by some control or selection expressions and the terminal nodes are labeled by some operations.

## 2.4 Complexity of generation of exhaustive set of test patterns for OLT

Present state	Control inputs (cin1, cin2)	Next state	Control outputs
• S2	• (1 0)	• S3	• (1 0 1 0)
S2	(1 1)	S4	(1 1 1 1)
• •	• •	• •	• •

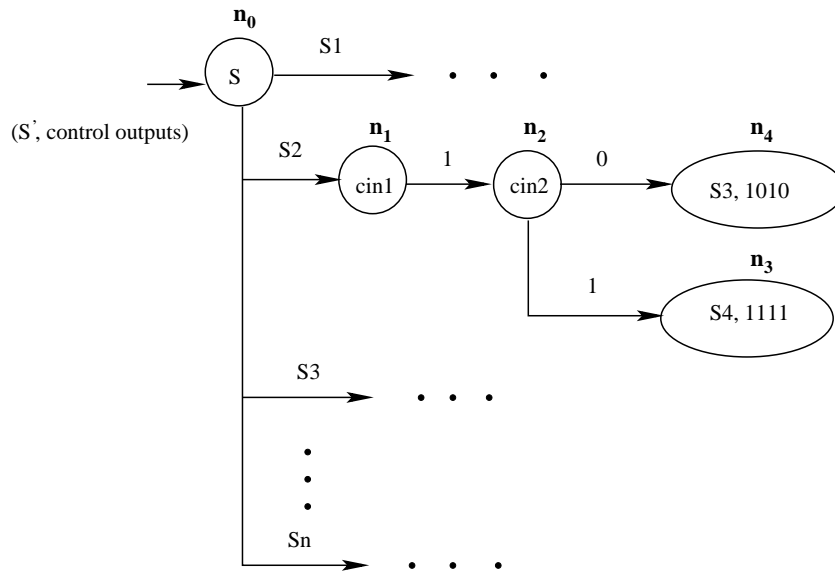


Figure 2.15: Decision Diagram representation of a control part segment when current state is  $S2$

In similar way, the control part of an RTL circuit is represented using another HLDD model. The upper part of Figure 2.15 shows an example of a portion of the control part of an RTL circuit in form of FSM state table and its the corresponding HLDD representation is shown in lower part of the figure. In the control HLDD model, the non-terminal nodes correspond to the current *state status* and FSM *input control signals (conditions)* whereas, terminal nodes hold a vector which includes *values of next state* along with the values of FSM *output control signals*. Here, the FSM state table shows behavior of the circuit when the present state is  $S2$ . The initial node  $n_0$  in the HLDD model represents present state and is associated with current state status  $S$ . The non-terminal nodes  $n_1$  and  $n_2$  represent FSM inputs and are associated with control signals  $cin1$  and  $cin2$ , respectively. The terminal nodes  $n_3$  and  $n_4$  represent next state and FSM outputs when the values of  $\langle cin1\ cin2 \rangle$  is 10 and 11, respectively.

### 2.4.2 Testing of digital circuits using Decision Diagrams

In last subsection, we have discussed different types of DDs and their uses for representation of digital circuits. Among them Ordered Binary Decision Diagram (OBDD) has been used as an efficient data structure for OLT of digital circuits at gate level [9,12,13]. The OLT schemes reported in papers [9,12,13] directly generate test patterns from the OBDD representation of the circuit and design on-line tester circuit using these test patterns. Each output of the circuit is represented using separate OBDDs under normal and faulty conditions (say  $OBDD_{normal}$  and  $OBDD_{faulty}$ ). Then logical XOR operation is performed between  $OBDD_{normal}$  and  $OBDD_{faulty}$  and resulting XORed OBDD (say  $OBDD_{xor}$ ) is constructed. Finally, test patterns are generated by applying “satisfy-all-1” operation on the  $OBDD_{xor}$ . For example, let  $f_N(a, b, c) = ab' + a'b + a'c$  be an output function of a circuit under normal condition and  $f_F(a, b, c) = a'c + ab'c$  be the output function under faulty condition. The OBDD representation of  $f_N$  is shown in Figure 2.16 and OBDD representation of  $f_F$  is shown in Figure 2.17. The XOR operation is performed between normal and faulty OBDDs and resulting XOR-OBDD is shown in Figure 2.18. The test patterns to detect that fault can be generated by applying the “satisfy-all-1” operation on the  $OBDD_{xor}$ . Here, the test patterns ( $\langle a, b, c \rangle$ ) are  $\langle 1, 0, 0 \rangle$  and  $\langle 0, 1, 0 \rangle$ . The feasibility of the test patterns can be verified by applying them on the normal and faulty OBDDs; for both the test patterns, in case  $OBDD_{normal}$  ( $OBDD_{faulty}$ ) they generate output as 1 (0). Thus, the obtained test patterns are valid and can successfully detect the fault. Once all test patterns for all possible faults of the CUT are generated using the XOR-OBDD procedure, then the on-line tester circuit is designed using these test patterns. The on-line tester executes concurrently with the CUT and detects the occurrence of faults during normal operation.

The OLT schemes reported in [9,12,13] use OBDD in a straight forward manner for generation of test patterns for the circuits modeled at gate level. However, this procedure of generation of test patterns using XOR of OBDDs cannot be directly applied for addressing the challenges of OLT discussed in Section 2.3.

- **Measurement limitation:** When some lines of the CUT are not tapped (under measurement limitation) by the on-line tester then generation of test patterns using OBDDs is not a straight forward procedure. This is because the test patterns generated using the above procedure under full measurement case (tapping all lines of the CUT) may not remain so under a given measurement limitation. Thus, test pattern generation under measurement limitation cannot be directly performed using the above XOR-OBDD based scheme.

2.4 Complexity of generation of exhaustive set of test patterns for OLT

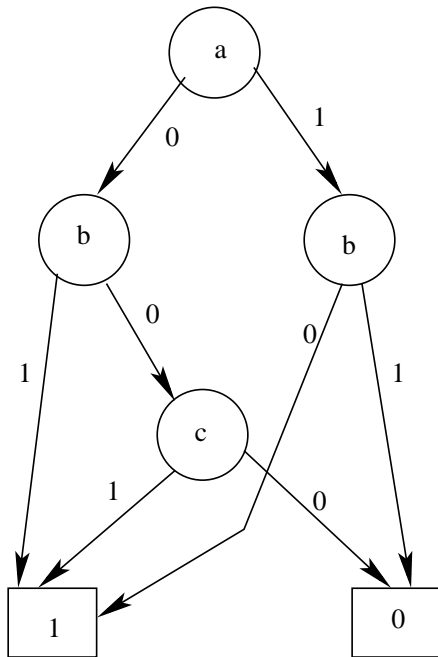


Figure 2.16:  $OBDD_{normal}$ : representing  $f_N(a,b,c) = ab' + a'b + a'c$

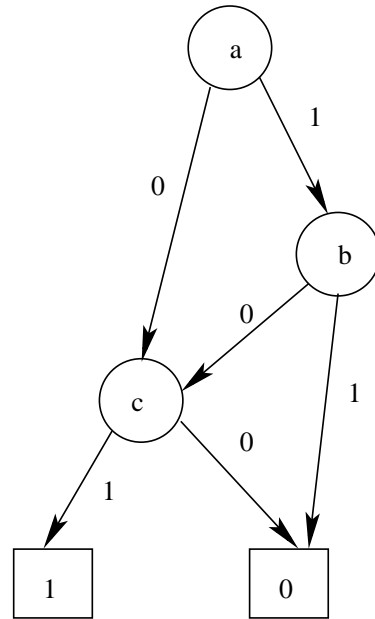


Figure 2.17:  $OBDD_{faulty}$ : representing  $f_F(a,b,c) = a'c + ab'c$

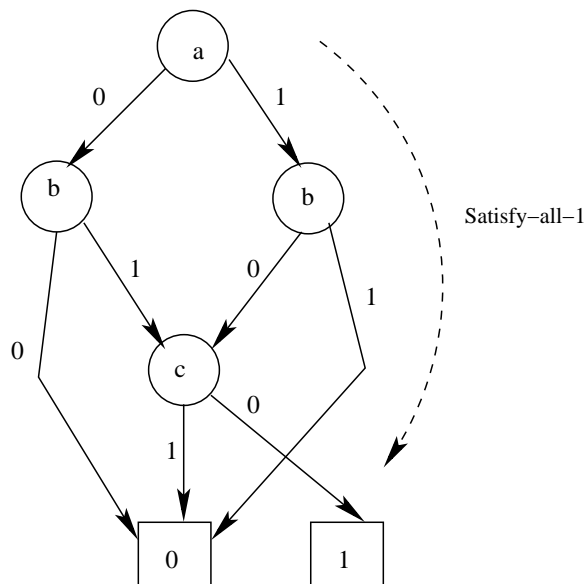


Figure 2.18:  $OBDD_{xor}$ : representing  $OBDD_{normal} \text{ XOR } OBDD_{faulty}$

- **Feedback bridging fault:** The simple XOR based procedure of generation of test patterns using OBDDs may not be a direct approach for feedback bridging faults because in some cases they create oscillations.
- **Scalability:** In case of OLT scheme at higher description level like behavioral level, register transfer level, etc., the procedure of generation of test patterns using OBDDs cannot be applied because OBDDs model the circuits at the gate level.
- **OLT for asynchronous circuits:** OBDDs have not yet been applied for OLT of asynchronous circuits. So a study is required to find whether the XOR-OBDD procedure is applicable to OLT of asynchronous circuits.

## 2.5 Conclusion

In this chapter we have discussed different types of OLT techniques for digital VLSI circuits along with their pros and cons. It is seen that partial replication technique is widely used compared to other techniques because of the advantages like non-intrusiveness, simplicity, flexibility, etc. However, there are some shortfalls in this technique which are addressed in the thesis; these are—(i) measurement limitation based flexibility, (ii) coverage for feedback bridging faults, (iii) improvement in scalability and (iv) handling asynchronous circuits. Also, different types of decision diagrams and their application in modeling and testing of digital circuits have been discussed in this chapter. It is seen that OBDD is used in a straight forward manner for generation of test patterns for OLT of circuits at gate level. However, such a procedure of generation of test patterns using OBDDs cannot be directly applied to the problems in case of measurement limitation, feedback bridging faults, circuits modeled at higher level of abstractions and asynchronous circuits. So several extensions are required to the XOR-OBDD procedure to address these problems.

In the next chapter we will address our first problem, i.e., designing a flexible OLT scheme with the concept of measurement limitation using OBDD.



# Chapter 3

## On-line Testing with Measurement Limitation

### 3.1 Introduction

On-line Testing (OLT) is performed when the circuit is in operational mode. It basically involves continuous monitoring of the circuit and detecting the occurrence of a fault within a finite time of its occurrence. Broadly speaking, there are four primary parameters that are considered in design of an on-line tester—i) fault coverage, ii) fault detection latency, iii) area overhead and iv) power overhead (Chapter 2, Subsection 2.1.4). The area and power overheads of the on-line testers are high because they are designed using the exhaustive set of test patterns for each fault of the circuit. If some faults and test patterns are dropped then area and power overheads reduce, however, at the cost of fault coverage and detection latency. Thus, one of the main requirements of OLT is to provide flexibility in the on-line tester circuitry design. The OLT schemes reported in the literature [9, 12, 13] provide flexibility in terms of trade-offs between area overhead of the tester versus fault coverage and detection latency. These schemes have lowered the area overhead by considering a subset of test patterns for design of the on-line tester circuit. However, the subset of test patterns is selected in a fashion such that for all faults, at least one test pattern is present. Experimental results in [9, 12, 13] have illustrated that very high fault coverage can be achieved even with low area overheads. It is also shown that the impact of lowering the test patterns is almost linear with the detection latency.

The on-line tester circuitry executes concurrently with the Circuit Under Test (CUT) and needs to tap certain lines of the CUT. As the on-line tester is fabricated on the same chip with the CUT, any point of the CUT can be easily tapped. This enables easy measurement

### 3.1 Introduction

---

of any required digital parameter of the CUT by the tester. So, most of the works on OLT [9, 12, 13] (Chapter 2, Section 2.3) have ignored the issue of tap points or measurement limitation. It may be noted that measurement limitation reduces load (fan-outs) on the gates of the CUT which drive the tap points. This in turn reduces the number of additional buffers required for driving the tester by the CUT, thereby decreasing the area overhead of the tester. However, minimization of tap points also compromise fault coverage and detection latency. This is because some of the test patterns generated for the full measurement case no longer retain their capability to detect faults under measurement limitation. Therefore, “number of tap points” can be used as a parameter to trade-off area overhead versus fault coverage and detection latency.

In this chapter, we aim at developing a partial replication based OLT scheme for digital circuits with measurement limitation. We also study the effect of minimizing tap points on fault coverage, detection latency and area overhead, from the OLT perspective. The scheme starts with generation of test patterns, called Fault Detecting transitions (*FD*-transitions), for each fault of the circuit under full measurement. Following that, the *FD*-transitions that remain so under a given measurement limitation are determined. Finally, on-line tester, called Fault versus Normal condition detector (*FN*-detector), is designed using these *FD*-transitions. The procedure of generation of *FD*-transitions and determination of *FD*-transitions under measurement limitation are implemented using Ordered Binary Decision Diagrams (OBDDs). Experimental results on ISCAS 89 benchmarks have been presented, which illustrate that measurement limitation can be used as a trade-off parameter to minimize area overhead to a great extent with minimal compromise in fault coverage and detection latency. It is also found that for a given detection latency and coverage, area overhead of the proposed scheme is lower compared to other similar schemes reported in the literature.

This chapter is organized as follows. In Section 3.2 we discuss circuit modeling using Finite State Automata (FSA) framework and *FN*-detector construction under measurement limitation. Section 3.3 illustrates use of Ordered Binary Decision Diagrams (OBDDs) to generate *FD*-transitions efficiently for construction of the *FN*-detector, which makes the approach scalable. Section 3.4 presents experiential results regarding area overhead, fault coverage and detection latency versus measurement limitation of the *FN*-detector. Finally we conclude in Section 3.5.

## 3.2 FSA framework under measurement limitation: Circuit modeling and $FN$ -detector design

In this section, we model a digital sequential circuit having a single clock using the FSA framework. Figure 3.1 illustrates the basic block diagram of a sequential circuit with the on-line tester. First we consider the Next State Function (NSF) block and Flip-Flops (FFs) for OLT. The mechanism can be easily extended for the Output Function (OF) block, which is a combinational circuit; this will be illustrated in Subsection 3.3.3. In other words, first only the two sub-parts of the circuit, i.e., NSF block and the FFs are considered as the CUT. Later we will demonstrate how the scheme is applied for the OF block of the circuit.

A sequential circuit without the OF block is modeled as FSA  $G = \langle V, X, X_0, \Sigma, \mathfrak{S} \rangle$ , where  $V = \{v_1, v_2, \dots, v_n\}$  is a finite set of Boolean variables,  $X$  is a finite set of  $G$ -states (also called set of states),  $X_0 \subseteq X$  is the set of initial states,  $\Sigma$  is a finite set of input symbols and  $\mathfrak{S}$  is a finite set of transitions. The set  $V$  of variables can be partitioned into two subsets, namely (i)  $S = \{v_1, v_2, \dots, v_k\}$  representing the state variables and (ii)  $I = \{v_{k+1}, v_{k+2}, \dots, v_n\}$  representing the input variables. A  $G$ -state or state  $x \in X$  is a mapping  $x : S \rightarrow \{0, 1\}$ . Similarly, any input symbol  $\sigma \in \Sigma$  is a mapping  $\sigma : I \rightarrow \{0, 1\}$ . Thus, a state is represented by a binary  $k$ -tuple, where  $k = \lceil \log_2 |X| \rceil$ . Similarly, any input symbol can be represented as a binary  $i$ -tuple, where  $i = n - k$  and  $|\Sigma| = 2^{n-k}$ .

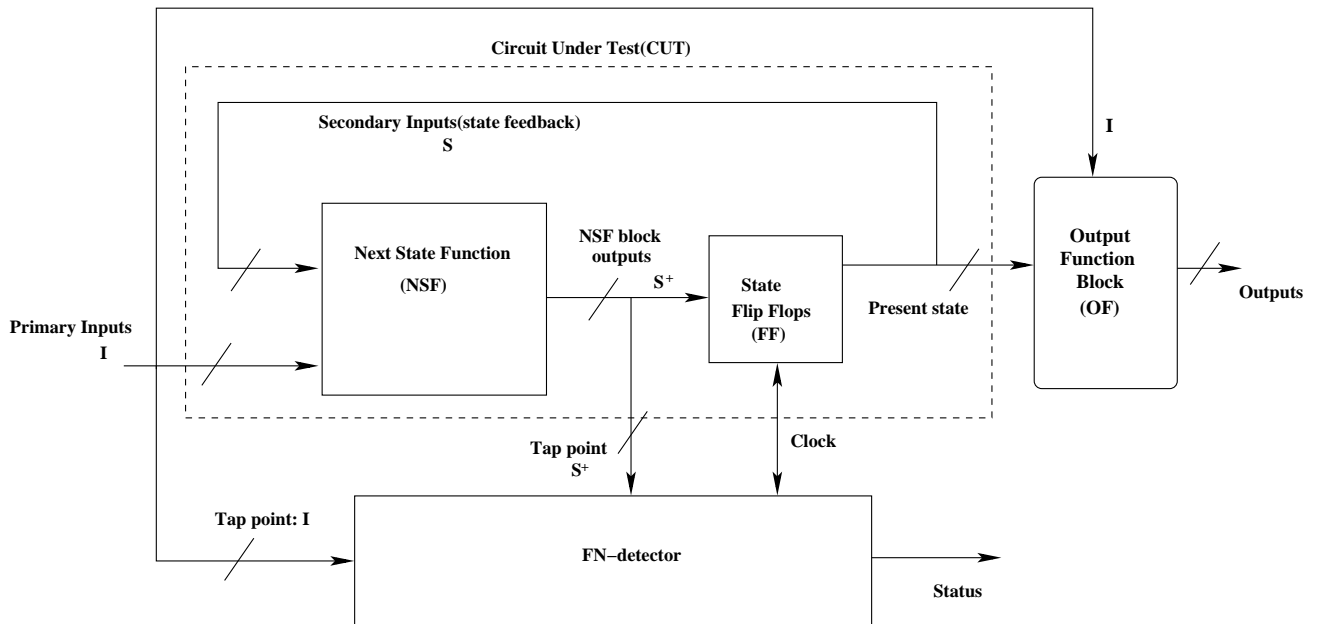


Figure 3.1: Basic architecture of a sequential circuit with on-line tester ( $FN$ -detector)

### 3.2 FSA framework under measurement limitation: Circuit modeling and $FN$ -detector design

---

All input and state variables are not measurable. Let  $I_m \subset I$  and  $S_m \subset S$  be the subsets of measurable input and state variables, respectively. The unmeasurable state (input) variables correspond to register-outputs (primary input lines) which are not tapped by the on-line tester. The measurable input alphabet  $\Sigma_m = \{\sigma|_{I_m} \text{ such that } \sigma \in \Sigma\}$  and the measurable set of states  $X_m = \{x|_{S_m} \text{ such that } x \in X\}$ <sup>1</sup>.

A *transition*  $\tau \in \mathfrak{S}$  from a state  $x$  to another state  $x^+$  is an ordered three-tuple  $\tau = \langle x, \sigma, x^+ \rangle$  where,  $x$  (*initial*( $\tau$ )) is the initial state of the transition,  $x^+$  (*final*( $\tau$ )) is the final state of the transition and  $\sigma \in \Sigma$  (*input*( $\tau$ )) is the input symbol of the transition.

#### 3.2.1 Circuit modeling under single stuck-at fault

Single stuck-at (s-a) faults are represented in the FSA model of a circuit using the following steps:

- The variable set  $V$  is extended to include a subset  $C$  of  $l = \lceil \log_2(p+1) \rceil$  *status variables*. Thus,  $V = S \cup I \cup C$ , where  $S$  and  $I$  are the sets of state and input variables respectively, as given before, and  $p$  is the number of possible faults in the circuit.
- The state mappings are extended so that each becomes a mapping from  $S \cup C$  to  $\{0, 1\}$ .  $\bigcup_{x \in X} x(C) = \{N, F_1, F_2, \dots, F_p\}$ , where  $N$  stands for normal status and  $F_i$ ,  $1 \leq i \leq p$ , stands for the  $i^{\text{th}}$  fault status. The image  $x(C)$  of  $C$  under  $x$  is called the fault label of the state  $x$ .

The set of status variables are unmeasurable. The FSA model of a circuit (capturing both normal and fault status) can be conveniently conceived as a collection of sub-machines, one for the normal condition and one each for the faults  $F_1, F_2, \dots, F_p$ . The onset of a fault  $F_i$  is captured by a transition from a state  $x_1$  with  $x_1(C) = N$  to a state  $x_2$  with  $x_2(C) = F_i$ ; such transitions are termed as  $s_i$ -transitions (for the start of fault  $F_i$ ) and are represented as  $s_i = \langle x_1, T, x_2 \rangle$ , where  $x_1(C) = N$ ,  $x_2(C) = F_i$  and “ $T$ ” stands for “always true”. Due to the occurrence of an  $s_i$ -transition, only the status variable changes its value from  $N$  to  $F_i$  and all other state variables remain unchanged. Thus,  $s_i$ -transitions are unmeasurable. These transitions need not occur at the triggering edges of the clock, i.e., they are asynchronous. Their enabling conditions do not depend on any input variable combinations as they are always true.

We use a flat indexing like  $x_1, x_2, \dots, x_l$  when no differentiation needs to be made among

---

<sup>1</sup> $x|_{S_m}$  is the restriction of values  $x$  to set  $S_m$ . For example, if  $x = \langle v_1 v_2 v_3 \rangle = \langle 110 \rangle$  and  $S_m = \{v_1, v_2\}$ , then  $x|_{S_m}$  returns  $\langle 11 \rangle$ .

the sub-machines (normal or faulty). When we need to make a distinction between normal and faulty sub-machines, the states for the normal sub-machine are designated as  $x_{0j}$ ,  $1 \leq j$ , and those of the  $F_i$ -sub-machine are designated as  $x_{ij}$ ,  $1 \leq j$ ; likewise for the transitions.

**Definition 3.1. *N*-state:** A *G*-state is called normal (i.e., *N*-state), denoted as  $x_{0j}$ ,  $1 \leq j$ , if  $x_{0j}(C) = N$ . The set of all normal states is denoted as  $X_N$ .

**Definition 3.2.  $F_i$ -state:** A *G*-state is called an  $F_i$ -state, denoted as  $x_{ij}$ ,  $1 \leq j$ , if  $x_{ij}(C) = F_i$ . The set of all  $F_i$  states is denoted as  $X_{F_i}$ .

**Definition 3.3. Normal *G*-transition and Faulty *G*-transition:** A *G*-transition  $\langle x, \sigma, x^+ \rangle$  is called a Normal (Faulty  $F_i$ ) *G*-transition if  $x, x^+ \in X_N (X_{F_i})$ .

Since faults are assumed to be *permanent*, there is no transition from any  $X_{F_i}$  state to any  $X_N$  state.

**Definition 3.4. Measurement equivalent states:** Two states  $x_1$  and  $x_2$  are measurement equivalent, denoted as  $x_1 E x_2$ , if  $x_1|_{S_m} = x_2|_{S_m}$ .

**Definition 3.5. Measurement equivalent transitions:** Two transitions  $\tau_1 = \langle x_1, \sigma_1, x_1^+ \rangle$  and  $\tau_2 = \langle x_2, \sigma_2, x_2^+ \rangle$  are measurement equivalent, denoted as  $\tau_1 E \tau_2$ , if  $x_1|_{S_m} = x_2|_{S_m}$ ,  $x_1^+|_{S_m} = x_2^+|_{S_m}$  and  $\sigma_1|_{I_m} = \sigma_2|_{I_m}$ .

In other words, two transitions are measurement equivalent if their source states are measurement equivalent, destination states are measurement equivalent and so are the inputs.

Throughout this chapter the simple example circuit given in Figure 3.2 is used to illustrate the theory. A single s-a-1 fault  $F_1$  is assumed at the fanout branch marked *A* in Figure 3.2. Figure 3.3 shows the FSA model for the circuit corresponding to the normal and faulty behaviour.

### 3.2.2 *FN*-detector design for FSA model of a circuit

Let us first consider the circuit of Figure 3.2 under the case of full measurement i.e.,  $S_m = S$  and  $I_m = I$ . If we compare the transitions under normal condition with the corresponding ones after the s-a-1 fault in the FSA model given in Figure 3.3, it is seen that there is one transition namely,  $\langle x_{11}, 1, x_{13} \rangle : \tau_{16}$ , that implies a change in the circuit behaviour after the fault. This is because, for transition  $\langle x_{11}, 1, x_{13} \rangle : \tau_{16}$  the corresponding transition in normal condition is  $\langle x_{01}, 1, x_{02} \rangle : \tau_{06}$ , where  $x_{01}|_{S_m} = x_{11}|_{S_m} = 10$ ,  $\sigma_{06} = \sigma_{16} = 1$  but  $x_{02}|_{S_m} = 00 \neq x_{13}|_{S_m} = 01$ . All other  $F_1$ -transitions have an equivalent *N*-transition, e.g.,

### 3.2 FSA framework under measurement limitation: Circuit modeling and $FN$ -detector design

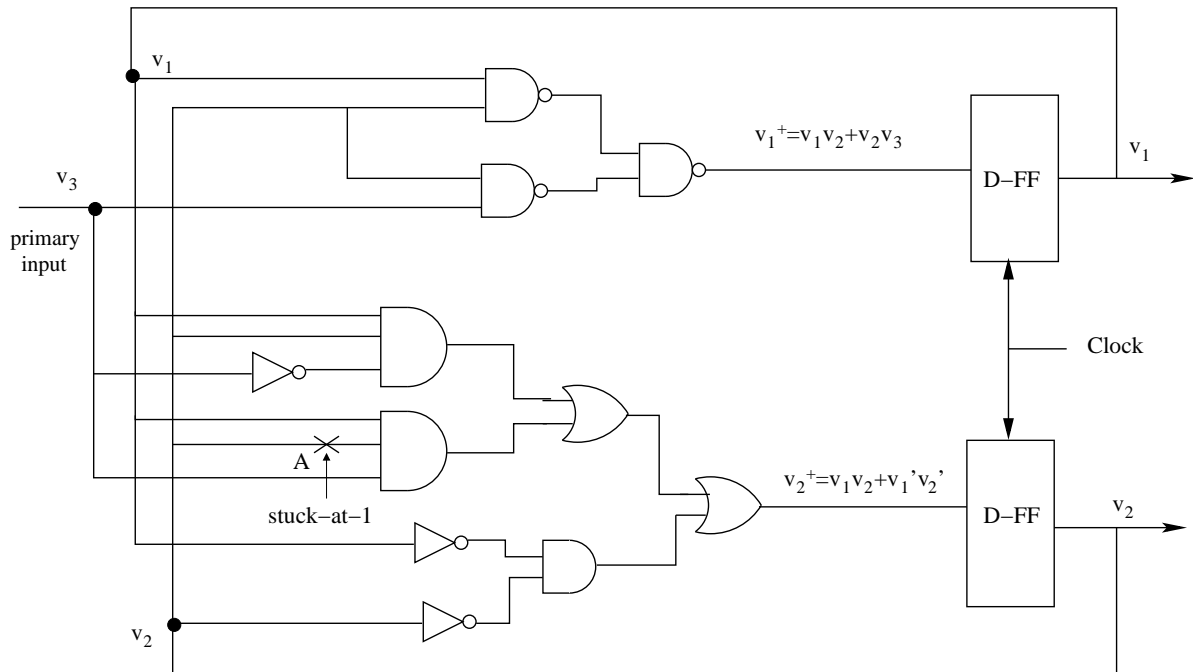


Figure 3.2: A simple sequential circuit with a s-a-1 fault

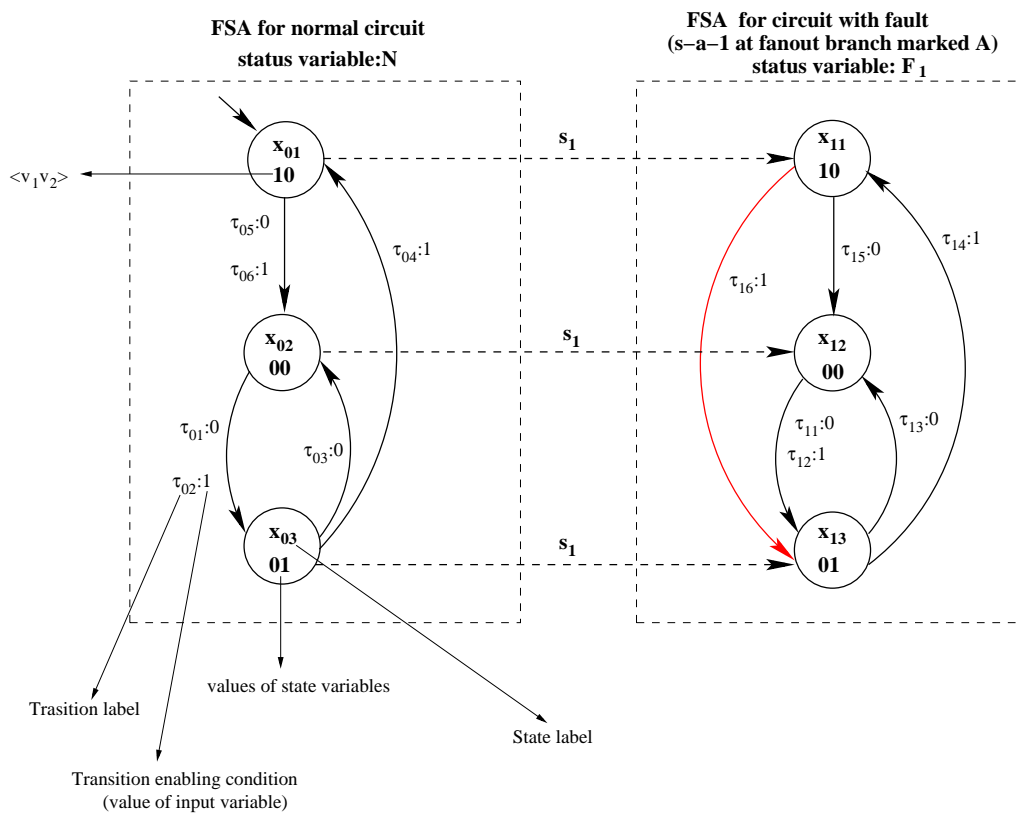


Figure 3.3: FSA model for the circuit of Figure 3.2

$\tau_{01}E\tau_{11}$  ; so they cannot detect the fault. Hence, a Finite State Machine (FSM) can be designed to determine if the following takes place. The CUT is in state  $x_{01}$  or in  $x_{11}$  (i.e., measured state variables are 10) and after that at input 1 the next state is  $x_{13}$  (i.e., the measured state variables in the next clock period become 01); this indicates the s-a-1 fault. We term this machine as an *FN*-detector (Fault versus Normal condition detector) and the transition(s), that detect the faults, as *FD*-transitions (Fault Detecting transitions).

From the above observation, it appears that the *FN*-detector needs to monitor both the NSF block outputs and the state flip-flop outputs. In case of the CUT of Figure 3.2, the *FN*-detector may measure  $v_1, v_2$  along with the NSF block outputs  $v_1^+, v_2^+$  and the input  $v_3$ . If the input vector  $\langle v_1, v_2, v_3, v_1^+, v_2^+ \rangle = \langle 10101 \rangle$ , then the *FN*-detector can move to a fault indicating state; else, on encountering  $\langle 10100 \rangle$  (or any other *don't care* pattern), it can loop back to the same state.

Since the number of state variables in a typical VLSI circuit is quite high, the number of inputs to the *FN*-detector circuit should be restricted. In this work, we are able to do so by allowing the the *FN*-detector to monitor only the NSF outputs and detect an *FD*-transition in two steps (in two consecutive clock cycles). The *FN*-detector, in the first clock cycle, verifies whether the CUT is going to be in the initial state of the *FD*-transition. If it has happened, then the detector, in the next clock cycle, examines if the primary input and the NSF block output match, respectively, the input and the final state of the *FD*-transition. Obviously, both these steps can be performed by measuring only the NSF block outputs. It is to be observed that the technique still allows the *FN*-detector to move in step with the CUT, i.e., both the *FN*-detector and the CUT can be driven by the same clock edge. The basic schematic of the *FN*-detector vis-a-vis the CUT is shown in Figure 3.1. The process of *FN*-detector construction from *FD*-transition is first demonstrated for the CUT of Figure 3.2 and then we give a generalized treatment.

The state transition diagram of the *FN*-detector of the FSA model of the CUT, shown in Figure 3.3, is given in Figure 3.4. This *FN*-detector detects the *FD*-transition  $\langle x_{11}, 1, x_{13} \rangle : \tau_{16}$ . The detector starts from  $z_0$  (the initial state). State  $z_1$  is reached by the transition  $t_2$  when the CUT traverses to the state  $x_{11} = \text{inital}(\tau_{16})$ , i.e., the measured NSF block outputs  $v_1^+$  and  $v_2^+$  are 1 and 0, respectively. The value of the input variable  $v_3$  is a don't care ( $d$ ) because the *FN*-detector depends only on the next state of the CUT to reach  $z_1$ . If the CUT moves to a state other than  $x_{11}$ , (or  $x_{01}$ ), then  $t_1$ , the self-loop transition, takes place. So, the *FN*-detector reaches the state  $z_1$  simultaneously with the CUT moving to the state  $x_{11}$  (or  $x_{01}$ ). The transition  $t_3$  from the state  $z_1$  represents the fact that the *FD*-transition  $\tau_{16}$  will occur in the CUT in the next clock edge because the NSF block outputs

### 3.2 FSA framework under measurement limitation: Circuit modeling and $FN$ -detector design

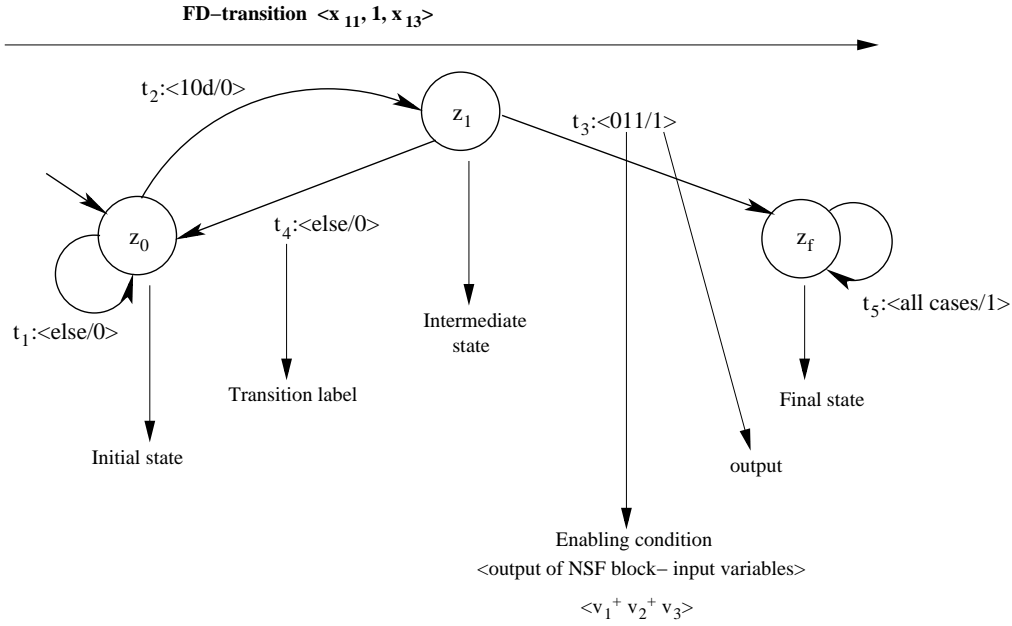


Figure 3.4:  $FN$ -detector for the FSA model of the circuit with a s-a-1 fault (Figure 3.3)

$v_1^+ = 0$  and  $v_2^+ = 1$  and the input variable  $v_3 = 1$ , as given by the 3-tuple  $\langle v_1^+ v_2^+ v_3 \rangle = \langle 011 \rangle$ . Thus, the transition  $t_3$  leads the  $FN$ -detector to the final state  $z_f$  yielding the output 1, indicating that the s-a-1 fault has occurred at the fanout branch marked  $A$ . If such an input-next state combination is not found in the state  $z_1$ , then the  $FN$ -detector traverses back to  $z_0$  by the transition  $t_4$ . If the final state  $z_f$  is reached, the detector always remains in that state since the faults are permanent; the output is 1 indicating fault detection.

Now, we formally define the  $FD$ -transitions and the  $FN$ -detector.

**Definition 3.6.  $FD$ -transition:** An  $F_i$ - $G$ -transition  $\tau_{ik} = \langle x_{ik}, \sigma_{ik}, x_{ik}^+ \rangle$  is an  $FD$ -transition, for fault  $F_i$  (denoted as  $FD_i$ -transition), if there is a normal- $G$ -transition  $\tau_{0l} = \langle x_{0l}, \sigma_{0l}, x_{0l}^+ \rangle$  such that  $x_{0l} E x_{ik}, \sigma_{0l} |_{I_m} = \sigma_{ik} |_{I_m}$  and  $x_{0l}^+ \notin x_{ik}^+$ .

The set of all  $FD_i$ -transitions is denoted as  $\mathfrak{S}_{FD_i}$ . The set of all  $FD$ -transitions for all faults is denoted as  $\mathfrak{S}_{FD}$ . Let  $\mathfrak{S}_{FD_i} = \{\tau_{i1}, \tau_{i2}, \dots, \tau_{il}\}$ , where,  $1 \leq j \leq l$ ,  $\tau_{ij} = \langle x_{ij}, \sigma_{ij}, x_{ij}^+ \rangle$ . The  $FN$ -detector is driven by the same clock edge as the CUT. In general, there are three types of states in any  $FN$ -detector – an initial state  $z_0$ , a set of intermediate states  $z_1, z_2, \dots, z_l$  and a single final state  $z_f$ . The initial state  $z_0$  keeps track of the next  $G$ -state by monitoring the outputs of the NSF block  $v_1^+, v_2^+, \dots, v_k^+$ . The input variables  $v_{k+1}, v_{k+2}, \dots, v_n$  are don't cares for the transitions emanating from  $z_0$ . Whenever the CUT is going to be in any state  $x_{ij} |_{S_m}$ , for some  $\tau_{ij} \in \mathfrak{S}_{FD_i}$ , at the next clock edge, the  $FN$ -detector moves to an intermediate state  $z_k$ . Thus, there is a transition from  $z_0$  to  $z_k$  (for

$\tau_{ij}$ ), labeled with the values of the measurable state variables corresponding to  $x_{ij}|_{S_m}$  (i.e.,  $\text{initial}(\tau_{ij})$ ); the outputs associated with all these transitions from  $z_0$  are 0. In the state  $z_k$ , the *FN*-detector keeps track of those outputs of the NSF block  $v_1^+, v_2^+, \dots, v_k^+$  which are in  $S_m$  and inputs from  $v_{k+1}, v_{k+2}, \dots, v_n$  which are in  $I_m$ . If the input pattern matches with  $\sigma_{ij}|_{I_m}$  (i.e.,  $\text{input}(\tau_{ij})$ ) and the NSF block output pattern matches with  $x_{ij}^+|_{S_m}$  (i.e.,  $\text{final}(\tau_{ij})$ ), then the *FN*-detector moves to the final state  $z_f$  yielding an output 1; else it moves back to  $z_0$ . Thus, there is a transition from  $z_k$  to  $z_f$  (for  $\tau_{ij}$ ), labeled with the values of the measurable state variables corresponding to the state  $x_{ij}^+$  and the measurable values of the input variables corresponding to  $\sigma_{ij}$ . The set of *FN*-detector states, therefore, is given by  $Z = \{z_0, z_1, z_2, \dots, z_l, z_f\}$ , where  $z_1, z_2, \dots, z_l$  correspond to the initial states of the *FD*-transitions. In a similar way *FD*-transitions of all other faults need to be incorporated in the *FN*-detector by associating intermediate states with each transition. It is possible to merge two intermediate states  $z_k$  and  $z_n$  into a single one if the corresponding *FD*-transitions  $\tau_{ij} = \langle x_{ij}, \sigma_{ij}, x_{ij}^+ \rangle$  and  $\tau_{ln} = \langle x_{ln}, \sigma_{ln}, x_{ln}^+ \rangle$  are such that  $x_{ij}|_{S_m} = x_{ln}|_{S_m}$ . Thus, the *FN*-detector is a finite state machine given by the six-tuple,

$$G_{FN} = \langle Z, z_0, \Sigma_Z, \delta_Z, Y_Z, z_f \rangle, \quad (3.1)$$

where  $Z$  is the set of states,  $z_0$  is the initial state,  $\Sigma_Z = X_m \times \Sigma_m$  is the input alphabet,  $\delta_Z$  is the transition function,  $Y_Z$  is the output function and  $z_f$  is the final state. Here,  $\delta_Z : Z \times \Sigma_Z \rightarrow Z$  and  $Y_Z : Z \times \Sigma_Z \rightarrow \{0, 1\}$ . The following steps are used for the construction of the *FN*-detector.

1. Create an initial state  $z_0$  and final state  $z_f$ .
2. For each *FD*-transition  $\tau_{ij}$ , repeat Step 3 and Step 4.
3. Create an intermediate state  $z_k$ . Add a transition  $t_k$  from  $z_0$  to  $z_k$ . Input of  $t_k$  is  $v_1^+, v_2^+, \dots, v_k^+ = \text{initial}(\tau_{ij})$  co-joined with  $v_{k+1}, v_{k+2}, \dots, v_n$ , which are don't cares. Output of  $t_k$  is 0.
4. Add a transition  $t_l$  from  $z_k$  to  $z_f$ . Input of  $t_l$  is  $v_1^+, v_2^+, \dots, v_k^+ = \text{final}(\tau_{ij})$  co-joined with  $v_{k+1}, v_{k+2}, \dots, v_n = \text{input}(\tau_{ij})$ . Output of  $t_l$  is 1.
5. For each pair of intermediate states  $z_k$  and  $z_n$ , merge them into a single state, if the corresponding *FD*-transitions  $\tau_{ij} = \langle x_{ij}, \sigma_{ij}, x_{ij}^+ \rangle$  and  $\tau_{ln} = \langle x_{ln}, \sigma_{ln}, x_{ln}^+ \rangle$  are such that  $x_{ij}|_{S_m} = x_{ln}|_{S_m}$ .
6. From each intermediate state  $z_k$ , add a transition to  $z_0$ . The enabling condition of the transition is any value of  $v_1^+, v_2^+, \dots, v_k^+, v_{k+1}, v_{k+2}, \dots, v_n$  other than the ones

### 3.2 FSA framework under measurement limitation: Circuit modeling and $FN$ -detector design

---

corresponding to enabling conditions of transitions emanating from  $z_k$  and leading to  $z_f$ . The output is 0.

7. Add a self loop in  $z_0$ , whose enabling condition is any value of  $v_1^+, v_2^+, \dots, v_k^+, v_{k+1}, v_{k+2}, \dots, v_n$  other than the ones corresponding to enabling conditions of transitions emanating from the initial state. The output is 0.
8. Add a self loop in  $z_f$ , whose enabling condition is always TRUE (i.e., any value of  $v_1^+, v_2^+, \dots, v_k^+, v_{k+1}, v_{k+2}, \dots, v_n$ ) and output is 1.

#### $FN$ -detector under measurement limitation

Let us now examine the feasibility of an  $FN$ -detector under measurement limitation  $S_m = \{v_2\}$  and  $I_m = \{v_3\}$ , i.e.,  $v_1$  is not tapped. In this case, the transition  $\tau_{16} = \langle x_{11}, 1, x_{13} \rangle$  is an  $FD_1$ -transition because there is a normal- $G$ -transition namely,  $\tau_{06} = \langle x_{01}, 1, x_{02} \rangle$  such that  $x_{01}|_{S_m} = x_{11}|_{S_m} = 0$ ,  $\sigma_{06}|_{I_m} = \sigma_{16}|_{I_m} = 1$  and  $x_{02}|_{S_m} \neq x_{13}|_{S_m}$  because  $x_{02}|_{S_m} = 0$  and  $x_{13}|_{S_m} = 1$ .

Interestingly, however,  $\tau_{16}$  cannot detect the fault  $F_1$  in an  $FN$ -detector as explained below. Suppose we proceed to construct an  $FN$ -detector as follows. Since  $\tau_{16}$  is measured as  $\langle x_{11}|_{S_m}, v_3|_{I_m}, x_{13}|_{S_m} \rangle = \langle v_2, v_3, v_2^+ \rangle = \langle 0, 1, 1 \rangle$ , on detecting  $v_2^+$  to be 0, the  $FN$ -detector would go to an intermediate state. Following that, if the input  $v_3$  is measured to be 1, and  $v_2^+$  is measured as 1, then the final state of the  $FN$ -detector is visited indicating fault  $F_1$ . However, the transition  $\tau_{02} = \langle x_{02}, 1, x_{03} \rangle$  will also be measured as  $\langle 0, 1, 1 \rangle$ ; in other words,  $\tau_{02}$  is measurement equivalent to  $\tau_{16}$ . Thus, under the measurement limitation being considered, the  $FN$ -detector cannot detect the fault. So, we may say that  $\tau_{16}$  no longer remains so under measurement limitation  $S_m = \{v_2\}$  and  $I_m = \{v_3\}$ . Let us now examine the feasibility of an  $FN$ -detector under another measurement limitation  $S_m = \{v_1, v_2\}$  and  $I_m = \{\}$ , i.e., input  $v_3$  is not tapped. In this case, the transition  $\tau_{16} = \langle x_{11}, 1, x_{13} \rangle$  is an  $FD_1$ -transition because there is a normal- $G$ -transition namely,  $\tau_{06} = \langle x_{01}, 1, x_{02} \rangle$  such that  $x_{01}|_{S_m} = x_{11}|_{S_m} = 10$ ,  $\sigma_{06}|_{I_m} = \sigma_{16}|_{I_m} = \phi$  and  $x_{02}|_{S_m} \neq x_{13}|_{S_m}$  because  $x_{02}|_{S_m} = 00$  and  $x_{13}|_{S_m} = 01$ . Interestingly, unlike measurement restriction for  $v_1$ ,  $\tau_{16}$  (measurement restriction for  $v_3$ ) can detect the fault  $F_1$  in an  $FN$ -detector as explained below. Suppose we proceed to construct an  $FN$ -detector as follows. Since  $\tau_{16}$  is measured as  $\langle x_{11}|_{S_m}, v_3|_{I_m}, x_{13}|_{S_m} \rangle = \langle v_1 v_2, \phi, v_1^+ v_2^+ \rangle = \langle 10, \phi, 01 \rangle$ , on detecting  $v_1^+ v_2^+$  to be 10, the  $FN$ -detector would go to an intermediate state. Following that, if  $v_1^+ v_2^+$  is measured as 01, then the final state of the  $FN$ -detector is visited indicating fault  $F_1$ . It may be noted that in the normal sub-machine (Figure 3.3) there is no transition which is measured as  $\langle 10, \phi, 01 \rangle$ , thereby successfully completing the  $FN$ -detector construction. So,

in this case of measurement limitation, the  $FN$ -detector is capable of detecting the fault. In other words, we may say that  $\tau_{16}$  remains an  $FD_1$ -transition under measurement limitation  $S_m = \{v_1, v_2\}$  and  $I_m = \{\}$ .

Thus, it may be concluded that for some measurement limitation, certain  $FD_i$ -transition (under full measurement) becomes non- $FD_i$ -transition. Before we proceed to the next section, we formally define  $FD$ -transition under measurement limitation  $I_m$  and  $S_m$ .

**Definition 3.7.**  *$FD_i$ -transition under  $I_m$  and  $S_m$ :* An  $F_i$ - $G$ -transition  $\tau_{ij} = \langle x_{ij}, \sigma_{ij}, x_{ij}^+ \rangle$  is an  $FD_i$ -transition under  $I_m$  and  $S_m$ , if there is a normal- $G$ -transition  $\tau_{0l} = \langle x_{0l}, \sigma_{0l}, x_{0l}^+ \rangle$  such that  $x_{0l}Ex_{ij}, \sigma_{0l}|_{I_m} = \sigma_{ij}|_{I_m}$  and  $x_{0l}^+ \notin x_{ij}^+$ . Further, there should not be any normal- $G$ -transition  $\tau_{0m} = \langle x_{0m}, \sigma_{0m}, x_{0m}^+ \rangle$  such that  $x_{0m}Ex_{ij}, \sigma_{0m}|_{I_m} = \sigma_{ij}|_{I_m}$  and  $x_{0m}^+Ex_{ij}^+$ . The set of all  $FD_i$ -transitions for fault  $F_i$  under  $I_m$  and  $S_m$  is denoted as  $\mathfrak{S}_{FD_i|I_m, S_m}$ .

The inherent problem of constructing the  $FN$ -detector from the FSA model is that the method becomes prohibitively complex even for simple VLSI circuits because the explicit FSA model of a circuit is exponential in number of flip-flops in the circuit. In the next section, we propose a scheme which is capable of detecting the  $FD$ -transitions (with measurement limitation) directly from the circuit description without the need of the explicit FSA model and, therefore, can be applied to fairly complex circuits.

### 3.3 Efficient construction of $FN$ -detector

The NSF block is a combinational circuit with two types of inputs namely, the primary inputs  $I$  and the secondary inputs  $S$  (which are feedback from the flip-flop outputs). The NSF block outputs, denoted collectively as  $S^+$ , determine the next state. This is illustrated in Figure 3.5.

The NSF block can be described by the tuple  $\mathfrak{S} = \langle \Sigma_S, S^+ \rangle$ , where  $\Sigma_S = X \times \Sigma$  is the alphabet of input symbols (patterns) and  $S^+ = \{v_1^+, v_2^+, \dots, v_k^+\}$  is the set of outputs lines. For each  $v_i^+ \in S^+$ ,  $1 \leq i \leq k$ ,  $v_i^+ : \Sigma_S \rightarrow \{0, 1\}$ . Thus, an NSF output line  $v_i^+$  also designates the switching function realized on this line. An input combination  $\sigma_s \in \Sigma_S$  is a mapping from  $V = \{v_1, v_2, \dots, v_k, \dots, v_n\}$  to  $\{0, 1\}$  represented as an  $n$ -tuple  $\langle \sigma_s(v_1), \sigma_s(v_2), \dots, \sigma_s(v_k), \sigma_s(v_{k+1}), \dots, \sigma_s(v_n) \rangle$ , where the first  $k$  members constitute a  $k$ -tuple of the secondary inputs and the remaining  $(n - k)$  members constitute an  $(n - k)$ -tuple of the primary inputs.

Let  $S_i^+ = \{v_{i1}^+, v_{i2}^+, \dots, v_{ik}^+\}$  denote the output maps represented by the NSF block under fault  $F_i$ ; similarly let  $S_0^+ = \{v_{01}^+, v_{02}^+, \dots, v_{0k}^+\}$  denote the output maps represented by

### 3.3 Efficient construction of $FN$ -detector

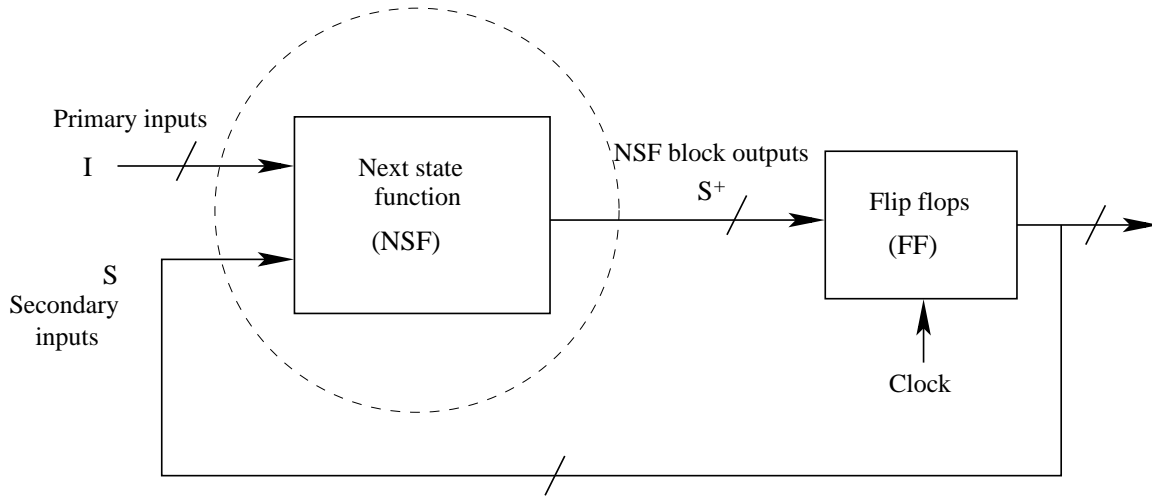


Figure 3.5: Input-output of the NSF block

the NSF block under normal condition. If we speak of the NSF block without the context of faults (i.e., only in the normal condition), then  $S^+ = \{v_1^+, v_2^+, \dots, v_k^+\}$  denotes its outputs. An  $FD_i$ -transition  $\tau_{im} = \langle x_{im}, \sigma_{im}, x_{im}^+ \rangle$  can be determined from the NSF block netlist description in the following manner:

For the given s-a fault  $F_i$ , determine a value of the input combination of the NSF block i.e.,  $\sigma_s \in \Sigma_S$  which sensitizes the fault and propagates the effect through the NSF block in at least one of its outputs, i.e.,  $\exists j, 1 \leq j \leq k, v_{ij}^+(\sigma_s) \neq v_{0j}^+(\sigma_s)$ . As the secondary inputs of the NSF block are the outputs of the state flip-flops, a secondary input pattern denotes the current state from where there is an  $FD$ -transition. Hence, the first  $k$ -tuple of  $\sigma_s = initial(\tau_{im}) = x_{im}$ . Similarly, the second  $(n - k)$ -sub-tuple of  $\sigma_s = input(\tau_{im}) = \sigma_{im}$ . The output of the NSF block (with fault  $F_i$ ) corresponding to the input  $\sigma_s$  gives  $final(\tau_{im}) = x_{im}^+$  as  $\langle v_{i1}^+(\sigma_s), v_{i2}^+(\sigma_s), \dots, v_{ik}^+(\sigma_s) \rangle$ . To determine the set  $\mathfrak{S}_{FD_i}$ , all possible values of  $\sigma_s$  are to be determined such that  $\exists j, 1 \leq j \leq k, v_{ij}^+(\sigma_s) \neq v_{0j}^+(\sigma_s)$ .

Now we study  $FD$ -transitions under measurement limitation. Given  $\mathfrak{S}_{FD_i}$ , subject to measurement limitation  $I_m$  and  $S_m$ , some of the  $FD_i$ -transitions may not remain so. An input combination  $\sigma_s \in \Sigma_S$  under  $I_m, S_m$  is represented as an  $n$ -tuple  $\langle \sigma_s(v_1), \sigma_s(v_2), \dots, \sigma_s(v_k), \sigma_s(v_{k+1}), \dots, \sigma_s(v_n) \rangle$ , where  $\sigma_s(v_i)$  is  $d$  (don't care), if  $v_i \notin S_m \cup I_m$ . For example,  $\langle d, \sigma_s(v_2), \dots, \sigma_s(v_k), d, \dots, \sigma_s(v_n) \rangle$  represents the input combination when  $v_1 \notin S_m$  and  $v_{k+1} \notin I_m$ , i.e., NSF block output lines  $v_1^+$  and  $v_{k+1}^+$  are not measured. The input combination  $\sigma_s \in \Sigma_S$  under  $I_m, S_m$  represents a set of input combinations (under full measurement) which are obtained by replacing each  $d$  with 0 and 1. For example, if  $\sigma_s = \langle d, \sigma_s(v_2), \dots, \sigma_s(v_k), d, \dots, \sigma_s(v_n) \rangle$  under  $v_1 \notin S_m$  and  $v_{k+1} \notin I_m$ , then  $\sigma_s|_{I_m, S_m} = \{ \langle 0, \sigma_s(v_2), \dots, \sigma_s(v_k), 0, \dots, \sigma_s(v_n) \rangle, \langle 1, \sigma_s(v_2), \dots, \sigma_s(v_k), 1, \dots, \sigma_s(v_n) \rangle \}$ .

$\langle 0, \sigma_s(v_2), \dots, \sigma_s(v_k), 1, \dots, \sigma_s(v_n) \rangle, \langle 1, \sigma_s(v_2), \dots, \sigma_s(v_k), 0, \dots, \sigma_s(v_n) \rangle, \langle 1, \sigma_s(v_2), \dots, \sigma_s(v_k), 1, \dots, \sigma_s(v_n) \rangle \}$ .

An  $FD_i$ -transition  $\tau_{im} = \langle x_{im}, \sigma_{im}, x_{im}^+ \rangle$  remains so under  $I_m$  and  $S_m$  if

- Fault propagation is through a measured NSF output line: If  $\sigma_s$  (here  $x_{im} \times \sigma_{im}$ ) sensitizes the fault and propagates the effect through the NSF block in at least one of its *measured* outputs, i.e.,  $\exists j, 1 \leq j \leq k, v_{ij}^+(\sigma_s) \neq v_{0j}^+(\sigma_s) \wedge v_j \in S_m$ .
- Under measurement limitation  $\tau_{im}$  does not become equivalent to any  $N$ -transition:  $\nexists$   $N$ -transition  $\tau_{0l} = \langle x_{0l}, \sigma_{0l}, x_{0l}^+ \rangle$ , such that  $\exists(x_{0l} \times \sigma_{0l}) \in \sigma_s|_{I_m, S_m}$  and  $v_{0j}^+(x_{0l} \times \sigma_{0l}) = v_{ij}^+(\sigma_s), \forall v_j \in S_m$ .

For example,  $\tau_{16} = \langle x_{11}, 1, x_{13} \rangle$  (Figure 3.2) is an  $FD$ -transition. Here,  $x_{11} = 10, \sigma_{16} = 1, x_{13} = 01$ . Also, input combination is  $\sigma_s \equiv \langle \sigma_s(v_1), \sigma_s(v_2), \sigma_s(v_3) \rangle = x_{11} \times 1 = 101$ . If  $S_m = \{v_1, v_2\}$  and  $I_m = \{\}$ , then input combination set  $\sigma_s|_{I_m, S_m} \equiv 101|_{v_3}$  is  $10d = \{100, 101\}$ . Here,  $v_{01}^+(100) = v_{11}^+(101) = 0$  but  $v_{02}^+(100) = 0 \neq v_{12}^+(101) = 1$ . Similarly,  $v_{01}^+(101) = v_{11}^+(101) = 0$  but  $v_{02}^+(101) = 0 \neq v_{12}^+(101) = 1$ . So  $\tau_{16} = \langle x_{11}, 1, x_{13} \rangle$  remains a  $FD_1$ -transition even under  $S_m = \{v_1, v_2\}$  and  $I_m = \{\}$ . Now let us consider measurement limitation  $S_m = \{v_2\}$  and  $I_m = \{v_3\}$ ; input combination set  $\sigma_s|_{I_m, S_m} \equiv 101|_{v_1}$  is  $d01 = \{001, 101\}$ . Here,  $v_{01}^+(001) = v_{11}^+(101) = 0$  and  $v_{02}^+(001) = v_{12}^+(101) = 1$ . So  $\tau_{16} = \langle x_{11}, 1, x_{13} \rangle$  does not remain an  $FD_1$ -transition under  $S_m = \{v_2\}$  and  $I_m = \{v_3\}$ . The same conclusion was arrived at in Subsection 3.2.2

Given a netlist description of the NSF block of the circuit, the set of  $FD$ -transitions under  $I_m$  and  $S_m$  can be determined in the following manner:

1. Simulate the NSF block under normal condition to determine output responses for all input combinations.
2. Insert the s-a fault at the proper point in the NSF.
3. Simulate the NSF block with the fault for all possible input combinations.
4. Determine all possible values of inputs such that the output is different under fault and normal condition; the corresponding transitions are  $FD$ -transitions under full measurement (also called test patterns in off-line test terminology [17]).
5. For each  $FD$ -transition check if it remains so, under  $I_m$  and  $S_m$ .
6. Repeat Steps (1) to (5) for all possible s-a faults.

### 3.3 Efficient construction of $FN$ -detector

---

Step (1) through Step (4) basically involve determining all possible values of input combinations for the NSF block that sensitize the fault and propagate its effect through at least one NSF block output; this is called exhaustive test pattern generation [17]. Exhaustive test pattern generation is a computationally hard problem. Further, to determine whether a test pattern under full measurement remains so, even under a given measurement limitation requires  $O(2^k)$ , where  $k = n - (|S_m| + |I_m|)$ , times analysis of the normal circuit. In other words, a test pattern under full measurement represents a set of patterns under measurement limitation, which are obtained by replacing each unmeasurable input by 0 and 1 ( $O(2^k)$  in number). So, like exhaustive test pattern generation procedure, this process of checking test patterns under measurement limitation also involves exponential complexity. Hence, we require optimized techniques for this problem.

The subsections that follow provide the details of these optimization steps. In essence, these optimizations result by representing the NSF outputs as OBDDs [16] and devising processing steps to work on these OBDD representations.

#### 3.3.1 OBDD based procedure for exhaustive test pattern generation for the NSF block under full measurement

In this section we discuss the procedure for exhaustive test pattern generation for a fault  $F_i$  for a given output line of the NSF block (under full measurement). Without compromising fault detection capability, we assume that even if  $F_i$  is manifested at more than one NSF output lines, any one of these lines can be used for its detection. Given an NSF block output  $v_j^+$  and a fault  $F_i$ , two OBDDs are generated for the Boolean functions  $v_{0j}^+$  and  $v_{ij}^+$ , the former for the normal condition and the latter under  $F_i$ . The two OBDDs are XORed and the exhaustive set of input test vectors for  $F_i$  (that is, the exhaustive set of test patterns) is the result of “satisfy-all-1” operation on the resulting XORed OBDD because all paths leading to 1 in the XORed OBDD represent the exhaustive set of input patterns for which the output under normal condition is different from that under the fault. The output response  $v_{ij}^+, 1 \leq j \leq k$ , for the fault  $F_i$ , for the given set of input test vectors, can be easily obtained from the OBDD for  $v_{ij}^+$  by applying the test patterns; this process can go hand in hand as the test patterns are generated. Let us now illustrate this procedure for the s-a-1 fault, termed as  $F_1$ , at the fanout net marked  $A$  in the circuit shown in Figure 3.2. In this example, we illustrate the OBDD with the ordering  $v_1 \prec v_2 \prec v_3$ . Figure 3.6 represents the OBDD for the Boolean function  $v_{02}^+ = v_1v_2 + v_1'v_2'$ . Figure 3.7 represents the OBDD for the Boolean function of  $v_{12}^+ = v_1v_2v_3' + v_1v_3 + v_1'v_2'$ . Figure 3.8 represents the OBDD corresponding to  $v_{02}^+ \oplus v_{12}^+$  obtained by XORing the normal OBDD and the  $F_1$ -OBDD illustrated in Figures 3.6 and 3.7,

respectively. The exhaustive set of input patterns to test the fault  $F_1$  is obtained using the *satisfy-all-1* operation on the XORed OBDD (Figure 3.8) as  $\{\langle v_1 = 1, v_2 = 0, v_3 = 1 \rangle\}$ , which corresponds to the single path from the root node ( $v_1$ ) of the XORed OBDD to the leaf node 1. The output response under fault ( $F_1$ ) for this input test pattern can be easily determined using the  $F_1$ -OBDD shown in Figure 3.7 as  $v_{12}^+ = 1$ . Thus, for the given fault  $F_1$  and the NSF block output  $v_2^+$ , the exhaustive test pattern set corresponding to the tuple  $\langle v_1 v_2 v_3 \rangle$  is given by  $\{\langle 101 \rangle\}$ . The output for  $\{\langle 101 \rangle\}$  corresponding to the tuple  $\langle v_1^+ v_2^+ \rangle$  is  $\{\langle d1 \rangle\}$ . Thus, the  $FD$ -transition set for fault  $F_1$  and the NSF block output  $v_2^+$  is  $\{\langle 10, 1, d1 \rangle\}$ .

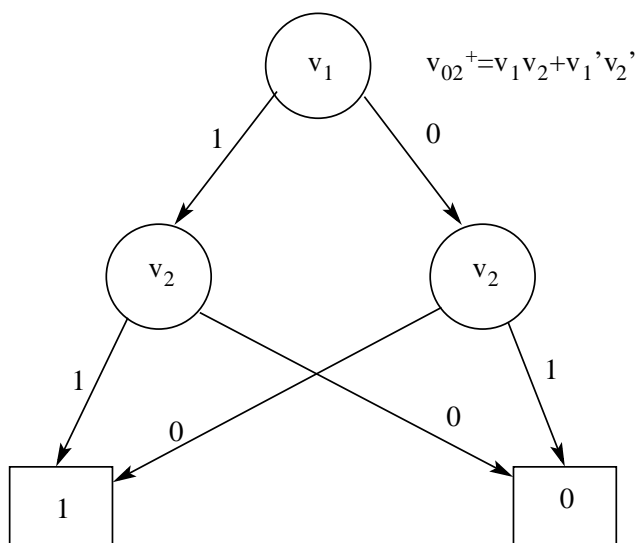


Figure 3.6: OBDD for the function  $v_{02}^+$  (circuit shown in Figure 3.2)

$FD$ -transitions determined by the procedure discussed in the last paragraph detects a fault by monitoring its manifestation at one NSF block output. However, it may happen that for a given test pattern,  $F_i$  is manifested at one output line (say  $v_1^+$ ) of the NSF block and for another test pattern,  $F_i$  is manifested at some other output line (say  $v_2^+$ ). While generating the exhaustive  $FD$ -transitions for the output  $v_1^+$ , we ignore the  $FD$ -transitions which may lead to manifestation of  $F_1$  through  $v_2^+$ . Ignoring these  $FD$ -transitions corresponding to  $v_2^+$  may lead to rise in detection latency because they may include some input combinations which are not covered in the  $FD$ -transitions for  $v_1^+$ . To address this problem, therefore, the exhaustive  $FD$ -transition sets are generated for each NSF output and for each  $F_i$ , which are then used for designing an  $FN$ -detector for the entire NSF block. Let  $\tau_{im}^j = \langle x_{im}^j, \sigma_{im}^j, x_{im}^{+j} \rangle$  denote the  $m^{th}$   $FD$ -transition for the fault  $F_i$  determined at the NSF block output  $v_j^+$ . The values of state variables in  $x_{im}^j$  are don't care values for members of  $S^+$  whose corresponding

### 3.3 Efficient construction of $FN$ -detector

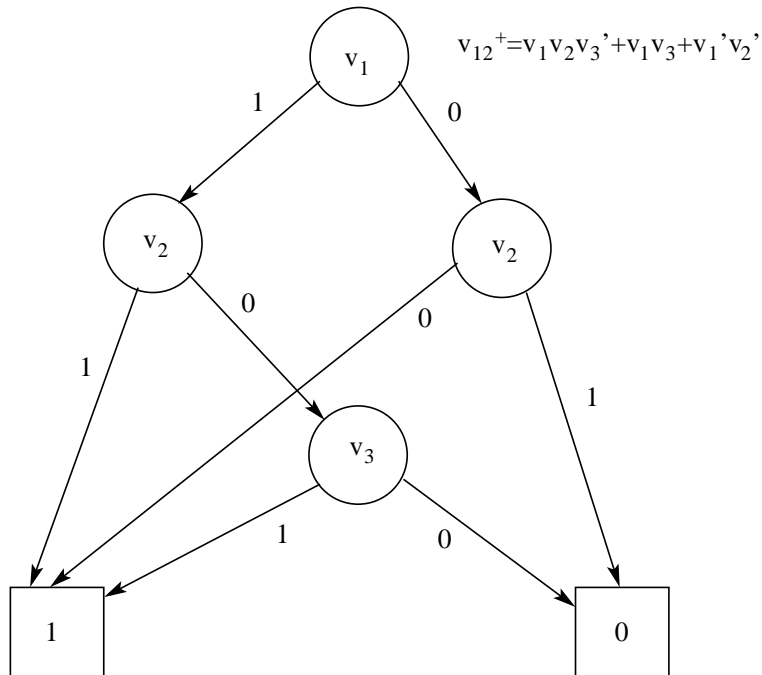


Figure 3.7: OBDD for the function  $v_{12}^+$  (circuit shown in Figure 3.2)

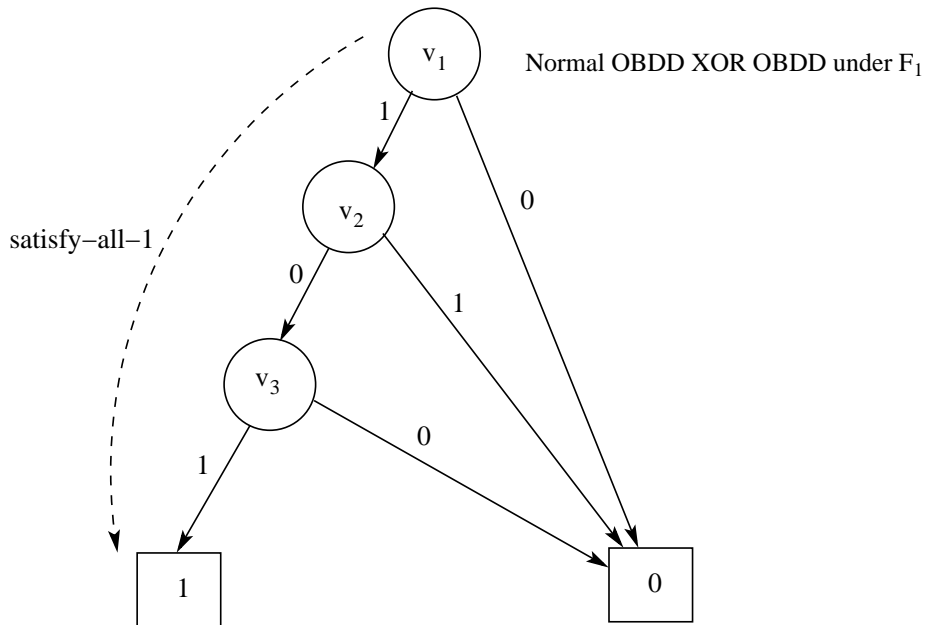


Figure 3.8: XOR of  $v_{02}^+$  and  $v_{12}^+$  OBDD (circuit shown in Figure 3.2)

members in  $S$  do not fall under the cone of influence <sup>2</sup> of the NSF block output ( $v_j^+$ ) being considered. Further, as the values of the variables corresponding to  $x_{im}^j$  conjoined with  $\sigma_{im}^j$  are determined using OBDD (based XOR operation), even some of these variables that fall in the cone of influence of  $v_j^+$  may be don't cares. Also, it may be noted that *only one variable* in  $x_{im}^{+j}$ , namely,  $v_j^+$ , that corresponds to the NSF block output through which the fault manifestation is monitored has a Boolean value of 0 or 1; rest are don't cares.

Once the exhaustive set of  $FD$ -transitions are generated for each fault, we check whether the  $FD$ -transitions remain so under a given measurement limitation.

### 3.3.2 OBDD based procedure for determination of $FD$ -transitions under measurement limitation

Consider an  $FD$ -transition  $\tau_{im}^j = \langle x_{im}^j, \sigma_{im}^j, x_{im}^{+j} \rangle$  for the fault  $F_i$  determined at the NSF block output  $v_j^+$ . Now we discuss the procedure to check if  $\tau_{im}^j = \langle x_{im}^j, \sigma_{im}^j, x_{im}^{+j} \rangle$  remains an  $FD_i$ -transition under measurement limitation  $I_m$  and  $S_m$ , using OBDDs. Obviously, only those NSF block outputs are considered whose corresponding  $v_j \in S_m$  (i.e., are measurable). In other words, all  $FD$ -transitions where fault manifestation is only through NSF outputs which are unmeasurable, can be directly dropped. So in this case, if  $v_j$  is measurable (i.e.,  $v_j \in S_m$ ) then we proceed for further verification steps. Following that, we determine the value of the NSF output ( $v_j^+$ ) under failure condition for input  $\sigma_{sm}^j = x_{im}^j \times \sigma_{im}^j$  by tracing the path in the OBDD (representing output function for  $v_{ij}^+$ ) corresponding to values of the variables in  $\sigma_{sm}^j$ ; let the value be  $val_{im}^j \in 0, 1$ . Now, for each input combination under measurement limitation  $I_m, S_m$  i.e.,  $\sigma_s \in \sigma_{sm}^j|_{I_m, S_m}$ , we need to determine the value of NSF output ( $v_j^+$ ) under normal condition for input  $\sigma_s$  by tracing the path in the OBDD (representing output function for  $v_{0j}^+$ ) corresponding to values of the variables in  $\sigma_s$ ; let the value be  $val_{0\sigma_s}^j \in 0, 1$ . If  $val_{0\sigma_s}^j \neq val_{im}^j$ , for all  $\sigma_s$ , then  $\tau_{im}^j$  remains an  $FD_i$ -transition under measurement limitation  $I_m$  and  $S_m$ . Alternatively, if  $val_{0\sigma_s}^j = val_{im}^j$  for any input condition  $\sigma_s \in \sigma_{sm}^j|_{I_m, S_m}$ , then for that  $\sigma_s$ , the corresponding NSF output  $v_j^+$  gives same value both in normal and faulty case;  $\tau_{im}^j$  does not remain an  $FD_i$ -transition under measurement limitation.

Now we will illustrate the concept with the failure s-a-1 in line A (of Figure 3.2, whose FSA model is shown in Figure 3.3) for measurement limitation (i)  $I_m = \{\}$  and  $S_m = \{v_1, v_2\}$  (ii)  $I_m = \{v_3\}$  and  $S_m = \{v_2\}$ . The  $FD_1$ -transition is  $\tau_{16}^2 = \langle 10, 1, d1 \rangle$ , corresponding to NSF output  $v_2$ . Here,  $\sigma_{s6}^2 = 10 \times 1$ . If we traverse the OBDD for  $v_{12}^+$  (for the fault, shown in Figure 3.7) for the input combination 101 we have  $val_{16}^2 = 1$ . For  $I_m = \{\}$  and

---

<sup>2</sup>In terms of VLSI testing the sub-circuit that is in the transitive fanins of an (NSF) output,  $v_j^+$  say, is called the “sub-circuit in the cone of influence of  $v_j^+$ ” [17]

### 3.3 Efficient construction of $FN$ -detector

---

$S_m = \{v_1, v_2\}$ ,  $\sigma_s \in \sigma_{s6}^2|_{I_m, S_m} = \{100, 101\}$ . From the OBDD for  $v_{02}^+$  (for the normal circuit, shown in Figure 3.6), we have  $val_{0\sigma_s}^2 = 0$  for both the input combinations of  $\sigma_s = 100$  and  $101$ , which is not equal to  $val_{16}^2 = 1$ . So  $\langle 10, 1, d1 \rangle$  remains an  $FD_1$ -transition.

For  $I_m = \{v_3\}$  and  $S_m = \{v_2\}$ ,  $\sigma_s \in \sigma_{16}^2|_{I_m, S_m} = \{001, 101\}$ . From the OBDD for  $v_{02}^+$ , we have  $val_{0\sigma_s}^2 = 1$  for combination  $\sigma_s = 001$  which is equal to  $val_{16}^2 = 1$ . So  $\langle 10, 1, d1 \rangle$  does not remain an  $FD_1$ -transition.

**Note:** The above procedure to check if  $\tau_{im}^j$  remains an  $FD$ -transition under measurement limitation  $I_m, S_m$  requires exponential number (with respect to unmeasurable lines) of checks in the normal OBDD. However, using OBDD we can perform this step efficiently as discussed below. In the OBDD representing the NSF output corresponding to  $v_j^+$ , under normal condition, the following steps are required.

1. If  $v_k \in S_m \cup I_m$  and  $\sigma_{sm}^j(v_k) = 0$  (or 1) then in the node of the OBDD corresponding to  $v_k$ , eliminate the edge corresponding to 1 (or 0).
2. Delete all edges and nodes unreachable from the root after elimination of the edge.
3. Repeat Step 1 and Step 2 for all  $v_k \in S_m \cup I_m$ .
4. In the resultant OBDD if there is a path from root to leaf whose value is same as that of the corresponding faulty OBDD for input combination  $\sigma_{sm}^j$ , then  $\tau_{im}^j$  does not remain an  $FD_i$ -transition under measurement limitation; else it remains an  $FD_i$ -transition.

In simple words, given an  $FD_i$ -transition, we first replace all the variables of the input combination with  $d$  which are unmeasurable. Now, in the normal OBDD, given a variable of the input combination, we determine the corresponding nodes and keep the edge representing 0 or the edge representing 1 or both the edges, if the value of the variable is 0 or 1 or  $d$ , respectively. This process is repeated for all variables of the input combination. In the resultant OBDD, if there is a path to a leaf node whose value is same as that of the faulty OBDD for the input combination of the given  $FD_i$ -transition, then it does not remain an  $FD_i$ -transition under the given measurement limitation.

Let us consider the same s-a-1 fault (of Figure 3.2, whose FSA model is shown in Figure 3.3) for measurement limitation  $I_m = \{v_3\}$  and  $S_m = \{v_2\}$ . The  $FD_1$ -transition in this case is  $\tau_{16}^2 = \langle 10, 1, d1 \rangle$  corresponding to the NSF output  $v_2$ . As already discussed,  $val_{16}^2 = 1$ . In the normal OBDD (Figure 3.6), as  $v_1 \notin S_m$  we retain both the edges for the variable  $v_1$ . As  $v_2 \in S_m$  and value in the  $FD$ -transition is 0, we eliminate the edges corresponding to 1 in the nodes for  $v_2$ . Finally, as  $v_3 \in I_m$  and value in the  $FD$ -transition is 1, we need to eliminate the edges corresponding to 0 in the nodes for  $v_3$ ; however, this need not be done as the nodes

for  $v_3$  are redundant and already eliminated by the OBDD construction. Figure 3.9 shows the normal OBDD for  $v_{02}^+$  after edges and nodes for  $FD$ -transition  $\langle 10, 1, d1 \rangle$  are eliminated for  $I_m = \{v_3\}$  and  $S_m = \{v_2\}$ . It may be noted that there is path from the root node to leaf node with value 1, which is same as in the faulty OBDD (Figure 3.7) for input combination  $\langle 101 \rangle$ . So  $\langle 10, 1, d1 \rangle$  does not remain an  $FD_1$ -transition. In a similar way, it can be shown that  $\tau_{16}^2$  remains  $FD_1$ -transition under measurement limitation  $I_m = \{\}$ ,  $S_m = \{v_1, v_2\}$ . The  $FN$ -detector comprising  $FD_1$ -transition  $\tau_{16}^2 = \langle 10, 1, d1 \rangle$  under measurement limitation  $I_m = \{\}$  and  $S_m = \{v_1, v_2\}$  for NSF output  $v_2^+$  is shown in Figure 3.10.

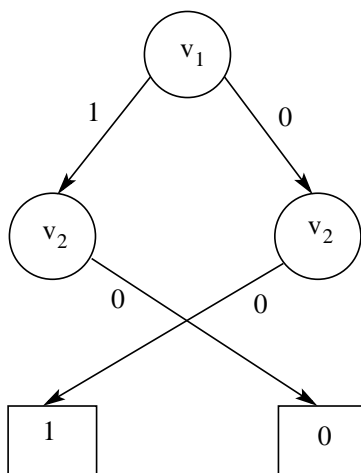


Figure 3.9: OBDD for  $v_{02}^+$  after edges and nodes for  $FD$ -transition  $\langle 10, 1, d1 \rangle$  being eliminated for  $I_m = \{v_3\}$  and  $S_m = \{v_2\}$

### 3.3.3 $FN$ -detector design for Output Function block of the circuit

The above procedure of design of the  $FN$ -detector can be easily applied to the Output Function (OF) block of the circuit shown in Figure 3.1. To elaborate, we represent each cone of the OF block using separate OBDDs under normal and faulty conditions. The same OBDD based operations (applied for NSF block) are performed to generate the  $FD$ -transitions under full measurement and determine the  $FD$ -transitions that retain their capability under a given measurement limitation. Finally, the  $FN$ -detector is designed using these  $FD$ -transitions. Since the OF block is a combinational circuit, its  $FN$ -detector design is much simpler than that of the NSF block. An  $FD$ -transition generated for the OF block consists of a combination of input values and its faulty response, whereas an  $FD$ -transition for the NSF block, as discussed in Subsection 3.2.2, consists of initial state values, input and final (faulty) state values. So, the FSM of the  $FN$ -detector for the OF block involves only two state—initial state ( $z_0$ ) and final state ( $z_f$ ) and any transition from  $z_0$  to  $z_f$  indicates the

### 3.3 Efficient construction of $FN$ -detector

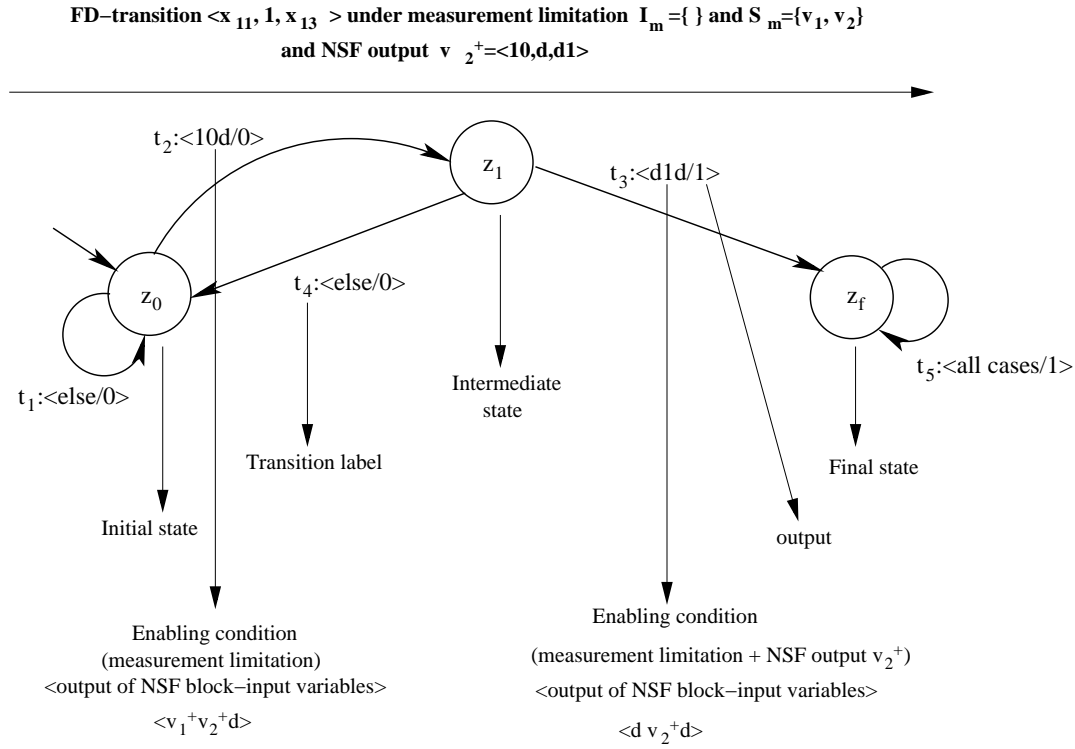


Figure 3.10: The  $FN$ -detector for  $FD$ -transition  $\tau_{16}$  under  $I_m = \{ \}$ ,  $S_m = \{v_1, v_2\}$  and NSF output  $v_2^+$

occurrence of a fault in the OF block. It may be noted that the fault detection in the OF block is performed in a single clock cycle, whereas it requires two consecutive clock cycles for the NSF block of the circuit.

We demonstrate the design of the  $FN$ -detector for the OF block using a simple combinational circuit and avoid the detail formalisms. Figure 3.11 shows an OF block having inputs— $a, b, c, d$  and  $e$ , and outputs— $OP_1$  and  $OP_2$ . First, we partition the OF block into cones with respect to its outputs as shown in the figure. Let us consider a s-a-0 fault at point B (of Figure 3.11). As the fault belongs to cone of  $OP_2$ , so we can propagate the effect of the fault only through  $OP_2$ . Under full measurement the test patterns to detect the fault are  $\langle a, b, c, d, e \rangle \langle 10110 \rangle$  and  $\langle 01110 \rangle$ . These patterns produce output  $OP_2$  as 1 (0) under normal (faulty) condition. Suppose line  $a$  is not tapped by the  $FN$ -detector, then the test pattern  $\langle d0110 \rangle$  does not retain its capability to detect the fault. This is because the test pattern  $\langle d0110 \rangle$  comprises patterns  $\langle 00110 \rangle$  and  $\langle 10110 \rangle$  and the pattern  $\langle 00110 \rangle$  cannot detect the s-a-0 fault at B; value of  $OP_2$  is same under normal and faulty conditions (i.e.,  $OP_2 = 0$ ). However, the test pattern  $\langle d1110 \rangle$  retains its capability to detect the fault because it comprises patterns  $\langle 01110 \rangle$  and  $\langle 11110 \rangle$  and both can detect the s-a-0 fault at point B; value of  $OP_2$  is 1 (0) under normal (faulty) condition. The FSM of the  $FN$ -detector

to detect the s-a-0 fault at B under measurement limitation (line  $a$  is not tapped) is shown in Figure 3.12.

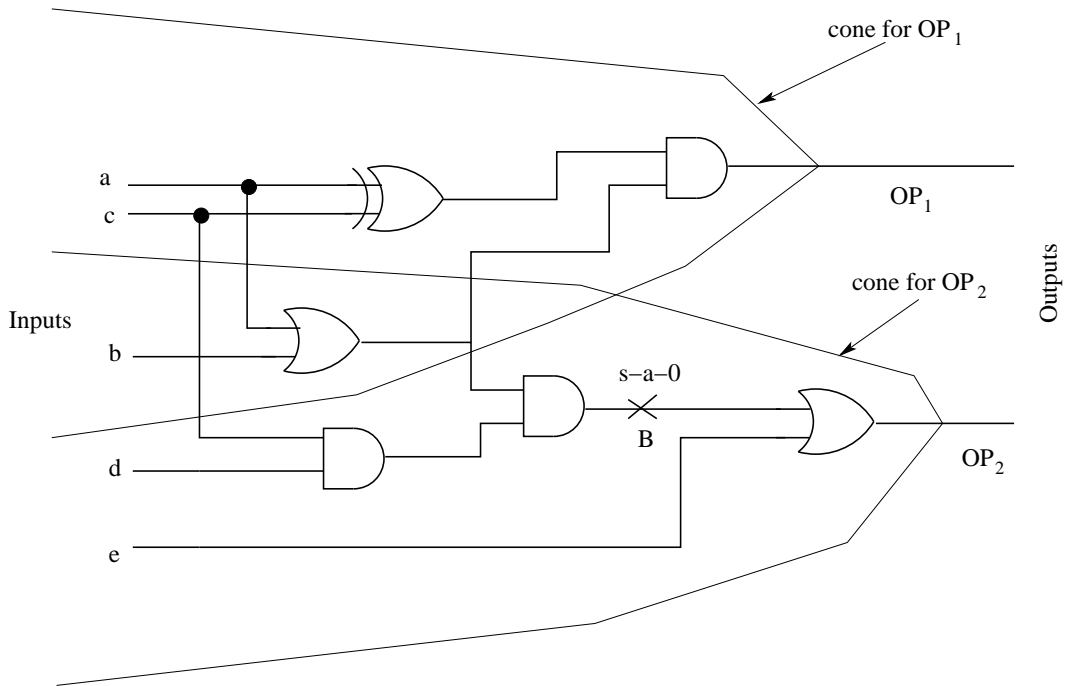


Figure 3.11: Example of OF block

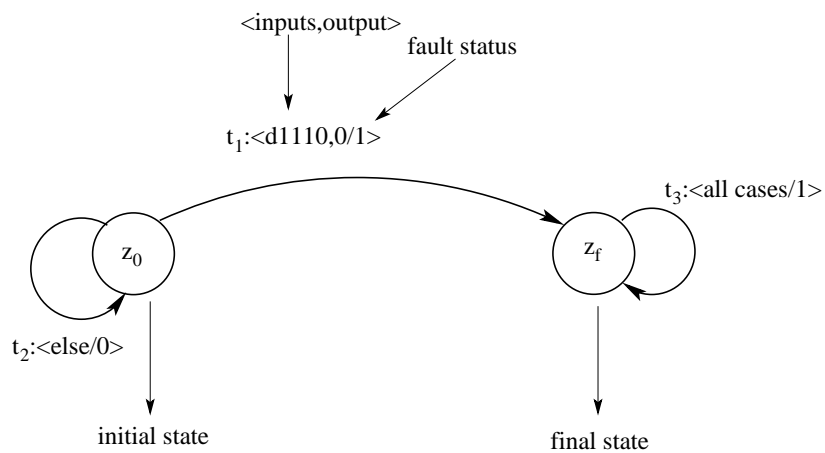


Figure 3.12:  $FN$ -detector for the OF block (Figure 3.11) where line  $a$  is not tapped

## 3.4 Experimental evaluation

The techniques discussed in Section 3.2 and Section 3.3 are used to design a tool “ML-OLT”, which generates an *FN*-detector (in Verilog RTL) given a digital sequential circuit (in netlist format). It basically involves the following steps:

1. Extract the the part of the netlist that corresponds to the NSF block.
2. Eliminate the flip-flops and partition the netlist (into sub-circuits) according to cones of influence corresponding to each of the flip-flops. The output of each of the sub-circuits is the corresponding input to the flip-flop.
3. Repeat the following for all the sub-circuits generated in Step 2.
  - (a) Insert s-a faults in all possible locations.
  - (b) Repeat the following for all the faults
    - i. Generate OBDD for the sub-circuit under normal condition.
    - ii. Generate OBDD for the sub-circuit under the fault condition.
    - iii. XOR the two OBDDs. The variable values corresponding to the paths to leaf node “1”, are the input combinations for the *FD*-transitions. The faulty OBDD output for an input combination determines the final state of the *FD*-transition.
    - iv. Determine all the *FD*-transitions which remain so under the given measurement limitation and drop the remaining ones.
4. Generate the FSM of the *FN*-detector with the remaining *FD*-transitions and translate the FSM to Verilog code [24].
5. Generate the FSM of the *FN*-detector for OF block under measurement limitation and translate the FSM to Verilog code.

In this thesis, we have used CUDD (Colorado University Decision Diagram) package for the manipulation of OBDDs in order to generate *FD*-transitions. The CUDD package is considered as the best-manipulated BDD package and is freely available. The package provides a large set of operations on BDDs, like performing boolean operations (AND, OR, XOR, etc.) on BDDs, Satisfying all 1/0 operations on BDD, etc.

The Verilog code can be synthesized using any standard synthesis tool, design library and user defined constraints. Following that area overhead of the *FN*-detector can be

determined for a given measurement limitation. As already discussed, along with area overhead, other important parameters for the *FN*-detector are detection latency and fault coverage. In the next sub-section we discuss regarding these parameters and how trade-offs can be exploited in the *FN*-detector design.

### 3.4.1 Trade-offs in *FN*-detector design: detection latency, fault coverage, measurement limitation and area overhead

The performance of an *FN*-detector in terms of fault detection can be represented in terms of—(i) fault coverage and (ii) detection latency. The former deals with coverage of all possible faults conforming to the single s-a fault model. Detection latency implies the number of times a fault is manifested at some output of the CUT due to occurrence of an *FD*-transition, however, is not detected because that *FD*-transition is not considered in the *FN*-detector due to measurement limitation. Detection latency may increase due to two factors namely, i) some *FD*-transitions may be kept out of the purview of the *FN*-detector or ii) measurement limitation, which in turn eliminates some *FD*-transitions. So, when all the *FD*-transitions are used to design the *FN*-detector, any fault is detected immediately after it results in the first measurable difference in the output (compared to the normal condition); thus, the detection latency is zero. Clearly, if some of the *FD*-transitions are dropped in the construction of the *FN*-detector, then the detection latency may increase. This is because the *FD*-transitions that are not taken in the *FN*-detector may occur before the *FD*-transitions that are taken.

In [12], the area overhead was reduced by eliminating some *FD*-transitions. In the present work we will use measurement limitation as a trade-off factor to minimize area overhead by compromising detection latency and fault coverage. In [12], for most of the cases (i.e., for the *FD*-transition set selected for the *FN*-detector) all primary inputs and output lines had to be measured. In the experimental results we will show that similar detection latency, fault coverage and area overhead can be achieved by the proposed scheme compared to [12], however, with reduction in the lines to be measured.

The CAD tool “ML-OLT” is used to generate OLT circuits for different ISCAS’89 benchmark circuits under various measurement limitations. First we illustrate results (as graphs) for fault coverage, detection latency and area overhead of the circuit s1488 under different combinations of measurement limitations. We have illustrated results where 1 or 2 lines are considered unmeasurable. The following measures were used to determine the values of fault coverage, detection latency and area overhead for a tester given a measurement limitation.

### 3.4 Experimental evaluation

---

- **Fault Coverage (FC):** We consider a fault to be covered if at least one  $FD$ -transition of the fault remains in the  $FN$ -detector under measurement limitation. Fault coverage =  $((\text{number of faults covered})/(\text{number of faults in the circuit})) \times 100 \%$ .
- **Detection Latency (DL):** For a fault  $F_i$  (which is covered), let there be  $nFD_i$  number of  $FD$ -transitions under full measurement. After measurement limitation let  $nmlFD_i$  be the number of  $FD$ -transitions that remain. Detection latency is  $(\lceil nFD_i/nmlFD_i \rceil) - 1$ .
- **Area Overhead (AO):** Area Overhead =  $(\text{Area of the } FN\text{-detector after synthesis})/(\text{Area of the CUT after synthesis})$ .

Figure 3.13, Figure 3.14 and Figure 3.15 illustrate detection latency, area overhead and fault coverage, respectively of s1488 versus different combinations of measurement limitations of one and two input lines of the NSF. Under this case of one and two input lines being unmeasured, s1488 has 105 combinations of unmeasurable lines. In the graph, points in the  $x$ -axis represent the line(s) not being measured; for example, the first point  $V0$  represents that input  $V0$  is not measured whereas  $V0\_V1$  represents that  $V0$  and  $V1$  are not measured. To keep the markings of the  $x$ -axis legible we illustrate only 55 combinations. The following points may be noted:

- Figure 3.13: Impact of not measuring different (single or double) input lines may have different impact on detection latency. As already discussed, making line(s) unmeasurable results in converting some  $FD$ -transitions to non- $FD$ -transitions which leads to rise in detection latency. Broadly speaking, the input lines whose transitive fanouts have more fault sites (i.e., gates) have higher sensitivity to detection latency.
- Figure 3.14: Lower the detection latency, higher the area overhead. Higher detection latency implies that unmeasurable lines resulted in converting more  $FD$ -transitions to non- $FD$ -transitions compared to a situation with lower detection latency. Generally, speaking an  $FN$ -detector with less  $FD$ -transitions involve less states resulting in lower area and vice-versa. Same detection latency (due to different combinations of unmeasured lines) may also result in different area overheads. Detection latency implies that some  $FD$ -transitions are not considered, however, it does not specify which  $FD$ -transitions. As circuit area does not only depend on the number of minterms but also on the specific minterms and don't cares [61], same detection latency (same number of  $FD$ -transitions) may also result in different area overheads.



### 3.4 Experimental evaluation

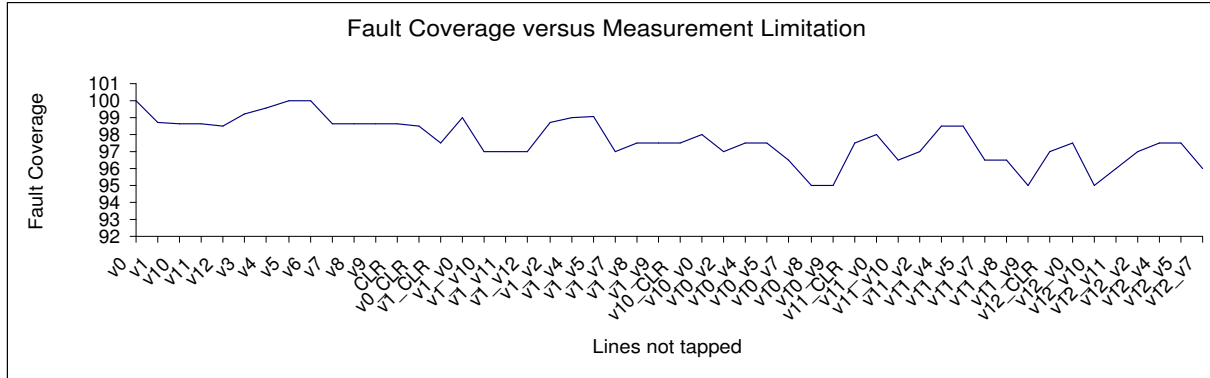


Figure 3.15: Fault coverage for s1488 versus different combinations of measurement limitations of one and two input lines of the NSF

high coverage could be achieved. We have mainly dealt with area overhead and detection latency because they are the most sensitive parameters.

Columns 1-2 provide information about the circuit. Columns 3, 5 and 7 correspond to the lowest (best) area overhead obtained among all combinations of 1, 2 and 3 unmeasured lines, respectively. Columns 4, 6 and 8 correspond to the highest (worst) area overhead obtained among all combinations of 1, 2 and 3 unmeasured lines, respectively. In Column 9, we report the amount of CPU time taken to generate the exhaustive set of  $FD$ -transitions. Corresponding to each circuit (i.e., row 4 to row 13) we have reported values regarding, i) AO: Area overhead of the  $FN$ -detector for the corresponding combination of unmeasured lines ii) DL: detection latency due to the particular combination of unmeasured lines and iii) AO[]: Area overhead of the  $FN$ -detector designed using the scheme of [12,36] to achieve the particular detection latency; given a detection latency these schemes eliminate  $FD$ -transitions randomly such that the given latency is maintained. For example, row 4-column 4, represents the single input line in circuit s27 (NSF block), whose unmeasurability gives the best area overhead. The first element “AO:2.41” states that best case area overhead is 2.41 for the corresponding single line being unmeasured. The second element “DL:2” states that for the corresponding single line being unmeasured we get detection latency as 2. The third element “AO[]:2.45” states that for detection latency 2, the area overhead of the  $FN$ -detector designed using the scheme [12,36] is 2.45. The following conclusions can be derived.

- Trends are similar to the case of s1488.
- The ranges between best case area overhead and worst case area overhead are fairly high. Different input lines have different impact on transforming  $FD$ -transitions to

### 3.4 Experimental evaluation

Table 3.1: Area Overhead (AO) for different combinations of measurement limitations, resulting Detection Latency (DL), AO comparison with [12, 36] and CPU time to generate  $FD$ -transitions\*

Circuit description		AO for different combinations of measurement limitations						CPU Time (Secs.)
Circuit	No. of FFs- (Gates)	one line		two lines		three lines		
		Best case AO	Worst case AO	Best case AO	Worst case AO	Best case AO	Worst case AO	
S27	3-(10)	AO:2.41 DL:2 AO[]:2.45	AO:2.99 DL:1 AO[]:2.99	AO:2.34 DL:4 AO[]:2.39	AO:2.66 DL:1 AO[]:2.99	AO:2.11 DL:9 AO[]:2.19	AO:2.51 DL:2 AO[]:2.45	19
S298	14-(119)	AO:0.86 DL:2 AO[]:1.01	AO:1.36 DL:1 AO[]:1.88	AO:0.63 DL:4 AO[]:0.78	AO:1.34 DL:1 AO[]:1.88	AO:0.42 DL:8 AO[]:0.62	AO:1.32 DL:1 AO[]:1.88	228
S386	6-(118)	AO:0.86 DL:2 AO[]:1.11	AO:1.38 DL:1 AO[]:1.80	AO:0.62 DL:4 AO[]:0.85	AO:1.25 DL:1 AO[]:1.80	AO:0.51 DL:7 AO[]:0.70	AO:1.13 DL:1 AO[]:1.80	411
S510	6-(211)	AO:0.79 DL:2 AO[]:1.1	AO:1.2 DL:1 AO[]:1.75	AO:0.70 DL:3 AO[]:0.88	AO:1.1 DL:1 AO[]:1.75	AO:0.60 DL:6 AO[]:0.72	AO:1.0 DL:1 AO[]:1.75	1027
S5378	179-(2779)	AO:0.4 DL:2 AO[]:0.44	AO:0.98 DL:1 AO[]:0.98	AO:0.23 DL:3 AO[]:0.31	AO:0.98 DL:1 AO[]:0.98	AO:0.18 DL:6 AO[]:0.25	AO:0.97 DL:1 AO[]:0.98	74141
S9234	228-(5597)	AO:0.35 DL:2 AO[]:0.39	AO:0.99 DL:1 AO[]:0.99	AO:0.21 DL:3 AO[]:0.3	AO:0.97 DL:1 AO[]:0.99	AO:0.15 DL:6 AO[]:0.21	AO:0.97 DL:1 AO[]:0.99	221529
S15850	597-(9772)	AO:0.3 DL:2 AO[]:0.36	AO:0.99 DL:1 AO[]:0.99	AO:0.20 DL:3 AO[]:0.29	AO:0.99 DL:1 AO[]:0.99	AO:0.18 DL:5 AO[]:0.25	AO:0.98 DL:1 AO[]:0.99	481115
S35932	1728-(16065)	AO:0.28 DL:2 AO[]:0.35	AO:0.95 DL:1 AO[]:0.98	AO:0.20 DL:3 AO[]:0.28	AO:0.94 DL:1 AO[]:0.97	AO:0.17 DL:5 AO[]:0.24	AO:0.93 DL:1 AO[]:0.97	1023461
S38417	1636-(22179)	AO:0.27 DL:2 AO[]:0.33	AO:0.89 DL:1 AO[]:0.95	AO:0.17 DL:3 AO[]:0.27	AO:0.88 DL:1 AO[]:0.94	AO:0.16 DL:5 AO[]:0.23	AO:0.87 DL:1 AO[]:0.93	1253624
S38584	1452-(19253)	AO:0.27 DL:2 AO[]:0.34	AO:0.90 DL:1 AO[]:0.95	AO:0.18 DL:3 AO[]:0.28	AO:0.88 DL:1 AO[]:0.94	AO:0.17 DL:5 AO[]:0.24	AO:0.87 DL:1 AO[]:0.94	1221015

\*Executed in AMD Phenom IIX3 710 Processor with 4 GB RAM in Linux OS.

### 3.5 Conclusion

---

non  $FD$ -transitions. This range can be utilized as a design parameter to trade-off area overhead versus detection latency.

- For a given detection latency area overhead for the proposed scheme is lower compared to that of [12, 36]. The scheme of [12, 36] randomly eliminates  $FD$ -transitions while the proposed scheme performs this elimination by not measuring some input lines. Not measuring some input lines of the NSF implies that they are not tapped by the  $FN$ -detector. This reduces the fanouts of those input lines, resulting in less buffering (drivers) and hence lower area.

### 3.5 Conclusion

In this chapter we have proposed an OBDD based OLT scheme of digital circuits with measurement limitation (i.e., minimization of tap points of the CUT). The scheme provides flexibility in terms of area overhead of the tester versus fault coverage and detection latency with measurement limitation. The scheme uses “minimization of tap points” as a new trade-off parameter to reduce area overhead at the cost of fault coverage and detection latency. Experimentally, it has been shown that the minimization of tap points do not have high impact on fault coverage and detection latency but it reduces area overhead of the on-line tester. It is also observed that for a given detection latency, area overhead of the scheme is lower compared to other similar schemes reported in the literature.

The s-a fault model is widely used in testing (and also in OLT) for its simplicity, however, this model cannot capture more a fraction of real defects in modern day VLSI circuits. So, advanced fault models such as bridging faults, delay faults, etc., are introduced in testing in order to capture a large number of real defects. In next chapter, we will address another important issue of OLT, i.e., OLT for advanced fault models. We have taken bridging fault as the advanced fault model where both non-feedback and feedback versions are considered.

# Chapter 4

## On-line Testing for Feedback Bridging Faults

### 4.1 Introduction

In majority of the works on OLT, single stuck-at (s-a) fault model is considered. However in modern integration technology, single s-a fault model can capture only a small fraction of real defects and as a remedy, advanced fault models such as bridging faults, transition faults, delay faults, etc., are now being adopted [135]. In this chapter, we focus towards OLT of one of the most important advanced fault model, i.e., bridging faults. The first work on OLT for bridging fault is reported in [73], which is based on self-checking design where the outputs are encoded with error detecting codes and presence of any bridging fault would result in a non-coded word as output. Biswas et al. in [13] have proposed an OLT scheme for bridging faults which is based on the partial replication technique, where they have illustrated that area overhead for OLT of bridging faults is not higher compared to that of s-a faults. The main drawback of these two schemes is that they have only considered non-feedback bridging faults and ignored feedback bridging faults. It may be noted that in some cases feedback bridging faults cause oscillations and detecting them on-line using logic testing is difficult. However, not all feedback bridging faults create oscillations and even if some does, there are test patterns for which the fault effect is manifested logically. Directly dropping all feedback bridging faults lead to significant compromise in fault coverage. Das et al. attempted to test feedback bridging faults on-line in cluster based FPGAs [32]. There are two main issues with this approach namely, intrusiveness of the design and use of asynchronous elements (Muller-C elements). It may be noted that design of asynchronous tester for OLT of synchronous circuit is not desirable. The details about these OLT schemes for bridging faults can be

## 4.2 Circuit modeling and FN-detector design using FSA framework

---

found in Chapter 2, Subsection 2.3.2.

Based on the literature review, in this chapter we propose a partial replication based OLT scheme for wired AND-OR bridging faults. The scheme first determines the bridging faults which do not lead to oscillations i.e., all non-feedback and some feedback bridging faults. Following that, exhaustive set of test patterns for these faults are generated. Also, it is checked if there are patterns, even in case of oscillating feedback bridging faults, which can detect these faults without oscillations. All these test patterns taken together are used to design the on-line tester, called *FN*-detector (i.e., fault versus normal condition detector). All major steps of the scheme namely, checking if a feedback bridging fault causes oscillations, generating exhaustive test patterns for non-feedback bridging faults and determining test patterns that do not lead to oscillations in feedback bridging faults, etc., are implemented using Ordered Binary Decision Diagrams (OBDDs) [16]. Application of OBDD enables the proposed scheme to handle fairly complex circuits. On-line testers have been designed for ISCAS 89 benchmarks. Experimental results illustrate that consideration of feedback bridging faults along with non-feedback ones improve fault coverage with a marginal increase in area overhead compared to schemes only involving non-feedback faults.

The chapter is organized as follows. Finite State Automata (FSA) based modeling of the Circuit Under Test (CUT) with bridging faults and *FN*-detector construction are explained in Section 4.2. To handle the issue of complexity of *FN*-detector construction, several optimization techniques namely, partitioning the CUT using cones of influence, use of OBDDs to generate fault detecting transitions without explicit state modeling, etc., have been applied and are discussed in Section 4.3. Section 4.4 presents experimental results regarding fault coverage and area overhead. Finally we conclude in Section 4.5.

## 4.2 Circuit modeling and FN-detector design using FSA framework

The modeling procedure of sequential circuits for bridging faults using FSA is same as the modeling framework discussed in the previous chapter (Chapter 3, Section 3.2). However, we reproduce the FSA framework in brief for readability.

The basic architecture of a sequential circuit with on-line tester is shown in Figure 3.1 (Chapter 3). A sequential circuit (i.e., the CUT) comprises three blocks namely, Next State Function (NSF), Flip-Flops (FFs) and Output Function(OF). In this work we mainly consider the NSF block and FFs for OLT. The mechanism can be easily extended for the OF block as it is a combinational circuit and is illustrated in Chapter 3, Subsection 3.3.3 for s-a

faults. The same philosophy is applied for bridging faults and we do not present explicitly in this chapter. A sequential circuit without the OF block can be modeled as an FSA  $G$ , defined below.

$$G = \langle V, X, X_0, \Sigma, \mathfrak{S} \rangle \quad (4.1)$$

where  $V = \{v_1, v_2, \dots, v_n\}$  is the finite set of Boolean variables,  $X$  is the finite set of states,  $X_0 \subseteq X$  is the set of initial states,  $\Sigma$  is the finite set of input symbols and  $\mathfrak{S}$  is the finite set of transitions. The set of variables  $V$  can be partitioned into two subsets—(i) state variables  $S = \{v_1, v_2, \dots, v_k\}$  and (ii) input variables  $I = \{v_{k+1}, v_{k+2}, \dots, v_n\}$ . A state  $x \in X$  is a mapping  $x : S \rightarrow \{0, 1\}$ . Similarly, any input symbol  $\sigma \in \Sigma$  is a mapping  $\sigma : I \rightarrow \{0, 1\}$ . Thus, a state is represented by a binary  $k$ -tuple, where  $k = \lceil \log_2 |X| \rceil$ ; the value of the tuple is called encoding of the state. Similarly, any input symbol can be represented as a binary  $i$ -tuple, where  $i = n - k$  and  $|\Sigma| = 2^{n-k}$ .

A transition  $\tau = \langle x, \sigma, x^+ \rangle \in \mathfrak{S}$  is an ordered three-tuple, where  $x$  is the initial state of the transition, denoted as  $initial(\tau)$ ,  $x^+$  is the final state of the transition, denoted as  $final(\tau)$  and  $\sigma \in \Sigma$  is the input symbol of the transition, referred as  $input(\tau)$ .

### 4.2.1 Circuit modeling under bridging faults

The present subsection explains how sequential circuits having bridging faults are modeled as FSA. In most of the works on bridging faults, short is assumed between any two lines in the CUT. Ideally speaking, a bridging fault may involve any number of lines of a circuit, however, that would make the number of all possible faults exponentially high. So, in the widely accepted bridging fault models only two lines are assumed to be involved [17]. As per the fault model, the manifestation is in terms of logic AND and logic OR between the two lines. This fault model is called wired AND-OR fault model. In the CUT, the fault is represented once by adding an AND gate and then by adding an OR gate between the two lines involved in the fault. Henceforth in this chapter, the term fault will be used to refer to wired AND-OR bridging fault. Whenever, any other fault needs to be referred to, it would be explicitly mentioned.

Fault is modeled as a part of the same FSA which is used to model the CUT under normal condition. To elaborate, the FSA is divided into sub-systems (i.e., a sub-set of states and transitions) and each sub-system is used to represent the CUT under a fault or normal condition. So, the variable set  $V$  is extended as  $V = S \cup I \cup C$ , where  $C$  is a set of  $k (= \lceil \log_2(p+1) \rceil)$  status variables (normal or fault), where  $p$  is the total number of possible faults in the CUT.  $\bigcup_{x \in X} x(C) = \{N, F_1, F_2, \dots, F_p\}$ , where  $N$  stands for normal status and

## 4.2 Circuit modeling and FN-detector design using FSA framework

---

$F_i$ ,  $1 \leq i \leq p$ , stands for the  $i^{\text{th}}$  fault status. The image  $x(C)$  of  $C$  under  $x$  is called the fault label of the state  $x$ . The state mapping is modified as  $(S \cup C) \rightarrow \{0, 1\}$ . It may be noted that status variables are dummy variables only used for modeling and are unmeasurable. It may be noted that if status variables are measurable then failure detection problem is trivial.

The occurrence of a fault (on the fly)  $F_i$  is captured by a transition from a state  $x_1$  with  $x_1(C) = N$  (in normal sub-system) to a state  $x_2$  with  $x_2(C) = F_i$  (in  $F_i$  sub-system). For a fault  $F_i$  such a transition is called  $s_i$ -transition (i.e., start of fault  $F_i$ ) and is represented as  $s_i = \langle x_1, T, x_2 \rangle$ , where  $x_1(C) = N, x_2(C) = F_i$ . Firing of an  $s_i$ -transition does not depend on input variables, rather it is “ $T$ ” implying “always true”. Due to occurrence of an  $s_i$ -transition, only the status variable changes its value from  $N$  to  $F_i$  and all the other variables remain unchanged. Thus,  $s_i$ -transitions are unmeasurable. In synchronous circuits the state register changes only at the triggering edges of the clock depending upon the inputs. So, even if faults occur on the fly (in the NSF block) their effects are not manifested before the next active clock edge when the circuit moves to a state that is different from the normal condition. <sup>1</sup>

Now we repeat the definitions of some terminologies in brief which are related to the FSA model  $G$ . The detailed about the definitions can be found in Chapter 3, Section 3.2.

**Definition 4.1.  $N$ -state and  $F_i$ -state:** A  $G$ -state is called normal (i.e.,  $N$ -state), denoted as  $x_{0j}$ ,  $j \geq 1$ , if  $x_{0j}(C) = N$ . The set of all normal states is denoted as  $X_N$ .

A  $G$ -state is called an  $F_i$ -state, denoted as  $x_{il}$ ,  $l \geq 1$ , if  $x_{il}(C) = F_i$ . The set of all  $F_i$  states is denoted as  $X_{F_i}$ .

**Definition 4.2. Normal  $G$ -transition and Faulty  $G$ -transition:** A  $G$ -transition  $\langle x, \sigma, x^+ \rangle$  is called a Normal (Faulty  $F_i$ )  $G$ -transition if  $x, x^+ \in X_N(X_{F_i})$ .

**Definition 4.3. Measurement equivalent states:** Two states  $x_1$  and  $x_2$  are measurement equivalent, denoted as  $x_1 E x_2$ , if  $x_1|_S = x_2|_S$ ;  $x_1|_S$  denotes the projection (i.e., values) of the state variables in  $S$ .

**Definition 4.4. Measurement equivalence transitions:** Two transitions  $\tau_1 = \langle x_1, \sigma_1, x_1^+ \rangle$  and  $\tau_2 = \langle x_2, \sigma_2, x_2^+ \rangle$  are measurement equivalent, denoted as  $\tau_1 E \tau_2$ , if  $x_1|_S = x_2|_S$ ,  $x_1^+|_S = x_2^+|_S$  and  $\sigma_1|_I = \sigma_2|_I$ .

---

<sup>1</sup>For explanation of our proposed OLT scheme we consider faults only in the NSF block. A bridging fault in the flip-flops can be represented using a bridging fault involving the input and output lines of the NSF block. It may be noted from Figure 3.1 that outputs and (secondary) inputs of NSF block are input lines and output lines respectively, of the flip-flops.

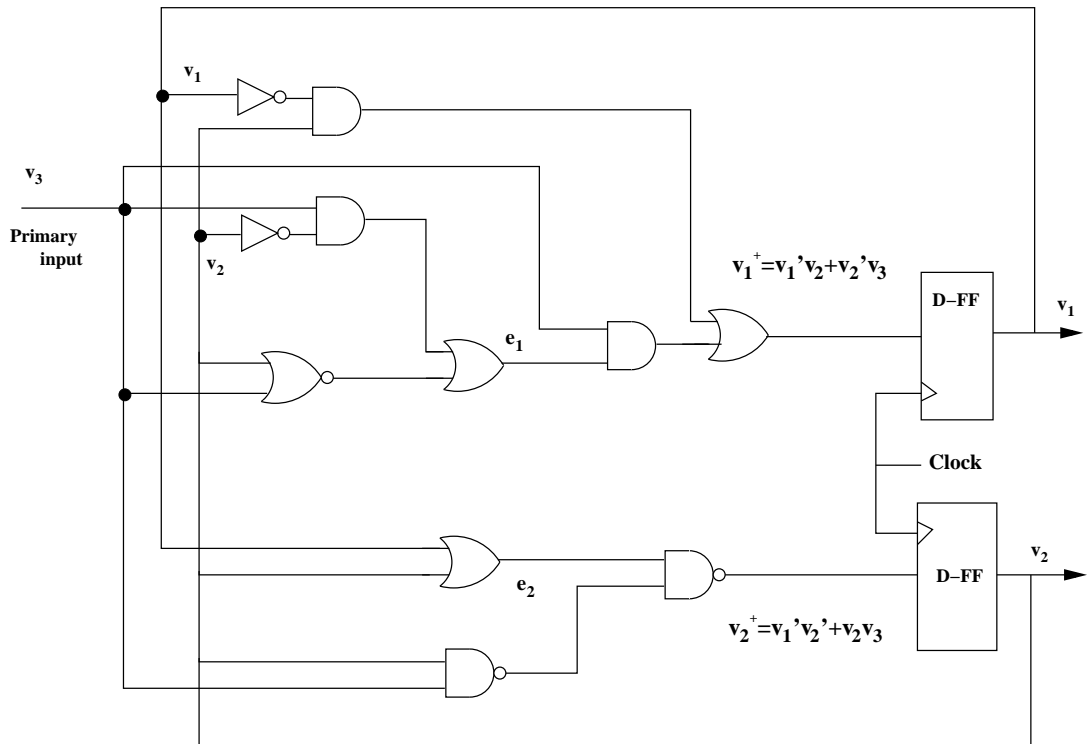


Figure 4.1: A simple sequential circuit.

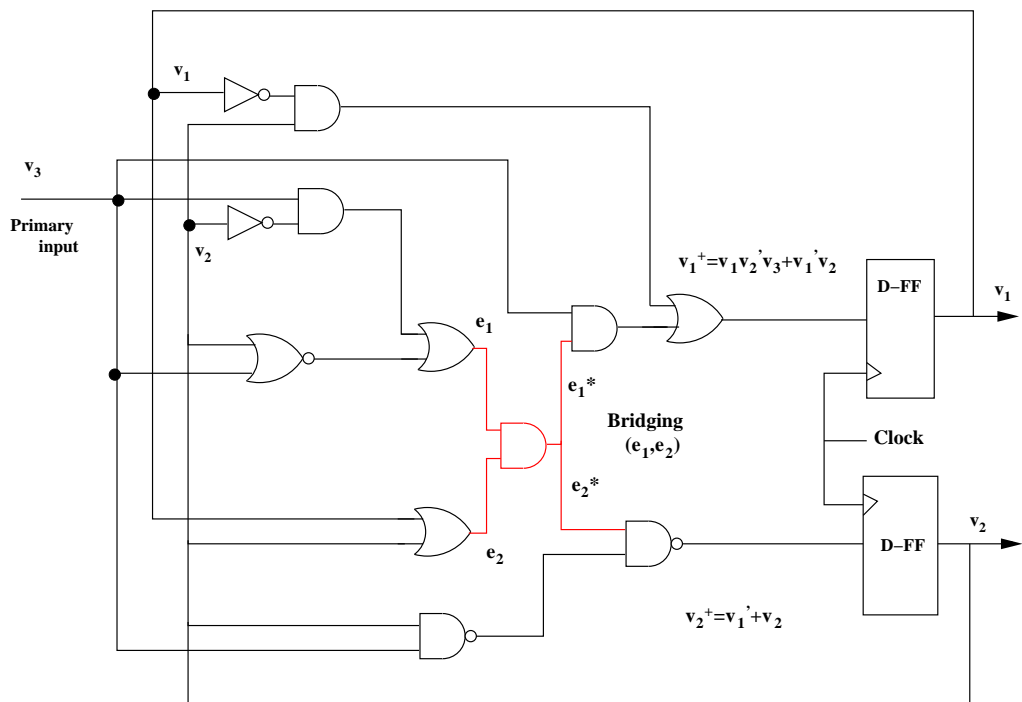


Figure 4.2: Sequential circuit with AND-bridging between lines  $e_1$  and  $e_2$ .

## 4.2 Circuit modeling and FN-detector design using FSA framework

---

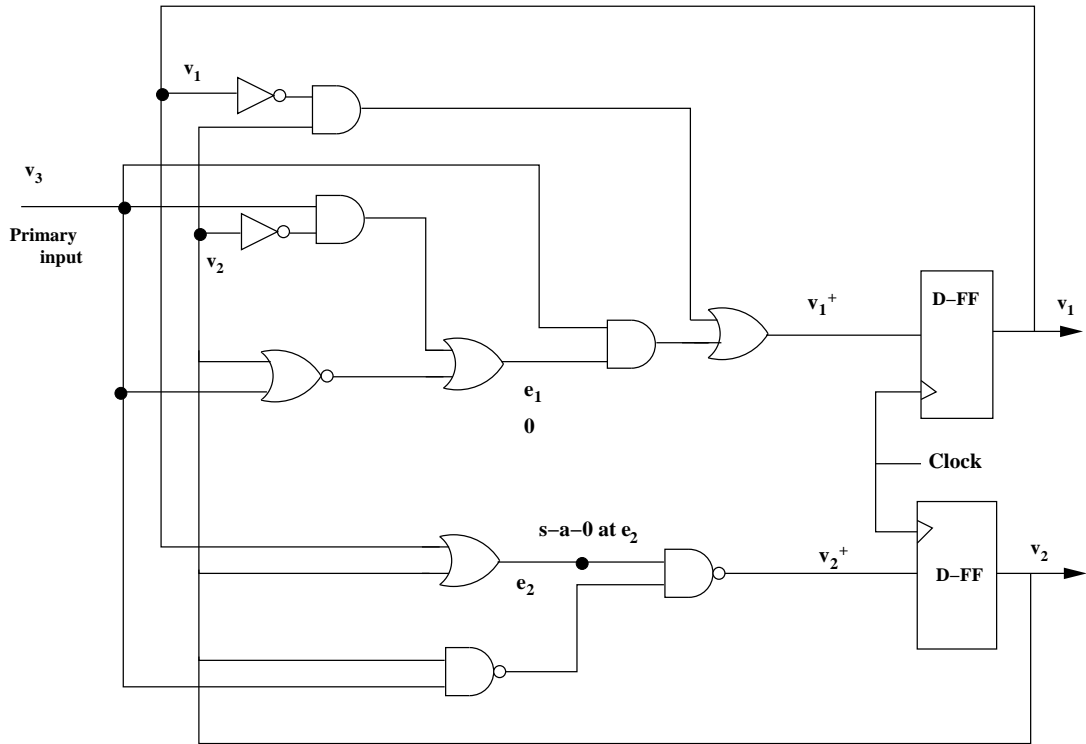
In this work, we have taken a simple sequential circuit, shown in Figure 4.1, for illustration of the theory. We assume a wired AND-bridging fault (denoted as  $F_1$ ) between lines  $e_1$  and  $e_2$ , as shown in Figure 4.2. The lines marked  $e_1^*$  and  $e_2^*$  represent the values of lines  $e_1$  and  $e_2$  under the fault. All possible values at  $e_1e_2$  are 00, 01, 10, 11. Among all these four possibilities, 00 and 11 do not lead to any difference in logic values at any net in the circuit under fault condition compared to the normal condition. However, if  $e_1e_2 = 01$  then  $e_1^*e_2^* = 00$  and if  $e_1e_2 = 10$  then  $e_1^*e_2^* = 00$ . So, the wired AND-bridging fault between two lines  $e_1$  and  $e_2$  is active only when these lines have different logic values. When  $e_1e_2 = 01$ , then fault is manifested through only line  $e_2^*$ , because  $e_1 = e_1^* = 0$  (i.e., there is no change in  $e_1^*$  compared to  $e_1$  under fault) however,  $e_2 = 1 \neq e_2^* = 0$  (i.e., there is change in  $e_2^*$  compared to  $e_2$  under fault). In a similar way, when  $e_1e_2 = 10$ , then fault is manifested through only line  $e_1^*$ . So, it can be stated that in wired AND-bridging fault the line which has the logic value 0 (e.g.,  $e_2$  when  $e_1e_2 = 10$ ) is “*dominating*” over the line, called “*dominated*” (e.g.,  $e_1$  when  $e_1e_2 = 10$ ), which has the value 1. In other words, in wired AND-bridging fault the logic value at the *dominating* line is 0 which overrides the value at the *dominated* line by pulling it from 1 to 0. This implies that wired AND-bridging fault results in s-a-0 fault at the *dominated* line when the *dominating* line has the value 0.

Thus, test patterns for detecting the wired AND-bridging fault between lines  $e_1$  and  $e_2$  involve the following steps:

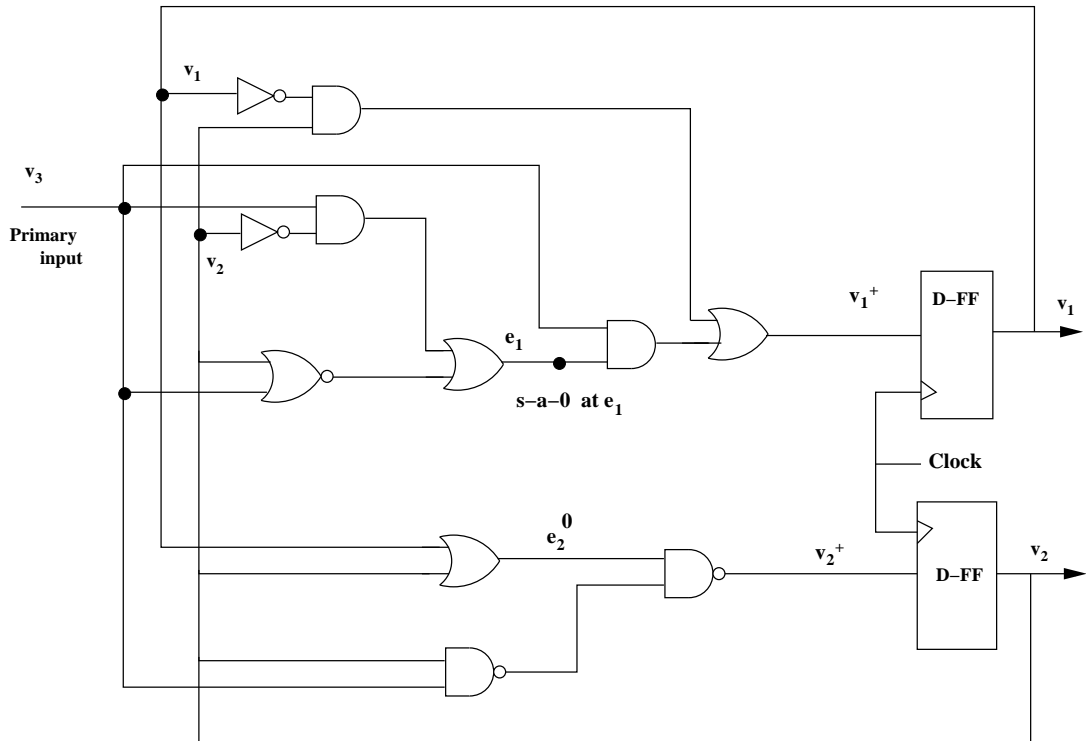
- All input patterns which result in  $e_1 = 0$  (*dominating*) and detect s-a-0 fault at  $e_2$  (*dominated*), by propagating the fault effect at an output. This is illustrated in Figure 4.3(a).
- All input patterns which result in  $e_2 = 0$  (*dominating*) and detect s-a-0 fault at  $e_1$  (*dominated*), by propagating the fault effect at an output. See Figure 4.3(b).

**Note:** In this chapter we will limit our discussion only on wired AND-bridging fault. The mechanism for AND-bridging fault can be directly applied for OR-bridging fault by applying the duality principle. For example, in case of OR-bridging the *dominating* line has a value of 1 and it pulls the *dominated* line from 0 to 1, i.e., a s-a-1 fault.

As shown in Figure 4.1, under normal condition the expressions for the NSF block outputs are  $v_1^+ = v_1'v_2 + v_2'v_3$  and  $v_2^+ = v_1'v_2' + v_2v_3$ . The presence of the bridging fault changes the output expressions to  $v_1^+ = v_1v_2'v_3 + v_1'v_2$  and  $v_2^+ = v_1' + v_2$  (Figure 4.2). Figure 4.4 shows the FSA model for the normal and faulty behavior of the circuit. In the circuit modeling, states for the normal submachine will be designated as  $x_{0j}$ ,  $1 \leq j$ , and those of the  $i^{th}$  fault (i.e.,  $F_i$ -submachine) are designated as  $x_{ij}$ ,  $1 \leq j$ ; likewise for the transitions. In this example



(a) AND-bridging where  $e_1$  dominates  $e_2$ .



(b) AND-bridging where  $e_2$  dominates  $e_1$ .

Figure 4.3: AND-bridging fault

## 4.2 Circuit modeling and FN-detector design using FSA framework

as there is a single fault denoted as  $F_1$ , the faulty states and transitions are designated as  $x_{1j}$ ,  $1 \leq j$  and  $\tau_{1j}$ ,  $1 \leq j$ , respectively. The occurrence of the fault is captured by the transitions marked  $s_1$ .

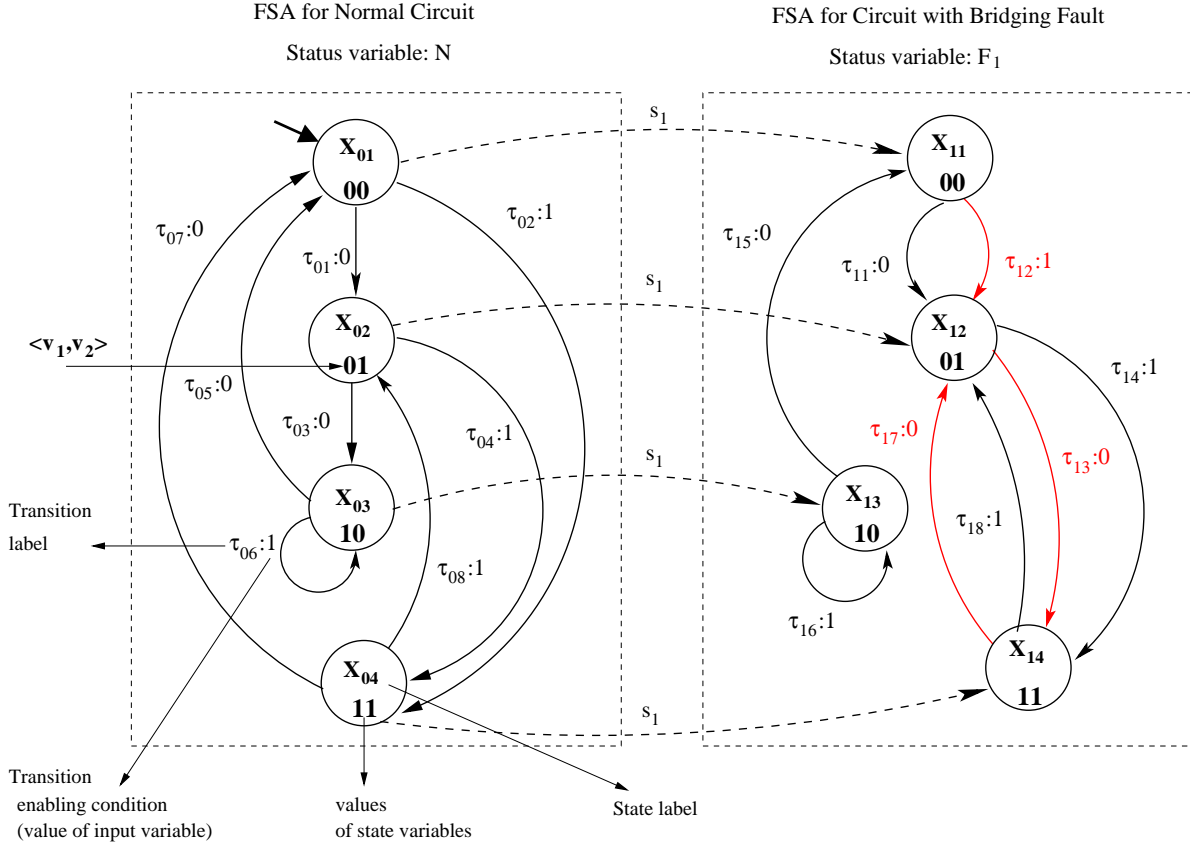


Figure 4.4: FSA model for the circuit (of Figure 4.1) under normal and faulty condition

Now comparing the transitions under normal condition with the corresponding ones after the bridging fault in the FSA model given in Figure 4.4, it is noted that there are three transitions that reflect a change in behavior after bridging fault. These transitions are  $\tau_{12} : \langle x_{11}, 1, x_{12} \rangle$ ,  $\tau_{13} : \langle x_{12}, 0, x_{14} \rangle$  and  $\tau_{17} : \langle x_{14}, 0, x_{12} \rangle$ . This is because, for transition  $\tau_{12} : \langle x_{11}, 1, x_{12} \rangle$  the corresponding transition in normal condition is  $\tau_{02} : \langle x_{02}, 1, x_{04} \rangle$ , where  $x_{01}|_S = x_{11}|_S = 00$ ,  $\sigma_{02} = \sigma_{12} = 1$  but  $x_{04}|_S (= 11) \neq x_{12}|_S (= 01)$ . In simple words, in these three transitions, for a given state and input variable combination the values of the state variables in the next state are different in the normal model compared to its faulty counterpart. Such transitions that result in manifestation of faults are termed as *FD*-transitions (i.e., Fault Detecting transitions). All other transitions in the normal model have an equivalent counterpart in the faulty model; e.g.,  $\tau_{01} E \tau_{11}$  because,  $\tau_{01} : \langle x_{01}, 0, x_{02} \rangle$ ,  $\tau_{11} : \langle x_{11}, 0, x_{12} \rangle$  and  $x_{01}|_S = x_{11}|_S = 00$ ,  $\sigma_{01} = \sigma_{11} = 0$ ,  $x_{02}|_S = x_{12}|_S = 01$ .



### 4.3 Efficient construction of $FN$ -detector for bridging faults

---

$$G_{FN} = \langle Z, z_0, \Sigma_Z, \delta_Z, Y_Z, z_f \rangle, \quad (4.2)$$

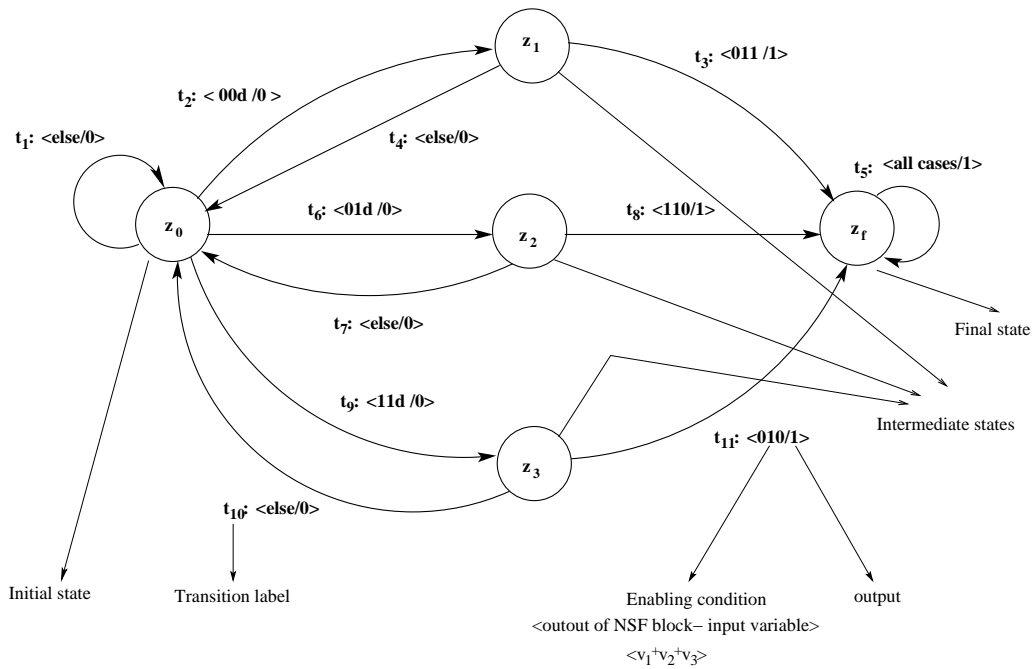
where  $Z$  is the set of states,  $z_0$  is the initial state,  $\Sigma_Z = X \times \Sigma$  is the input alphabet,  $\delta_Z : Z \times \Sigma_Z \rightarrow Z$  is the transition function,  $Y_Z : Z \times \Sigma_Z \rightarrow \{0, 1\}$  is the output function and  $z_f$  is the final state.

Figure 4.6 represents the state transition diagram of the  $FN$ -detector for the FSA model of the circuit under consideration. As discussed before the  $FD$ -transitions are  $\tau_{12}, \tau_{13}$  and  $\tau_{17}$ . In the detector, transitions  $t_1, t_2, t_3, t_4, t_5$  are responsible for checking if  $FD$ -transition  $\tau_{12}$  has occurred in the CUT. The detector starts from its initial state  $z_0$ . Following that, if the NSF block outputs  $\langle v_1^+, v_2^+ \rangle = 00$  then the CUT is going to be in state  $x_{11} = \text{initial}(\tau_{12})$  (if fault has occurred) or  $x_{01} = \text{initial}(\tau_{02})$  (if CUT is normal) in the next clock edge. The detector reaches state  $z_1$  by the transition labeled  $t_2$  with the same clock edge. So the detector reaches  $z_1$  along with the CUT reaching  $x_{11}$  or  $x_{01}$ . It may be noted that enabling condition of  $z_1$  is  $00d$ , which implies that measured values of  $v_1^+, v_2^+ = 00$  and  $v_3$  is don't care ( $d$ ). In simple words, for each  $FD$ -transition, in the  $FN$ -detector there is a transition from the initial state to intermediate state with enabling condition as "NSF outputs equal to values of state variables of the initial state of the  $FD$ -transition". From state  $z_1$ , the detector needs to verify whether transition  $\tau_{12}$  is going to occur in the CUT in the next clock edge. The transition  $t_3$  from state  $z_1$  corresponds to this fact because enabling condition of  $t_3$  is  $011$ , which implies NSF block outputs as  $v_1^+ = 0, v_2^+ = 1$  and primary input as  $v_3 = 1$ . Thus, the transition  $t_3$  leads the  $FN$ -detector to the final state  $z_f$  yielding output 1, indicating that the bridging fault has occurred. If the enabling condition of  $t_3$  is not satisfied in state  $z_1$  (i.e.,  $v_1^+ = 1, v_2^+ = 1$  and primary input as  $v_3 = 1$ , corresponding to transition  $\tau_{02}$ ), the  $FN$ -detector moves back to the initial state by the transition  $t_4$ . Once the final state  $z_f$  is reached, the  $FN$ -detector remains in that state forever maintaining the output as 1 since the faults are assumed to be permanent.

In a similar way, the working of the detector for the other two  $FD$ -transitions  $\tau_{13}$  and  $\tau_{17}$  can be explained; transitions  $t_1, t_6, t_7, t_8, t_5$  and  $t_1, t_9, t_{10}, t_{11}, t_5$  correspond to  $\tau_{13}$  and  $\tau_{17}$ , respectively.

### 4.3 Efficient construction of $FN$ -detector for bridging faults

While the procedure discussed in the last section can construct the  $FN$ -detector but its complexity is prohibitively high. The reason is selection of the  $FD$ -transitions from the


 Figure 4.6:  $FN$ -detector for the FSA model of the circuit shown in Figure 4.4

FSA model in which the number of states can be exponential with respect to the number of flip-flops in the CUT. In this section we propose an efficient scheme for construction of  $FN$ -detector. The technique involves several optimization steps namely, partitioning the CUT into smaller sub-parts based on cones of influence, determining  $FD$ -transitions without explicitly constructing the FSA models using OBDD, etc., which have enabled design of on-line testers for circuits having of the order of about ten thousand gates.

### 4.3.1 Partition of the CUT into sub-circuits using cones of influence

From the basic architecture of a sequential circuit with on-line tester (shown in Chapter 3, Figure 3.1), it may be noted that the NSF block of the CUT has two types of inputs; primary inputs (I) and the secondary inputs (S). The secondary inputs are fed back from the outputs of the flip-flops and represent the present state of the CUT. The outputs of the NSF block are the next state of the CUT and denoted as  $S^+$ . So, the NSF block can be described as  $\mathbb{S} = \langle \Sigma_S, S^+ \rangle$ , where  $\Sigma_S = X \times \Sigma = v_1, v_2, \dots, v_k, v_{k+1}, \dots, v_n$  is the NSF input and  $S^+ = \{v_1^+, v_2^+, \dots, v_k^+\}$  is the NSF output. An input combination  $\sigma_s \in \Sigma_S$  is a mapping from  $V = \{v_1, v_2, \dots, v_n\}$  to  $\{0, 1\}$ , which can be represented as an  $n$ -tuple  $\langle \sigma_s(v_1), \sigma_s(v_2), \dots, \sigma_s(v_k), \sigma_s(v_{k+1}), \dots, \sigma_s(v_n) \rangle$ , where the first  $k$  members correspond to

### 4.3 Efficient construction of $FN$ -detector for bridging faults

---

secondary inputs (present state) and the remaining  $(n - k)$  members correspond to primary inputs. For each  $v_j^+ \in S^+, 1 \leq j \leq k, v_j^+ : \Sigma_S \rightarrow \{0, 1\}$ .

Let  $S_0^+ = \{v_{01}^+, v_{02}^+, \dots, v_{0k}^+\}$  denote the NSF outputs under normal condition and  $S_i^+ = \{v_{i1}^+, v_{i2}^+, \dots, v_{ik}^+\}$  denote the outputs under bridging fault  $F_i, 1 \leq i \leq p$ , where  $p$  is the number of possible bridging faults. The  $j^{\text{th}}$   $FD_i$ -transition  $\tau_{ij} = \langle x_{ij}, \sigma_{ij}, x_{ij}^+ \rangle$  can be determined from the NSF block directly, without explicit construction of the FSA model, in the manner discussed below.

For a given bridging fault  $F_i$ , determine an input pattern of the NSF block, i.e.,  $\sigma_s \in \Sigma_S$  which sensitizes the fault and propagates the effect through at least one of the NSF outputs, i.e., if output of the faulty ( $F_i$ ) NSF block for input  $\sigma_s$  is  $\langle v_{i1}^+(\sigma_s), v_{i2}^+(\sigma_s), \dots, v_{ik}^+(\sigma_s) \rangle$ , then  $\exists m, 1 \leq m \leq k$ , such that  $v_{im}^+(\sigma_s) \neq v_{0m}^+(\sigma_s)$ . It may be noted that the first  $k$ -tuple of  $\sigma_s = \text{initial}(\tau_{ij}) = x_{ij}$ . The second  $(n - k)$ -sub-tuple of  $\sigma_s = \text{input}(\tau_{ij})$  and the output of the NSF block ( $\langle v_{i1}^+(\sigma_s), v_{i2}^+(\sigma_s), \dots, v_{ik}^+(\sigma_s) \rangle$ ) gives  $\text{final}(\tau_{ij}) = x_{ij}^+$ .

Given a netlist description of the NSF block of the CUT, the exhaustive set of  $FD$ -transitions for the fault  $F_i$  (i.e.,  $\mathfrak{S}_{FD_i}$ ) can be generated as follows:

1. For all  $\sigma_s \in \Sigma_S$  simulate the NSF block under normal condition to determine the output response  $\langle v_{01}^+(\sigma_s), v_{02}^+(\sigma_s), \dots, v_{0k}^+(\sigma_s) \rangle$ .
2. Insert the bridging fault ( $F_i$ ) at proper position in the NSF.
3. Simulate the NSF block with the fault  $F_i$  with each input  $\sigma_s$  to get the corresponding output response  $\langle v_{i1}^+(\sigma_s), v_{i2}^+(\sigma_s), \dots, v_{ik}^+(\sigma_s) \rangle$ .
4. Select those  $\sigma_s$  such that  $\exists m, 1 \leq m \leq k, v_{im}^+(\sigma_s) \neq v_{0m}^+(\sigma_s)$ . All such  $\sigma_s$  conjoined with the outputs of the NSF block (for those  $\sigma_s$ ), comprise the exhaustive set of  $FD_i$ -transitions.
5. Repeat Steps 2 – 4 for all possible bridging faults.

The complexity of the above procedure for determining the exhaustive set of  $FD$ -transitions is exponential with respect to the number of inputs of the NSF block (i.e.,  $O(2^n)$ ) because  $|\Sigma_S| = 2^n$ . In case of reasonably complex VLSI circuits,  $n$  is of the order of thousands and therefore there is a requirement of optimization techniques for exhaustive test pattern generation. In this work, we address the issue using two techniques (i) divide the NSF into sub-circuits using the principle of “cones of influence” with respect to the NSF output lines. This technique divides the problem into sub-problems thereby lowering complexity; (ii) OBDDs [16] have been used for all Boolean function operations required for test pattern generation, checking if a pattern creates oscillation, etc.

---

### 4.3 Efficient construction of $FN$ -detector for bridging faults

---

A combinational circuit can be represented as a Directed Acyclic Graph (DAG) where a gate is represented by a node, the inputs to the gate are represented by directed edges into the node and the gate outputs are represented by directed edges out from the node. The nets in the circuit are represented by edges in the DAG. In this graph model, there are also nodes representing primary inputs (called as source nodes) and primary outputs (called sink nodes). The DAG representation of a circuit is defined as a tuple  $\langle N, E \rangle$ , where  $N$  is the set of nodes and  $E$  is the set of edges. An edge  $e \in E$  is denoted by a tuple  $\langle n_1, n_2 \rangle, n_1, n_2 \in N$ . The node set is partitioned into three subsets— $N_{Si}$ : set of sink nodes (for primary outputs),  $N_{Sc}$ : set of source nodes (for primary inputs) and  $N_I$ : set of intermediate nodes (for gates). There is no input edges into the source nodes and no output edges from the sink nodes.

A cone of influence of a net is a sub-circuit, which contains all the gates, nets and inputs that are transitive fan-ins of the net (for which cone is being computed). Given a DAG  $\langle N, E \rangle$  of a combinational circuit, Algorithm 4.1 generates cones (i.e., sub-graphs of  $\langle N, E \rangle$ ) corresponding to a net  $e_1$ .

---

**Algorithm 4.1** Algorithm for generation of cone of influence for a net  $e_1$ .

---

**Input:**  $\langle N, E \rangle$ : DAG representation of the circuit

$e_1$ : Net for which cone is to be generated.

**Output:**  $gate\_cones(e_1)$ : set of gates in cone for  $e_1$

$net\_cones(e_1)$ : set of nets in cone for  $e_1$

Create  $\langle N', E' \rangle$ : Modified DAG of  $\langle N, E \rangle$  where direction of all edges are reversed;

$node\_cones(e_1) \leftarrow \phi$

$edge\_cones(e_1) \leftarrow \phi$

Determine the node  $n_{e_1}$ , such that  $\langle n_{e_1}, n \rangle$ , where  $n \in N$ , is the edge corresponding to  $e_1$ ;

*/\*  $n_{e_1}$  is the node from which the edge corresponding to net  $e_1$  emanates \*/*

Perform Breadth First Search (BFS) in  $\langle N', E' \rangle$ , where root node is  $n_{e_1}$ ;

$node\_cones(e_1) \leftarrow$  all gates corresponding to nodes visited in the BFS traversal;

$edge\_cones(e_1) \leftarrow$  all nets corresponding to edges visited in the BFS traversal;

---

Using the above algorithm for each of the NSF outputs, it can be divided in cones. Following that, OBBD based Boolean function manipulation techniques would be used to generate the  $FD$ -transitions for the bridging faults. If the bridging fault is between two nets from different cones then only those two cones need to be considered at a time for generating the  $FD$ -transitions. However, in case of faults involving nets from a single cone, OBBDs need to operate only on a single cone at a time. So, partitioning using cones of influence limits the size of the CUT that needs to be handled at a time to a great extent.

### 4.3 Efficient construction of $FN$ -detector for bridging faults

---

In the next two subsections we discuss in details the OBDD based scheme of generating  $FD$ -transitions for non-feedback bridging faults and feedback bridging faults, respectively.

#### 4.3.2 OBDD based procedure for generation of exhaustive set of $FD$ -transitions for non-feedback bridging faults

In this section we discuss the procedure for applying OBDD for generating the exhaustive set of  $FD$ -transitions for a given non-feedback bridging fault  $F_i$ , between two lines  $e_1$  and  $e_2$ . As the fault is non-feedback,  $e_1$  does not lie in cone of influence of  $e_2$  and vice versa. Initially, the normal circuit NSF is partitioned using cones of influence for each of the NSF output lines. Let  $e_1$  be the *dominated* line and  $e_2$  be the *dominating* line.  $F_i$  is introduced in the NSF block by inserting s-a-0 fault at the *dominated* line. Then the faulty NSF is partitioned into cones for each of its outputs and those cones are selected which comprise the *dominated* line. For each of these selected cones the following OBDD based operations generate the set of  $FD$ -transitions for the fault.

1. Let the cone for  $v_m^+$  be one of the selected cones. Generate an OBDD for this cone. This OBDD represents the Boolean function corresponding to  $v_m^+$  under s-a-0 fault at the *dominated* line; let this OBDD be termed as “faulty OBDD”.
2. Consider the cone for NSF output  $v_m^+$  under normal condition (whose Boolean function is  $v_{0m}^+$ ) and represent it using an OBDD; it is termed as “normal OBDD”.
3. The two OBDDs (normal and faulty) are XORed and “satisfy-all-1” operation is applied on the resulting XORed OBDD. The “satisfy-all-1” operation on an OBDD generates all paths in terms of values of variables (of the Boolean function it represents) that lead to leaf node with value 1. In the XORed OBDD, the paths leading to leaf node with value 1 correspond to input patterns of the NSF cone under consideration, which result in different values at NSF output  $v_m^+$ , under faulty (s-a-0 fault at *dominated* line) condition compared to normal condition. Let  $IP_{s-a-0,dominated}$  be the set of such input patterns.
4. Generate a cone for *dominating* line in the NSF corresponding to the normal circuit. Let the Boolean function corresponding to the *dominating* line be  $v_{dominating}$ , which is represented using another OBDD, termed as “dominating OBDD”.
5. The “satisfy-all-0” operation is applied on the dominating OBDD, which generates all the input patterns for which the value at the *dominating* line is 0. The set of such input patterns is  $IP_{0,dominating}$ .

6. The required test patterns that detect  $F_i$  (drives 0 to *dominating* line and detects s-a-0 fault at *dominated* line) is obtained by the intersection of  $IP_{s-a-0,dominated}$  and  $IP_{0,dominating}$ . These test patterns can be mapped to the initial state and input of the  $FD_i$ -transitions. The final state of the  $FD_i$ -transitions can be obtained by applying these patterns to the faulty OBDD, because the fault is manifested at the NSF output  $v_m^+$ .

**Note:** Let  $\tau_{ij} = \langle x_{ij}, \sigma_{ij}, x_{ij} \rangle$  be the  $j^{th}$   $FD_i$ -transition that detects fault  $F_i$  through NSF output corresponding to  $v_m^+$ .  $\tau_{ij}$  can be obtained by mapping an input pattern (Step 3) to  $initial(\tau_{ij})$  conjoined with  $input(\tau_{ij})$ . The faulty output through the cone for  $v_m^+$  against the pattern under consideration (Step 6) can be mapped to  $final(\tau_{ij})$ . The values of state variables in  $initial(\tau_{ij})$  and input variables in  $input(\tau_{ij})$  are don't cares which do not fall under the cone of influence of  $v_m^+$ . Also, only one variable in  $final(\tau_{ij})$  namely,  $v_{im}^+$  that corresponds to the NSF block output through which the fault effect is monitored has a Boolean value of 0 or 1; rest are don't cares. We denote  $\tau_{ij}^m = \langle x_{ij}^m, \sigma_{ij}^m, x_{ij}^{+m} \rangle$  as the  $j^{th}$   $FD_i$ -transition which detects fault through cone corresponding to output  $v_m^+$ .

It may be noted that the procedure discussed above generates the exhaustive set of  $FD_i$ -transitions when  $e_1$  is the *dominated* line and  $e_2$  be the *dominating* line. This is only half of the task, and it needs to be repeated by changing the roles of  $e_1$  and  $e_2$ .

Now we explain the above procedure with the help of the circuit and the fault  $F_1$  shown in Figure 4.2. The partitioning of the NSF block (under normal condition) using cones of influence on the NSF outputs is shown in Figure 4.7. First we assume that  $e_1$  is the *dominated* line and  $e_2$  is the *dominating* line. The bridging fault under this case needs inserting a s-a-0 fault at line  $e_1$  and enforcing 0 at  $e_2$ . Following that, the faulty NSF is divided into cones on its outputs; this is shown in Figure 4.8(a). It may be observed from the figure that only cone for NSF output  $v_1^+$  comprises  $e_1$ . So OBDD based operations for generating the  $FD$ -transitions are to be done only on the cone for  $v_1^+$ .

The OBDD for cone of NSF output  $v_1^+$  under normal condition (expression  $v_1'v_2 + v_2'v_3$ ) is shown in Figure 4.9(a). Figure 4.9(b) illustrates the OBDD for NSF output  $v_1^+$  under s-a-0 condition at  $e_1$  (expression  $v_1'v_2$ ). The OBDD obtained after XORing the normal and faulty OBDDs is shown in Figure 4.9(c). The “satisfy-all-1” operation on the XORed OBDD generates the set  $IP_{s-a-0,dominated}$  as  $\{v_1 = 1, v_2 = 0, v_3 = 1; v_1 = 0, v_2 = 0, v_3 = 1\}$ . Here,  $e_2$  is the dominating line and  $v_{dominating} = v_1 + v_2$ , which is represented by the dominating OBDD shown in Figure 4.9(d). “satisfy-all-0” operation on this OBDD generates the set  $IP_{0,dominating}$  as  $\{v_1 = 0, v_2 = 0, v_3 = d\}$ , where  $d$  is don't care, implying  $IP_{0,dominating} = \{v_1 = 0, v_2 = 0, v_3 = 0; v_1 = 0, v_2 = 0, v_3 = 1\}$ . The intersection of

### 4.3 Efficient construction of $FN$ -detector for bridging faults

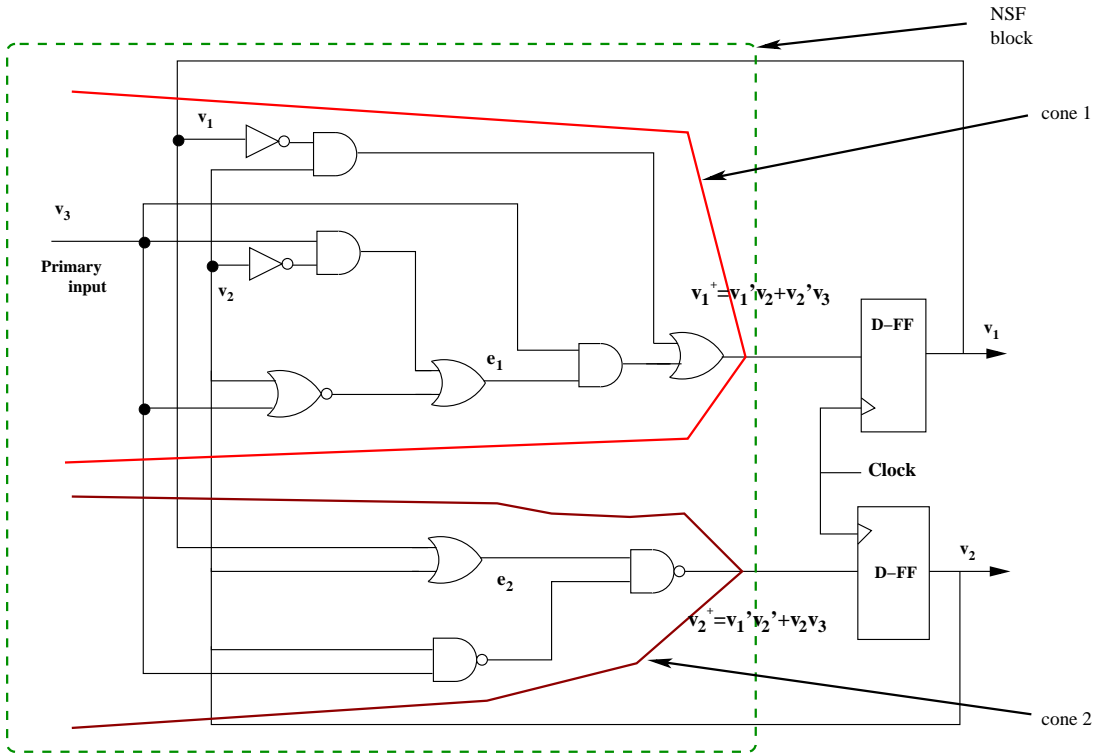


Figure 4.7: NSF (normal condition) partitioned using cones of influence on its outputs.

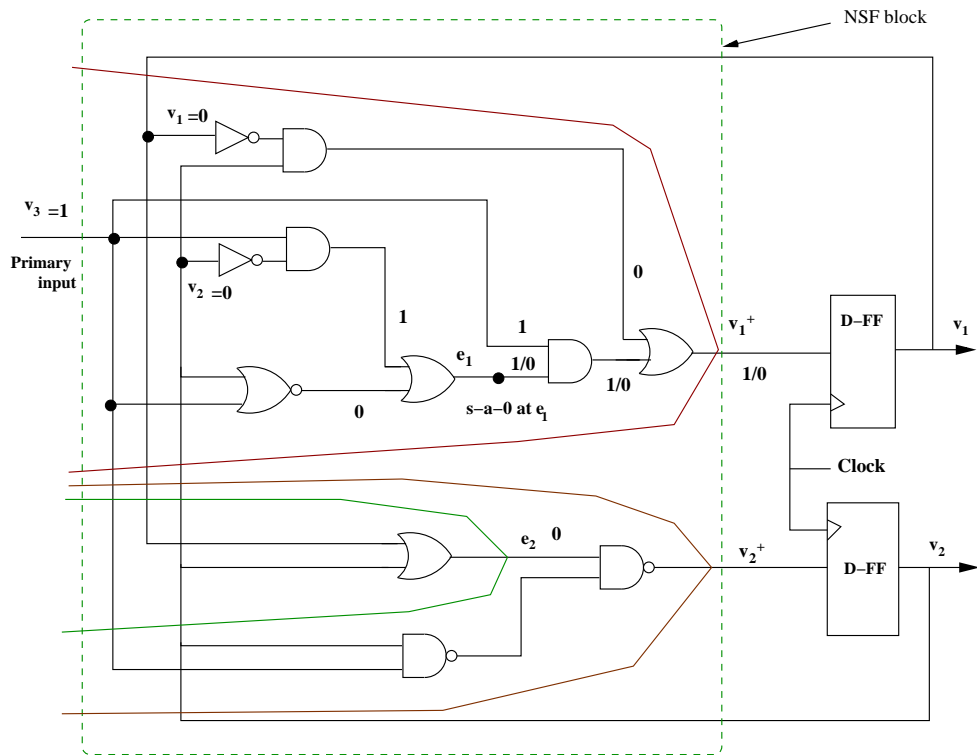
$IP_{s-a-0,dominated}$  and  $IP_{0,dominating}$  gives the set of test patterns as  $\{v_1 = 0, v_2 = 0, v_3 = 1\}$ . Signal values at the nets of the NSF block under s-a-0 fault at  $e_1$  for the test pattern  $\{v_1 = 0, v_2 = 0, v_3 = 1\}$  is shown in Figure 4.8(a). In the figure “1/0” implies that under normal condition (s-a-0 fault at  $e_1$ ) the signal value at the corresponding net is 1(0). The fault (s-a-0) manifestation at  $v_1^+$ , when  $\{v_1 = 0, v_2 = 0, v_3 = 1\}$  is obtained by applying the pattern to the faulty OBDD, which comes to be 0. So the  $FD_1$ -transition obtained from the input pattern and fault manifestation is  $\langle 00, 1, 0d \rangle$ , which corresponds to transition  $\tau_{12}$  (Figure 4.4).

In a similar way, we determine the remaining  $FD_1$ -transitions by reversing the roles of  $e_1$  and  $e_2$  (Figure 4.8(b)); the  $FD$ -transitions obtained are  $\langle 01, 0, d1 \rangle$  and  $\langle 11, 0, d1 \rangle$ , which correspond to  $\tau_{13}$  and  $\tau_{17}$ , respectively.

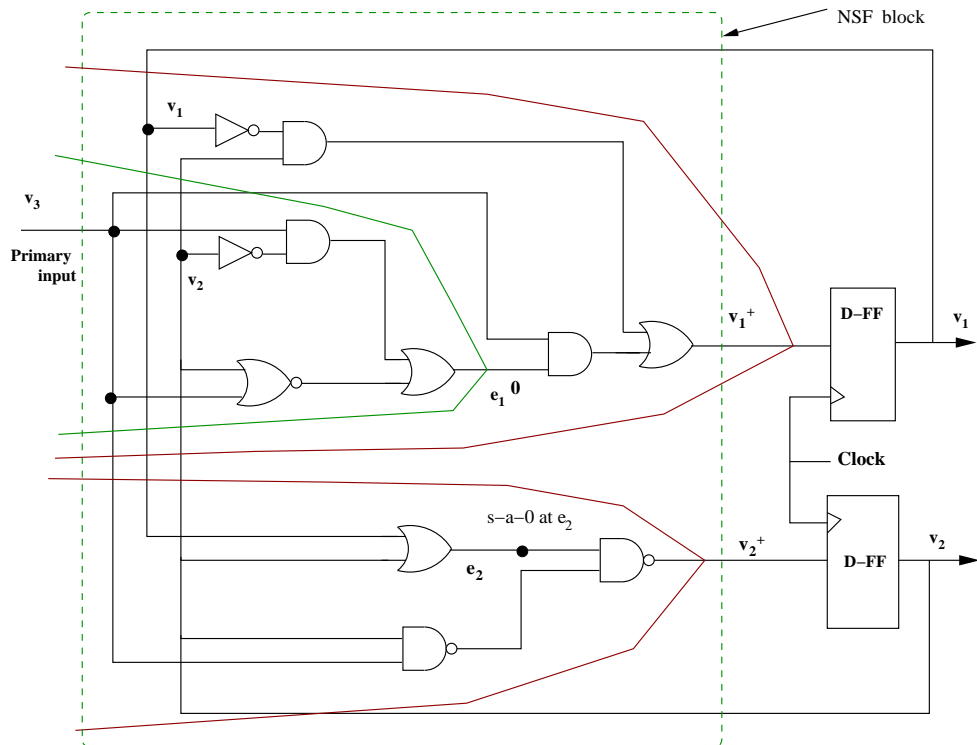
#### 4.3.3 OBDD based procedure for generation of exhaustive set of $FD$ -transitions for feedback bridging faults

As already discussed, the bridging between two lines is called feedback bridging if there exists at least one path between these two lines. We refer the two lines involved in the feedback

### 4.3 Efficient construction of $FN$ -detector for bridging faults



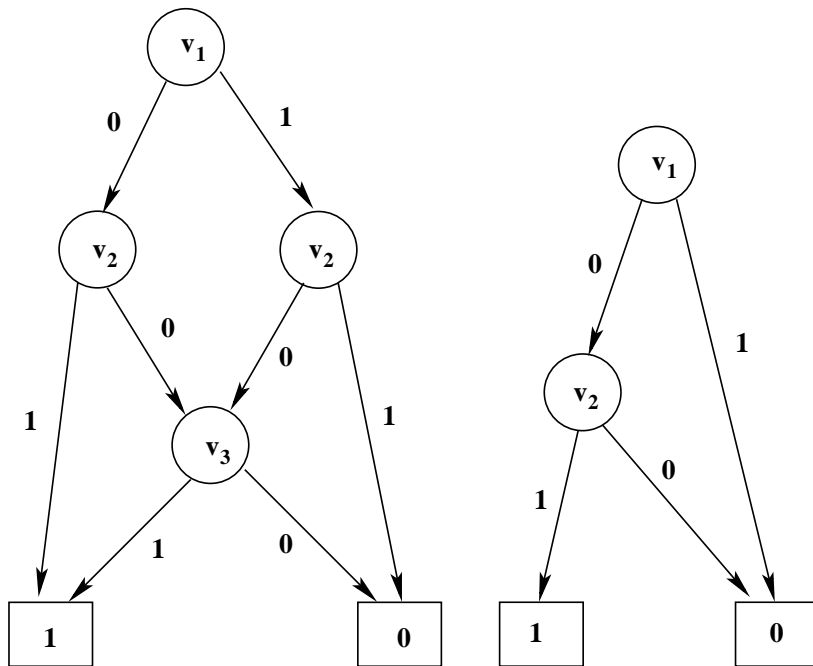
(a) NSF with fault, partitioned into cones, when  $e_2$  dominates  $e_1$ .



(b) NSF with fault, partitioned into cones, when  $e_1$  dominates  $e_2$ .

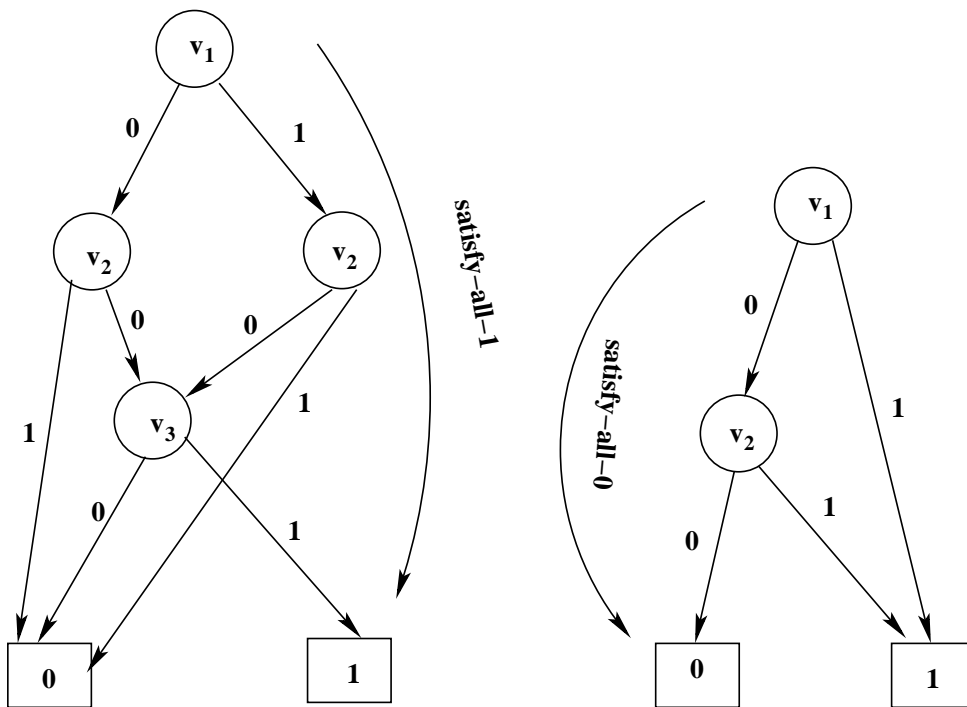
Figure 4.8: NSF with faults ( $e_2$  dominates  $e_1$  and  $e_1$  dominates  $e_2$ )

4.3 Efficient construction of  $FN$ -detector for bridging faults



(a) Normal OBDD for cone of NSF output  $v_1^+$ .

(b) Fault OBDD for cone of NSF output  $v_1^+$  (s-a-0 at  $e_1$ ).



(c) XORed OBDD for the normal and faulty OBDDs.

(d) Dominating OBDD for line  $e_2$ .

Figure 4.9: OBDDs for non-feedback bridging fault when  $e_2$  dominates  $e_1$

bridging fault as the *back line*( $b$ ) and the *front line*( $f$ ), where  $b$  is closer to the primary inputs and  $f$  is closer to the primary outputs. In other words, there is path from  $b$  to  $f$ . The procedures of generation of test patterns for feedback bridging faults are discussed in two parts. The first part discusses the procedure where  $f$  becomes the *dominating* line and  $b$  becomes the *dominated* line and the second part deals with the reverse of that.

**Part 1: Generation of exhaustive set of  $FD$ -transitions for feedback bridging fault– the *front line* dominates the *back line***

The procedure for generation of the exhaustive set of  $FD$ -transitions for feedback bridging faults (where  $f$  dominates  $b$ ) involves all the steps required for the non-feedback bridging faults (Subsection 4.3.2) namely, partitioning the normal NSF using cones of influence for each of the outputs, introduction of fault by inserting s-a-0 fault at the *dominated* line, partitioning the faulty NSF and finally generating the  $FD$ -transitions using OBDD based operations.

However, additional steps are required in this case of feedback bridging fault to determine if the  $FD$ -transitions cause oscillations. To elaborate, a test pattern that drives 0 to the *dominating* line (here  $f$ ) and detects s-a-0 fault at the *dominated* line (here  $b$ ) may not qualify to become an  $FD$ -transition, if the fault effect at line  $b$  propagates through line  $f$  and makes it 1. It is easy to observe that for sensitizing the fault, line  $f$  is driven to 0 and effect of s-a-0 fault at line  $b$  is propagated to the NSF output, however, if the fault effect makes  $f = 1$ , then there is oscillation.

The following steps based on OBDD are performed to check if the test patterns generated using the scheme for non-feedback bridging faults (Subsection 4.3.2) cause oscillations for the given feedback bridging fault where  $f$  dominates  $b$ .

Let  $TP$  be the set of test patterns obtained from the intersection of  $IP_{s-a-0,dominated}$  and  $IP_{0,dominating}$ .  $TP$  is obtained using the steps discussed in Subsection 4.3.2, for the case when  $e_1$ , the *dominated* line is  $b$  and  $e_2$ , the *dominating* line is  $f$ .

1. Generate a cone for the *dominating* line (i.e.,  $f$ ) in the faulty NSF (s-a-0 at  $b$ ). Let “dominating faulty OBDD” be the OBDD representation for the Boolean expression corresponding to the *dominating* line  $f$  under the fault. Apply the “satisfy-all-1” operation on the “dominating faulty OBDD”, which generates all the input patterns for which the value at *dominating* line  $f$  becomes 1 under the fault at *dominated* line  $b$ . The set of such input patterns be  $IP_{f=1,s-a-0\_at\_dominated}$ .
2. If there is a test patten  $tp$  in the intersection of  $TP$  and  $IP_{f=1,s-a-0\_at\_dominated}$ , then  $tp$

### 4.3 Efficient construction of $FN$ -detector for bridging faults

needs to be eliminated from the set  $TP$ . It may be noted that test pattern  $tp$ , implies (i) 0 in the *dominating* line  $f$  under normal condition, (ii) different values in the NSF output  $v_m^+$  under normal condition compared to s-a-0 fault at the *dominated* line  $b$ , (iii) however, under fault, the *dominating* line  $f$  is pulled to 1. So,  $tp$  results in oscillation under the fault.

The remaining set of test patterns in  $TP$  are mapped to  $FD$ -transitions.

A test pattern which remains in  $TP$  after the check implies (i) 0 in the *dominating* line  $f$  under normal condition as well as faulty condition, (ii) different values in the NSF output  $v_m^+$  under normal condition compared to s-a-0 fault at the *dominated* line  $b$ . So such a test pattern can detect the fault without oscillation.

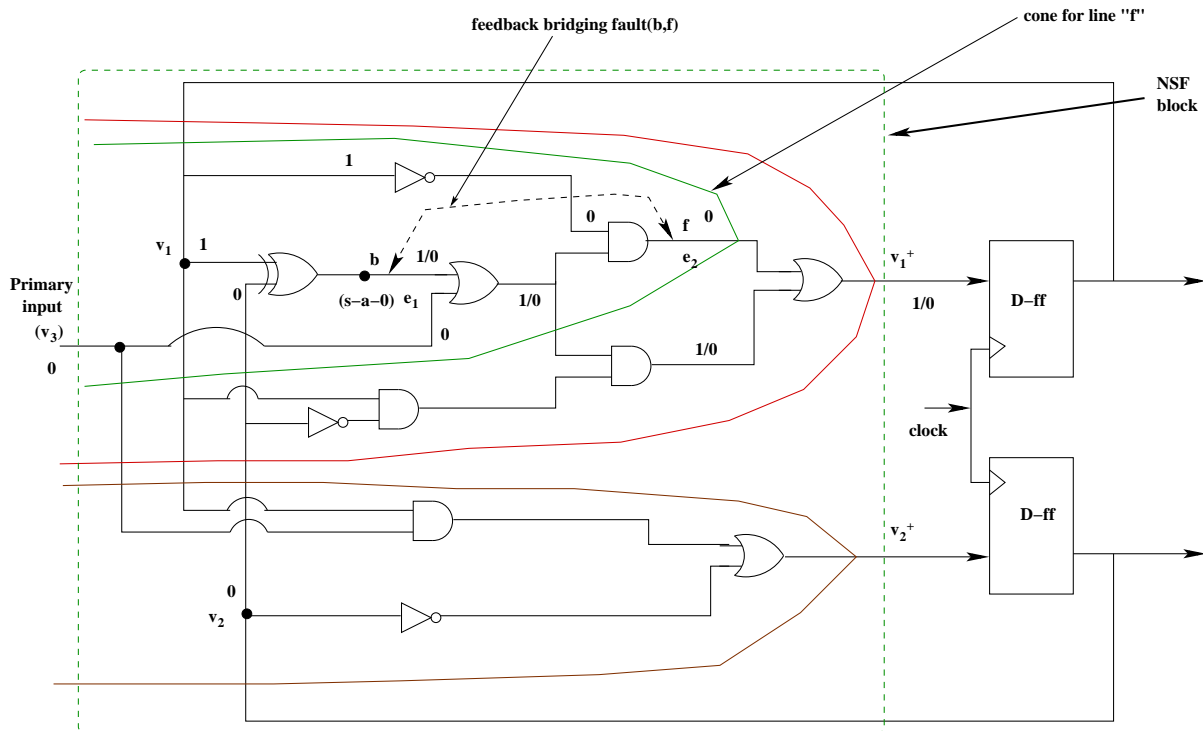
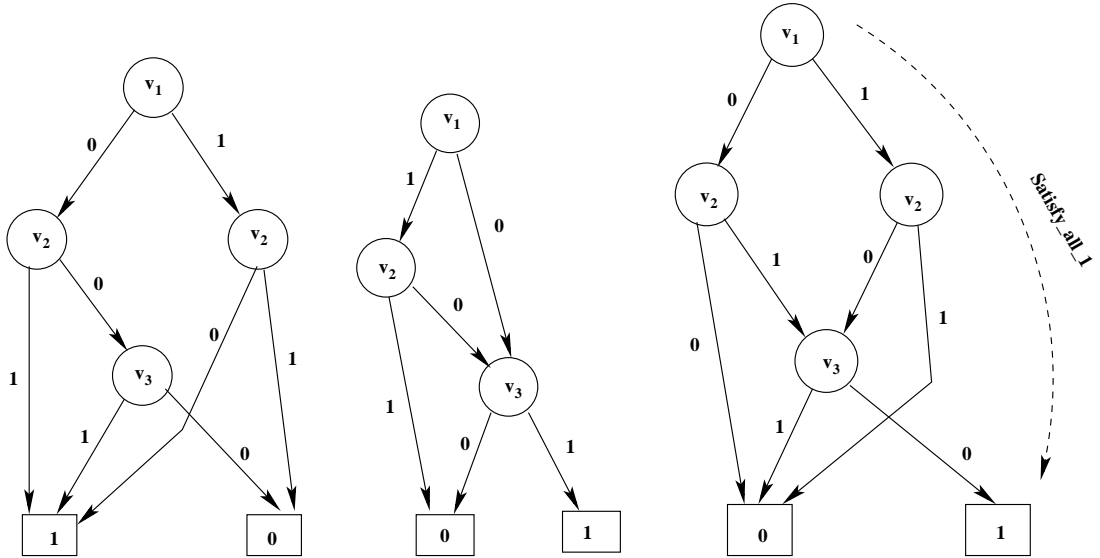


Figure 4.10: NSF with fault, partitioned into cones, when  $f$  dominates  $b$ .

Now we explain the above procedure with the help of a simple sequential circuit with feedback bridging fault  $F_1$  between lines  $e_1$  and  $e_2$ , as shown in Figure 4.10. Let  $e_1$  be the *dominated* line ( $b$ ) and  $e_2$  be the *dominating* line ( $f$ ). The partitioning of the NSF into cones on its outputs and on the *dominating* line are also shown in the figure.

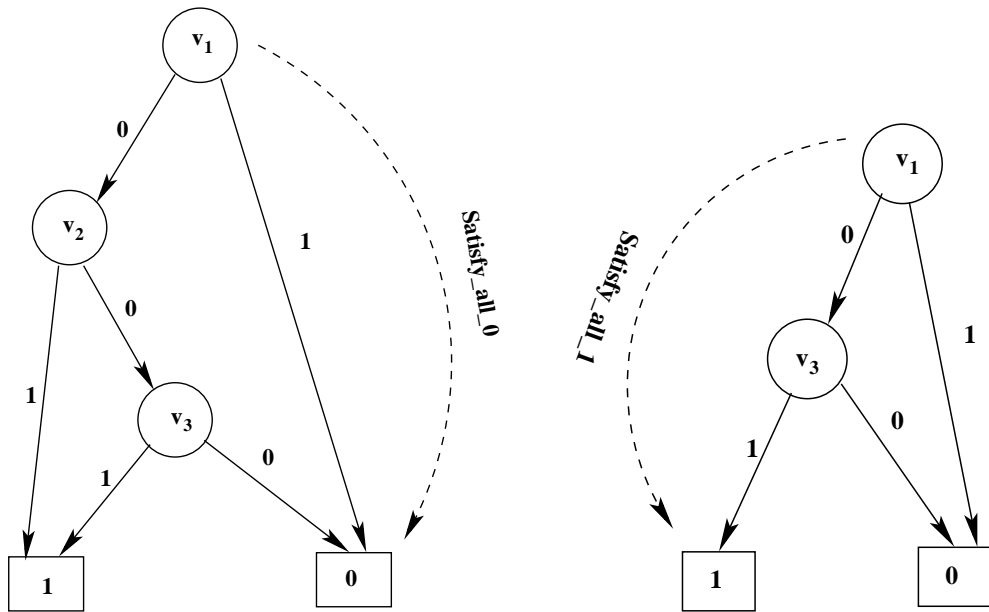
The OBDDs for the cone of NSF output  $v_1^+$  under normal condition (expression  $v_1v_2' + v_1'v_2 + v_1'v_3$ ) and s-a-0 condition at  $e_1$  (expression  $v_1'v_3 + v_1v_2'v_3$ ) are shown in Figure 4.11(a) and Figure 4.11(b), respectively. The OBDD obtained from XORing normal



(a) Normal OBDD for cone of NSF output  $v_1^+$ .

(b) Faulty OBDD for cone of NSF output  $v_1^+$  (s-a-0 at line  $b$ ).

(c) XORed OBDD for the normal and faulty OBDDs.



(d) Dominating OBDD for the line  $f$  under normal condition.

(e) Dominating faulty OBDD for the line  $f$  (under  $s - a - 0$  at  $b$ ).

Figure 4.11: OBDDs for feedback bridging fault when  $f$  dominates  $b$

### 4.3 Efficient construction of $FN$ -detector for bridging faults

---

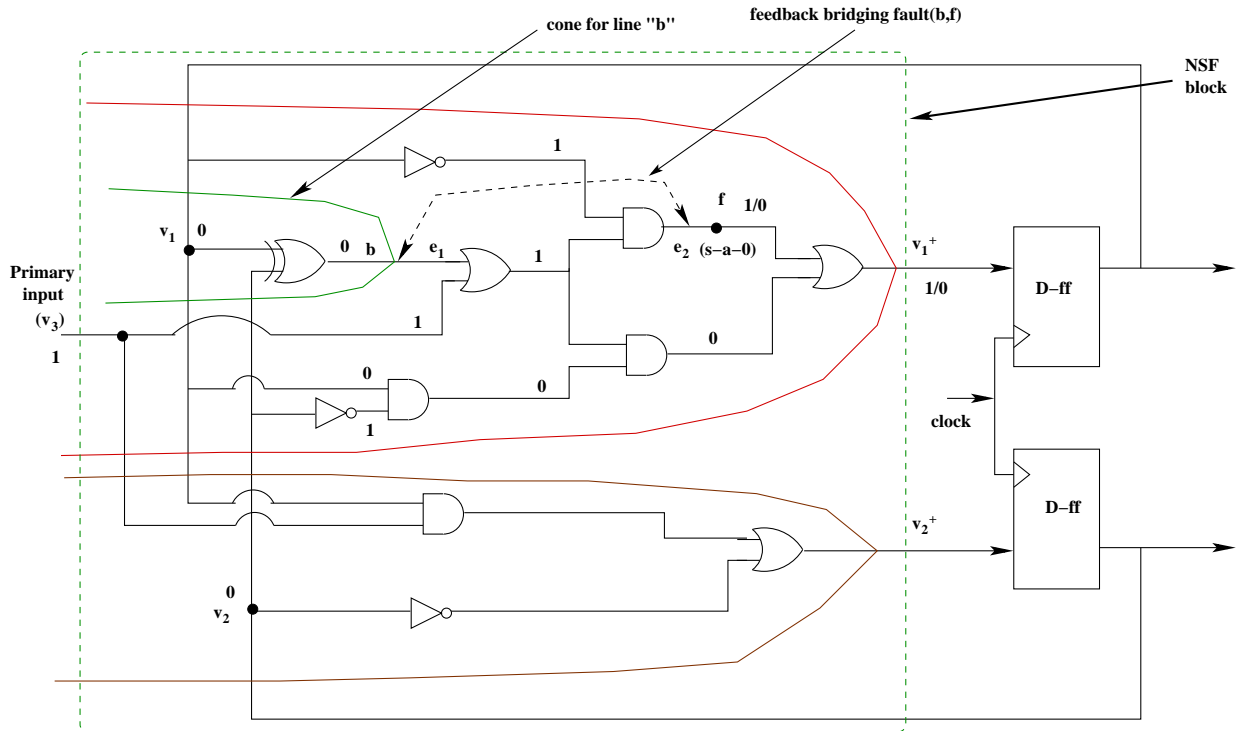
and faulty OBDDs is shown in Figure 4.11(c). The “satisfy-all-1” operation on XORed OBDD generates the set  $IP_{s-a-0,dominated}$  as  $\{v_1 = 1, v_2 = 0, v_3 = 0; v_1 = 0, v_2 = 1, v_3 = 0\}$ . Here, the dominating line is  $e_2(f)$  and  $v_{dominating} = v'_1v_2 + v'_1v_3$ , which is represented by the dominating OBDD shown in Figure 4.11(d). The “satisfy-all-0” operation is applied on this dominating OBDD which generates the set  $IP_{0,dominating} = \{v_1 = 1, v_2 = 0, v_3 = 0; v_1 = 1, v_2 = 0, v_3 = 1; v_1 = 1, v_2 = 1, v_3 = 0; v_1 = 1, v_2 = 1, v_3 = 1; v_1 = 0, v_2 = 0, v_3 = 0\}$ . The intersection of  $IP_{s-a-0,dominated}$  and  $IP_{0,dominating}$  gives the test pattern set  $TP$  as  $\{v_1 = 1, v_2 = 0, v_3 = 0\}$ .

Now, we check if the test pattern  $\{v_1 = 1, v_2 = 0, v_3 = 0\}$  causes oscillation under fault. The “dominating faulty OBDD” for the line  $e_2(f)$  (expression is  $v_1v_3$ ) is shown in Figure 4.11(e). Then “satisfy-all-1” operation is applied on this OBDD to generate the set  $IP_{f=1,s-a-0,at\_dominated}$  as  $\{v_1 = 0, v_2 = 0, v_3 = 1; v_1 = 0, v_2 = 1, v_3 = 1\}$ . Now the intersection of  $TP$  and  $IP_{f=1,s-a-0,at\_dominated}$  is  $\phi$ , which implies that test pattern  $\{v_1 = 1, v_2 = 0, v_3 = 0\}$  can detect the feedback bridging fault  $F_1$ , when  $f$  dominates  $b$ , as it does not cause oscillation. The fault (s-a-0) manifestation at  $v_1^+$  for the test pattern  $\{v_1 = 1, v_2 = 0, v_3 = 0\}$  is 0, thereby mapping to  $FD_1$ -transition as  $\langle 10, 0, 0d \rangle$ .

As discussed before, to generate the exhaustive set of  $FD_1$ -transitions, now we need to repeat this procedure when the roles of *front line* and *back line* are reversed i.e., generation of exhaustive set of  $FD$ -transitions for feedback bridging fault, when *back line* dominates the *front line*.

#### **Part 2: Generation of exhaustive set of $FD$ -transitions for feedback bridging fault– the *back line* dominates the *front line***

In the circuit considered in Part 1 (Figure 4.10), if the roles of *front line* and *back line* are reversed we obtain the circuit given in Figure 4.12. In this case, as *back line* ( $e_1$ ) dominates the *front line* ( $e_2$ ), we drive 0 to the  $e_1$  and test for s-a-0 fault at  $e_2$ . Using the OBDD based operations to generate the test patterns (discussed in Subsection 4.3.2), we obtain  $TP$  as  $\{v_1 = 0, v_2 = 0, v_3 = 1\}$ . Now, it needs to be verified if the test pattern causes oscillation under fault i.e., under fault, the *dominating* line  $b$  is pulled to 1. It may be noted that this is not possible because fault effect cannot be propagated from the *dominated* line to the *dominating* line. The reason is obvious, as there is no path from the *dominated* line to the *dominating* line. So  $FD_1$ -transition corresponding to this test pattern is  $\langle 00, 1, 0d \rangle$ , as NSF output  $v_1^+$  for this test pattern under fault is 0. So the exhaustive set of  $FD_1$ -transitions is  $\{\langle 00, 1, 0d \rangle, \langle 10, 0, 0d \rangle\}$ .


 Figure 4.12: NSF with fault, partitioned into cones when  $b$  dominates  $f$ .

**Note:** For any feedback bridging fault, all the test patterns generated for the case “ $b$  dominates  $f$ ” can be directly mapped to  $FD$ -transitions and used for  $FN$ -detector construction (as they do not cause oscillation).

#### 4.3.4 OBDD based procedure for illustration of an oscillating feedback bridging fault

Now, we illustrate an example of a circuit where a feedback bridging fault ( $f$  dominates  $b$ , case) causes oscillation.

The circuit in Figure 4.13 shows a feedback bridging fault  $F_1$  between lines  $e_1$  and  $e_2$ . As we are illustrating oscillation,  $e_1$  is the *dominated* line ( $b$ ) and  $e_2$  is the *dominating* line ( $f$ ). The partitioning of the NFS into cones on its outputs and on the *dominating* line are also shown in the figure. Using the OBDD based operations to generate the test patterns, we obtain  $TP$  as  $\{v_1 = 1, v_2 = 1, v_3 = 0\}$ . The expression for the line  $e_2(f)$  under s-a-0 fault at line  $e_1(b)$  is  $v_1' + v_3'$ . So,  $IP_{f=1, s-a-0, at, dominated}$  is  $\{v_1 = 0, v_2 = 0, v_3 = 0; v_1 = 0, v_2 = 0, v_3 = 1; v_1 = 0, v_2 = 1, v_3 = 0; v_1 = 0, v_2 = 1, v_3 = 1; v_1 = 1, v_2 = 0, v_3 = 0; v_1 = 1, v_2 = 1, v_3 = 0\}$ . As test pattern  $\{v_1 = 1, v_2 = 1, v_3 = 0\}$  is included in the set  $IP_{f=1, s-a-0, at, dominated}$ , it implies that the test pattern under fault would pull the *dominating* line ( $f$ ) to 1, leading to

## 4.4 Experimental evaluation

oscillation. So this test pattern cannot be included in the set of  $FD_1$ -transitions. Also, it may be noted that in this case there are no more test patterns. Hence,  $F_1$  cannot be tested when *front line* dominates the *back line*.

However, in case of this fault when *back line* dominates the *front line*, the test patterns are  $\{v_1 = 1, v_2 = 0, v_3 = 0; v_1 = 0, v_2 = 0, v_3 = 1; v_1 = 0, v_2 = 0, v_3 = 0; v_1 = 0, v_2 = 1, v_3 = 0\}$ , which map to  $FD_1$ -transitions  $\{\langle 10, 0, 0d \rangle, \langle 00, 1, 0d \rangle, \langle 00, 0, 0d \rangle, \langle 01, 0, 0d \rangle\}$ , respectively.

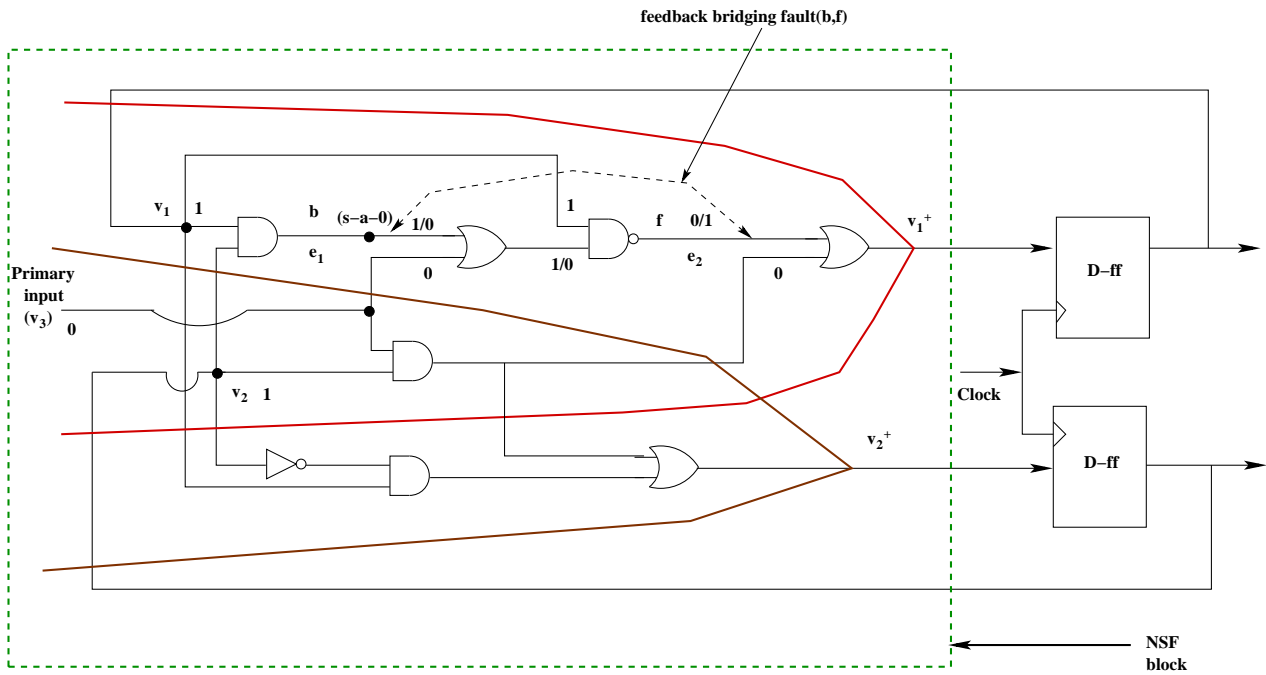


Figure 4.13: NSF with fault causing oscillation, partitioned into cones when  $f$  dominates  $b$

**Note:** Due to possibility of oscillation in case of feedback bridging faults, most of the works on OLT of bridging fault have considered only the non-feedback faults. However, as shown in the last subsection, there are feedback bridging faults for which there are test patterns (even in case of  $f$  dominates  $b$ ) which do not cause oscillation and hence can detect the fault. Further, as discussed before, for all feedback bridging faults in case of  $b$  dominates  $f$ , no test pattern causes oscillation. So, if all feedback bridging faults are dropped, there is a substantial fall in fault coverage.

## 4.4 Experimental evaluation

Using the above techniques discussed in the last section we have designed a tool “OLT-FBF”, which produces the  $FN$ -detector (in Verilog) for detecting bridging faults, given the netlist

of a digital sequential circuit. On-line testers have been designed for several ISCAS'89 benchmark circuits using the tool OLT-FBF and performance in terms of fault coverage, detection latency and area overhead have been analyzed.

$$\text{Fault Coverage (FC):} = \frac{\text{Number of faults covered}}{\text{Total number of bridging faults in CUT}} \times 100\%$$

$$\text{Area Overhead (AO):} = \frac{\text{Area of the FN-detector (after synthesis)}}{\text{Area of the Circuit Under Test(CUT)}}$$

**Detection Latency (DL):** Detection latency for  $F_i$  is  $(\lceil nFD_i/nmlFD_i \rceil) - 1$ , where  $nFD_i$  is total number of  $FD_i$ -transitions and  $nmlFD_i$  be the number of  $FD_i$ -transitions that are considered in the  $FN$ -detector.

#### 4.4.1 Fault coverage analysis

Table 4.1 shows the details of bridging fault coverage <sup>2</sup> achieved by the proposed scheme for different ISCAS'89 benchmark circuits and comparison with [13]. Column 1 provides information about the circuit i.e., circuit name (number of flip-flops, number of gates). Column 2 shows the number of all possible AND-OR bridging faults. In Column 3, we report the percentage of bridging faults which are non-feedback. The same column also represents the fault coverage of the scheme proposed in [13]. It may be noted that the scheme reported in [13] only handles non-feedback bridging faults. Percentage of non-oscillating feedback bridging faults and oscillating feedback bridging faults <sup>3</sup> are reported in Column 4 and Column 5, respectively. Column 6 represents the coverage of the proposed scheme i.e., sum of non-feedback and non-oscillating feedback bridging faults. Strictly speaking, the proposed scheme also covers the oscillating bridging faults *partially*, because even for such faults  $FD$ -transitions are present in the  $FN$ -detector when  $b$  dominates  $f$ . In Column 7, we report the CPU time taken to generate the exhaustive set of  $FD$ -transitions.

The following points may be noted:

- Broadly, about 10 to 20 percentage of bridging faults are feedback bridging faults. However, among them only a small fraction (less than 1 percent) creates oscillations. So neglecting all feedback bridging faults leads to substantial reduction in coverage, which is the case in [13]. By filtering out the oscillating bridging faults and covering the remaining bridging faults, i.e., non-feedback and non-oscillating feedback bridging

<sup>2</sup>detection latency was zero, i.e., all  $FD$ -transitions were considered in the  $FN$ -detector for the faults covered

<sup>3</sup>in this table a bridging fault is considered oscillating if there is a test pattern for which the circuit oscillates, when the *front\_line* dominates the *back\_line*

## 4.4 Experimental evaluation

---

faults, more than 99 percentage of fault coverage is obtained for all the benchmark circuits by the proposed OLT scheme.

- The number of feedback bridging faults is higher in circuits where the average number of gates per cone of influence of the NSF outputs are large. The reason is explained as follows. As we have seen, for a feedback bridging fault the *back line* should be within the same cone as the *front line*. Obviously, larger cones imply more nets and more such combinations of *back lines* and *front lines*.

It can be observed that the percentage of feedback bridging faults for the benchmark circuit *s382* having 21 flip-flops and 158 gates is 9.89 %. Whereas for the circuit *s386*, having 6 flip-flops and 159-gates, the percentage is 15.17 %. It may be noted that these two circuits have almost equal number of gates but only difference is in the number of flip-flops. The average number of gates per cone in circuit *s386* is 26.5, whereas in case of *s382* it is only 7.52. Similar trend can be seen for other circuits as well.

- The percentage of feedback bridging faults causing oscillations is low (less than 1 percent). In most of cases we have observed that a feedback bridging fault creates oscillation if the *back line* involved in the fault has no other path for fault propagation except through the *front line*; if *back line* belongs to more than one cones then probability of this situation is low. It may be observed from Table 4.1 that in most of the cases, higher the number of flip-flops (i.e., cones) in a circuit, lower is the number of oscillating feedback bridging faults.

### 4.4.2 Area overhead analysis

If we design an *FN*-detector with highest possible fault coverage and target zero detection latency (i.e., incorporate all *FD*-transitions for all faults in the *FN*-detector), area overhead of the detector is high. So depending on the tolerable detection latency, some *FD*-transitions may be dropped from each fault, thereby leading to reduction in area overhead.

**Note:** The scheme of blindly dropping *FD*-transitions based on given detection latency is not applied for all faults. It has been observed that for some faults the number of *FD*-transitions is quite less compared to others; such faults are called “difficult to test faults”. If *FD*-transitions for such faults are dropped using the formula of detection latency (given above), extremely low number or no *FD*-transition will be present in the *FN*-detector for such faults. This would practically imply that the fault is dropped, leading to compromise in fault coverage, which is not desirable. So, in this work, a threshold is determined based on the input space of the CUT and all faults whose number of *FD*-transitions are less than

Table 4.1: Fault coverage by the proposed method, comparison with the existing technique [13] and CPU time to generate  $FD$ -transitions \*

<b>ISCAS'89 benchmark</b>	<b>Total#BFs<sup>+</sup></b>	<b>#Non-FBFs(%)<sup>+</sup></b>	<b>#FBF(%)<sup>+</sup></b>	<b>#Oscillating-FBFs(%)</b>	<b>Fault coverage(%)</b>	<b>CPT Time (Secs.)</b>
<b>circuits-(FFs, GATEs)</b>		<b>Fault coverage(%) [13]</b>			<b>Proposed scheme</b>	
s298-(14,119)	9180	90.94	9.06	0.860	99.14	329
s344-(15,160)	16836	85.96	14.04	0.623	99.377	780
s382-(21, 158)	16471	90.11	9.89	0.631	99.369	720
s386-(6,159)	14706	84.83	15.17	0.904	99.096	522
s713-(19,393)	99681	76.73	23.27	0.985	99.015	3410
s838-(32,446)	130816	91.15	8.85	0.623	99.377	3823
s1238-(18,508)	145530	89.25	10.75	0.717	99.283	5012
s1423-(74,657)	279378	83.07	16.93	0.608	99.392	11215
s5378-(179,2779)	4477528	79.86	20.14	0.598	99.402	155730
s9234-(228,5597)	17073246	78.72	21.28	0.611	99.389	485982
s13207-(669,7951)	37415575	78.12	21.88	0.602	99.398	811764
s15850-(597,9772)	53898153	77.13	22.87	0.590	99.410	942365
s35932-(1728,16065)	158909878	75.28	24.72	0.537	99.463	2267521
s38417-(1636,22179)	284232403	74.14	25.86	0.522	99.478	2872524
s38584-(1452,19253)	214586686	74.27	25.73	0.525	99.475	2512320

<sup>+</sup>BFs: bridging faults, FBFs: feedback bridging faults, Non-FBFs: non-feedback bridging faults.

\*Executed in AMD Phenom IIX3 710 Processor with 4 GB RAM in Linux OS.

## 4.4 Experimental evaluation

---

the threshold are marked as difficult to test faults. All  $FD$ -transitions corresponding to such faults are included in the  $FN$ -detector. This rarely leads to a significance rise in area overhead because of the low number of extra transitions that are required to be explicitly included in the  $FN$ -detector.

Table 4.2 shows the area overhead of the  $FN$ -detector for different ISCAS'89 benchmark circuits under different values of detection latency.

The following points may be noted

- As expected, increase in detection latency results in reduction in area overhead of the  $FN$ -detector.
- For a given detection latency, area overhead decreases with increase in size of the circuit and finally saturates. For partial replication based OLT for s-a faults, Drineas et al. in [35] identified the fact that area overhead ratio is approximately  $\alpha + 1/k$ , where  $\alpha$  is the fraction of the test patterns incorporated in the tester design (i.e., detection latency in our case) and  $k$  is the number of state bits (generally proportional to circuit size). It can be observed from Table 4.2 that the dependence of area overhead ratio with detection latency adheres (approximately) to the above-mentioned fact, even for bridging faults. For example, in case of a small circuit (s298), where the number of state bits is 14, area overhead is nearly three times even for detection latency of 9. However, the area overhead for a large circuit (s9234), where state bits are 228, is less than one fourth for the same latency. From the table it may be noted that this trend follows for all the benchmark circuits considered.

Thus, for most of the practical circuits (which generally have more than tens of thousands of gates), near hundred percent bridging fault coverage can be achieved with reasonably low area overheads by suitably compromising detection latency.

- For a given latency, the proposed scheme leads to slightly higher area overhead compared to [13]. The reason is, more  $FD$ -transitions in the detector due to the additional coverage of feedback bridging faults in the proposed scheme compared to [13].
- It can be seen in Table 4.2 that the area overheads for small sized circuits (i.e., from s298 to s713) are more than 200% even for detection latency 9, where as for large sized circuits it gradually decreases to around 10%. So it may be concluded that the proposed scheme provides high fault coverage and tolerable latency at reasonable area overhead for circuits having more than thousand gates (which is typically the case for most of the practical circuits).

Table 4.2: Area overhead for the proposed method and comparison with [13]

ISCAS'89 benchmark circuits-(FFs,GATEs)	Area overhead for Detection latency							
	For Detection latency=0		For Detection latency=4		For Detection latency=9			
	[13]	Proposed work	[13]	Proposed work	[13]	Proposed work	[13]	Proposed work
s298-(14,119)	2.85	3.03	2.80	2.86	2.64	2.72		
s344-(15,160)	2.83	3.04	2.74	2.85	2.43	2.49		
s382-(21, 158)	2.9	3.12	2.81	2.90	2.53	2.58		
s386-(6,159)	2.88	3.28	2.78	2.94	2.48	2.61		
s713-(19,393)	2.37	2.96	1.98	2.16	1.82	1.90		
s838-(32,446)	1.5	1.64	1.38	1.52	1.21	1.32		
s1238-(18,508)	1.48	1.54	1.18	1.31	1.13	1.22		
s1423-(74,657)	1.44	1.51	1.10	1.21	1.05	1.11		
s5378-(179,2779)	1.25	1.32	0.5	0.61	0.213	0.225		
s9234-(228,5597)	1.23	1.29	0.44	0.57	0.209	0.219		
s13207-(669,7951)	1.22	1.27	0.41	0.53	0.206	0.217		
s15850-(597,9772)	1.18	1.22	0.33	0.45	0.178	0.190		
s35932-(1728,16065)	1.05	1.13	0.167	0.215	0.121	0.131		
s38417-(1636,22179)	1.02	1.11	0.159	0.192	0.113	0.123		
s38584-(1452,19253)	1.03	1.12	0.158	0.183	0.110	0.117		

## 4.5 Conclusion

---

- Since the area overheads of all the above benchmark circuits are greater than 100% for zero detection latency, it can be argued that simply duplicating the original circuit and comparing the responses would be much simpler and effective technique. However, the main drawback of this full duplication scheme is that, same type of fault may occur in both the circuits (original and duplicate) and in such case fault detection is not possible. Such faults are called common-mode failures and it has been identified by Mitra et al. [75] that their number is reasonably high, which reduces the efficacy of pure duplication based OLT.

## 4.5 Conclusion

In this chapter, we have proposed an OBDD based OLT scheme of digital circuits for AND-OR bridging faults. Most of the reported works on OLT of bridging faults cover only non-feedback bridging faults, whereas the proposed scheme covers both feedback and non-feedback bridging faults. Experimentally, it has been shown that on an average 20% of all possible bridging faults are feedback, however, only less than 1% of them cause oscillations. So, significant improvement in fault coverage is achieved by considering both feedback and non-feedback bridging faults. It is also observed that there is marginal increase in area overhead of the proposed scheme compared to the techniques considering only non-feedback bridging faults.

None of the OLT schemes including the OBDD based ones, could scale up to the level of complexity incurred in modern day circuits which have tens of thousands of gates. The major reason being most of these OLT schemes work at gate level, leading to the state explosion problem. So, one of the most important issues of the gate level OLT schemes is scalability. In the next chapter, we will address the issue of scalability by proposing an OLT scheme for the circuits at Register Transfer Level (RTL). The scheme uses High Level Decision Diagram (HLDD) instead of OBDD in OLT (for circuits at gate level).

# Chapter 5

## On-line Testing at Register Transfer Level

### 5.1 Introduction

One of the important issues of OLT in modern deep sub-micron design is scalability. Most of the OLT schemes reported in the literature including the ones proposed in Chapter 3 and Chapter 4 work at logic gate level and are scalable only up to a certain extent, i.e., circuits having about 30 thousand gates and 500 flip-flops. This is because these schemes are designed at logic gate level leading to the state explosion problem. In order to solve this issue, i.e., to improve the scalability, a number of OLT schemes at higher description level have been proposed [43, 57, 58]. The details about these schemes can be found in Chapter 2, Subsection 2.3.3. The OLT schemes at Register Transfer Level (RTL) presented in [43, 58] are based on replicating each operation and executing them using different functional units in the idle computational clock cycles. Outputs of these functional units are compared and the faulty functional units are detected. The scheme discussed in [57] is based on exploiting RTL implementation diversity to detect both transient and permanent faults on-line. The technique applies allocation diversity by changing operation-to-operator allocation and data diversity by shifting operands before re-computation. Faults can be detected by comparing the results obtained from normal computation and re-computation. All of these OLT schemes have a number of drawbacks—(i) they are intrusive in nature since they require some special properties in the circuit structure, (ii) they have high latency because they depend on idle times of different functional units of the CUT, (iii) they are architecture specific because of the use of secondary functional units, etc.

Similar to the schemes discussed in Chapter 3 and Chapter 4, in this work we develop

## 5.2 High-Level Decision Diagram

---

a partial replication based OLT scheme at RTL in order to overcome the drawbacks of the schemes reported in [43, 57, 58]. However, unlike the use of OBDD for gate level circuits (in Chapter 3 and Chapter 4), this scheme uses High Level Decision Diagram (HLDD) for circuits at RTL. The CUT is partitioned into a number of sub-circuits and each sub-circuit is represented using different HLDDs under normal and faulty conditions. For each fault, Fault Detecting control patterns (*FD*-control-patterns) are generated from HLDD representations. Finally, on-line tester, called Fault versus Normal condition detector (*FN*-detector), is designed using these *FD*-control-patterns. Application of HLDD enables the scheme to handle fairly complex circuits. Experimental results illustrate that similar fault coverage is achieved with lower area overhead and lower computational time compared to OLT schemes at gate level. Further, the scheme is non-intrusive in nature, architecture independent and can be easily applied to all types of circuits at RTL

The chapter is organized as follows. Section 5.2 presents the preliminaries of HLDD and Section 5.3 illustrates modeling of RTL circuits under normal and faulty conditions using the HLDD framework. Generation of the exhaustive set of *FD*-control-patterns and design of the *FN*-detector are discussed in Section 5.4. We have reported experimental results in Section 5.5 and finally concluded in Section 5.6.

## 5.2 High-Level Decision Diagram

HLDD is a mathematical model used to represent digital systems at higher levels of abstraction. Since the last two decades HLDDs have been used for high level and hierarchical test generation for complex digital circuits [91–93]. HLDD can be defined as a directed acyclic graph

$$G_{DD} = (N, n_0, \mathfrak{S}, \Gamma, \lambda, X), \quad (5.1)$$

where  $N$  is the finite set of *nodes* and  $n_0 \in N$  is the initial node. The set  $N$  is partitioned into two sets as  $N = NT \cup T$ , where  $NT$  is the set of non-terminal nodes and  $T$  is the set of terminal nodes. Each non-terminal node (say  $n_i$ ) is associated with an expression (say  $exp_{n_i}$ ). The expression may be a control signal or a condition. Similarly, each terminal node is associated with an operation.  $\mathfrak{S} = \{\tau_1, \tau_2, \tau_3, \dots\}$  is the finite set of transitions.  $\Gamma = \{\Gamma_1, \Gamma_2, \Gamma_3, \dots\}$  is the finite set of functions defined on non-terminal nodes to evaluate the expressions associated with them. The expression associated with each non-terminal node  $n_i$  (i.e.,  $exp_{n_i}$ ) is evaluated by its corresponding function  $\Gamma_i$ , where  $1 \leq i \leq |NT|$ .  $\lambda = \{\lambda_1, \lambda_2, \lambda_3, \dots\}$  is the finite set of functions defined on terminal nodes to evaluate the operations associated with them. The operation associated with each terminal

node  $n_j$  (i.e.,  $op_{n_j}$ ) is evaluated by its corresponding function  $\lambda_j$ , where  $1 \leq j \leq |T|$ .  $X = \{x(\tau_1), x(\tau_2), x(\tau_3), \dots\}$  is the finite set of constants associated with the transitions. The transition from a non-terminal node  $n_i$  is decided by evaluating the expression associated with it (i.e.,  $exp_{n_i}$ ) and the number of outgoing transitions from  $n_i$  is the number of possible outcomes of  $\Gamma_i(exp_{n_i})$ . Now we define a transition as:

A transition  $\tau \in \mathfrak{S}$  from a node  $n_\tau$  to another node  $n_\tau^+$  is an ordered pair as

$$\tau = \langle n_\tau, n_\tau^+ \rangle \quad (5.2)$$

where

- $n_\tau \in NT$  is the initial node of the transition, denoted as  $initial(\tau)$ .
- $n_\tau^+ \in N$  is the final node of the transition, denoted as  $final(\tau)$ .
- The transition,  $\tau = \langle n_\tau, n_\tau^+ \rangle$ , is said to occur successfully if the evaluated value of the expression associated with  $n_\tau$  (that is  $exp_{n_\tau}$ ) is equal to  $x(\tau)$ . That means  $\Gamma_\tau(exp_{n_\tau}) = x(\tau)$ .

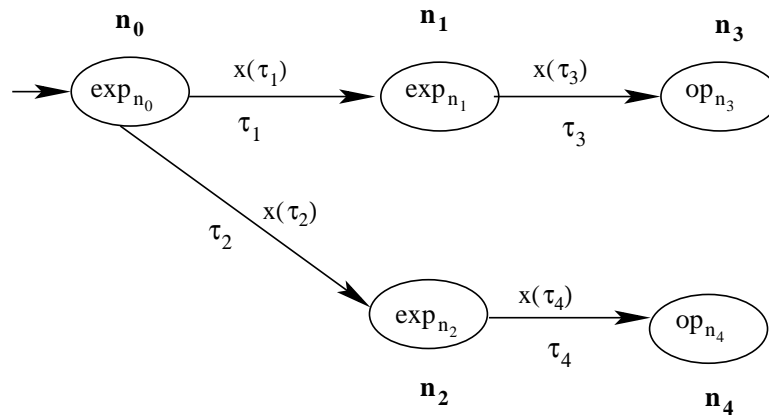


Figure 5.1: Graphical representation of a HLDD model.

Figure 5.1 shows a graphical representation of the HLDD model  $G_{DD}$ , where  $N = \{n_0, n_1, n_2, n_3, n_4\}$  is the set of nodes,  $NT = \{n_0, n_1, n_2\}$  is the set of non-terminal nodes,  $T = \{n_3, n_4\}$  is the set of terminal nodes,  $\mathfrak{S} = \{\tau_1, \tau_2, \tau_3, \tau_4\}$  is the set of transitions and  $n_0$  is the initial node.  $x(\tau_i)$  is the constant value associated with transition  $\tau_i$ , where  $1 \leq i \leq 4$ . Different expressions and operations are associated with the nodes and are shown in the figure. Consider a non-terminal node  $n_0$ ; the function  $\Gamma_0(exp_{n_0})$  evaluates the expression associated with  $n_0$ . There are two possible transitions from the node  $n_0$ . If  $\Gamma_0(exp_{n_0}) = x(\tau_1)$

### 5.3 Circuit modeling at RTL: Normal and faulty conditions

---

then the transition  $\tau_1$  occurs in the model. On the other hand, if  $\Gamma_0(exp_{n_0}) = x(\tau_2)$  then the transition  $\tau_2$  occurs in the model. Similarly, for each terminal node  $n_i \in T$ ,  $\lambda_i(op_{n_i})$  evaluates the operation associated with  $n_i$ . The value obtained from  $\lambda_i(op_{n_i})$  is referred to as the output of the path, starting from the initial node to the terminal node  $n_i$  in the model. For example, the value obtained from  $\lambda_4(op_{n_4})$  is referred to as the output of the path from  $n_0$  to  $n_4$ . Now, we formally define *path* in the HLDD model as:

**Definition 5.1. Path in HLDD:** A path  $p_{(i,j)}$  from node  $n_i$  to node  $n_j$  in the HLDD model  $G_{DD}$  is a sequence of transitions of  $G_{DD}$ , denoted as  $p_{(i,j)} = \langle \tau_1, \tau_2, \dots, \tau_k \rangle$ , where  $initial(\tau_1) = n_i$ ,  $final(\tau_k) = n_j$  and the consecutive property holds, i.e.,  $initial(\tau_{l+1}) = final(\tau_l)$ , where  $1 \leq l \leq (k - 1)$ .

We denote the path from initial node  $n_0$  to any other node  $n_j$  in  $G_{DD}$  as  $p_j$ .

For example, the path from initial node  $n_0$  to node  $n_4$  in the above HLDD is denoted as  $p_4$ . This path includes two transitions— $\tau_2$  and  $\tau_4$ . The path  $p_4$  is established if both the transitions have occurred successfully. That means,  $\Gamma_0(exp_{n_0}) = x(\tau_2)$  and  $\Gamma_2(exp_{n_2}) = x(\tau_4)$ . Thus, we can say the *path constraints* for  $p_4$  are  $exp_{n_0} = x(\tau_2)$  and  $exp_{n_2} = x(\tau_4)$ . Path constraints can be formally defined as:

**Definition 5.2. Path constraints:** The path constraints  $C_{p_j}$  for a path  $p_j = \langle \tau_1, \tau_2, \tau_3, \dots \rangle$  corresponds to the values of the expressions that have to be satisfied for establishment of that path. i.e.,  $C_{p_j} = \langle x(\tau_1), x(\tau_2), x(\tau_3), \dots \rangle$ .

There are two important tasks for testing circuits at RTL. The first task is modeling the circuit at RTL and the second one is applying appropriate high level fault models which have strong correlation with physical defects. In next section, we discuss the modeling of circuits at RTL using HLDDs.

### 5.3 Circuit modeling at RTL: Normal and faulty conditions

The circuit description at RTL is partitioned into two parts—data path and control part [30, 126]. The data path is viewed as an interconnection of modules and the control part is represented a Finite State Machine (FSM). The modules of the data path are different units like registers, multiplexers, functional units, etc. The modules are decided depending on number of inputs, number and type of operations required to implement the required algorithm, sequence of these operations, data transfers, etc. [30, 126].

### 5.3 Circuit modeling at RTL: Normal and faulty conditions

---

In order to explain the procedure of modeling circuits at RTL, we have considered the example of Greatest Common Divisor (GCD), which is also treated as a standard benchmark in different high level testing schemes [92,93]. The pseudo-code to calculate GCD of two unsigned integers is shown in Algorithm 5.1. Figure 5.2 shows the data path of the GCD algorithm at RTL which is obtained by applying high-level synthesis to the algorithm description [29]. The data path consists of 2 registers, 6 multiplexers and 3 functional units, whereas the control part is described using an FSM having five states which is shown in Table 5.1. These five states carry out the function of the control part as follows—initial state  $q_0$  enables the two registers to hold the input values. State  $q_1$  checks equality between two input values and moves to state  $q_2$  if they are not equal, otherwise the FSM remains in state  $q_1$  and outputs the GCD value. State  $q_2$  compares these two unequal values and moves either to state  $q_3$  or  $q_4$ . In states  $q_3$  and  $q_4$  subtraction is performed and finally the FSM moves back to state  $q_1$  for next iteration.

---

**Algorithm 5.1** Algorithm of Greatest Common Divisor (GCD) of two unsigned integers.

---

```
1: Begin
2:  $V_1 \leftarrow IN_1$ 
3:  $V_2 \leftarrow IN_2$ 
4: while  $V_1 \neq V_2$  do
5: if  $V_1 < V_2$  then
6:  $V_2 \leftarrow V_2 - V_1$ 
7: else
8:  $V_1 \leftarrow V_1 - V_2$ 
9: end if
10: end while
11:  $Output \leftarrow V_1$ 
12: End
```

---

Now, we discuss how the GCD operation is performed in the RTL architecture shown in Figure 5.2 with the control signals given in Table 5.1. The control signals at state  $q_0$  where *reset* signal is 1 are as follows;  $sel1 = 1, sel2 = 1, sel34 = 0, sel56 = d$ . The control signals  $sel1 = 1, sel2 = 1$  load the registers with input values which are selected by  $sel34 = 0$  in both *mux3* and *mux4*, as shown in Figure 5.2. At state  $q_0$  the control signal *sel56* has no impact, thus, it contains don't care value( $d$ ). The values of the two registers ( $regA(= V_1)$  and  $regB(= V_2)$ ) remain unchanged and are used for checking equality and less than conditions in states  $q_1$  and  $q_2$ , respectively. This is possible through the control signals  $sel1 = 0, sel2 = 0, sel34 = d, sel56 = d$  in both the states. At state  $q_3$

### 5.3 Circuit modeling at RTL: Normal and faulty conditions

---

Table 5.1: FSM representation of the control part of the GCD algorithm

Present state	Conditions			Next state	Control signals			
	Reset	NEQ	LT		sel1	sel2	sel34	sel56
$q_0$	1	d	d	$q_1$	1	1	0	d
$q_1$	0	1	d	$q_2$	0	0	d	d
$q_1$	0	0	d	$q_1$	0	0	d	d
$q_2$	0	d	1	$q_3$	0	0	d	d
$q_2$	0	d	0	$q_4$	0	0	d	d
$q_3$	0	d	d	$q_1$	0	1	1	1
$q_4$	0	d	d	$q_1$	1	0	1	0

( $sel1 = 0, sel2 = 1, sel34 = 1, sel56 = 1$ ), contents of  $regB$  (i.e.,  $V_2$ ) and  $regA$  (i.e.,  $V_1$ ) are selected by  $sel56 = 1$  in  $mux5$  and  $mux6$ , respectively. Then the subtract operation, i.e.,  $V_2 - V_1$  is performed by  $SUBRT$  module and the subtracted value is loaded into register  $regB$  by the control signals  $sel2 = 1, sel34 = 1$ . Even though  $sel34 = 1$  at  $q_3$ , the content of  $regA$  (i.e.,  $V_1$ ) remains unchanged because the control signal  $sel1 = 0$ . Similarly at state  $q_4$ , the operation,  $V_1 - V_2$ , is performed and the subtracted value is loaded into  $regA$ . All the details about the control signals can be found in Table 5.1.

It can be observed in the above example that the control part generates signals, using which different operations are carried out at the data path of the RTL circuit. The data path does not perform operations for all possible values of the control signals. For example, the data path performs a subtract operation, i.e.,  $V_2 - V_1$  when the values of the control signals  $\langle sel1, sel2, sel34, sel56 \rangle = \langle 0, 1, 1, 1 \rangle$  and does not perform any operation when the values of the control signals  $\langle sel1, sel2, sel34, sel56 \rangle = \langle 1, 1, 1, 1 \rangle$  (Table 5.1). Thus, the values of the control signals for which there is a distinct operation are called *valid control signals* and the values of the control signals for which there is no operation are called *invalid control signals*. Valid and invalid control signals can be defined as.

**Definition 5.3. Valid and Invalid control signals:** *The values of control signals ( $\langle sel1, sel2, \dots \rangle$ ) are said to be valid if the circuit performs a distinct operation using these signal values. Otherwise, they are called invalid control signals.*

Testing a circuit at RTL requires testing both the data path and the control part of the circuit. Since the control part is represented in the form of FSM, its testing is comparatively easier than that of the data path. Several OLT techniques have been proposed for testing of FSMs [60, 65]. The basic idea of testing the control part is to first model it as an FSM. Then state sequences of the FSM traversed during execution of the circuit is compared with the state sequences under normal condition. Fault is detected if any mismatch is found

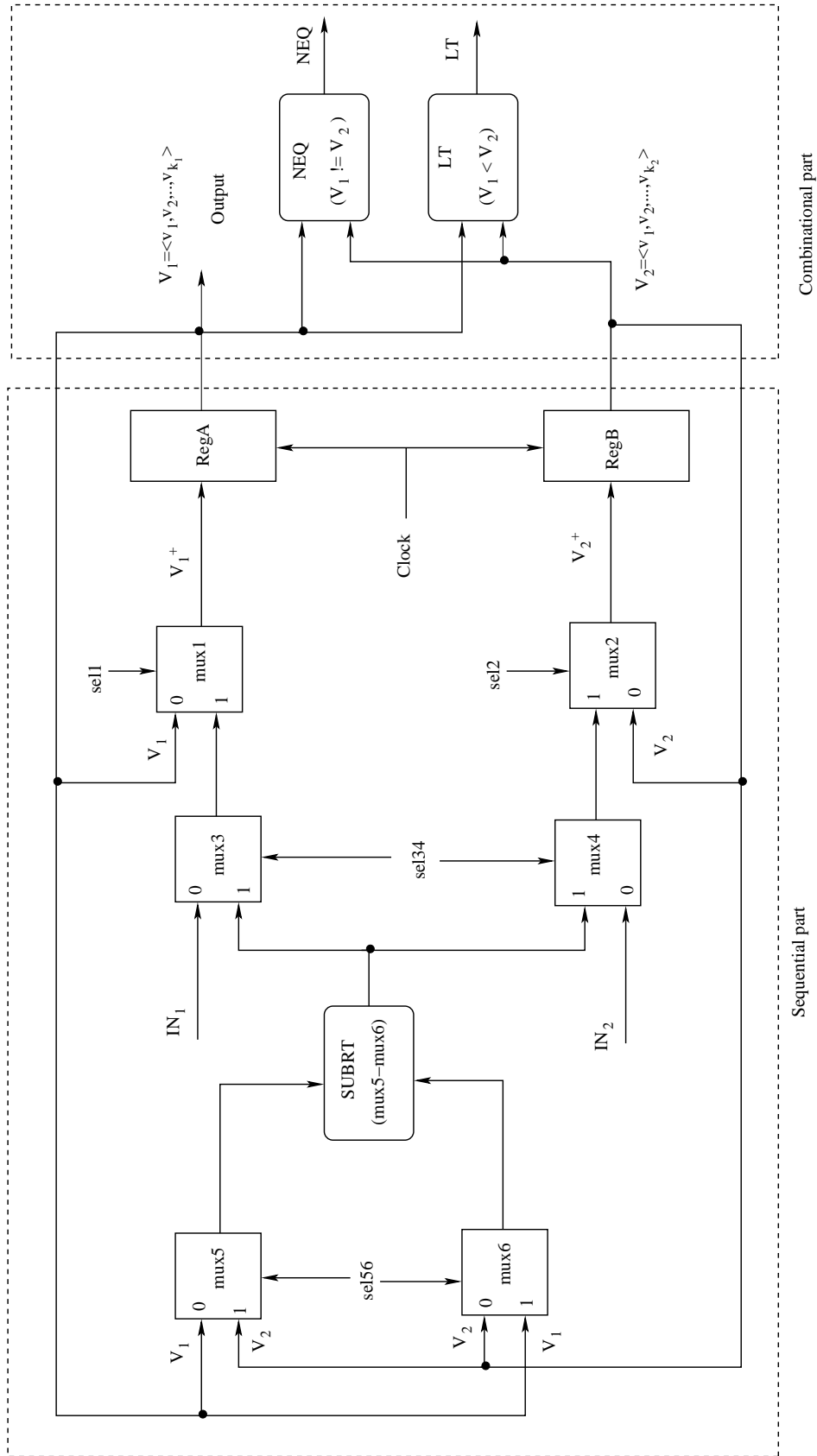


Figure 5.2: Data path of the GCD algorithm at RTL.

### 5.3 Circuit modeling at RTL: Normal and faulty conditions

---

between these two state sequences. In this work, we are interested to design an OLT scheme for testing of data path of the RTL circuits. Again, the data path can be divided into a sequential part and a combinational part, which is shown in the Figure 5.2 for the GCD circuit. First, we consider the sequential part and design on-line tester for it. Later, we discuss the design of on-line tester for the combinational part in brief.

#### 5.3.1 Circuit modeling using HLDD

This subsection explains how the data path of an RTL circuit is modeled using HLDD. We first partition the CUT (sequential part of the data path) into smaller sub-parts based on cones of influence with respect to the registers [15]. A cone is a sub-circuit corresponding to an input of a register, which contains all modules, nets and inputs that are transitive fan-ins of the register. Figure 5.3 shows the partitioning of the CUT into cones. It may be noted that the cone has two types of inputs; primary inputs and secondary inputs. Let  $P = \{IN_1, IN_2, \dots, IN_g\}$  be the set of primary inputs and  $V = \{V_1, V_2, \dots, V_h\}$  be the set of secondary inputs of the CUT, which are fed back from the outputs of the registers. The inputs of the registers (i.e., outputs of the cones) are treated as values of the registers at the next clock pulse and are denoted as  $V^+ = \{V_1^+, V_2^+, \dots, V_h^+\}$ ; they can be found in Figure 5.3. Thus, the CUT without registers can be described as  $Z = (\Sigma_Z, V^+)$ , where  $\Sigma_Z = P \times V = \{IN_1, IN_2, \dots, IN_g, V_1, V_2, \dots, V_h\}$  is the set of inputs and  $V^+ = \{V_1^+, V_2^+, \dots, V_h^+\}$  is the set of outputs. Once the CUT is divided into a number of cones, next we represent each cone using a HLDD.

**Note:** It may be noted that in RTL the inputs and outputs of the CUT consisting of multiple number of bits are considered and processed together, whereas in gate level, the inputs and outputs are considered and processed as individual bits. Thus, the complexity of representing circuits at gate level can be reduced at RTL.

Since the last few years HLDDs have been widely used to represent circuits at RTL [91–93] because of their simplicity and uniform graph based representation. In this work we follow the same formalism to represent each cone of the CUT using a HLDD. The non-terminal nodes of the HLDD correspond to multiplexers or data selectors whereas terminal nodes correspond to functional units. We have considered constant assignments and data transfers as special cases of operations. In the GCD circuit, the CUT is divided into two cones, *cone1* and *cone2*, which are shown in Figure 5.3. The set of primary and secondary inputs are  $P = \{IN_1, IN_2\}$  and  $V = \{V_1, V_2\}$ , respectively. Here, *cone1* corresponds to *RegA* and its output is denoted as  $V_1^+$ . Similarly, *cone2* corresponds to *RegB* and its output

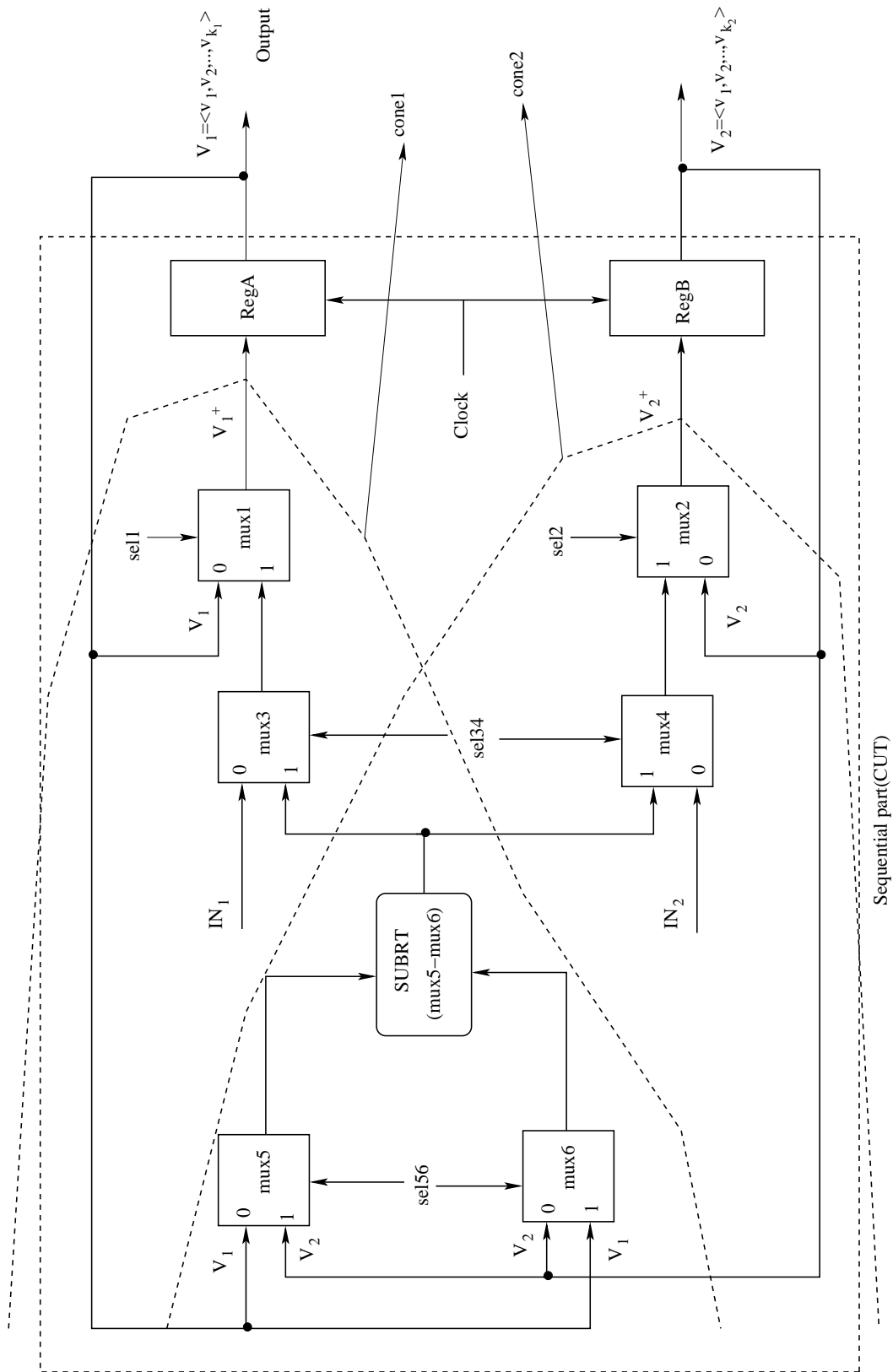


Figure 5.3: Partitioning the CUT into sub-parts based on cones of influence.

### 5.3 Circuit modeling at RTL: Normal and faulty conditions

is denoted as  $V_2^{+1}$ . The HLDD representation of  $V_1^+$  consists of 7 nodes, which is shown in Figure 5.4. Nodes  $n_0$ ,  $n_1$  and  $n_2$  are the non-terminal nodes and the nodes  $n_3$ ,  $n_4$ ,  $n_5$  and  $n_6$  are the terminal nodes. Expressions associated with the non-terminal nodes are different control expressions (multiplexer selection lines) and operations associated with the terminal nodes are subtractions and assignment operations. Initial node  $n_0$  of the HLDD shown in Figure 5.4 represents *mux1* and is associated with expression *sel1*, i.e, selection line of *mux1*. If  $\Gamma_0(sel1) = 0$  (that means  $sel1 = 0$ ), then we reach the node  $n_3$ , which is associated with an assignment operation. The terminal node  $n_3$  is evaluated by the function  $\lambda_3(op_{n_3})$  which assigns present value of  $V_1$  to  $V_1^+$ . If  $\Gamma_0(sel1) = 1$ , then we reach the node  $n_1$  in the HLDD which represents *mux3* and the expression associated with  $n_1$  is *sel34*. If  $\Gamma_1(sel34) = 0$ , then we reach the node  $n_4$ , which assigns the input value of  $IN_1$  to  $V_1^+$ . Again, if  $\Gamma_1(sel34) = 1$ , then we reach the node  $n_2$ , which represents both *mux5* and *mux6* and the expression associated with  $n_2$  is *sel56*. If  $\Gamma_2(sel56) = 0$ , then we reach the node  $n_5$  where subtraction is performed by the function  $\lambda_5(op_{n_5}) = \lambda_5(V_1 - V_2)$ . Similarly, if  $\Gamma_2(sel56) = 1$ , then we reach the node  $n_6$ , where subtraction is performed by the function  $\lambda_6(op_{n_6}) = \lambda_6(V_2 - V_1)$ .

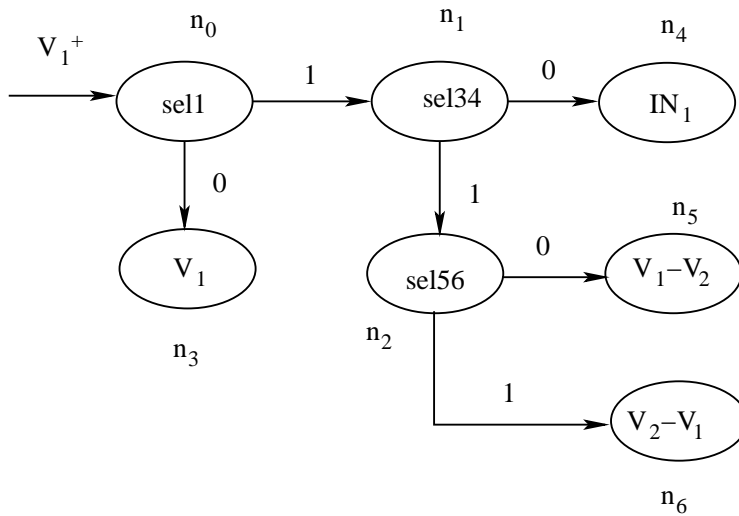


Figure 5.4: HLDD representing  $V_1^+$  .

One of the hardest problem of testing circuits at RTL is the lack of widely accepted fault models unlike at the gate level. Some high level fault models have been reported in literature review section where the authors have attempted to establish a correlation between the high

<sup>1</sup>Number of bits in  $V_1^+(V_2^+)$  is same as the number of bits in *RegA (RegB)*. Let  $V_1^+ = \langle v_1^+, v_2^+, \dots, v_{k_1}^+ \rangle$  contain  $k_1$ -bits and  $V_2^+ = \langle v_1^+, v_2^+, \dots, v_{k_2}^+ \rangle$  contain  $k_2$ -bits. Similarly, inputs also consist of multiple number of bits, e.g.,  $IN_1 = \langle i_1, i_2, \dots, i_{k_3} \rangle$  consists of  $k_3$ -bits and  $IN_2 = \langle i_1, i_2, \dots, i_{k_4} \rangle$  consists of  $k_4$ -bits.

level fault coverage and gate-level fault coverage [18, 25, 46, 59]. In the next subsection we illustrate one of the RTL fault models presented in [59] and following that, modeling of a circuit under faulty condition [59] using HLDD is discussed.

#### 5.3.2 RTL fault model and circuit modeling under fault.

##### RTL fault model

M. Karunaratne et al. [59] presented a number of RTL fault models for different conditional and control expressions. They have introduced three faulty behaviors for *if-else* control expression which is shown in Table 5.2. The first faulty behavior is generated by interchanging the *if* and *else* blocks. The second (and third) faulty behavior is generated by selecting *if* (*else*) block always without depending on the value of the condition.

Table 5.2: RTL faults for *if* and *else* blocks

Normal behavior	Faulty behavior 1	Faulty behavior 2	Faulty behavior 3
begin	begin	begin	begin
if(condition)	if(condition)	if(condition)	if(condition)
Output=input1;	<b>Output=input2;</b>	Output=input1;	<b>Output=input2;</b>
else	else	else	else
Output=input2;	<b>Output=input1;</b>	<b>Output=input1;</b>	Output=input2;
end	end	end	end

In general, *if-else* control expression is used to select one of the two sets of operations to be performed depending on the condition. If the condition is satisfied it executes the *if*-block statements, otherwise it executes the *else*-block statements. In RTL, the equivalent of *if-else* statement can be designed with the help of a multiplexer, where the inputs are *if*-block and *else*-block statements and one of these input blocks is selected for execution by the selection line of the multiplexer. So, the fault models associated with the *if-else* control statement can be applied to the multiplexer in the RTL design. Figure 5.5 shows a multiplexer and its equivalent circuit at gate level. In the multiplexer we have 3 faults (shown in Table 5.2) whereas its equivalent circuit at gate level has  $9 \times 2 = 18$  s-a faults (each line can be s-a-1 and s-a-0). Thus, it can be noted that for a circuit the number of RTL faults is less than that of gate level faults. At the same time it has also found that RTL faults have good correlation with gate level faults. So if all the RTL faults are tested, then quality of testing at RTL remains comparable with that of the gate level.

There is a number of high level fault models associated with different operations (addition, multiplications, subtraction, comparator, etc.) and conditional statements

### 5.3 Circuit modeling at RTL: Normal and faulty conditions

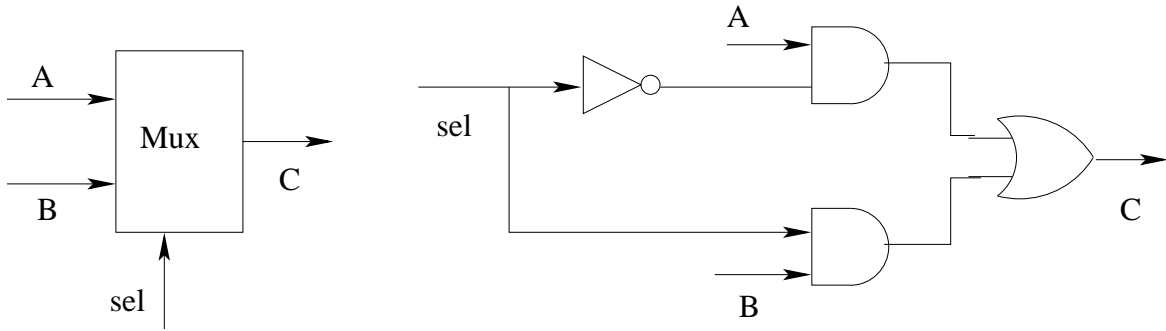


Figure 5.5: Multiplexer and its equivalent circuit at logic gate level

[18, 25, 46, 59]. In this work, we have applied them to the corresponding modules in RTL architecture of the CUT. Next we are going to discuss modeling of the CUT under fault using HLDD.

#### Circuit modeling under fault using HLDD

Like modeling of the circuit under normal condition, we introduce a fault at a module of the CUT and partition the CUT into smaller sub-parts based on cones of influence with respect to the registers. Let  $V_0^+ = \{V_{01}^+, V_{02}^+, V_{03}^+, \dots, V_{0h}^+\}$  denote the set of cone outputs under normal condition and  $V_i^+ = \{V_{i1}^+, V_{i2}^+, V_{i3}^+, \dots, V_{ih}^+\}$  denote the outputs under fault  $F_i$ ,  $1 \leq i \leq p$ , where  $p$  is the number of all possible faults. For modeling the CUT under faulty conditions the following steps are executed—i) for each fault  $F_i$ , find the cones which include  $F_i$ . ii) for each such cone, its output is represented using two HLDDs—1) under normal and 2) faulty ( $F_i$ ) condition.

In order to illustrate RTL fault modeling using HLDD, we consider the GCD circuit and fault at module *mux5*. We take the fault for *if-else* control expression presented in [59] and apply it (shown in 2nd column of Table 5.2) to *mux5* (say  $F_1$ ) in the GCD circuit. Since  $F_1$  belongs to both the cones, *cone1* and *cone2*, we must consider both of them for modeling the fault. Let  $V_{01}^+$  denote the output of *cone1* under normal condition and  $V_{11}^+$  denote the output of *cone1* under fault  $F_1$ . In normal case, *mux5* selects  $V_1$  ( $V_2$ ) when the selection line *sel56* is 0 (1). The HLDD to represent *cone1* under normal condition, i.e.,  $V_{01}^+$  is shown in Figure 5.6. After applying fault  $F_1$  at *mux5*, the behavior of *mux5* becomes the reverse, i.e., it selects  $V_2$  ( $V_1$ ) when *sel56* is 0(1). Now the behavior of *mux5* becomes identical with *mux6*, i.e., both select  $V_2$  ( $V_1$ ) when *sel56* is 0(1). Figure 5.7 shows the details about the HLDD representation for *cone1* under fault  $F_1$  (i.e.,  $V_{11}^+$ ). Like *cone1*, we can represent output of *cone2*, i.e.,  $V_2^+$ , using HLDD under normal and faulty ( $F_1$ ) conditions. Figure 5.8 and

Figure 5.9 show the HLDDs to represent  $V_{02}^+$  and  $V_{12}^+$ , respectively.

The HLDDs shown in Figure 5.6 and Figure 5.7 represent the cone output  $V_1^+$  under normal and faulty conditions, respectively. It can be observed in the figures that the path constraints of  $p_5$  (to node  $n_5$ ) in both the HLDDs is  $C_{p_5} = \langle sel1 = 1, sel34 = 1, sel56 = 0 \rangle$ . For the values of control signals  $\langle sel1, sel34, sel56 \rangle = \langle 1, 1, 0 \rangle$ , the values evaluated at node  $n_5$  (i.e.,  $\lambda_5(op_{n_5})$ ) in the normal HLDD (Figure 5.6) and in the faulty HLDD (Figure 5.7) are different. This is because the value of  $\lambda_5(op_{n_5}) = V_1 - V_2$  under normal condition is never equal to zero since  $V_1$  and  $V_2$  have distinct values (i.e.,  $\lambda_5(op_{n_5}) \neq 0$ ), whereas the value of  $\lambda_5(op_{n_5}) = V_2 - V_2$  under fault  $F_1$  is always equal to zero (i.e.,  $\lambda_5(op_{n_5}) = 0$ ). The control signals ( $\langle sel1 = 1, sel34 = 1, sel56 = 0 \rangle$ ) along with faulty output ( $V_{11}^+ = 0$ ) can detect fault  $F_1$ . Such values of control signals that result in manifestation of faults through the cone outputs are termed as *FD-control-patterns* (fault detecting control patterns). Now we can formally define *FD-control-pattern* as follows:

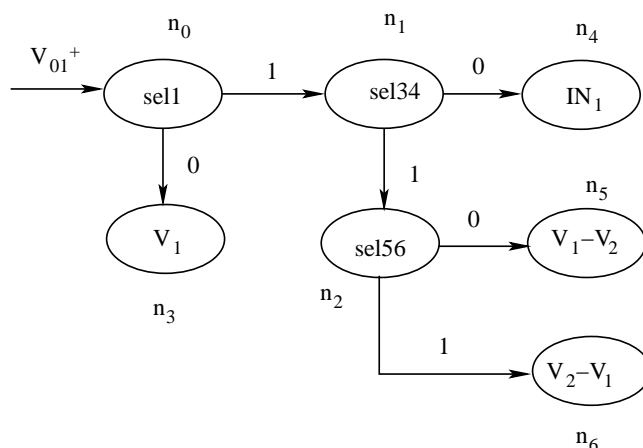


Figure 5.6: HLDD representing  $V_1^+$  under normal condition.

**Definition 5.4. *FD-control-pattern:*** The path constraint  $C_{p_k}$  for path  $p_k$  to node  $n_k$  (i.e., values of control signals  $\langle sel1, sel2, \dots \rangle$ ) is called “*FD-control-pattern for fault  $F_i$  manifested through cone for  $V_j^+$* ”, if the values of  $V_j^+$  under normal and faulty conditions are different. That means  $V_{0j}^+ \neq V_{ij}^+$  for these control signal values.

In the next section, we discuss the procedure of generation of exhaustive set of *FD-control-patterns* for all possible faults using HLDDs. Following that, the procedure of design of the *FN-detector* is discussed using the set of *FD-control-patterns* and their faulty outputs.

### 5.3 Circuit modeling at RTL: Normal and faulty conditions

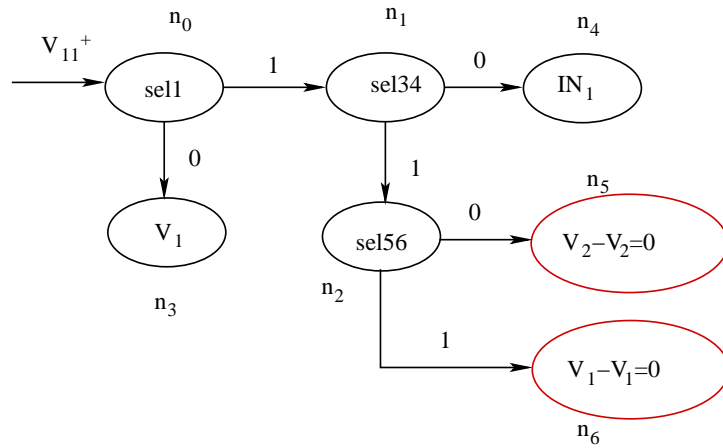


Figure 5.7: HLDD representing  $V_1^+$  under fault  $F_1$ .

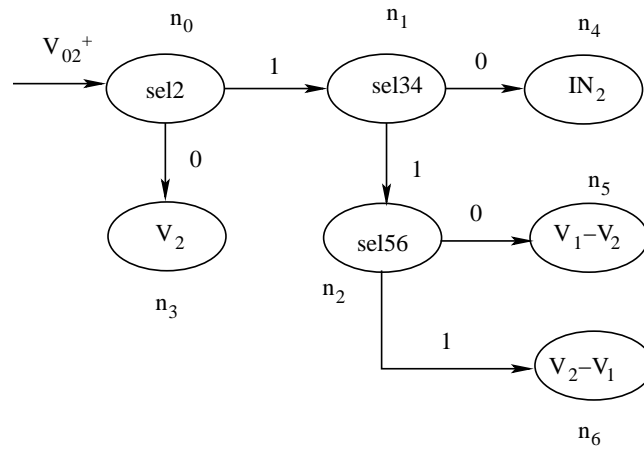


Figure 5.8: HLDD representing  $V_2^+$  under normal condition.

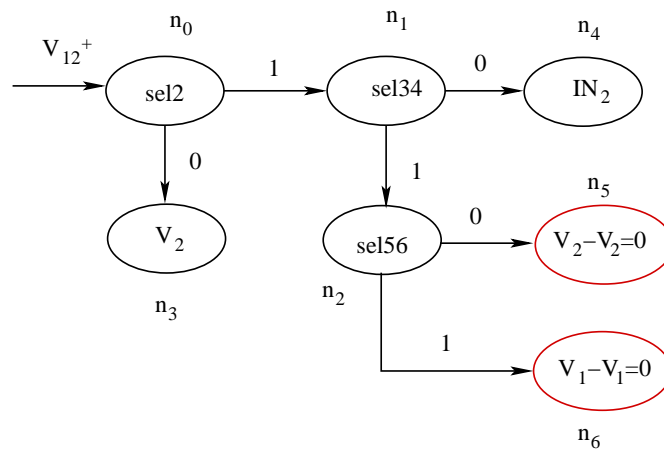


Figure 5.9: HLDD representing  $V_2^+$  under fault  $F_1$ .

## 5.4 Generation of exhaustive set of $FD$ -control-patterns and design of $FN$ -detector

As discussed in Chapter 4, Section 4.3, the steps for efficient construction of  $FN$ -detector involves– partitioning the CUT into smaller sub-parts based on cones of influence, representation of output of each cone under normal and faulty conditions using separate OBDDs, generation of  $FD$ -transitions from the OBDDs and finally design of the  $FN$ -detector using the  $FD$ -transitions. In similar way, in this work we start with partitioning of the CUT into a number of sub-circuits based on cones of influence with respect to the registers, then represent output of each cone under normal and faulty conditions using separate HLDDs. We generate  $FD$ -control-patterns from the HLDDs and design the  $FN$ -detector using the  $FD$ -control-patterns. In this section, we discuss the procedure of generation of the exhaustive set of  $FD$ -control-patterns and design of the  $FN$ -detector.

Consider the fault  $F_i$  at a module  $m$  of the CUT. Initially, the CUT is partitioned using cones of influence with respect to the registers. Let the module  $m$  belong to  $n$  different cones. The following HLDD based operations are executed for each cone in order to generate the exhaustive set of  $FD$ -control-patterns for  $F_i$ .

1. Let the cone  $V_j^+$  be the one of the cones that contains  $F_i$ . Generate HLDDs for this cone under normal condition as well as under fault  $F_i$ . Let  $G_{DDN}$  be the HLDD to represent  $V_j^+$  under normal condition (i.e.,  $V_{0j}^+$ ) and  $G_{DDF_i}$  be the HLDD to represent  $V_j^+$  under fault  $F_i$  (i.e.,  $V_{ij}^+$ ).
2. Traverse the HLDDs,  $G_{DDN}$  and  $G_{DDF_i}$ , starting from their initial nodes to the corresponding terminal nodes  $n_{k_N}$  and  $n_{k_{F_i}}$  in the respective HLDDs, where the path constraints  $C_{p_{k_N}}$  (to  $n_{k_N}$ ) and  $C_{p_{k_{F_i}}}$  (to  $n_{k_{F_i}}$ ) in both the HLDDs are same.
  - (a) Find the terminal nodes  $n_{k_{F_i}}$  in  $G_{DDF_i}$  (corresponding to  $n_{k_N}$  in  $G_{DDN}$ ) where  $\lambda_k(op_{n_{k_{F_i}}}) \neq \lambda_k(op_{n_{k_N}})$ . Let  $TN$  be the set of such terminal nodes.
3. For each terminal node  $n_{k_{F_i}} \in TN$ , find path  $p_{k_{F_i}}$  to  $n_{k_{F_i}}$  in  $G_{DDF_i}$  and its path constraint  $C_{p_{k_{F_i}}}$ . Let  $CP$  be set of such path constraints.
4. The  $FD$ -control-pattern that manifest fault ( $F_i$ ) effect through  $V_j^+$  can be obtained by mapping each path constraint in  $CP$  into control signals of the CUT. Let  $X_{FD_i}$  be the set of such  $FD$ -control-patterns.

## 5.4 Generation of exhaustive set of $FD$ -control-patterns and design of $FN$ -detector

---

5. For each  $FD$ -control-pattern  $fd \in X_{FD_i}$ , check if  $fd$  is an *invalid control signal*; if so, drop  $fd$  from  $X_{FD_i}$ . Eventually,  $X_{FD_i}$  becomes the exhaustive set of  $FD$ -control-patterns for the fault  $F_i$  through cone  $V_j^+$ .
6. For each  $FD$ -control-pattern  $fd \in X_{FD_i}$ , the faulty output for  $V_j^+$  can be obtained by applying the values of control signals in  $fd$  to the faulty HLDD (i.e.,  $G_{DDF_i}$ ).

Now we explain the above procedure with the help of the GCD circuit and fault  $F_1$  (i.e., fault at *mux5*). The partitioning of the CUT using cones of influence with respect to the registers is shown in Figure 5.3. Here, both the cones *cone1* and *cone2* include the fault  $F_1$ . Let us first consider *cone1* whose output is  $V_1^+$  and generate the set of  $FD$ -control-patterns for  $F_1$ . The HLDDs for  $V_1^+$  under normal condition (i.e.,  $V_{01}^+$ ) and under fault  $F_1$  (i.e.,  $V_{11}^+$ ) are shown in Figure 5.6 and Figure 5.7, respectively. Now we traverse both the HLDDs starting from their initial nodes to each terminal node and evaluate the operations associated with them. Here, terminal nodes  $n_5$  and  $n_6$  in the faulty HLDD give different values compared to the terminal nodes with same path constraints in the normal HLDD. Next, we find path constraints to these terminal nodes. The path constraints to node  $n_5$  and  $n_6$  for the control signals  $\langle sel1, sel34, sel56 \rangle$  are  $\langle 1, 1, 0 \rangle$  and  $\langle 1, 1, 1 \rangle$ , respectively. The  $FD$ -control-patterns to detect  $F_1$  through cone  $V_1^+$  for the values of  $\langle sel1, sel2, sel34, sel56 \rangle$  are  $\langle 1, d, 1, 0 \rangle$  and  $\langle 1, d, 1, 1 \rangle$ , where  $sel2 = d$  indicates that  $sel2$  does not belong to HLDD for  $V_1^+$ . The faulty output for  $V_1^+$  can be obtained by applying the  $FD$ -control-patterns to the faulty HLDD shown in Figure 5.7. For both the  $FD$ -control-patterns, the faulty output manifested through  $V_1^+$  is 0.

Similarly,  $FD$ -control-patterns can be generated by considering *cone2* and these are  $\langle d, 1, 1, 0 \rangle$  and  $\langle d, 1, 1, 1 \rangle$ . For these  $FD$ -control-patterns, the faulty output manifested through  $V_2^+$  is 0. Now the exhaustive set of  $FD$ -control-patterns for  $F_1$  is  $\{\langle 1, d, 1, 0 \rangle, \langle 1, d, 1, 1 \rangle, \langle d, 1, 1, 0 \rangle, \langle d, 1, 1, 1 \rangle\}$ . Among them, the  $FD$ -control-patterns  $\langle 1, d, 1, 1 \rangle$  and  $\langle d, 1, 1, 0 \rangle$  are not considered in the  $FN$ -detector design because these are *invalid control signals*, which cannot be found in Table 5.1. Thus, we have only two  $FD$ -control-patterns for fault  $F_1$  and these are  $\langle 1, d, 1, 0 \rangle$  and  $\langle d, 1, 1, 1 \rangle$ . The  $FD$ -control-pattern  $\langle 1, d, 1, 0 \rangle$  manifests  $F_1$  through  $V_1^+$  with faulty response 0 and the  $FD$ -control-pattern  $\langle d, 1, 1, 1 \rangle$  manifests  $F_1$  through  $V_2^+$  with faulty response 0.

In next subsection, we explain how to design the  $FN$ -detector using the exhaustive set of  $FD$ -control-patterns with their faulty responses.

### 5.4.1 Design of $FN$ -detector

The  $FN$ -detector runs in parallel with the Circuit Under Test (CUT) by tapping the control signals and cone outputs (values of registers). The interconnection of the CUT and the  $FN$ -detector is shown in Figure 5.10. If an  $FD$ -control-pattern appears in the CUT and it results in faulty output, then the  $FN$ -detector makes the status as high to indicate that fault has occurred in the CUT. We first illustrate the design of the  $FN$ -detector for the  $FD$ -control-pattern  $\langle 1, d, 1, 0 \rangle$  (say  $fd$ ), shown in Figure 5.11. Following that, we shall discuss a generalized procedure for its design.

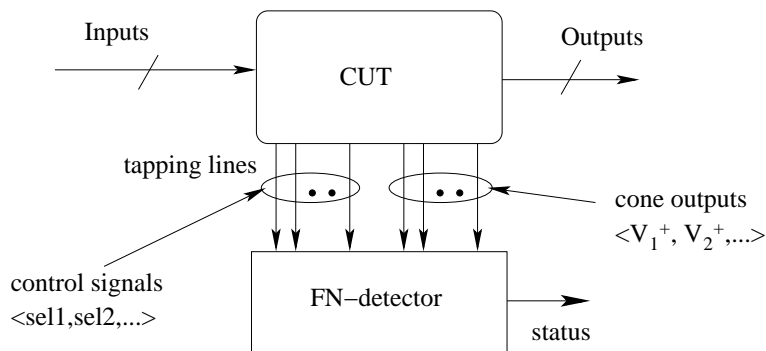


Figure 5.10: Interconnection of the CUT and the  $FN$ -detector.

As already discussed, in case of  $fd = \langle 1, d, 1, 0 \rangle$  the value of  $V_1^+$  becomes 0 under fault  $F_1$ , whereas in the normal case it has non-zero values. So, for detection of  $F_1$  the  $FN$ -detector needs to monitor control signals ( $\langle sel1, sel2, sel34, sel56 \rangle$ ) and the cone output ( $V_1^+$ ). Checking the occurrence of fault can be accomplished in two clock cycles. The timing diagrams of the CUT and the  $FN$ -detector are shown in Figure 5.12. The  $FN$ -detector runs in parallel with the CUT and both are driven by the same clock. In the first clock cycle, the  $FN$ -detector checks whether the values of the control signals generated by the CUT are same as  $fd$  (i.e.,  $\langle sel1, sel2, sel34, sel56 \rangle = \langle 1, d, 1, 0 \rangle$ ); this can be simply verified by measuring only the control signals of the CUT and measuring the value of cone output (i.e.,  $V_1^+$ ) is not required (shown by the 1<sup>st</sup> dotted line in Figure 5.12). Following that, in the next clock cycle the  $FN$ -detector examines if the output of the cone matches the value under faulty condition, i.e.,  $\langle V_1^+ = 0 \rangle$ ; this can be verified by measuring only the cone output and the values of control signals are not necessary to be measured. Again, while considering one cone, the output of other cones are not required to be measured. Since we have considered the cone for  $V_1^+$ , thus, the value of  $V_2^+$  is not required to be measured. So the cone outputs measured in second clock cycle are  $\langle V_1^+, V_2^+ = 0, d_{k_2} \rangle$  (shown by the 2<sup>nd</sup> dotted line in Figure 5.12), where  $d_{k_2}$  represents  $k_2$ -bits as don't care values. If it happens,

## 5.4 Generation of exhaustive set of $FD$ -control-patterns and design of $FN$ -detector

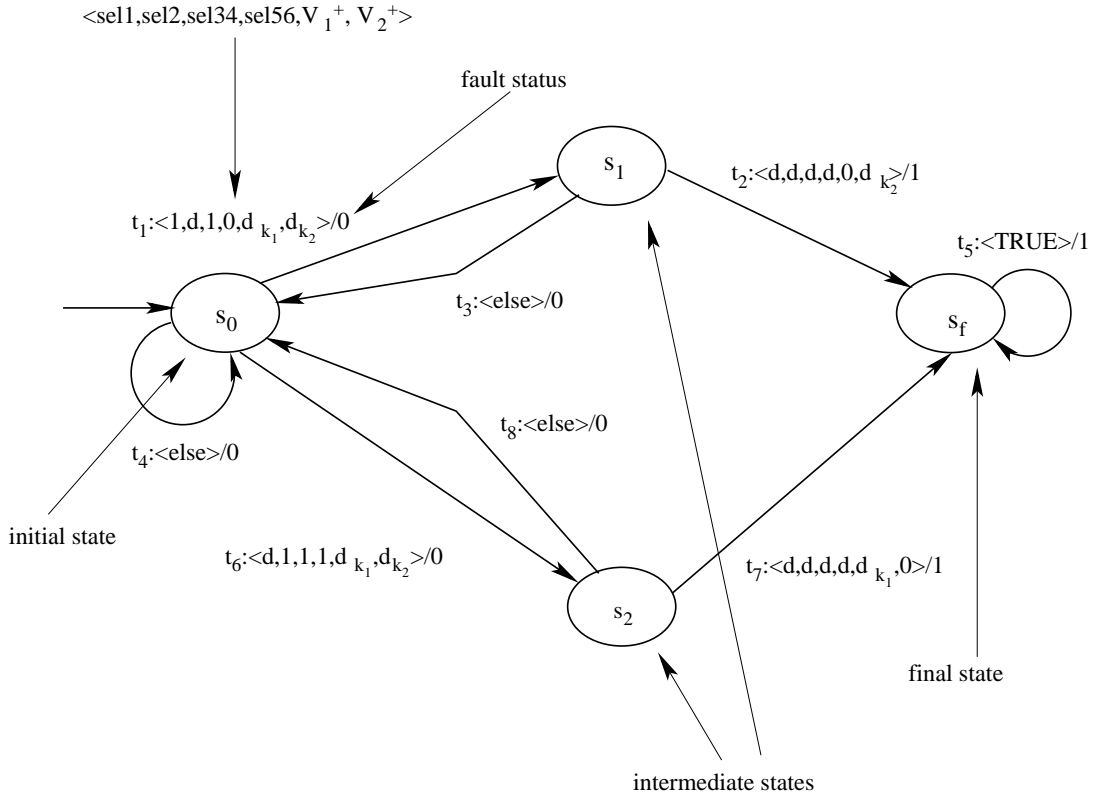


Figure 5.11: State transition diagram for the  $FN$ -detector.

then the status signal becomes high which indicates that fault ( $F_1$ ) has occurred in the CUT.

The state transition diagram of the  $FN$ -detector of the CUT to detect  $F_1$  is shown in Figure 5.11. In the detector, the transitions  $t_1$ ,  $t_2$  and  $t_3$  correspond to  $fd$ . The  $FN$ -detector starts from its initial state  $s_0$  and reaches the intermediate state  $s_1$  when the CUT satisfies the values of control signals  $\langle sel1, sel2, sel34, sel56 \rangle = \langle 1, d, 1, 0 \rangle$ . This is captured by the transition  $t_1 : \langle 1, d, 1, 0, d_{k_1}, d_{k_2} \rangle / 0$ . It may be noted that enabling condition of  $t_1$  is  $\langle 1, d, 1, 0, d_{k_1}, d_{k_2} \rangle$ , which implies that the values of  $sel1 = 1$ ,  $sel2 = d$ ,  $sel34 = 1$ ,  $sel56 = 0$ ,  $V_1^+ = d_{k_1}$  and  $V_2^+ = d_{k_2}$ , where  $d_{k_1}$  and  $d_{k_2}$  represent  $k_1$ -bits and  $k_2$ -bits as don't care values, respectively. The output bit of  $t_1$  is 0, which indicates fault has not yet been detected. In simple words, for each  $FD$ -control-pattern there is a transition from initial state to intermediate state with enabling signals same as the  $FD$ -control-pattern. From state  $s_1$ , the detector needs to verify whether  $F_1$  has occurred in the CUT in the next clock cycle. This is accomplished by transition  $t_2 : \langle d, d, d, d, 0, d_{k_2} \rangle$  from  $s_1$ . The enabling condition of  $t_2$  implies the values of control signals and  $V_2^+$  are don't cares and the value of  $V_1^+$  is 0 (faulty output). Thus, the transition  $t_2$  leads the  $FN$ -detector to the final state  $s_f$  yielding output 1, which indicates that  $F_1$  has occurred in the CUT. If the enabling condition of

## 5.4 Generation of exhaustive set of $FD$ -control-patterns and design of $FN$ -detector

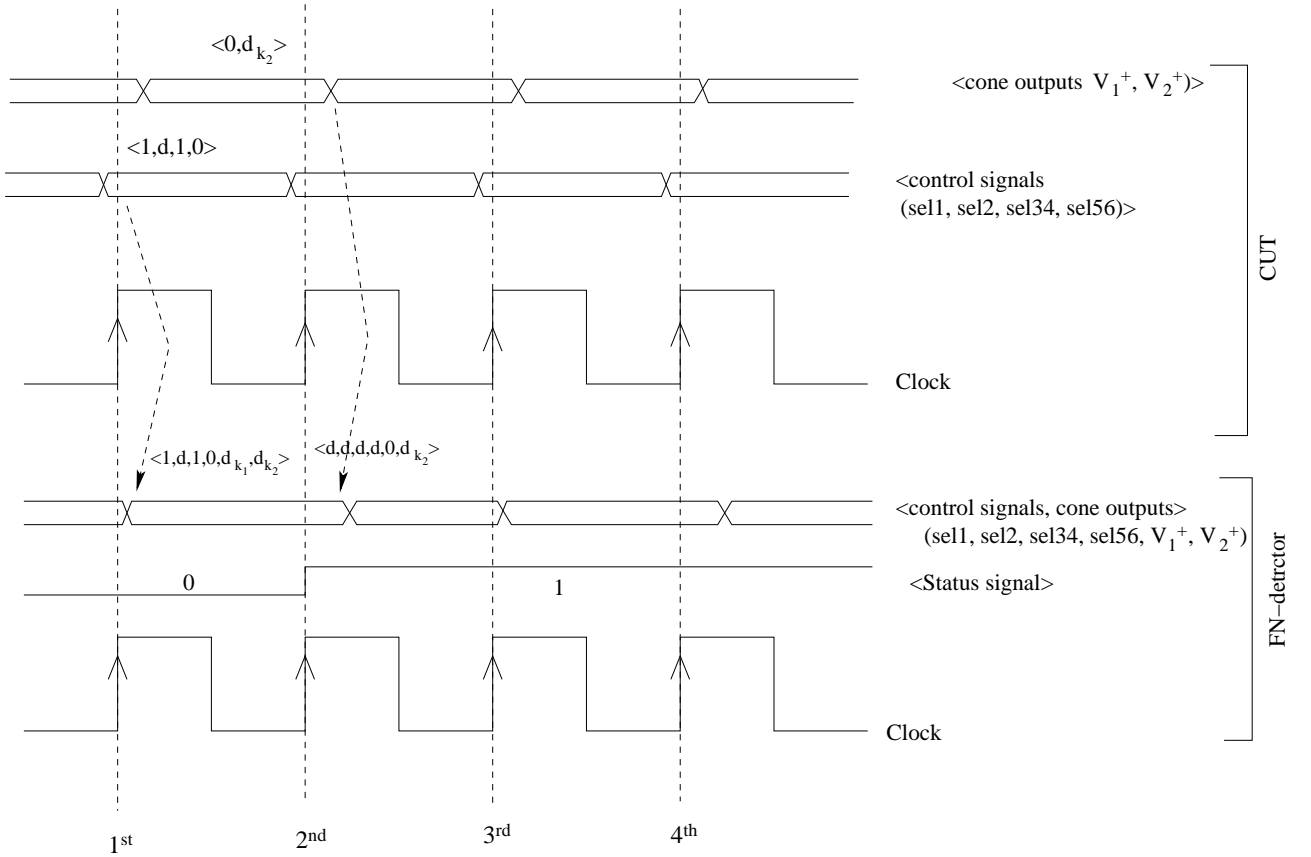


Figure 5.12: Timing diagram of the CUT versus  $FN$ -detector under fault  $F_i$ .

$t_2$  is not satisfied in the state  $s_1$  (i.e.,  $V_1^+ \neq 0$ ), then the  $FN$ -detector moves back to the initial state  $s_0$  by the transition  $t_3$ . Once the final state  $s_f$  is reached, the  $FN$ -detector remains in that state forever maintaining output as 1, since the faults are assumed to be permanent. This is accomplished by transition  $t_5$ , whose enabling condition is always TRUE.

In similar way, the working of  $FD$ -control-pattern  $\langle d, 1, 1, 1 \rangle$  with faulty output ( $V_2^+ = 0$ ) can be explained using transitions  $t_6$ ,  $t_7$  and  $t_8$ . Thus, the  $FN$ -detector has three type of states; a) an initial state ( $s_0$ ), b) a final state ( $s_f$ ) and c) a set of intermediate states, for each  $FD$ -control-pattern. Thus, the  $FN$ -detector is an FSM given by six-tuples

$$G_{FN-detector} = \langle S, s_0, \Sigma, \delta, Y, s_f \rangle, \quad (5.3)$$

where  $S$  is the set of states,  $s_0$  is the initial state,  $\Sigma$  is the input variables (control signals and cone outputs),  $\delta : S \times \Sigma \rightarrow S$  is the transition function,  $Y : S \times \Sigma \rightarrow \{0, 1\}$  is the output function and  $s_f$  is the final state. The  $FN$ -detector can be constructed by using the steps given below for each  $FD$ -control-pattern. Let  $fd$  be an  $FD$ -control-pattern that manifests

## 5.4 Generation of exhaustive set of $FD$ -control-patterns and design of $FN$ -detector

---

fault  $F_i$  through cone output  $V_m^+$  with faulty response  $R_f$ .

1. Create an initial state  $s_0$  and a final state  $s_f$ .
2. For each  $FD$ -control-pattern  $fd$ , repeat Step 3 and Step 4.
3. Create an intermediate state  $s_k$  and add a transition  $t_k$  from state  $s_0$  to  $s_k$ . Inputs of  $t_k$  are the same as the values of the signals in  $fd$  co-joined with the cone outputs, which are don't cares. Output of  $t_k$  is 0.
4. Add a transition  $t_l$  from  $s_k$  to  $s_f$ . Input of  $t_l$  includes don't cares for the control signals co-joined with the cone outputs, which are also don't cares except for the cone  $V_m^+$ . The value of  $V_m^+$  is equal to  $R_f$ . The output of  $t_l$  is 1.
5. From each intermediate state  $s_k$ , add a transition to  $s_0$ . The enabling condition of the transition is any value of the control signals and the cone outputs other than the one corresponding to the enabling condition of the transition from  $s_k$  to  $s_f$ . The output of the transition is 0.
6. Add a self loop at  $s_0$ , whose enabling condition is any value of control signals and cone outputs other than the ones corresponding to the enabling conditions of the transitions emanating from  $s_0$ . The output of the transition is 0.
7. Add a self loop at  $s_f$ , whose enabling condition is TRUE, i.e., any value of control signals and cone outputs, and its output is 1.

### 5.4.2 $FN$ -detector design for combinational part of the RTL circuit

The procedure of designing the  $FN$ -detector for the combinational part of the RTL circuit is similar to that of the sequential part of the circuit. We discuss the design procedure in brief using the example of the GCD circuit in this subsection. Like the sequential part, we partition the combinational part into a number of sub-circuits based on the cones of influence with respect to its outputs. Figure 5.13 shows the combinational part of the GCD circuit. The combinational part is partitioned into two sub-parts (cones), one is for the “not equal (NEQ)” module’s output and another is for the “less than (LT)” module’s output, which is shown in Figure 5.14. In order to illustrate the procedure of design of the  $FN$ -detector for the combinational part, we consider the cone for NEQ module and the same procedure can be applied for other modules (LT module). The inputs of the module are  $V_1$  and  $V_2$  and

the output is  $Y_1$ . Under normal condition, the output of the module (i.e.,  $Y_1$ ) is 1 (0) when  $V_1 \neq V_2$  ( $V_1 = V_2$ ). We have applied the RTL fault model presented in [25] at the NEQ module. Under faulty condition,  $Y_1$  is always 1, that implies, the difference between normal and faulty conditions is  $Y_1 = 1$ , when  $V_1 = V_2$ .

Like the sequential part, we model each cone of the combinational part under normal and faulty conditions using separate HLDDs and generate fault detecting patterns from the HLDDs. The fault detecting patterns are the inputs of the combinational part which produce different outputs under normal and faulty conditions. For this fault, the fault detecting patterns consist of all combinations of  $V_1$  and  $V_2$  where  $V_1 = V_2$ , i.e.,  $\langle V_1(k_1\text{-bits}), V_2(k_2\text{-bits}) \rangle = \langle 00\dots0, 00\dots0 \rangle, \langle 00\dots01, 00\dots01 \rangle, \langle 00\dots10, 00\dots10 \rangle, \dots, \langle 11\dots1, 11\dots1 \rangle$ . The faulty output obtained for these patterns is 1, i.e.,  $Y_1 = 1$ . The  $FN$ -detector for the combinational part is designed using the exhaustive set of fault detecting patterns and their faulty responses. The state transition diagram of the  $FN$ -detector to detect the fault at the module NEQ is shown in Figure 5.15. It involves only two states; initial state  $s_0$  and final state  $s_f$ . The transitions from  $s_0$  to  $s_f$  indicate that fault has occurred in the circuit. This is similar to the OLT at gate level for Output Function (OF) block of the circuit (Chapter 3, Subsection 3.3.3). It can be noted that the fault detection in combinational part is performed in a single clock cycle, while for the sequential part it requires two clock cycles. So, fault detection in the combinational part is more straightforward compared to the sequential part.

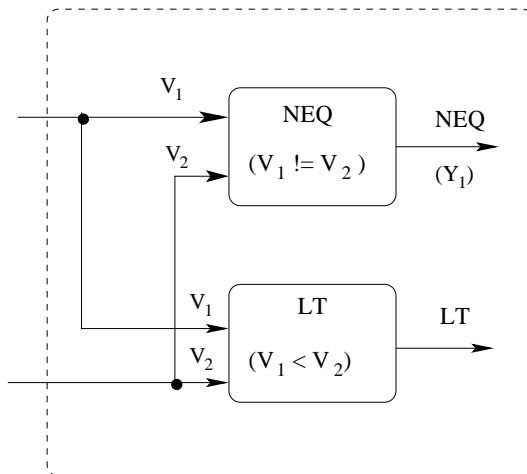


Figure 5.13: Combinational part of the GCD circuit.

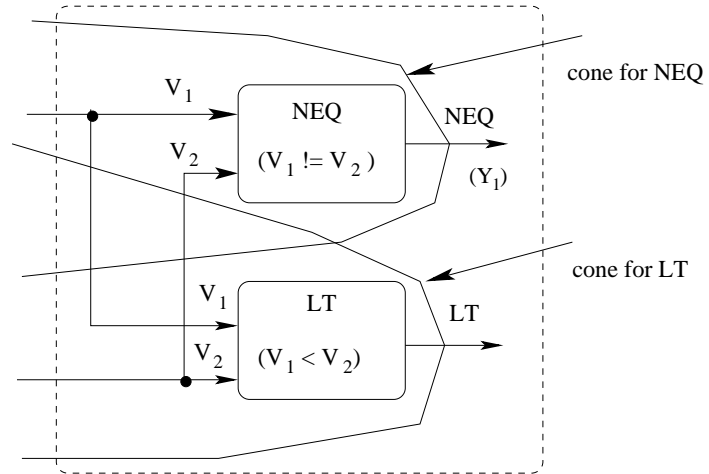


Figure 5.14: Partitioning of the combinational part using cones of influence.

In next section, we present experimental findings regarding fault coverage, test generation time and area overhead, and compare these results with gate level OLT schemes.

## 5.5 Experimental evaluation

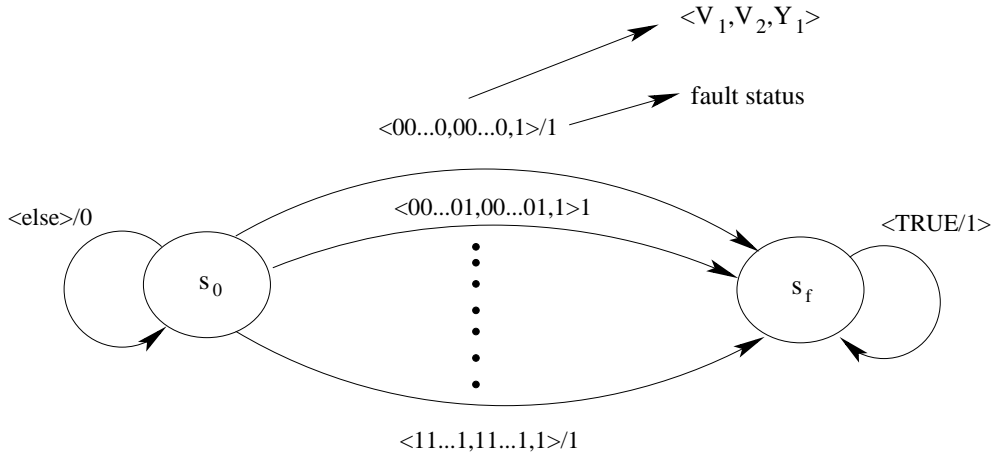


Figure 5.15: State transition diagram for the  $FN$ -detector of the combinational part.

## 5.5 Experimental evaluation

To show the feasibility of the proposed OLT scheme, we have selected different benchmark circuits. The benchmark circuits include Greatest Common Divisor (GCD), Sum of squares (sosq), 8-bit multiplier (mult8X8) and Differential equation (diffeq). These circuits have been taken from the HLSynth92 academic benchmark suit [1]. For each benchmark circuit, its RTL model is constructed from its behavioral description which is written in VHDL. Then data path of the RTL circuit is partitioned into a number of cones with respect to the registers. Appropriate high level fault models [18,25,46,59] have been chosen and applied into the different modules of the RTL data path. Using the HLDD based techniques discussed in the last two sections, we have generated the exhaustive set of  $FD$ -control-patterns for detecting faults at different modules and finally designed the  $FN$ -detector circuit using these  $FD$ -control-patterns.

The formulas for calculation of the performance parameters are as follows.

**Fault Coverage(FC):**  $FC = \frac{\text{Number of faults covered}}{\text{Total number of faults}} \times 100\%$

**Area Overhead(AO):**  $AO = \frac{\text{Area of } FN\text{-detector after synthesis}}{\text{Area of the CUT}}$

**Detection latency(DL):** For a fault  $F_i$ ,  $DL = (\lceil nfd_i / mfd_i \rceil) - 1$ , where  $nfd_i$  be the total number of  $FD$ -control-patterns for  $F_i$  and among them,  $mfd_i$  number of  $FD$ -control-patterns is considered in construction of the  $FN$ -detector.

### 5.5.1 Fault coverage analysis

Table 5.3 shows the details about RTL fault coverage and gate level stuck-at (s-a) fault coverage [36] [12] for different benchmark circuits. We have calculated the fault coverage with

0 detection latency, i.e., all the  $FD$ -control-patterns for each covered fault are considered in the construction of the  $FN$ -detector. Column 1 shows the name of the benchmark circuits, Column 2 shows the number of all possible RTL faults, Column 3 shows the percentage of coverage of the RTL faults. An RTL fault is not covered implies, we could not generate any  $FD$ -control-pattern for that fault. Column 4 shows the time required for the generation of the exhaustive set of  $FD$ -control-patterns. Column 5 shows the number of gate level s-a faults. Column 6 and Column 7 represent s-a fault coverage for the OLT scheme reported in [36] and [12], respectively. Column 8 and Column 9 represent the time taken for generation of the exhaustive set of test patterns for [36] and [12], respectively. The scheme reported in [36] works successfully only for small sized circuits because they have used FSM for circuit modeling, whereas the scheme reported in [12] is more scalable compared to [36] because of the use of OBDD.

Table 5.3: Fault coverage and exhaustive test set generation time of the proposed method and comparison with existing methods [36] and [12]

Circuit	RTL fault coverage and Time in seconds*			Gate level fault coverage and Time in seconds*				
	#Faults	Fault coverage(%)	Time	# Faults	Fault coverage(%)		Time	
					[36]	[12]	[36]**	[12]
GCD	19	89.47	56	844	92	93	NA	270
sosq	31	87.1	128	1938	88	87	NA	724
mult8X8	39	84.6	304	3915	NA	92	NA	1680
diffeq	46	95.65	823	15836	NA	95	NA	9876

\*Executed in AMD Phenom IIX3 710 Processor with 4 GB RAM in Linux OS.

\*\* [36] has not reported the execution time for test pattern generation

The fault coverage of the proposed scheme and the existing schemes ([36] and [12]) are almost same but the time taken to generate the  $FD$ -control-patterns is much lower than the time taken to generate the test patterns in [36] and [12]. The reason is that the proposed scheme generates  $FD$ -control-patterns at RTL whereas the existing schemes generate test patterns at gate level and the number of RTL faults of a circuit is less compared to s-a faults at gate level. It has been found that there exists close proximity between RTL and gate level faults [25, 59, 92]. Thus, the  $FD$ -control-patterns generated at RTL have good correlation with gate level test patterns. So there is no compromise in quality of testing at RTL. Further, the number of  $FD$ -control-patterns at RTL is less than that of test patterns at gate level for a circuit, thus, the proposed scheme has good impact on minimization of area overhead. In next subsection we will discuss the area overhead of the on-line tester in detail.

## 5.5 Experimental evaluation

### 5.5.2 Area overhead analysis

Table 5.4 shows the area overhead of the  $FN$ -detector for different benchmark circuits with different values of detection latency. Column 1 of the table shows the name of the benchmark circuits. Column 2 shows the area overhead of the proposed scheme when detection latency is equal to 0. Columns 3 and 4 show the area overheads of the schemes reported in [36] and [12], respectively, when detection latency is equal to 0. Similarly, Columns 5, 6 and 7 show the area overheads when the detection latency is equal to 3 and Columns 8, 9 and 10 show the area overheads when the detection latency is equal to 5. The following points may be noted.

Table 5.4: Area overhead of the proposed method and comparison with [36] and [12]

Circuit	Area overhead for different values of detection latency								
	For detection latency=0			For detection latency= 3			For detection latency=5		
	Proposed scheme	Existing schemes		Proposed scheme	Existing schemes		Proposed scheme	Existing schemes	
		[36]	[12]		[36]	[12]		[36]	[12]
GCD	0.97	2.4	2.34	0.93	2.2	2.25	0.88	2.1	2.08
sosq	0.92	1.65	1.67	0.90	1.52	1.48	0.86	1.3	1.23
mult8X8	0.83	NA	1.23	0.78	NA	0.95	0.63	NA	0.91
diffeq	0.74	NA	1.14	0.68	NA	0.92	0.57	NA	0.88

- Increase in the detection latency results in reduction of the area overhead of the  $FN$ -detector. For example, the area overhead of the proposed scheme for the circuit *diffeq* is 0.74 with 0 detection latency. The area overhead reduces to 0.68 when the detection latency increases to 3 and it reduces further to 0.57 when the detection latency increases to 5.
- For a given detection latency, the area overhead of the proposed scheme is always less compared to [36] and [12]. This is because the proposed scheme designs the on-line tester circuit using the  $FD$ -control-patterns which are generated at RTL, whereas the schemes in [36] and [12] designed the tester circuits using the test patterns which are generated at the gate level. To elaborate, since the the number of RTL faults of a circuit is less than that of gate level faults (s-a faults), the number of  $FD$ -control-patterns generated at RTL for a circuit is also less than that of test patterns generated at the gate level. It implies less number of  $FD$ -control-patterns in the  $FN$ -detector corresponding

to the RTL based representation, which results less area overhead compared to gate level testing.

- In RTL, we can decide the invalid  $FD$ -control-patterns for a fault and drop them in the design of the  $FN$ -detector circuit, thus the area overhead can be further reduced. Whereas, in the case of gate level circuits there is no such feature to decide invalid test patterns for a fault. So, in the gate level case, we include all the test patterns for a fault in on-line tester design which increases the area overhead.

## 5.6 Conclusion

In this chapter, we have proposed a HLDD based OLT scheme for digital circuits at RTL using different high level fault models. The proposed scheme mainly improves the scalability aspect of OLT. Experimentally, it is shown that the test generation time of the proposed scheme is much lower compared to the gate level techniques, thus, large circuits can be easily handled. It is also observed that the scheme achieves comparable fault coverage with low area overhead. The main reason for improvement in scalability is due to use of HLDD for modeling the circuits at RTL and generation of the exhaustive set of  $FD$ -control-patterns.

Most of the OLT schemes including our techniques proposed in the Chapters 3, 4 and 5 are designed for synchronous circuits. However, now-a-days asynchronous circuits are being used in the semiconductor industry, because of the advantages like no clock skew problem, higher degree of modularity, low power consumption, average case performance, etc. Thus, one of the challenges in OLT is to develop on-line testers for asynchronous circuits. In the next chapter, we extend our work by designing an OBDD based OLT scheme for Speed Independent asynchronous (SI) circuits.



# Chapter 6

## On-line Testing of Speed Independent Asynchronous Circuits

### 6.1 Introduction

Since the last two decades synchronous circuits have widespread use in VLSI design whereas asynchronous circuits have not been used in practice to that extent. However, compared to synchronous circuits, asynchronous circuits promise a number of advantages such as no clock skew problem, higher degree of modularity, low power consumption and average case performances rather than worst case executions [111]. In recent years, the use of the asynchronous circuits in the semiconductor industry has matured a lot because of the above advantages. Testing of asynchronous circuits as compared to synchronous circuits is considered difficult due to the absence of the global clock [50]. Also, On-line Testing (OLT) of such circuits is one of the challenging tasks. It is seen that most of the OLT schemes have been designed for synchronous circuits only. There are very few works that have been proposed on OLT of asynchronous circuits [107,109,129]. The details about these schemes can be found in Chapter 2, Subsection 2.3.4. The scheme proposed in [129] is based on traditional full replication technique, thus, it leads to more than 100% area and power overheads. The works reported in [107,109] are based on checking of a predefined protocol using Mutex elements. So, these schemes are protocol specific and use of Mutex elements make area overhead of these techniques high.

In this chapter, we aim at developing an efficient OLT scheme for asynchronous circuits which is protocol independent and incurs low area overhead. The proposed non-intrusive OLT scheme is easily applicable to all type of Speed Independent asynchronous circuits (SI circuits). The scheme starts with modeling of SI circuits along with their faults using Signal

## 6.2 SI circuit modeling using Signal Transition Graph and generation of $FD$ -transitions

---

Transition Graphs (STGs), then translating them into State Graphs (SGs), from which Fault Detecting transitions ( $FD$ -transitions) are generated. In case of OLT of synchronous circuits, the on-line tester circuit is a Finite State Machine (FSM) which detects the occurrence of  $FD$ -transitions (the procedure is discussed in Chapters 3 and Chapter 4). A synchronous circuit can be synthesized in a straightforward manner from the FSM specification that performs on-line testing. In similar way a synchronous circuit can be synthesized as the on-line tester for OLT of an asynchronous circuit, but the use of synchronous circuit for OLT of asynchronous circuit is not desirable. So, we propose a new technique for design of on-line tester, called Fault versus Normal condition detector ( $FN$ -detector), which can be synthesized as an SI circuit. The tester is designed as state graph model which is live and has Complete State Coding (CSC); these properties ensure its synthesizability as an SI circuit. Finally, we discuss the procedure of generation of  $FD$ -transitions in an efficient manner directly from the circuit description using Ordered Binary Decision Diagram (OBDD), without explicitly constructing the SG models whose complexity may be prohibitively high for large circuits.

The chapter is organized as follows. In Section 6.2, we discuss the modeling of an SI circuit using STG under normal and faulty conditions. Following that, conversion of STGs into SGs and generation of  $FD$ -transitions are discussed. In Section 6.3, we illustrate the design of the  $FN$ -detector using  $FD$ -transitions. Efficient generation of  $FD$ -transitions using OBDD is discussed in Section 6.4. Section 6.5 presents experimental results regarding area overhead and fault coverage of the  $FN$ -detector. Also, comparison of area overhead of the proposed scheme with other similar techniques is reported. Finally, we conclude in Section 6.6.

## 6.2 SI circuit modeling using Signal Transition Graph and generation of $FD$ -transitions

In this section, we start with modeling of an SI circuit using STG under normal and faulty conditions, then convert the STGs into SGs and generate  $FD$ -transitions. Just like modeling of synchronous circuits discussed in Chapter 3 and Chapter 4, the basic FSA framework is also used to model asynchronous circuits with slight modification. In case of synchronous circuits, state changes in the FSA occur only at the active edge of the register clock, irrespective of the time of changes in the inputs. On the other hand, in asynchronous circuits, state changes can occur immediately after a transition in the inputs. FSA used to model an asynchronous circuit is called an AFSA (Asynchronous FSA) [80]. An alternative to AFSA is Burst-mode (BM) state machines [80]. BM state machine and AFSA are similar

from the modeling perspective, however in case of the former, transitions are labeled with signal changes rather than their explicit values, which is the case in AFSAs. AFSAs and BM state machines assume that inputs change first followed by outputs and finally a new state is reached. Due to the strict sequence of signal changes all asynchronous protocols cannot be modeled using AFSAs or BM state machines. Petri net (PN) is widely accepted modeling framework for highly concurrent systems [27]. PN models a system using interface behaviors which are represented by allowed sequence of transitions or traces. The view of an asynchronous circuit as a concurrent system makes PN based models more appropriate than AFSAs and BM state machines for their analysis and synthesis. There are several variants of PNs among which Signal Transition Graph (STG) is generally used to model asynchronous circuits. The major reason is that the STG interprets transitions as signal transitions and specifies circuit behavior by defining casual relations among these signal transitions [71].

The SI circuit shown in Figure 6.1 (taken from [71]) will be considered as Circuit Under Test (CUT) to illustrate our proposed scheme. Traditionally synchronous circuits consist of blocks of combinational logic connected with clocked latches or registers, while in case of SI circuit designs, we basically have logic gates as building blocks with C-elements, which act as storage elements. Transistor level diagram of C-element is shown in Figure 6.2; logic function of the C-element can be described by the Boolean equation  $C = AB + AC' + BC'$ , where  $C$  is the next state and  $C'$  is the old state value [71, 106]. The output of C-element becomes logically high (low) when both the inputs are logically high (low), otherwise it keeps its previous logic value. There are two types of C-elements that are used in SI circuits; static C-element and dynamic C-element. The static version of C-element promises that the information inside it can be stored for unbounded periods. However, dynamic version of C-element provides gains in terms of area, power and delay [77, 105, 106, 120]. Since circuits having high operating speed, low area and power consumption are preferred in modern days, we have chosen SI circuits with dynamic C-elements instead of static ones.

Figure 6.3 shows the STG for the CUT being considered. Rising (falling) transitions on signals, indicated by  $+(-)$ , are shown in the STG. The dark circles along the arcs are called tokens. A token indicates one of possibly a set of signals that enable a transition to fire. If all input arcs for a signal transition have tokens then that signal transition is said to be enabled. For example, when signal  $Rin$  goes high (denoted by  $Rin+$ ) and signal  $Rout$  goes high (denoted by  $Rout+$ ), only then  $Aout+$  transition can take place. Upon firing  $Aout+$ , a token is placed on each of its outgoing arcs, thus enabling  $Rin-$ . Note that  $Rout-$  is enabled after  $Aout+$  and  $Ain+$ .

In this work we have considered SI circuits that contain C-elements (we assumed

## 6.2 SI circuit modeling using Signal Transition Graph and generation of *FD*-transitions

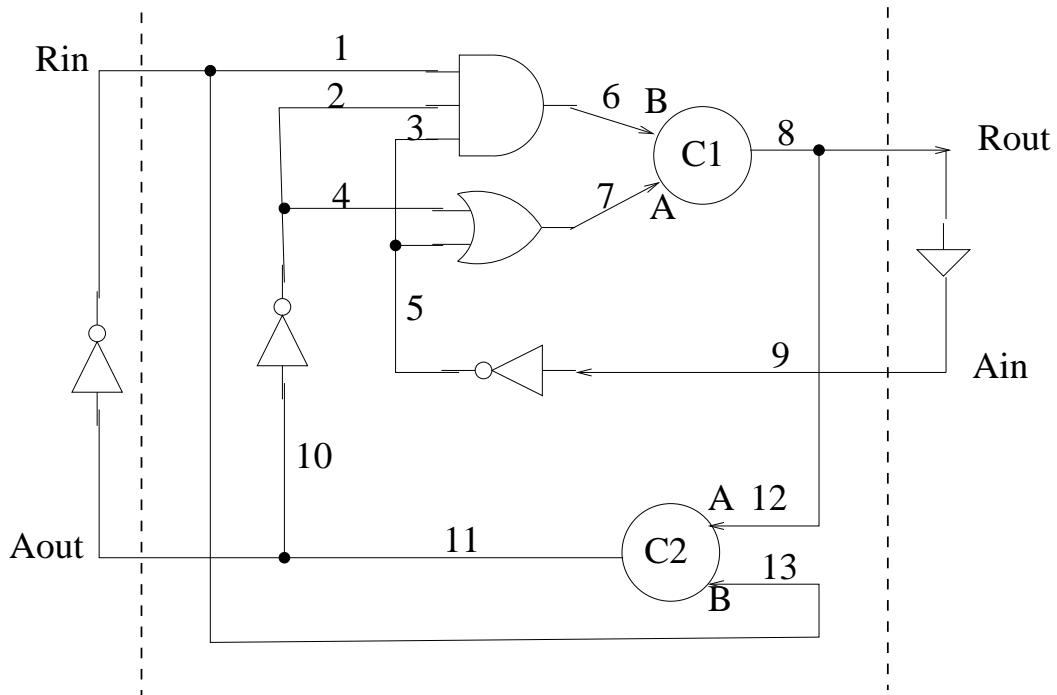


Figure 6.1: Example of speed independent circuit as CUT.

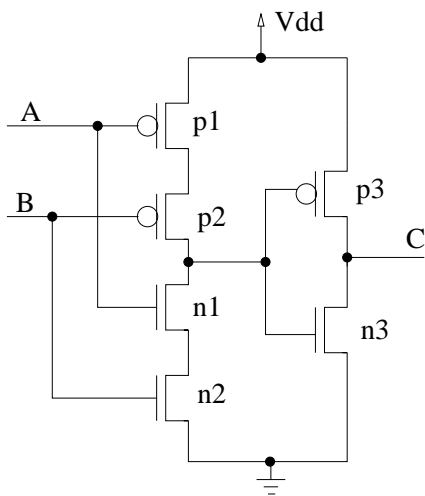


Figure 6.2: Transistor diagram of dynamic C-element.

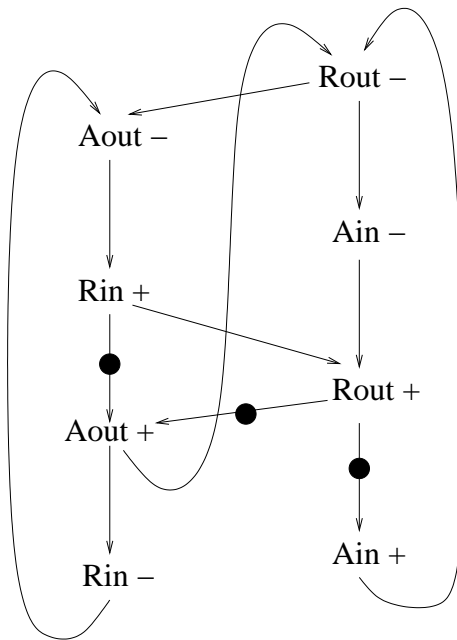


Figure 6.3: Signal Transition Graph of the sample circuit (Figure 6.1).

dynamic version) and logic gates. For the logic gates, the most popular fault model is the stuck-at (s-a) model. However, for the C-elements stuck-on and stuck-off faults for each transistor is an accepted fault model [71]. So we have chosen a mixed gate/transistor level description for modeling the faults. To illustrate fault modeling at both C-elements and basic gates, we consider the circuit example from [71] which is shown in Figure 6.1. We first model the faults in the gates and transistors (for the C-elements) and map them to STGs of the circuit. For the analysis, the signals attached to the inputs  $A$  and  $B$  of the C-elements are also indicated in the gate level circuit diagram of Figure 6.1. Now, we consider some of these faults (one at a time), analyze their effects, and finally modify the STG to model the faults.

Consider the C-element  $C2$  of Figure 6.1 and refer to transistor level circuit of Figure 6.2. The C-element  $C2$  has  $Rout$  and  $Rin$  as inputs and  $Aout$  as output. If the transistor  $n1$  has a stuck-on fault, this leads to an error in the circuit, where it needs to wait for only  $n2$  to be enabled to generate the output. When  $n2$  turns on, then a path to ground via  $n1$  and  $n2$  gets established, which makes  $p3$  on and  $n3$  off, making  $C$  high. So  $C2$  has to wait only for  $n2$  (i.e.,  $Rin+$  which corresponds to input  $B$  of  $C2$  to become 1) to turn on and change the output. In other words, it has to wait for only  $Rin+$  (and not also for  $Rout+$ , which is the requirement under normal condition) before it can generate  $Aout+$ . Thus, the fault in  $n1$  leads to premature firing of the  $Aout+$  transition. We represent this by including a token on the arc connecting  $Rout+$  to  $Aout+$ . Availability of this token will enable  $Aout+$  to fire as soon as  $Rin+$  arrives, without waiting for  $Rout+$ . This token is denoted by a '1' shown on the arc in Figure 6.4.

Now consider C-element  $C1$  producing output  $Rout$ , with transistor  $p1$  having stuck-on fault. As  $p1$  is on, the gate has to wait for  $p2$  to turn on before it can change the output. When  $p2$  turns on (by virtue of  $B = 0$ ) then there is no path to ground as  $n2$  is off, which makes  $p3$  off and  $n3$  on, making  $C$  low. Here,  $C1$  has to wait for the input  $B = 0$  to generate  $Rout-$ . Referring to Figure 6.1, for  $B$  to become 0, we need either  $Aout$  to become 1 (same as  $Rin$  becoming 0) or  $Ain$  to become 1. Thus, as soon as we have either  $Aout+$  or  $Ain+$ ,  $Rout-$  would fire. It may be noted that under normal condition, for  $Rout-$  to fire, we also require  $A = 0$ , which mandates both  $Aout+$  and  $Ain+$ . This failure condition is indicated in the STG by adding a '1' to the input arcs of  $Rout-$ , which is shown in Figure 6.5. To elaborate, Figure 6.5(a) (Figure 6.5(b)) shows that  $Rout-$  can be fired as soon as  $Ain+$  ( $Aout+$ ) fires and does not wait for  $Aout+$  ( $Ain+$ ).

As the third fault, let there be a stuck-on fault at  $n2$  of  $C1$ . The stuck-on fault at  $n2$  enforces the circuit to wait only for  $n1$  to be enabled for generating output  $Rout+$ . As  $n1$

## 6.2 SI circuit modeling using Signal Transition Graph and generation of $FD$ -transitions

---

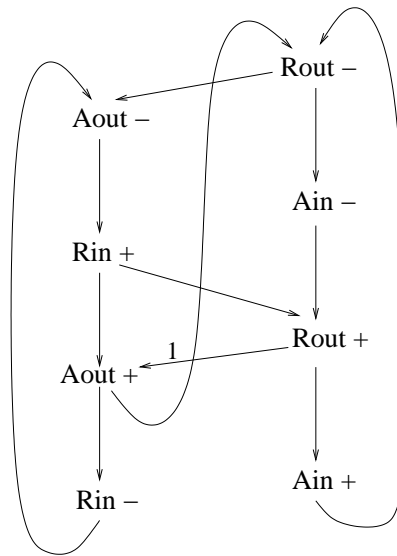


Figure 6.4: STG representation of stuck-on fault in  $n1$  of C2 (Figure 6.1).

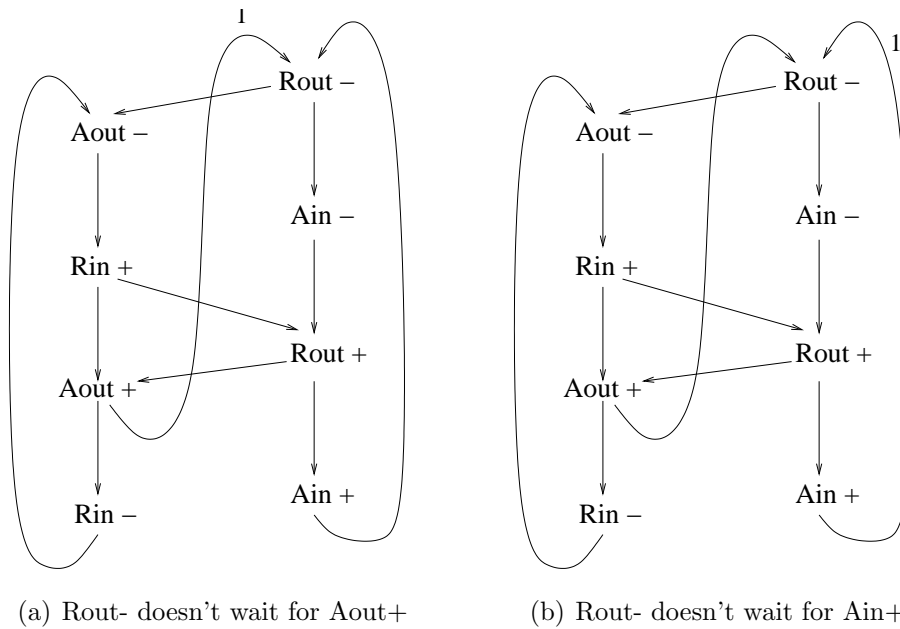


Figure 6.5: STG representation of stuck-on fault in  $p1$  of C1 (Figure 6.1).

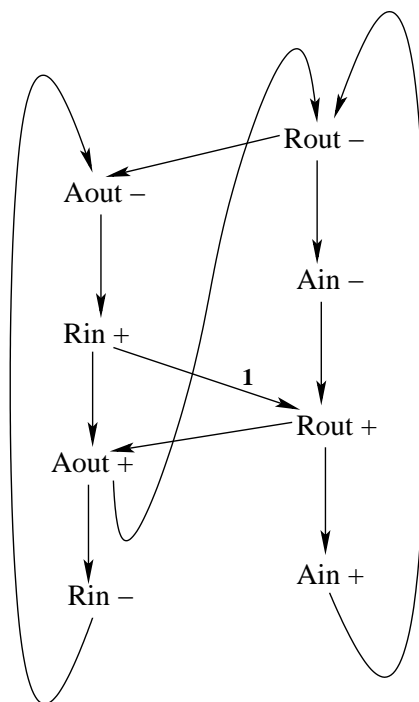


Figure 6.6: STG representation of stuck-on fault in  $n2$  of  $C1$  (Figure 6.1).

is connected to input  $A$ , which is logical ORing of  $Aout-$  and  $Ain-$ , transition  $Rout+$  can fire after  $Aout-$  or  $Ain-$  (without requiring to wait for  $Rin+$ ). This premature firing of the transition  $Rout+$  is indicated in the STG by adding a “1” to  $Rin+$ , which is shown in Figure 6.6.

For the gates, s-a-0 and s-a-1 faults are considered at their input and output nets. Let Line 2 of the AND gate from Figure 6.1 be affected by s-a-0 fault. This implies a s-a-0 fault at Line 6. As Line 6 is connected to the  $B$  input of the C-element  $C1$ , we have transistor  $p2$  on and transistor  $n2$  off. Note that, as  $n2$  is always off, there is no path to the ground. So the output  $Rout$  can never become 1, because  $p3$  can never turn on. In other words, we will never have the  $Rout+$  transition. This is indicated by adding a ‘0’ on the output arcs of  $Rout+$  in Figure 6.7. If Line 9 gets s-a-1, this will lead to Line 3 and Line 5 being affected by s-a-0 fault, further leading to Line 6 being s-a-0. As Line 6 is connected to the  $B$  input of the C-element, we will have the fault manifestation similar to the case of Line 2 s-a-0. Now we consider a s-a-0 fault at Line 13. As this line is connected to the  $B$  input of the C-element  $C2$ , it will lead to output  $Aout$  never becoming 1. That means, we will never have  $Aout+$  transition. The effect is shown by adding a ‘0’ to the output arcs of  $Aout+$ , in Figure 6.8.

## 6.2 SI circuit modeling using Signal Transition Graph and generation of $FD$ -transitions

---

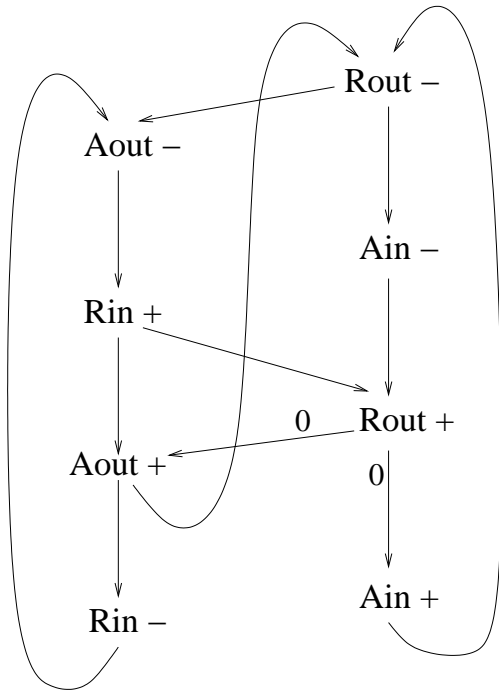


Figure 6.7: STG representation of s-a-0 fault in line-2 (Figure 6.1).

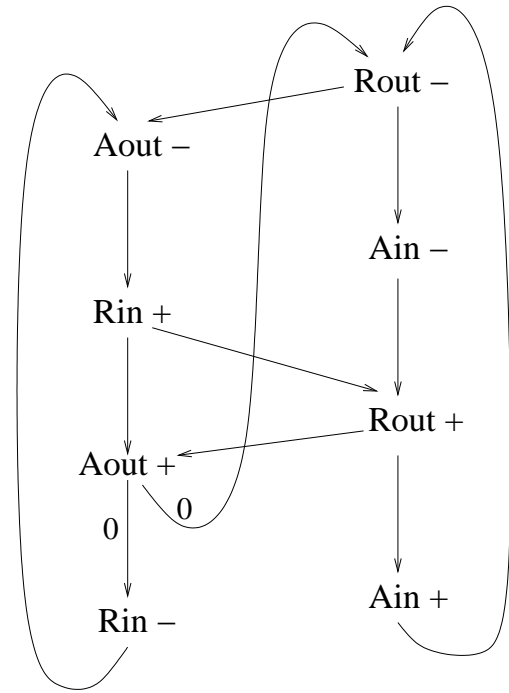


Figure 6.8: STG representation of s-a-0 fault in line-13 (Figure 6.1).

Now we consider an example of a redundant fault, i.e., no logical difference is observed in the operation of the circuit after the fault. An instance of such a fault is  $n1$  stuck-on fault in  $C1$ . This fault enforces the circuit to wait only for  $n2$  to be enabled (i.e.,  $B$  to be 1) for generating output  $Rout+$ . As  $n2$  is connected to input  $B$ , which is logical ANDing of  $Rin+$ ,  $Aout-$  and  $Ain-$ ,  $Rout+$  can fire only after three transitions, viz.  $Rin+$  and  $Aout-$  and  $Ain-$  fire. It may be noted that  $Aout-$  and  $Ain-$  also imply that input  $A$  (connected to  $n1$ ) of  $C1$  is 1, which in turn implies on condition for  $n1$ . As fault and normal condition both implies  $n1$  to be on, stuck-on fault at  $n1$  of  $C1$  do not generate any behavioral difference. Obviously, such faults cannot be detected under the single s-a fault assumption.

For the fault model considered the total number of faults in an SI circuit having dynamic C-elements is equal to 12 times the number of C-elements (each C-element consists of 6 transistors and each transistor can have stuck-on and stuck-off fault) plus twice the number of I/O lines of the gates (each line has either s-a-0 or s-a-1 fault). So the number of faults in case of the circuit considered in Figure 6.1 is not too small and listing them all would make a tabular representation long. So a partial list of faults and their effects on the STG are given in Table 6.1.

## 6.2 SI circuit modeling using Signal Transition Graph and generation of *FD*-transitions

---

Table 6.1: A partial list of faults and their effects on STG

Fault Type	Effect of fault on the transitions
Transistor n1 stuck-on fault for C1	Rout+ can only be fired after Rin+, Aout- and Ain- (same as normal condition)
Transistor n2 stuck-on fault for C1	Rout+ can be fired after either Aout- or Ain-
Transistor p1 stuck-on fault for C1	Rout- can be fired after either Aout+ or Ain+
Transistor p2 stuck-on fault for C1	Rout- can only be fired after Aout+ and Ain+
Transistor n1 stuck-on fault for C2	Aout+ can be fired after Rin+
Transistor n2 stuck-on fault for C2	Aout+ can be fired after Rout+
Transistor p1 stuck-on fault for C2	Aout- can be fired after Rin-
Transistor p2 stuck-on fault for C2	Aout- can be fired after Rout-
Transistor n1 stuck-off fault for C1	All arcs from Rout+ always 0
Transistor n2 stuck-off fault for C1	All arcs from Rout+ always 0
Transistor p1 stuck-off fault for C1	All arcs from Rout- always 0
Transistor p2 stuck-off fault for C1	All arcs from Rout- always 0
Transistor n1 stuck-off fault for C2	All arcs from Aout+ always 0
Transistor n2 stuck-off fault for C2	All arcs from Aout+ always 0
Transistor p1 stuck-off fault for C2	All arcs from Aout- always 0
Transistor p2 stuck-off fault for C2	All arcs from Aout- always 0
Transistor n3 stuck-on fault for C1	All arcs from Rout+ always 0
Transistor p3 stuck-off fault for C1	All arcs from Rout- always 0
Transistor p3 stuck-on fault for C1	All arcs from Rout- always 0
Transistor n3 stuck-off fault for C1	All arcs from Rout+ always 0
Transistor p3 stuck-on fault for C2	All arcs from Aout- always 0
Transistor n3 stuck-off fault for C2	All arcs from Aout+ always 0
Transistor n3 stuck-on fault for C2	All arcs from Aout+ always 0
Transistor p3 stuck-off fault for C2	All arcs from Aout- always 0
S-a-0 fault at Line 1 or Line 2 or Line 3 S-a-0 fault at Line 6 or Line 7 S-a-1 fault at Line 9 or Line 10	All arcs from Rout+ always 0
S-a-0 fault at Line 4 and Line 5	All arcs from Rout+ always 0
S-a-1 fault at Line 4 or Line 5 S-a-1 fault at Line 6 or Line 7 S-a-0 fault at Line 9 or Line 10	All arcs from Rout- always 0
S-a-0 fault at Line 8	All arcs from Rout+ always 0 and All arcs from Aout+ always 0
S-a-1 fault at Line 8	All arcs from Rout- always 0 and All arcs from Aout- always 0
S-a-0 fault at Line 11	All arcs from Rout- always 0 and All arcs from Aout+ always 0

## 6.2 SI circuit modeling using Signal Transition Graph and generation of $FD$ -transitions

---

S-a-1 fault at Line 11	All arcs from Rout+ always 0 and All arcs from Aout- always 0
S-a-0 fault at Line 12 or Line 13	All arcs from Aout+ always 0
S-a-1 fault at Line 12 or Line 13	All arcs from Aout- always 0

### 6.2.1 Converting STG into State Graph model and generation of $FD$ -transitions

A State Graph (SG)  $G$  is defined as  $G = \langle V, X, \mathfrak{S}, X0 \rangle$ , where  $V = \{v_1, v_2, \dots, v_n\}$ <sup>1</sup> is a finite set of Boolean variables, i.e., the domain of the variables is  $\{0, 1\}$ ,  $X$  is a finite set of states,  $\mathfrak{S}$  is a finite set of transitions and  $X0 \subseteq X$  is the set of initial states. A state  $x$  is a mapping of each variable to one of its domain elements. A *transition*  $\tau \in \mathfrak{S}$  from a state  $x$  to another state  $x^+$  is an ordered pair  $\langle x, x^+ \rangle$ , where  $x$  is denoted as *initial*( $\tau$ ) and  $x^+$  is denoted as *final*( $\tau$ ).

The stuck-on and stuck-off faults in the transistors of the C-elements of the circuit are captured by dividing the SG into sub-models and each sub-model is used to describe the system under normal or faulty conditions. To make differentiation among the sub-models, each state  $x$  is assigned a fault label by a status variable  $C$  with its domain being equal to  $\{N \cup F_1 \cup F_2 \cup \dots \cup F_p\}$ , where  $N$  is the normal status,  $F_i, 1 \leq i \leq p$ , is the fault status and  $p$  is the number of possible faults.

**Definition 6.1. Normal  $G$ -state:** A  $G$ -state  $x$  is normal if  $x(C) = N$ . The set of all normal states is denoted as  $X_N$ .

**Definition 6.2.  $F_i$ - $G$ -state:** A  $G$ -state  $x$  is fault state, or synonymously, an  $F_i$ -state, if  $x(C) = F_i$ . The set of all  $F_i$ -states is denoted as  $X_{F_i}$ .

**Definition 6.3. Normal- $G$ -transition:** A  $G$ -transition  $\langle x, x^+ \rangle$  is called a normal  $G$ -transition if  $x, x^+ \in X_N$ .

**Definition 6.4.  $F_i$ - $G$ -transition:** A  $G$ -transition  $\langle x, x^+ \rangle$  is called an  $F_i$ - $G$ -transition if  $x, x^+ \in X_{F_i}$ .

**Definition 6.5. Equivalent states:** Two states  $x$  and  $y$  are said to be equivalent, denoted as  $xEy$ , if  $x|_V = y|_V$  and  $x(C) \neq y(C)$ .

In other words two states are said to be equivalent if they have same values for state variables and different value for status variable.

---

<sup>1</sup>In case of modeling SI circuits as SG, the state variables are values of the I/O signals. So in this work, we will interchangeably use the terms signal and variable.

A transition  $\langle x, x^+ \rangle$ , where  $x(C) \neq x^+(C)$ , is called an  $s_i$ -transition (start of fault  $F_i$ ), indicating the first occurrence of fault  $F_i$  in the circuit. Faults are assumed to be permanent.

**Definition 6.6. Equivalent transitions:** *Two transitions  $\tau_1 = \langle x_1, x_1^+ \rangle$  and  $\tau_2 = \langle x_2, x_2^+ \rangle$  are equivalent, denoted as  $\tau_1 E \tau_2$ , if  $x_1 E x_2$ ,  $x_1^+ E x_2^+$  and they must associate with same signal change.*

Suppose there is a transition in faulty SG sub-model for which there is no corresponding equivalent transition in the normal SG sub-model, then that transition is called Fault Detecting transition (*FD*-transition). The fault is detected when the system traverses through the *FD*-transition. Thus, we can define *FD*-transition as:

**Definition 6.7. *FD*-transition:** *An  $F_i$ -G-transition of faulty SG sub-model  $\tau' = \langle x', x'^+ \rangle$  is an *FD*-transition, if there is no G-transition  $\tau = \langle x, x^+ \rangle$  in the normal SG sub-model such that  $\tau' E \tau$ .*

As already discussed, the first step of state based OLT is to generate normal and faulty models. For SI circuits, the STGs under normal and faulty conditions are obtained and then converted into separate SG models. We explain the concept using the example circuit of Figure 6.1 under normal and two faults, namely, stuck-on fault in  $n1$  of C2 and stuck-on fault in  $p1$  of C1.

The SG sub-model for the normal circuit is shown in Figure 6.9. It may be noted that in the circuit there are 4 I/O signals namely,  $Rin, Rout, Ain, Aout$ . In the SG model corresponding to each signal there is a discrete variable:  $\langle v_1 = Rin, v_2 = Rout, v_3 = Ain, v_4 = Aout \rangle$  which assumes values from the set  $\{0, 1\}$ . The set of states are  $X0$  to  $X13$  and  $X0$  is the initial state. State mappings and transitions are shown in Figure 6.9; e.g., state  $X0$  maps variables  $\langle Rin, Rout, Ain, Aout \rangle$  to  $\langle 1, 1, 0, 0 \rangle$ . In states  $X0$  and  $X1$  the mappings are  $\langle 1, 1, 0, 0 \rangle$  and  $\langle 1, 1, 0, 1 \rangle$ , respectively. So transition from  $X0$  to  $X1$  changes  $Aout$  from 0 to 1; this is indicated by the transition  $Aout+$ . Now, if we look at the STG for the normal circuit shown in Figure 6.3, we note that  $Aout+$  can fire if  $Rin+$  and  $Rout+$  have a token (i.e.,  $Rin = 1$  and  $Rout = 1$ ). In state  $X0$  as  $Rin = 1$  and  $Rout = 1$ , so  $Aout+$  can fire. Similarly, the whole SG is constructed.

The SG sub-model for the circuit under  $n1$  stuck-on fault in C2 is shown in Figure 6.10. The set of states are  $X'0$  to  $X'13$  and  $X'0$  is the initial state. The transitions and state mappings are shown in the figure. As discussed in the previous section,  $n1$  stuck-on fault in C2 results in premature firing of  $Aout+$  (i.e., it need not wait for  $Rout+$  and can fire only if  $Rin+$  holds). If we observe the faulty SG sub-model shown in Figure 6.10, we note that there are two dotted transitions, which correspond to the fault condition i.e., premature

## 6.2 SI circuit modeling using Signal Transition Graph and generation of *FD*-transitions

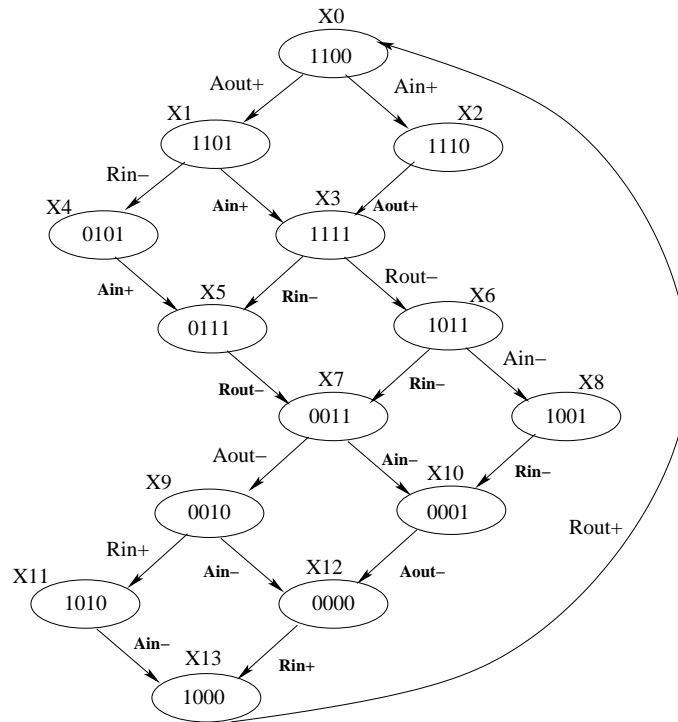


Figure 6.9: SG sub-model for the normal circuit (STG of Figure 6.3)

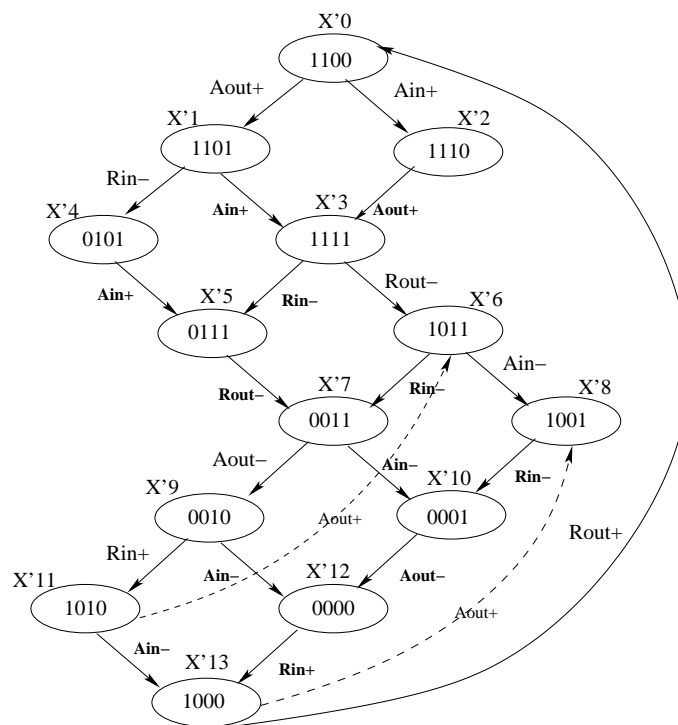


Figure 6.10: SG sub-model for the circuit with  $n_1$  stuck-on fault in C2 (STG of Figure 6.4).

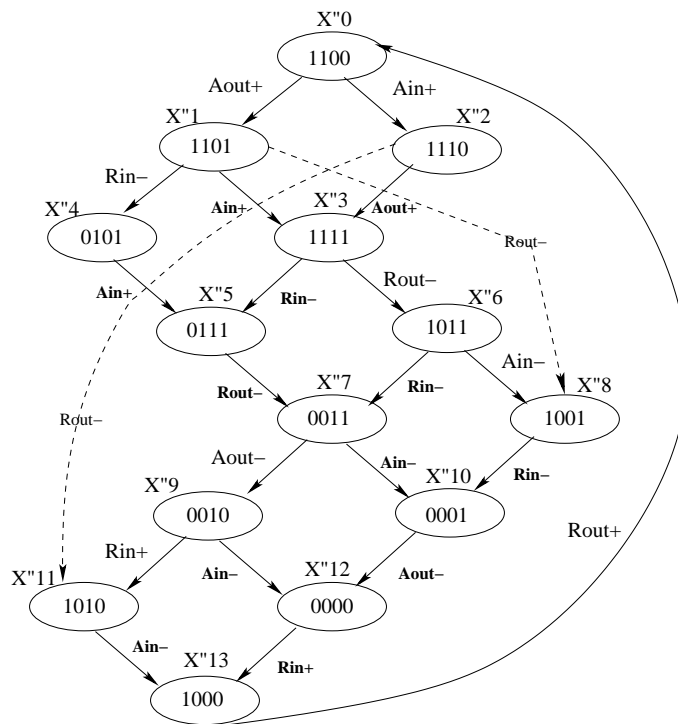


Figure 6.11: SG sub-model for the circuit with  $p1$  stuck-on fault in  $C1$  (STGs of Figure 6.5).

firing of  $Aout+$ . One dotted transition is between  $X''11$  and  $X''6$ . It may be noted that in  $X''11$  we have  $Rin = 1$ ,  $Rout = 0$ ,  $Ain = 1$  and  $Aout = 0$ ; where, even though  $Rout+$  is not enabled,  $Aout+$  fires because  $Rin+$  is enabled. A similar premature firing of  $Aout+$  occurs between  $X''13$  and  $X''8$ . So, for the fault  $n1$  stuck-on in  $C2$ , there are two *FD*-transitions namely,  $\langle X''11, X''6 \rangle$  and  $\langle X''13, X''8 \rangle$ .

The SG sub-model for the circuit under  $p1$  stuck-on fault in  $C1$  is shown in Figure 6.11. The set of states are  $X''0$  to  $X''13$  and  $X''0$  is the initial state. As discussed in the previous sub-section,  $p1$  stuck-on fault in  $C1$  results in premature firing of  $Rout-$  triggered by either  $Ain+$  or  $Aout+$ . This is captured by the dotted transitions  $\langle X''2, X''11 \rangle$  and  $\langle X''1, X''8 \rangle$  in faulty SG sub-model in Figure 6.11. The transition  $\langle X''2, X''11 \rangle$  represents firing of  $Rout-$  by  $Ain+$  in spite of  $Aout+$  not being enabled and the transition  $\langle X''1, X''8 \rangle$  represents firing of  $Rout-$  by  $Aout+$  in spite of  $Ain+$  not being enabled. Thus, for this fault there are two *FD*-transitions namely,  $\langle X''2, X''11 \rangle$  and  $\langle X''1, X''8 \rangle$ . The entire set of *FD*-transitions is shown in Table 6.2.

In the next section, we shall discuss the procedure for design of the on-line tester called *FN*-detector using *FD*-transitions and its synthesis as an SI circuit.

### 6.3 Design of $FN$ -detector using $FD$ -transitions

---

Table 6.2:  $FD$ -transitions

$FD$ -transitions	Start State	Final State	Effect
1	0001	0101	Premature fire of $Rout+$ before $Rin+$ (by $Ain-$ )
2	0000	0100	Premature fire of $Rout+$ before $Rin+$ (by $Ain-$ )
3	1110	1010	Premature fire of $Rout-$ before $Aout+$ (by $Ain+$ )
4	1010	1011	Premature fire of $Aout+$ before $Rout+$ (by $Rin+$ )
5	1000	1001	Premature fire of $Aout+$ before $Rout+$ (by $Rin+$ )
6	0111	0110	Premature fire of $Aout-$ before $Rout-$ (by $Rin-$ )
7	0101	0100	Premature fire of $Aout-$ before $Rout-$ (by $Rin-$ )
8	1011	1010	Premature fire of $Aout-$ before $Rin-$ (by $Rout-$ )
9	1001	1000	Premature fire of $Aout-$ before $Rin-$ (by $Rout-$ )
10	1101	1001	Premature fire of $Rout-$ before $Ain+$ (by $Aout+$ )

### 6.3 Design of $FN$ -detector using $FD$ -transitions

The detector is basically a state estimator which predicts whether the CUT traverses through normal or faulty states/transitions. Broadly speaking, the detector is constructed using transitions which can manifest the fault effects. In other words, such a transition is a faulty transition for which there is no corresponding equivalent normal transition. As already mentioned, we call such transitions as Fault Detecting transitions (i.e.,  $FD$ -transitions). In the circuit under consideration, comparing the normal (Figure 6.9) and  $n1$  stuck-on fault at  $C2$  SG sub-models, (Figure 6.10), we may note that there are two transitions (dotted)  $\langle X'11, X'6 \rangle$  and  $\langle X'13, X'8 \rangle$  which manifest the fault effect. Corresponding to these transitions there are no equivalent transitions in the normal sub-model. These two transitions are  $FD$ -transitions for the fault and are used in the  $FN$ -detector construction.

If the CUT is a synchronous circuit then obviously the on-line tester ( $FN$ -detector) is also a synchronous circuit that can be designed from the  $FD$ -transitions using straightforward FSM synthesis philosophy (discussed in Chapter 3 and Chapter 4). The detector FSM has three classes of states namely, initial, intermediate and final. The detector measures the I/O signals of the CUT (i.e., variables) to determine whether the following happens.

On startup, the detector is in its initial state and it checks if the CUT is in the initial state of any  $FD$ -transition. For example, if we consider only two faults in the circuit under consideration, stuck-on fault in  $n1$  of  $C2$  and stuck-on fault in  $p1$  of  $C1$ , then the  $FD$ -transition set is  $\{\langle X'11, X'6 \rangle, \langle X'13, X'8 \rangle, \langle X''2, X''11 \rangle, \langle X''1, X''8 \rangle\}$ . So in the initial state the detector checks if the signals  $Rin$ ,  $Rout$ ,  $Ain$  and  $Aout$  are 1, 0, 1 and 0 or 1, 0, 0, and 0 or 1, 1, 1 and 0 or 1, 1, 0 and 1. If so, the detector moves to an intermediate state (in the next clock edge) corresponding to the value matched. For each of the  $FD$ -transitions,

there is a corresponding intermediate state in the detector. For example, if  $Rin$ ,  $Rout$ ,  $Ain$  and  $Aout$  are measured to be 1, 0, 1 and 0 in the initial state of the detector, the detector moves to the intermediate state corresponding to *FD*-transition  $\langle X'11, X'6 \rangle$ . However, if the signals do not match the initial state of any *FD*-transition the detector loops in the initial state. In the intermediate state whether the values of the signals of the CUT match with the final state of the corresponding *FD*-transition is checked; if so, the fault is detected and the detector moves to the final state and is deadlocked there. Otherwise, it moves to the initial state. Continuing with the example, if the values of  $Rin$ ,  $Rout$ ,  $Ain$  and  $Aout$  are 1, 0, 1 and 1 respectively, from the intermediate state, *FD*-transition  $\langle X'11, X'6 \rangle$  is detected (i.e., stuck-on fault in  $n1$  of  $C2$ ) and the detector moves to the final state in the next clock edge. Otherwise, if  $Rin$ ,  $Rout$ ,  $Ain$  and  $Aout$  are 1, 0, 0 and 0 then CUT is normal and the detector moves to the initial state.

The above mentioned philosophy of constructing the detector and then synthesizing it into a synchronous system is widely used in OLT of synchronous circuits [10, 12]. Obviously, if the CUT is an SI circuit, so must be the detector circuit. However, it may be noted that the same philosophy cannot be directly used in the case of SI circuits. The reason is, the FSM of the detector designed above has liveness issue in the final state and has Complete State Coding (CSC) violations in the intermediate states. In this work, we propose a new technique for detector design which can be synthesized as an SI circuit. The detector is designed as state graph model which is live and has CSC, that ensure its synthesizability as an SI circuit. Before formalizing the algorithm for the design of the State Graph (SG) of the detector, we first introduce the basic philosophy of its working using the examples from the previous section.

An *FD*-transition in SI circuit design paradigm can be stated as “under fault, a signal  $s$  can change in the presence of signals  $y1, y2 \dots yn$ , ( $1 \leq n$ ) that is not possible under normal condition”. For example, in the case of  $n1$  stuck-on fault of  $C2$ ,  $\langle X'11, X'6 \rangle$  is an *FD*-transition which changes signal  $Aout$  from 0 to 1 (i.e.,  $Aout+$ ) and the other signals are  $Rin = 1, Rout = 0$ , and  $Ain = 1$  (Figure 6.10). It may be noted that in normal condition (shown in Figure 6.9) for changing  $Aout$  from 0 to 1 we need  $Rin = 1, Rout = 1$ , and  $Ain = 0$  (in state  $X0$ ) and  $Rin = 1, Rout = 1$ , and  $Ain = 1$  (in state  $X2$ ). Comparing with the faulty condition we may state that “under  $n1$  stuck-on fault of  $C2$ , signal  $Aout$  can change from 0 to 1 in presence of signals  $Rin = 1, Rout = 0$ , and  $Ain = 1$  which is not possible under normal condition”. So, to detect whether *FD*-transition  $\langle X'11, X'6 \rangle$  has occurred, the detector needs to tap lines  $Rout$  and  $Aout$  ( $Rin$  and  $Ain$  are not required to be monitored as their values are same under normal and faulty cases) of the CUT and

### 6.3 Design of *FN*-detector using *FD*-transitions

---

determine whether *Aout*+ has fired and at that time whether *Rout* = 0; if so, a status output line is made 1. If we consider the other *FD*-transition  $\langle X'13, X'8 \rangle$  for the fault, it can be detected by checking if *Aout*+ has fired and at that time whether *Rout* = 0; *Rin*, *Ain* are not required to be monitored as their values are same under normal and faulty cases. So, it may be stated that to detect the fault by *FD*-transitions  $\langle X'11, X'6 \rangle$  and  $\langle X'13, X'8 \rangle$  we need to check whether *Aout*+ has fired and at that time whether *Rout* = 0. Figure 6.12 illustrates the SG for detecting *n1* stuck-on fault at *C2* by *FD*-transitions  $\langle X'11, X'6 \rangle$  and  $\langle X'13, X'8 \rangle$ . The design and flow of the detector for these two *FD*-transitions are as follows:

1. The state encoding tuple is  $\langle Rout, Aout, Status \rangle$ . The initial state of the detector  $z_0$  is encoded as 100. The first two bits represent the complement of *Rout* = 0 and *Aout* = 1 i.e., complement of the value of *Rout* in state *X'11* and complement of the change of *Aout* by the *FD*-transition. The third bit represents *Status* output of the detector which is 0 until *FD*-transition is detected.
2. The detector waits for signal *Rout* to become 0 and if so, it moves to state  $z_1$  say, which is encoded as  $\langle 000 \rangle$ . However, from state  $z_0$ , if *Aout* becomes 1, *FD*-transition cannot be detected because this is normal situation (state *X0* in Figure 6.9) where *Aout*+ fires when *Rout* = 1; detector moves to state  $z_5$  having encoding  $\langle 110 \rangle$ . When *Aout* becomes 0 in state  $z_5$ , the detector moves back to  $z_0$  from where it again waits to detect whether the *FD*-transition occurs.

3. From state  $z_1$  the following may happen:

- (a) If *Rout* becomes 1, then *FD*-transition cannot be detected and so the detector moves back to  $z_0$ .
- (b) If *Aout* becomes 1, then *FD*-transition has occurred and hence, fault is detected. The detector moves to state  $z_2$  having encoding  $\langle 010 \rangle$ . Following that, the detector makes *Status* output high and moves to state  $z_3$  with encoding  $\langle 011 \rangle$ .

Once *Status* line is 1 i.e., fault is detected on-line, the system should switch to an alternative backup circuit, as under the single stuck-at fault model faults are assumed to be permanent [71]. By that logic, the detector should stop or loop in  $z_3$  indefinitely, however, it would lead to deadlock and is non-synthesizable as an SI circuit. To avoid this deadlock a simple modification is made in the detector SG without effecting the fault detection performance. We wait at state  $z_3$  for any signal to change (i.e., *Rout* from 0 to 1 or *Aout* from 1 to 0) and we move to state  $z_4$ ; let us select *Rout* for this purpose. State encoding of  $z_4$  is  $\langle 111 \rangle$ . From state  $z_4$  we have a transition to state  $z_3$  on change of *Rout* from 1 to 0.

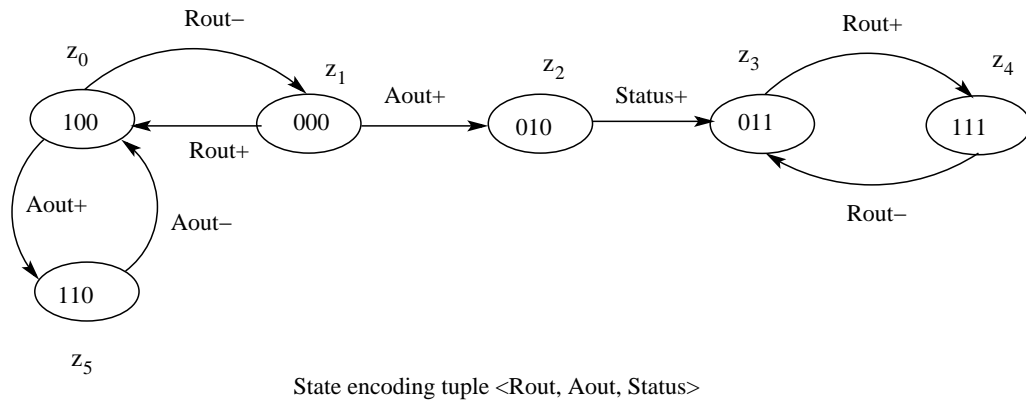


Figure 6.12: SG for detecting the  $FD$ -transitions  $\langle X'11, X'6 \rangle$  and  $\langle X'13, X'8 \rangle$

In similar way we can design SGs for the other  $FD$ -transitions shown in Table 6.2. However, it may be noted that different circuits may be required for the other  $FD$ -transitions because merging all  $FD$ -transitions in a single detector SG will lead to CSC problems. As shown in the example above, some  $FD$ -transitions can be merged into a single SG maintaining CSC. Figures 6.13, 6.14, 6.15 and 6.16 given below illustrate the SGs for some  $FD$ -transitions shown in Table 6.2. Also, the  $FD$ -transitions which could be merged are mentioned in the figures.

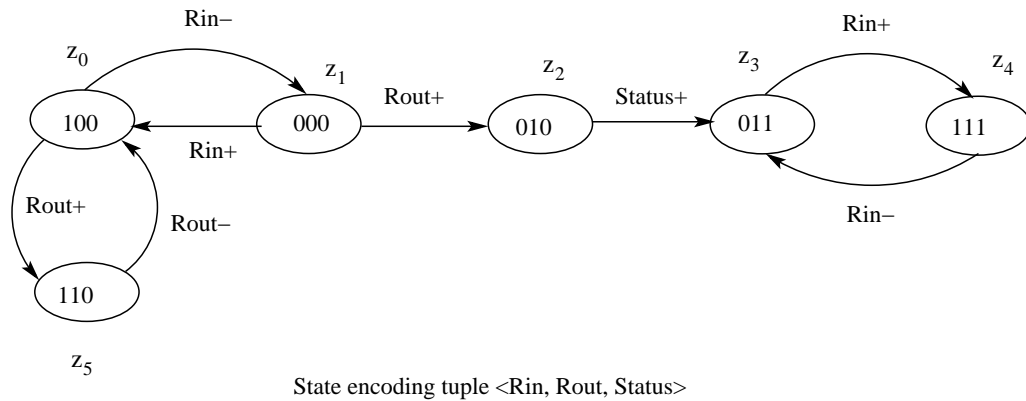


Figure 6.13: SG for detecting the  $FD$ -transitions—Sl. No. 1 and 2 of Table 6.2

Before discussing the algorithm for generating the detector SGs for a set of  $FD$ -transitions, we introduce the notion of compatible  $FD$ -transitions.

**Definition 6.8. Compatible  $FD$ -transitions:** Two  $FD$ -transitions  $\tau'1 = \langle X'1, X'1^+ \rangle$  and  $\tau'2 = \langle X'2, X'2^+ \rangle$  are compatible if the following holds:

- If  $s1$  is the signal change by  $\tau'1$  and  $s2$  is the signal change by  $\tau'2$ , then  $s1$  is same as  $s2$ . In other words, signal change by both the  $FD$ -transitions are same.

### 6.3 Design of *FN*-detector using *FD*-transitions

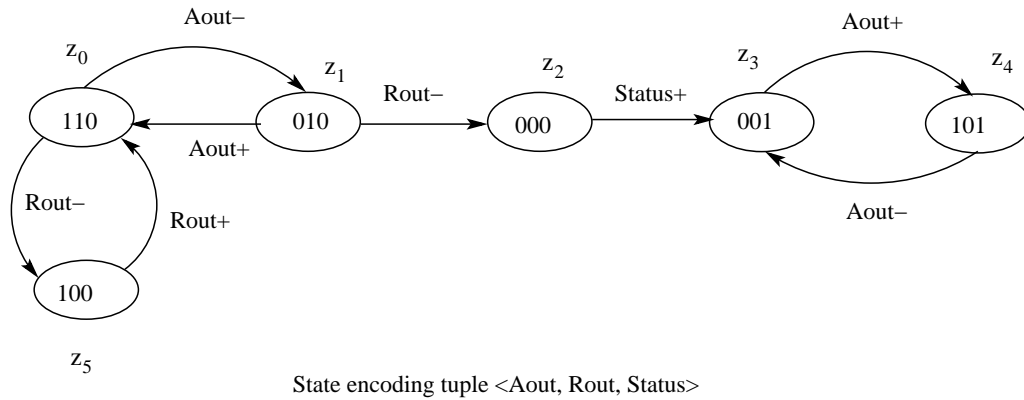


Figure 6.14: SG for detecting the *FD*-transition—Sl. No. 3 of Table 6.2

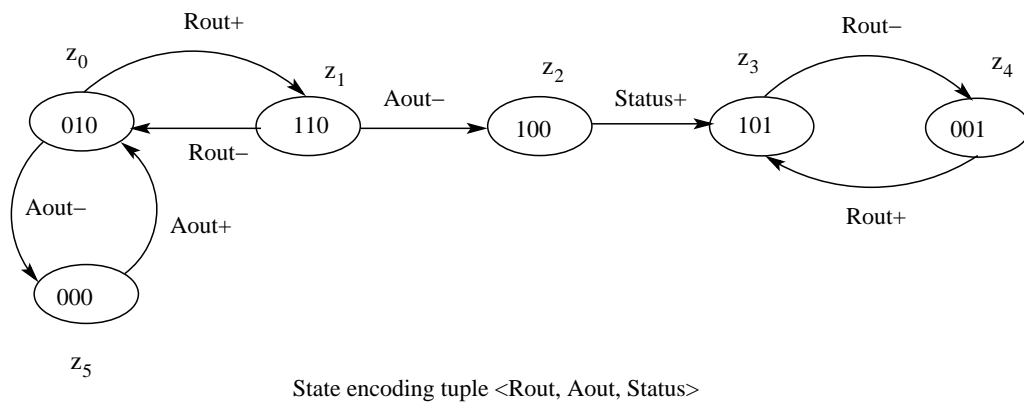


Figure 6.15: SG for detecting the *FD*-transitions—Sl. No. 6 and 7 of Table 6.2

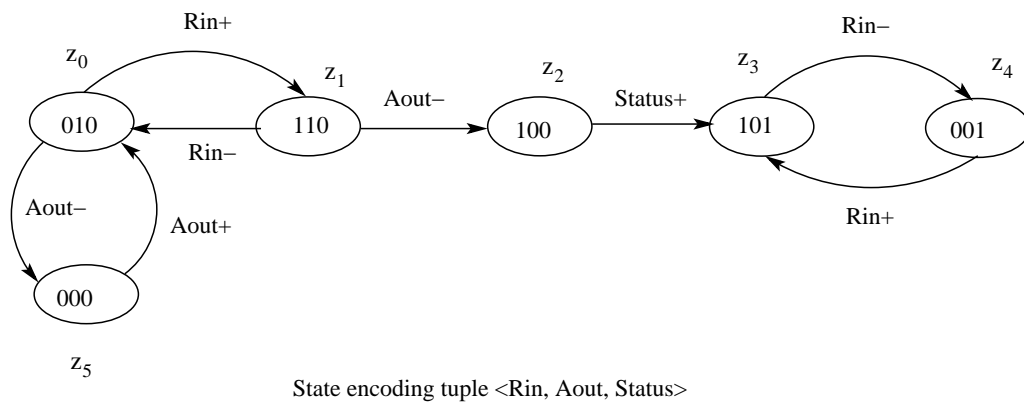


Figure 6.16: SG for detecting the *FD*-transitions—Sl. No. 8 and 9 of Table 6.2

- Let  $V'1 \subseteq V$  (for *FD*-transition  $\tau'1 = \langle X'1, X'1^+ \rangle$ ) be the set of variables whose values at  $X'1$  are different compared to state(s)  $Xi$ , where  $Xi$  is any state under normal condition (normal sub-model) from which  $s1$  is the signal change. Similarly, the set  $V'2 \subseteq V$  is calculated for *FD*-transition  $\tau'2 = \langle X'2, X'2^+ \rangle$ . Then  $V'1 \cap V'2 \neq \phi$ . In other words, there exists at least one signal (i.e., a variable) whose value is same in the initial states of both the *FD*-transitions and that is different compared to the initial state(s) of the corresponding transition(s) under normal condition.

For example, consider two *FD*-transitions  $\langle X'11, X'6 \rangle$  ( $= \tau'1$ , say) and  $\langle X'13, X'8 \rangle$  ( $= \tau'2$ , say). We calculate  $V'1$  for  $\tau'1$  as follows. The value of the variables at the initial state  $X'11$  are  $\{Rin = 1, Rout = 0, Ain = 1, Aout = 0\}$ . The signal change for  $= \tau'1$  is  $Aout+$ . We get two states ( $X0 = \{Rin = 1, Rout = 1, Ain = 0, Aout = 0\}$  and  $X2 = \{Rin = 1, Rout = 1, Ain = 1, Aout = 0\}$ ) in normal condition from which the signal change  $Aout+$  occurs. Thus,  $V'1 = \{Rout(= 0)\}$  because  $Rout$  is the only variable that is different in  $X'11$  compared to normal states  $X0$  and  $X2$ . Similarly, we calculate  $V'2$  for  $\tau'2$  as  $V'2 = \{Rout(= 0)\}$ . Since  $V'1 \cap V'2 \neq \phi = \{Rout(= 0)\}$ , thus, these two transitions are compatible and can be merged (as shown in SG of Figure 6.12). Algorithm 6.1 is used to construct SGs for the given set of *FD*-transitions.

#### 6.3.1 Circuit synthesis for *FN*-detector

It is clear from the construction of the SGs of the detectors that they have Complete State Coding (CSC) [26,69] and are live. So they can be synthesized as SI circuits using C-elements and logic gates by applying standard asynchronous circuit synthesis procedures [23,45].

Figure 6.17 illustrates some snapshots regarding the steps of synthesizing the SG of the detector shown in Figure 6.14 using the CAD tool Petrify [28]; Figure 6.17(a) is the description of the SG that is given as input to Petrify, Figure 6.17(b) illustrates the output of Petrify showing CSC and no liveness issues, and Figure 6.17(c) shows the equations obtained from Petrify. The circuit schematic (of the detector) that is synthesized for this SG is shown in Figure 6.18.

Now we explain some details of the Petrify equations. *INORDER* is a keyword of Petrify to represent all I/O signals of the corresponding SG. *OUTORDER* is the keyword to represent the output signals of the SG. Each subsequent line (denoted as [0], [1]...) represents a gate of the circuit in terms of the function it implements. In case of the circuit of Figure 6.18, *INORDER* =  $Aout, Rout, Status$  and *OUTORDER* =  $Status$ . The equations  $[0] = Aout'Rout'$  and  $[1] = 0$  represent the logic expressions of the internal Gate 4 and Gate

### 6.3 Design of *FN*-detector using *FD*-transitions

```

pradeep@pradeep-desktop:~/Desktop/asy work/example$ ./petrify FN.sg -gc -eqn FN.
eqn
The STG has CSC.
# File generated by ./petrify 4.2 (compiled 15-Oct-03 at 3:06 PM)
# from <FN.sg> on 25-Apr-14 at 1:09 PM
# CPU time: 0.01 sec -- Host: pradeep-desktop
# 0.00(trav)+0.00(init)+0.00(min)+0.00(enc)+0.00(CSC)+0.00(map)+0.00(regs)+0.0
0(irred)
# The original TS had (before/after minimization) 6/6 states
# Original STG: 3 places, 8 transitions, 13 arcs ( 5 pt + 5 tp + 3 tt)
# Current STG: 5 places, 7 transitions, 20 arcs ( 10 pt + 9 tp + 1 tt)
# It is a Petri net with 2 self-loop places
.model FN
.inputs Aout Rout
.outputs Status
.graph
Rout- p2
Rout+/1 p0 p3
Aout-/2 p3 p1
Aout+/3 p0 p3
Aout-/7 p4
Status+/5 p4
Aout+/6 Aout-/7
p0 Rout+/1 Aout-/2
p1 Aout+/3 Status+/5
p2 Rout+/1 Status+/5
p3 Rout- Aout-/2 Aout+/3
p4 Aout+/6
.marking { p0 p3 }
.end
pradeep@pradeep-desktop:~/Desktop/asy work/example$ █

.model FN.g
.inputs Aout Rout
.outputs Status
.state graph
z0_110 Rout- z5_100
z5_100 Rout+ z0_110
z0_110 Aout- z1_010
z1_010 Aout+ z0_110
z1_010 Rout- z2_000
z2_000 Status+ z3_001
z3_001 Aout+ z4_101
z4_101 Aout- z3_001
.marking {z0_110}
.end

```

(a) State graph

(b) Output of Petrify

```

# EQN file for model FN
# Generated by ./petrify 4.2 (compiled 15-Oct-03 at 3:06 PM)
# Outputs between brackets "[out]" indicate a feedback to input "out"
# Estimated area = 7.00

INORDER = Aout Rout Status;
OUTORDER = [Status];
[0] = Aout' Rout';
[1] = -0-;
[Status] = [1]' ([0] + Status) + Status [0];      # mappable onto gc
# The initial state is unstable. No reset information generated.
# Signal [1] enabled in the initial state.

```

(c) Output equations of Petrify

Figure 6.17: Screenshot showing the synthesis of on-line detector from SG using Petrify

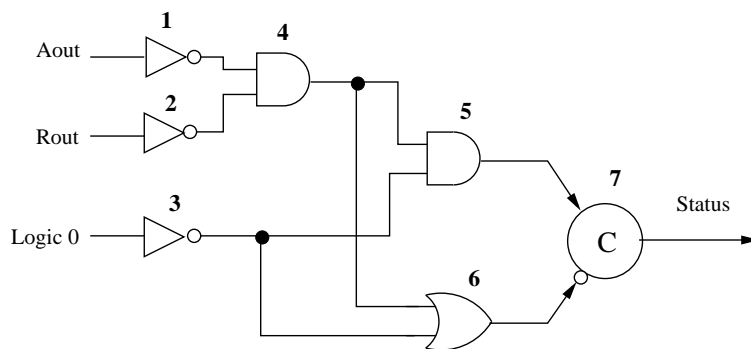


Figure 6.18: *FN*-detector circuit for the SG shown in Figure 6.14

**Algorithm 6.1** Algorithm for construction of detector SGs given the set of  $FD$ -transitions

**Input:**  $\mathfrak{S}_{FD}$ : Set of  $FD$ -transitions

**Output:** Detector SGs for determining occurrence of  $FD$ -transitions

1. Partition  $\mathfrak{S}_{FD}$  into compatible classes. Let  $\mathfrak{S}_{1FD}, \mathfrak{S}_{2FD}, \dots, \mathfrak{S}_{lFD}$  be the sets generated.
  2. For each of these sets ( $\mathfrak{S}_{iFD}, (1 \leq i \leq l)$ ) generate a detector SG using the Step (3) to Step (10).
  3.  $s$  is the signal changed by  $\tau' \in \mathfrak{S}_{iFD}$  and  $y$  is any signal whose value is the same in initial states of all  $\tau' \in \mathfrak{S}_{iFD}$ . Further, signal  $y$  is different in the initial state of the corresponding normal transition that also makes same change in  $s$ .
  4. Let state encoding of the detector be the tuple  $\langle y, s, Status \rangle$ .
  5. Create the initial state  $z_0$ . The values of the variables in  $z_0$  are as follows: (i)  $y$  in the tuple for  $z_0$  is complement of the value of the variable  $y$  in  $initial(\tau'), \tau' \in \mathfrak{S}_{iFD}$ , (ii)  $s$  in the tuple for  $z_0$  is complement of the value of the variable  $s$  after its change by  $\tau' \in \mathfrak{S}_{iFD}$ , (iii)  $Status$  in  $z_0$  is 0.
  6. Create state  $z_1$ , with transition from  $z_0$  to  $z_1$  labeled as  $y+$  ( $y-$ ) if value of  $y$  in  $z_0$  is 0 (1). Also, create a transition from  $z_1$  to  $z_0$  labeled with inverse of the signal change as in transition from  $z_0$  to  $z_1$ . Accordingly encode state  $z_1$ .
  7. Create state  $z_2$ , with transition from  $z_1$  to  $z_2$  labeled as  $s+$  ( $s-$ ) if value of  $s$  in  $z_1$  is 0 (1). Accordingly encode state  $z_2$ .
  8. Create state  $z_3$ , with transition from  $z_2$  to  $z_3$  labeled as  $Status+$ . Accordingly encode state  $z_3$ .
  9. Create state  $z_4$ , with transition from  $z_3$  to  $z_4$  labeled as  $y+$  ( $y-$ ) if transition from  $z_0$  to  $z_1$  is  $y-$  ( $y+$ ). Add a transition from  $z_4$  to  $z_3$  with inverse of the signal change as in transition from  $z_3$  to  $z_4$ . Accordingly encode state  $z_4$ .
  10. Create state  $z_5$ , with transition from  $z_0$  to  $z_5$  labeled as  $s+$  ( $s-$ ) if transition from  $z_1$  to  $z_2$  is  $s+$  ( $s-$ ). Add a transition from  $z_5$  to  $z_0$  with inverse of the signal change as in transition from  $z_0$  to  $z_5$ . Accordingly encode state  $z_5$ .
- 

3, respectively. The equation  $[Status] = [1]'([0] + Status) + Status[0]$  represents the output of the circuit.

In similar way, all SGs for the  $FD$ -transitions have been synthesized into different circuits. Then the final on-line tester circuit (called  $FN$ -detector) for CUT is constructed by simply ORing the outputs of these circuits. The output of the  $FN$ -detector becomes high when output of at least one individual detector becomes high, thereby detecting the fault.

Till now in this chapter, the procedure of generation of  $FD$ -transitions for the design of the  $FN$ -detector using SG model has been discussed. The procedure of generation of  $FD$ -transitions involves—i) modeling the SI circuit under normal and faulty conditions using STGs, ii) converting the STGs into SG sub-models, and iii) comparing each transition under normal and faulty SG sub-models. This process of generating  $FD$ -transitions from the SG

## 6.4 Efficient generation of $FD$ -transitions directly from circuit description using OBDD

---

framework becomes complex for large circuits because the number of states in the SG model grows exponentially with the variables/ signals of the circuit. Further, comparing each transition under normal and faulty sub-models in order to generate  $FD$ -transitions is a time taking task. In order to solve these problems we have devised a procedure which is capable of generating  $FD$ -transitions directly from the circuit description using OBDDs, without need of the explicit SG models.

### 6.4 Efficient generation of $FD$ -transitions directly from circuit description using OBDD

In this section, we discuss the procedure of generation of  $FD$ -transitions using OBDD based operations in detail. The steps are similar to our proposed works discussed in Chapter 3, Section 3.3 and Chapter 4, Section 4.3 with slight modifications. We first demonstrate the procedure of generation of  $FD$ -transitions using an example, following that the detailed procedure is discussed.

Consider  $n1$  stuck-on fault of  $C2$  (say  $F_1$ ) in the circuit shown in Figure 6.1, which leads to premature firing of  $Aout+$  transition. The STG model of the fault is shown in Figure 6.4 where  $Aout+$  is fired as soon as  $Rin+$  fires, without waiting for  $Rout+$ . In other words, we can say that under this fault  $Rout+$  is always true, (i.e.,  $Rout = 1$ ) and whenever  $Rin+$  occurs in the circuit then  $Aout+$  occurs. Since  $Aout$  is the output of  $C2$ , thus the Boolean expression for  $Aout$  under normal condition is  $RinRout + RoutAout' + RinAout'$  (say  $Aout_{normal}$ ). Similarly, the Boolean expression for  $Aout$  under  $n1$  stuck-on fault of  $C2$  is  $Rin + Aout'$  (say  $Aout_{faulty}$ ), which is obtained by substituting  $Rout = 1$  in the normal Boolean expression (i.e.,  $Aout_{normal}$ ). The OBDD representation of  $Aout_{normal} = RinRout + RoutAout' + RinAout'$  is shown in Figure 6.19 and the OBDD representation of  $Aout_{faulty} = Rin + Aout'$  is shown in Figure 6.20. Figure 6.21 represents the OBDD corresponding to  $Aout_{normal} \oplus Aout_{faulty}$  which is obtained by XORing the normal and faulty OBDDs illustrated in Figure 6.19 and Figure 6.20, respectively. The set of next states under faulty condition which are different compared to the normal condition is obtained by applying “satisfy-all-1” operation on the XORed OBDD, which is shown in Figure 6.21. In case of  $F_1$ , the set of next states obtained from “satisfy-all-1” operation on the XORed OBDD is  $\{\langle Rin = 1, Rout = 0, Ain = 0, Aout = 1 \rangle, \langle Rin = 1, Rout = 0, Ain = 1, Aout = 1 \rangle, \langle Rin = 0, Rout = 0, Ain = 0, Aout = 0 \rangle, \langle Rin = 0, Rout = 0, Ain = 1, Aout = 0 \rangle\}$ . Since the effect of fault  $F_1$  is premature firing of  $Aout+$ , so the value of  $Aout$  in the next states must be equal to 1. Therefore, we have considered the next states where  $Aout = 1$ . Now the set of

next state becomes as  $\{\langle Rin = 1, Rout = 0, Ain = 0, Aout = 1 \rangle, \langle Rin = 1, Rout = 0, Ain = 1, Aout = 1 \rangle\}$ . Corresponding to the next state  $\langle Rin = 1, Rout = 0, Ain = 0, Aout = 1 \rangle$ , the start/present state is  $\langle Rin = 1, Rout = 0, Ain = 0, Aout = 0 \rangle$  and the  $FD$ -transition is  $\langle 1000, 1001 \rangle$ . Similarly, corresponding to the next state  $\langle Rin = 1, Rout = 0, Ain = 1, Aout = 1 \rangle$ , the present state is  $\langle Rin = 1, Rout = 0, Ain = 1, Aout = 0 \rangle$  and the  $FD$ -transition is  $\langle 1010, 1011 \rangle$ . The same was found in the SG model for  $n1$  stuck-on fault in  $C2$  (shown Figure 6.10).

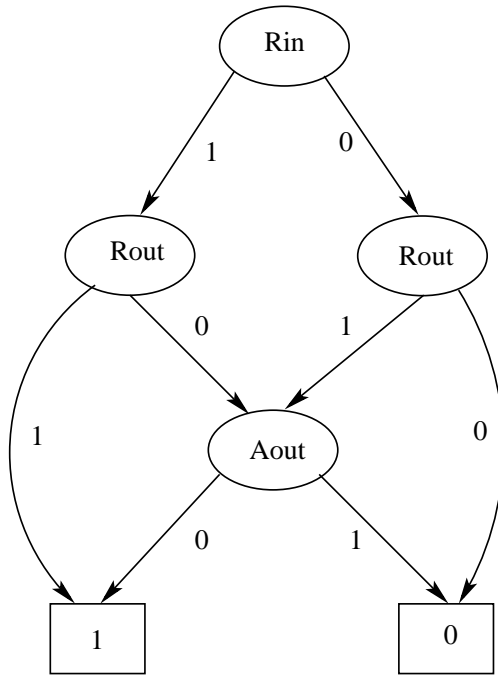


Figure 6.19: Normal OBDD for  $Aout_{normal}$

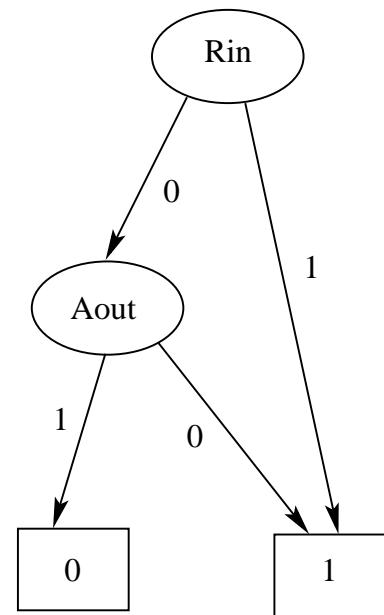


Figure 6.20: Faulty OBDD for  $Aout_{faulty}$

Next we discuss the procedure for applying OBDDs for generation of  $FD$ -transitions for a given fault (say  $F_i$ ). Initially, the effect of the  $F_i$  is found from the STG model of the fault. Let signal  $v_k$  be one of the affected signals for the fault  $F_i$  which fires prematurely. The following steps are used to generate  $FD$ -transitions to detect the premature fire of  $v_k$  due to the fault  $F_i$ .

1. Find the Boolean expression for  $v_k$  from the circuit description under normal condition (say  $v_{k_{normal}}$ ). Generate OBDD for  $v_{k_{normal}}$ . Let this OBDD be termed as “normal OBDD”.
2. Find the Boolean expression for  $v_k$  from the circuit description under fault  $F_i$  (say  $v_{k_{F_i}}$ ). Generate OBDD for  $v_{k_{F_i}}$ . Let this OBDD be termed as “faulty OBDD”.

## 6.4 Efficient generation of $FD$ -transitions directly from circuit description using OBDD

---

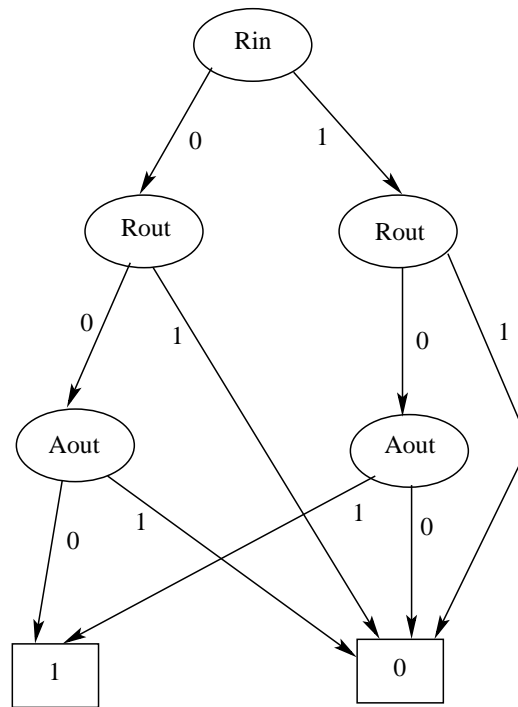


Figure 6.21: XOR OBDD for the normal and faulty OBDDs

3. The two OBDDs (normal and faulty) are XORed and “satisfy-all-1” operation is applied on the resulting XORed OBDD. This operation on the XORed OBDD generates the set of next states that are attained by the CUT on firing of  $v_k$  (rising or falling) signal under faulty  $F_i$ . Let  $NS_{v_k}$  be the set of such next states.
4. If  $F_i$  affects the rising signal of  $v_k$ , i.e.,  $v_{k+}$ , then remove the states from  $NS_{v_k}$  where the value of  $v_k$  is 0. Let  $NS_{v_{k+}}$  be the set of such next states.
5. If  $F_i$  affects the falling signal of  $v_k$ , i.e.,  $v_{k-}$ , then remove the next states from  $NS_{v_k}$  where the value of  $v_k$  is 1. Let  $NS_{v_{k-}}$  be the set of such next states.
6. Once the required set of next states (either  $NS_{v_{k+}}$  or  $NS_{v_{k-}}$ ) is determined, then for each state  $ns \in NS_{v_{k+}}$  ( $NS_{v_{k-}}$ ), its corresponding start/present state (say,  $ps$ ) is obtained by changing only the value of  $v_k$  in  $ns$  from 1 (0) to 0 (1) and other signal values remain unchanged. Finally, for each state  $ns \in NS_{v_{k+}}$  ( $NS_{v_{k-}}$ ), an  $FD$ -transition is generated which includes both start/present state and next state as  $\langle ps, ns \rangle$ , which detects the occurrence fault  $F_i$  in the CUT.

## 6.5 Experimental evaluation

To validate the efficacy of the scheme we analyze the area overhead ratio of the *FN*-detector to that of the CUT. Further, we also compare the overhead with other techniques reported in the literature. In our experiments we have considered some standard SI benchmark circuits [44]. Further, for comparison we have also implemented our scheme on the circuits used in [107].

The algorithm discussed in previous section is used to design a CAD tool OLT-ASYN which generates the *FN*-detector for OLT given an asynchronous circuit specification. We calculate performance parameters as follows.

**Fault Coverage (FC):**  $FC = (\text{Number of faults covered}) / (\text{Total number of faults}) \times 100$

**Area Overhead (AO):**  $AO = (\text{Area of the } FN\text{-detector after synthesis}) / (\text{Area of the CUT})$

Table 6.3 shows the number of gates, number of faults, fault coverage, area overhead ratio and execution time of the proposed approach for the different SI circuits being considered. The first three circuits in the table are simple examples whose gate level designs are shown in Figure 6.22, Figure 6.23 and Figure 6.24. The fourth and fifth circuits have been used in [107]. The others are standard asynchronous benchmarks [44] which are complex in terms of area, states and number of signals compared to first five circuits in the table. Broadly speaking, it can be observed in Table 6.3 that area overhead decreases with the increase of the size of the circuit. In [35], Drineas et al. have identified that the area overhead ratio for partial replication based OLT for s-a faults is approximately  $\alpha + 1/\beta$ , where  $\alpha$  is the fraction of test patterns incorporated in detector design ( $\alpha=1$  when all *FD*-transitions are incorporated in detector design) and  $\beta$  is the number of state bits required for circuit representation (i.e., proportional to the circuit size). In this work we have taken all possible *FD*-transitions and the obtained area overhead ratio acts (approximately) in accordance with the fact mentioned above.

From the discussion in the last section regarding design of the detector from the *FD*-transitions it may appear that a large number of such detectors may be required for complex circuits. In the worst case the number of detectors may be equal to the number of *FD*-transitions. Further, in case of large circuits as the number of nets and C-elements are high the number *FD*-transitions may be proportionally large. However, interestingly, the experiments illustrated reverse trends. Large circuits have high number of possible s-a faults, however, many of them are mapped to similar effects and hence same *FD*-transitions; this can be observed from Table 6.1 for the running example. Further, using the principle of compatible of *FD*-transitions, it was found that multiple *FD*-transitions fall in the same cluster thereby resulting in the fact that a single detector suffices for more than one *FD*-

## 6.5 Experimental evaluation

transition. To conclude, it was observed that a few detectors are actually required to cover all the faults. To the best of our knowledge such facts regarding OLT of asynchronous circuits were not reported in the literature.

It may be noted that percentage of fault coverage is more than 95% on the average. The number of faults that could not be detected were found to be redundant.

Table 6.3: Fault coverage, area overhead ratio and execution time for the *FN*-detector designed using the proposed approach

Circuits	Number of gates	Number of faults	% of fault coverage	Area overhead	Execution time(sec)*
Circuit 1	3	22	95	0.8	0.12
Circuit 2	5	32	96	1.5	0.23
Circuit 3	5	54	98	1.2	0.34
2 David cells [107]	6	44	94	1.6	0.22
4 David cells [107]	12	88	93	1	0.40
chu172	9	47	96	0.24	0.36
alloc-outbound	15	130	98	0.13	0.42
sbuf-read-ctl	19	152	95	0.12	0.51
sbuf-send-ctl	18	140	94	0.087	0.47
ram-read-sbuf	23	197	93	0.025	0.56

\*Executed in AMD Phenom (tm) IIX3 710 Processor with 4GB RAM in Linux OS

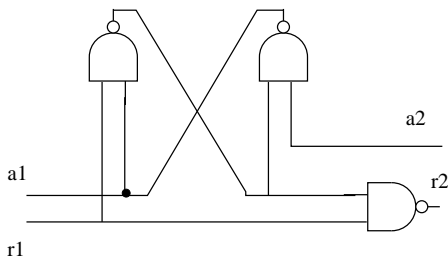


Figure 6.22: Circuit 1

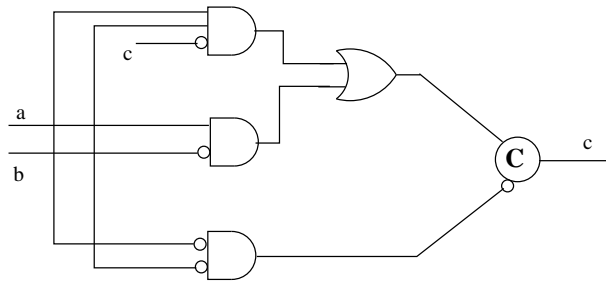


Figure 6.23: Circuit 2

### 6.5.1 Mutex approach to testing [107]

Now we will discuss in brief, the Mutex approach for on-line testing proposed in [107] and compare its area overhead ratio with our scheme. In [107] the scheme is demonstrated on the following specification of a handshaking protocol:

$req+ \rightarrow ack+ \rightarrow req- \rightarrow ack-$

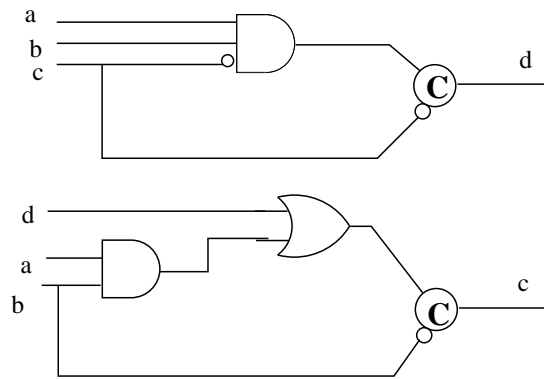


Figure 6.24: Circuit 3

OLT is performed using checkers which verify that sequencing of the signals as per the protocol is maintained, i.e., there is no premature or late firing of signals, no signal is s-a-0/s-a-1, etc. All the protocol signals are used as inputs for the checker. The checker has two functionalities namely, self checking and OLT of the handshaking protocol. The signal “mode” decides this selection. The block diagram of the checker is given in Figure 6.25. A part of the checker circuit is shown in Figure 6.26 which will be used to present the basic working of the checker. The full circuit diagram and functionality can be found in [107]. As shown in Figure 6.26, there are two Mutex components, one is used to arbitrate between  $req-$  and  $ack-$ , and another is used for the arbitration between  $mode+$ ,  $ga11+$ , and  $ga11e+$ ; the details of the signals  $ga11+$  and  $ga11e+$  are given below.

At the initial state the values of both the signals  $req$  and  $ack$  are 1, i.e., 11, which must be satisfied by the previous state. In order to provide the appropriate initial condition, the operation  $req+$  occurred before  $ack+$  in the previous state, which makes the signal  $gr11 = 1$ . As per the handshaking protocol, the operation  $req-$  should occur as the next signal change. Once  $req-$  has occurred, the signal  $ga11$  becomes 1 (left Mutex), because the signal  $ack$  is still high. So, the checker moves to next state 01, which indicates that there is no error in the protocol. Suppose there is an error in the protocol under test, that means the operation  $ack-$  precedes  $req-$ , and makes the signal  $ga11e = 1$ . This moves the checker along the faulty branch. When the  $mode$  signal is 1, then the three input arbiter (right Mutex in Figure 6.26) is used to arbitrate between  $mode+$ ,  $ga11+$  and  $ga11e+$ . This Mutex is used for self testing of the checker.

The asynchronous CUT (that realizes the above handshaking protocol), is implemented using David cells [107]. The partial checker circuit illustrated in Figure 6.26, basically tests the handshake protocol between a pair of David cells and performs self checking. Along with the partial circuit shown in Figure 6.26, there are four David cells (not shown), which

## 6.5 Experimental evaluation

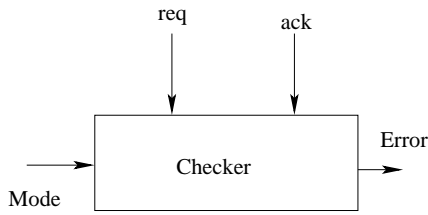


Figure 6.25: Block diagram of the checker

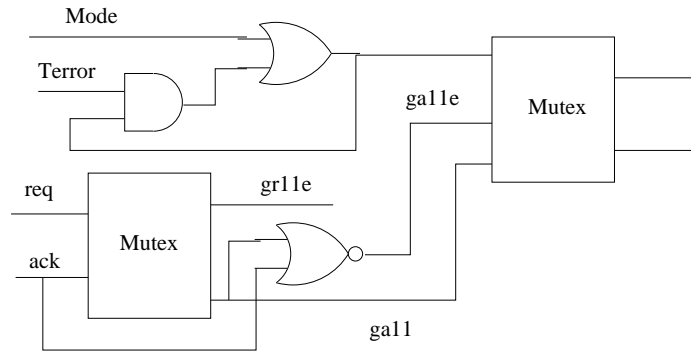


Figure 6.26: A part of the checker circuit [107]

together test the handshaking protocol (between a pair of David cells) and self testing of the checker. Among the two Mutex blocks and four David cells, half of them are used for testing the handshaking protocol and the other half is used for self testing. The logic gates are the shared resources for both the testings. In [107], both the CUT and the checker circuitry are implemented using David cells, based on the flow of converting a Petri net model to an asynchronous circuit [108].

Table 6.4: Area ratio for the Mutex approach

CUT	Circuits for OLT	Area overhead ratio for Mutex method
2 David cells	2 David cells + 2 Mutex elements + Gates	3.3
4 David cells	4 David cells + 4 Mutex elements + Gates	4.9

### 6.5.2 Comparison with the Mutex approach

The proposed approach for on-line testing does not involve self testing of the detector. So, for comparison of area overhead of the proposed scheme with [107], we require only half of the resources used in [107]. Table 6.4 shows area overhead ratio of the checker (for on-line testing only) for two circuits implementing handshaking protocols involving two and four David cells, respectively. The table also reports the number of David cells, Mutex elements and logic gates involved in the checker (for OLT). From Table 6.4 and Table 6.3 (fourth and fifth circuit) we can deduce that the area overhead requirement for the Mutex method is higher compared to that of the proposed scheme. The advantages of the proposed method over the Mutex approach are as follows.

1. The area overhead for the on-line tester circuit is less as compared to that of the Mutex approach by about 50%.

2. There is flexibility to trade-off area overhead, by reducing fault coverage depending upon the testability requirements. Such flexibility is not easy to achieve by the Mutex approach. It may be noted that the proposed scheme verifies that there is no s-a faults while the Mutex approach verifies a protocol. In particular, it checks for the correct sequencing of the outputs. Fault coverage can be easily traded off with area overhead in our approach, while it is difficult to achieve something like “partial verification of a protocol”.
3. In the detector of the proposed scheme, there is no dependency on the Mutex elements. The Mutex element itself can undergo a meta-stable state which needs to be handled by the meta-stability detector, adding to area overhead.

In this work, we could not compare fault coverage of our approach with the Mutex approach. The Mutex approach verifies on-line whether the output of the CUT follows the specified handshaking protocol. So, the Mutex approach basically follows functional testing. The proposed scheme works on structural testing and hence fault coverage can be given, while it is not possible for functional testing. It may be noted that the circuits considered in the Mutex-based OLT scheme [107] were simple. For comparison with our scheme we have manually implemented the Mutex-based tester design on those circuits.

## 6.6 Conclusion

In this chapter, we have proposed an OBDD based OLT scheme for SI circuits. The existing OLT schemes for asynchronous circuits are protocol dependent and have high area and power overheads, whereas the proposed scheme is protocol independent and involves low area overhead. The proposed scheme can handle all types of SI circuits irrespective of their specified design protocols. Experimentally, it has shown that the area overhead of the proposed scheme is less than that of the Mutex based approach.

In the next chapter we shall conclude the works carried out by the thesis, following that some of the directions for future work are also discussed.



# Chapter 7

## Conclusions and Future scope of work

### 7.1 Summary of the work

In this thesis, we have proposed a number of On-line Testing (OLT) schemes for digital VLSI circuits using decision diagrams. The proposed schemes basically work on the philosophy of partial replication and satisfy most of the parameters required for an efficient on-line tester design; these are i) non-intrusiveness, ii) low area overhead, iii) coverage for advanced fault models, iv) low detection latency, v) flexibility in terms of trade-offs between area overhead versus fault coverage and detection latency, vi) scalability, and vii) applicability for asynchronous circuits.

Providing flexibility in on-line tester design is one of the essential features of an efficient OLT scheme. It is found that most of the OLT schemes achieve flexibility in terms of trade-offs between area overhead of the tester versus fault coverage and detection latency by considering a subset of test patterns for design of the on-line tester circuit. However, reduction in tap points (i.e., measurement limitation) of the Circuit Under Test (CUT) by the on-line tester was not studied. In the first contribution of the thesis (Chapter 3), we have considered measurement limitation as a new mechanism to provide flexibility in OLT. Measurement limitation implies less lines to be tapped by the tester from the CUT. This lowers the number of driving buffers, thereby resulting in lower area overhead. The scheme illustrates how measurement limitation can be used as a trade-off parameter to minimize area overhead at the cost of detection latency. This work starts with the generation of exhaustive set of Fault Detecting transitions (*FD*-transitions) for all possible faults of a circuit under full measurement. Following that, the *FD*-transitions that retain their capability to detect faults under the given measurement limitation are determined. Finally, the on-line tester is designed using these *FD*-transitions. The procedure of generation

## 7.1 Summary of the work

---

of  $FD$ -transitions and determination of  $FD$ -transitions under measurement limitation are implemented using Ordered Binary Decision Diagrams (OBDDs). Application of OBDD enables the proposed scheme to handle complex circuits at gate level. Experimentally, it is verified that measurement limitation does not have high impact on fault coverage. Further, it is also found that for a given detection latency, area overhead of the proposed scheme is lower compared to other similar schemes reported in the literature.

Developing OLT schemes for advanced fault models like bridging faults, delay faults, transition faults, etc., is another important task in VLSI testing which is explored in Chapter 4. It is seen that most of the works on OLT of bridging faults cover only non-feedback faults because feedback faults may cause oscillations which are difficult to detect on-line. In this work, we have proposed an OLT scheme for AND-OR bridging faults and it is experimentally shown that on an average 20% of all possible bridging faults are feedback, however, only less than 1% of them cause oscillations. So directly dropping all feedback bridging faults leads to significant compromise in fault coverage. Therefore in this scheme, by carefully filtering out only the oscillating bridging faults, notable improvement in fault coverage is achieved compared to other works reported in the literature. Further, it has been shown that the increase in area overhead of the on-line tester due to consideration of feedback bridging faults is marginal, compared to the case involving only the non-feedback bridging faults. All major steps of the scheme namely, checking if a feedback bridging fault causes oscillation, generating exhaustive test patterns for non-feedback bridging faults and determining test patterns that do not lead to oscillations in feedback bridging faults are implemented using OBDDs.

Theoretically speaking, the schemes discussed in Chapter 3 and Chapter 4, can design on-line testers for any digital circuit. But the runtime complexity of the CAD tool developed based on the above methodologies may reach impractical limits, typically for circuits with more than a thousand inputs and state bits. This is because of the fact that in such cases generation of OBDDs itself become too complex. To handle this issue, it is required to enhance the scalability of these schemes from gate level to higher abstraction levels. In the third contribution, we have proposed an OLT scheme for digital circuits at Register Transfer Level (RTL) using High Level Decision Diagrams (HLDDs) (Chapter 5). Since there are no well accepted fault models at RTL like the stuck-at-fault model at the gate level, therefore, we have applied high level faults which have good correlations with gate level faults. The scheme starts with modeling the RTL circuits under normal and faulty conditions using separate HLDDs. Following that, Fault Detecting control patterns ( $FD$ -control-patterns) are generated from the normal and faulty HLDD representations and the on-line tester circuit

is designed using these  $FD$ -control-patterns. Experiments on a set of benchmark circuits show that the test generation time of the proposed scheme is significantly shorter compared to the OLT schemes at gate level, thus large circuit can be easily handled. Finally, it is shown that the proposed method achieves comparable fault coverage with low area overhead.

Now-a-days the use of asynchronous circuits in semiconductor industry has got acceptability because of the advantages promised by these circuits such as, no clock skew problem, higher degree of modularity, low power consumption, average case performances rather than worst case performances, etc. However, the number of OLT schemes proposed for asynchronous circuits is very few as compared to that of synchronous circuits. In the fourth contribution, we extended our work by proposing an OBDD based OLT scheme for Speed Independent asynchronous (SI) circuits (Chapter 6). We start by obtaining the Signal Transition Graph (STG) representation of the SI circuit under test using the tool Petrifly. After that, effects of stuck-at faults are represented in the STGs. The normal and faulty STGs are modeled into separate state graphs,  $FD$ -transitions are generated from the state graphs and finally the  $FN$ -detector is designed using the  $FD$ -transitions. An efficient way of generation of the  $FD$ -transitions directly from the circuit description using OBDD, without need of the explicit state graph model, is also discussed. The detector is synthesized as an SI circuit with C-elements which is to be placed on chip along with the CUT. Several circuits are considered as case studies and area overhead ratio of the detectors are studied. Results illustrated that area requirement of the detector of the proposed scheme is less than that of the Mutex approach [107] by 50% on the average. Apart from this, there are several other advantages of the proposed approach, namely, independence of circuit functionality, non-intrusiveness, Complete State Coding (CSC) and free from liveness problem. It may be noted that for synthesizability of the  $FN$ -detector as an SI asynchronous circuit the state graph of the detector should have CSC and no liveness issue.

## 7.2 Future scope of work

From the summary of the work it can be observed that the thesis basically focused on design of efficient OLT schemes for digital VLSI circuits. Several research challenges like non-intrusiveness, low area overhead, flexibility, scalability, applicability for asynchronous circuits, etc., have been addressed while designing these OLT schemes. Further, some new design objectives and interesting research challenges have been identified during the process of the thesis. Some of the potential directions to which the contribution of the thesis can be extended are discussed as follows:

## 7.2 Future scope of work

---

In this thesis, we have proposed four OLT schemes and studied three major performance parameters; area overhead, fault coverage and detection latency. Power overhead is another important issue in OLT, which poses the extra power required to operate the on-line tester circuit concurrently with the CUT. In this thesis, we have not studied power overhead of the proposed OLT schemes. Like area overhead, the power overhead can be studied and trade-offs can be provided between power overhead versus fault coverage and detection latency. Study of power overhead in OLT is also one of the challenges modern deep sub-micron technology and it should be explored separately.

In this thesis, we have proposed OLT schemes for digital VLSI circuits where on-line tester called *FN*-detector is designed from the *FD*-transitions/*FD*-control-patterns. These schemes facilitate trade-offs between area overhead versus fault coverage and detection latency by selecting a subset of *FD*-transitions/*FD*-control-patterns. The selection of *FD*-transitions/*FD*-control-patterns can be better accomplished by solving a multi-criterion optimization problem using area and power of the *FN*-detector, fault coverage, detection latency, importance of the *FD*-transitions/*FD*-control patterns in functionality of the circuit, number of tappings in the critical paths, etc., as optimization parameters. Further, in case of OLT with measurement limitation (Chapter 3), selection of unmeasured lines (not tapping lines) can be better performed by solving such type of multi-criteria optimization problem. The challenges and issues inherent with the multi-criteria based optimization for OLT can be explored as an extension of the problems addressed in the thesis.

We have illustrated measurement limitation for stuck-at faults as our first work in Chapter 3. In similar way, measurement limitation can also be applied in rest of the works in the thesis (Chapters 4, 5 and 6). In case of bridging faults (Chapter 4), the technique of determination of test patterns (*FD*-transitions) under measurement limitation using Ordered Binary Decision Diagram (OBDD) discussed in Chapter 3 can be directly applied to Chapter 4 without any modification. Whereas in Chapter 5 (OLT at RTL), it is required to design High Level Decision Diagram (HLDD) based algorithms to generate *FD*-control-patterns under measurement limitation. Also in case of OLT of asynchronous circuit (Chapter 6), measurement limitation can be applied with some constraints such as Complete State Coding (CSC) and liveness issues. These problems may arise during not tapping some of the lines of the circuit by the on-line tester. So, major research is required to study effect of measurement limitation in case of OLT of asynchronous circuits.

In this thesis, we have proposed an OLT scheme which is applicable only for SI circuits with dynamic implementation of C-elements. As a further direction of research, this scheme can be extended for other types of asynchronous circuits like Delay Insensitive (DI) circuits.

It is required to verify whether this proposed scheme can be directly applied for DI circuits or some modifications would be needed. Also, in case of SI circuits, the proposed scheme can be extended for static C-elements. OLT of static C-element may be comparatively more complex than that of the dynamic C-element because the dynamic C-element comprises less number of transistors than that of the static C-element. Clearly further research is required to solve these issues.

The recent advancements of nanometer technology in semiconductor industry allow design of core-based VLSI systems like System-On-Chip (SOC) and Network-On-Chip (NOC). The basic SOC architecture consists of a number of memory cells and various functional blocks known as cores, which are interconnected using a global bus structure. In NOC, a packet switch network is implemented on the chip to provide high performance communication among the cores. A typical NOC architecture consists of three main parts— i) a number of switches to route the data packets, ii) interconnections among the switches, and iii) interfaces that connect each core to a switch. Use of nano and deep sub-micron technologies in design of SOCs and NOCs make them more susceptible to faults during normal operation. In other words, on-line testing becomes essential for such systems. OLT of SOCs and NOCs involve multiple challenges due to their complex architectures and different types of faults such as faults at the switches, faults at the cores and faults at the interconnection links [70, 136]. So, a detailed study is required to design OLT schemes for such complex systems.

In all the works presented in this thesis, it is assumed that the on-line tester is free of faults. To make the OLT scheme more robust, testing of the on-line tester is required. This can be accomplished by designing another tester circuit for the on-line tester. Testing of the on-line tester can be performed either on-line or off-line. Off-line testing will incur less design issues, low area overhead, etc. However, in fault tolerant systems OLT of the on-line tester is necessary. The partial replication based technique discussed in the thesis can be applied for OLT of the on-line tester. As already discussed, the main distinguishing feature of partial replication based scheme over other techniques is non-intrusiveness but it has comparatively high area overhead. It may be noted that unlike the CUT, the feature of non-intrusiveness is not mandatory in OLT of the on-line tester. So, intrusive techniques like self-checking design using coding theory, signature monitoring, etc., which have low area and power overheads may be applied.



# References

- [1] Hlsynth92 benchmark directory URL. <https://people.engr.ncsu.edu/brglez/CBL/benchmarks/HLSynth92/> (last accessed 30<sup>th</sup> January, 2017).
- [2] Miron Abramovici, Melvin A Breuer, and Arthur D Friedman. *Digital systems testing and testable design*. IEEE press, 1994.
- [3] S.B. Akers. Binary decision diagrams. *IEEE Transactions on Computers*, C-27(6):509–516, 1978.
- [4] Hussain Al-Asaad. Efficient techniques for reducing error latency in on-line periodic built-in self-test. *IEEE instrumentation and measurement magazine*, 13(4):28–32, 2010.
- [5] F. A. Aloul, I. L. Markov, and K. A. Sakallah. Efficient gate and input ordering for circuit-to-BDD conversion. In *International Workshop on Logic Synthesis*, pages 137–142, 2002.
- [6] R Iris Bahar, Erica A Frohm, Charles M Gaona, Gary D Hachtel, Enrico Macii, Abelardo Pardo, and Fabio Somenzi. Algebraic decision diagrams and their applications. *Formal methods in system design, Springer*, 10(2-3):171–206, 1997.
- [7] Y. Balasubrahmanyam, G. L. Chowdary, and T. J. V. S. Subrahmanyam. A novel low power pattern generation technique for concurrent BIST architecture. *International Journal Computer Technology and Applications*, 3(2):561–565, 2012.
- [8] Anitha Balasubramanian, BL Bhuvana, LW Massengill, B Narasimham, RL Shuler, TD Loveless, and W Timothy Holman. A built-in self-test (BIST) technique for single-event testing in digital circuits. *IEEE Transactions on Nuclear Science*, 6(55):3130–3135, 2008.

## REFERENCES

---

- [9] S. Biswas, S. Mukhopadhyay, A. Patra, and D. Sarkar. Unified technique for on-line testing of digital circuits: Delay and stuck-at fault models. *Journal of Circuits, Systems and Computers, World Scientific*, 17(06):1069–1089, 2008.
- [10] S Biswas, G Paul, and S Mukhopadhyay. Methodology for low power design of on-line testers for digital circuits. *International Journal of Electronics, Taylor and Francis*, 95(8):785–797, 2008.
- [11] Santosh Biswas, Siddhartha Mukhopadhyay, and Amit Patra. A discrete event systems approach to online testing of digital VLSI circuits. In *International Conference on Systems, Man and Cybernetics*, volume 2, pages 1699–1704, 2004.
- [12] Santosh Biswas, Siddhartha Mukhopadhyay, and Amit Patra. A formal approach to on-line monitoring of digital VLSI circuits: theory, design and implementation. *Journal of Electronic Testing, Springer*, 21(5):503–537, 2005.
- [13] Santosh Biswas, P Srikanth, R Jha, Siddhartha Mukhopadhyay, Amit Patra, and Dipankar Sarkar. On-line testing of digital circuits for n-detect and bridging fault models. In *Asian Test Symposium*, pages 88–93, 2005.
- [14] C. Bolchini, R. Montandon, F. Salice, and D. Sciuto. Design of VHDL based totally self-checking finite state machine and data path descriptions. *IEEE Transactions on VLSI Systems*, 8(1):98–103, 2000.
- [15] DR Brasen and G Saucier. Using cone structures for circuit partitioning into FPGA packages. *IEEE Transactions on Computer-Aided Design of Integrated Circuits and Systems*, 17(7):592–600, 2006.
- [16] R. E. Bryant. Graph-based algorithms for Boolean function manipulation. *IEEE Transactions on Computers*, C-35(8):677–691, 1986.
- [17] M Bushnell and Vishwani Agrawal. *Essentials of Electronic Testing for Digital, Memory and Mixed-Signal VLSI Circuits*, volume 17. Springer Science and Business Media, 2006.
- [18] Tapan Chakraborty and Sumit Ghosh. On behavior fault modeling for combinational digital designs. In *International Test Conference on New Frontiers in Testing*, pages 593–600, 1988.

- 
- [19] Tapan J Chakraborty, Vishwani D Agrawal, and Michael L Bushnell. Delay fault models and test generation for random logic sequential circuits. In *Proceedings of Design Automation Conference*, pages 165–172, 1992.
- [20] W.-F. Chang and C.-W. Wu. Low-cost modular totally self-checking checker design for m-out-of-n code. *IEEE Transactions on Computers*, 48(8):815–826, 1999.
- [21] W.-F. Chang and C.-W. Wu. TSC Berger-code checker design for 2r-1-bit information. *Journal of Information Science and Engineering*, 15(3):429–440, 1999.
- [22] Yung-Yuan Chen. Concurrent detection of control flow errors by hybrid signature monitoring. *IEEE transactions on Computers*, 54(10):1298–1313, 2005.
- [23] T. A. Chu. Automatic synthesis and verification of hazard-free control circuits from asynchronous finite state machine specifications. In *International Conference on Computer Design: VLSI in Computers and Processors*, pages 407–413, 1992.
- [24] Ken Coffman. *Real World FPGA Design with Verilog*. Prentice Hall PTR, 1999.
- [25] E Corno, Gianluca Cumani, M Sonza Reorda, and Giovanni Squillero. An RT-level fault model with high gate level correlation. In *International High-Level Design Validation and Test Workshop*, pages 3–8, 2000.
- [26] J. Cortadella, M. Kishinevsky, A. Kondratyev, L. Lavagno, and A. Yakovlev. A region-based theory for state assignment in speed-independent circuits. *IEEE Transactions on CAD of Integrated Circuits and Systems*, 16(8):793–812, 1997.
- [27] Jordi Cortadella, Michael Kishinevsky, Alex Kondratyev, Luciano Lavagno, and Alex Yakovlev. Hardware and petri nets application to asynchronous circuit design. In *International Conference on Application and Theory of Petri Nets*, pages 1–15, 2000.
- [28] Jordi Cortadella, Michael Kishinevsky, Alex Kondratyev, Luciano Lavagno, and Alexandre Yakovlev. Petrify: a tool for manipulating concurrent specifications and synthesis of asynchronous controllers. *IEICE Transactions on information and Systems*, 80(3):315–325, 1997.
- [29] Philippe Coussy and Adam Morawiec. *High-Level Synthesis: from Algorithm to Digital Circuit*. Springer Science and Business Media, 2008.
- [30] Phillipe Coussy, Daniel D Gajski, Michael Meredith, and Andres Takach. An introduction to high-level synthesis. *IEEE Design and Test of Computers*, 26(4):8–17, 2009.

## REFERENCES

---

- [31] D. Das and N.A. Touba. Weight-based codes and their application to concurrent error detection of multilevel circuits. In *VLSI Test Symposium*, pages 370–377, 1999.
- [32] N. Das, P. Roy, and H. Rahaman. On line testing of single feedback bridging fault in cluster based FPGA by using asynchronous element. In *International On-Line Testing Symposium*, pages 190–191, 2008.
- [33] Nachiketa Das, Pranab Roy, and Hafizur Rahaman. Built-in-self-test technique for diagnosis of delay faults in cluster-based field programmable gate arrays. *IET Computers and Digital Techniques*, 7(5):210–220, 2013.
- [34] K. De, C. Natarajan, D. Nair, and P. Banerjee. RSYN: A system for automated synthesis of reliable multilevel circuits. *IEEE Transactions on VLSI Systems*, 2(2):186–195, 1994.
- [35] P. Drineas and Y. Makris. Non-intrusive design of concurrently self-testable FSMs. In *Asian Test Symposium*, pages 33–38, 2002.
- [36] P. Drineas and Y. Makris. SPaRre: Selective partial replication for concurrent fault-detection in FSMs. *IEEE Transactions on Instrumentation and Measurement*, 52(6):1729–1737, 2003.
- [37] J Drozd, A Drozd, and M Al-dhabi. A resource approach to on-line testing of computing circuits. In *East-West Design and Test Symposium*, pages 1–6, 2015.
- [38] R. D. Eldred. Test routines based on symbolic logical statements. *Journal of the ACM*, 6(1):33–36, 1959.
- [39] Petr Fišer, Pavel Kubalík, and Hana Kubátová. An efficient multiple-parity generator design for on-line testing on FPGA. In *Euromicro Conference on Digital System Design Architectures, Methods and Tools*, pages 96–99, 2008.
- [40] José Flich and Davide Bertozzi. *Designing network on-chip architectures in the nanoscale era*. Chapman and Hall/CRC, 2010.
- [41] M. Fujita, H. Fujisawa, and Y. Matsunaga. Variable ordering algorithms for ordered binary decision diagrams and their evaluation. *IEEE Transactions on CAD of Integrated Circuits and Systems*, 12(1):6–12, 1993.
- [42] Bibhas Ghoshal and Indranil Sengupta. A distributed bist scheme for NoC-based memory cores. In *Euromicro Conference on Digital System Design*, pages 567–574, 2013.

- 
- [43] O. Goubeva, M.S. Reorda, and M. Violante. An RT-level concurrent error detection technique for data dominated systems. In *On-Line Testing Symposium*, page 159, 2003.
- [44] Myers Research Group. *Atacs online demo (www.async.ece.utah.edu/atacs-bin/demo)*. 1999.
- [45] J. Gu and R. Puri. Asynchronous circuits synthesis with boolean satisfiability. *IEEE transactions on CAD of Integrated Circuits and Systems*, 14(8):961–973, 1995.
- [46] R.J. Hayne and B.W. Johnson. Behavioral fault modeling in a VHDL synthesis environment. In *VLSI Test Symposium*, pages 333–340, 1999.
- [47] Marcos Hervé, Pedro Almeida, Fernanda Lima Kastensmidt, Erika Cota, and Marcelo Lubaszewski. Concurrent test of network-on-chip interconnects and routers. In *Latin American Test Workshop*, 2010.
- [48] David A Hodges et al. *Analysis and Design of Digital Integrated Circuits, In Deep Submicron Technology (special Indian Edition)*. Tata McGraw-Hill Education, 2005.
- [49] Wonhak Hong, Rajashekhar Modugu, and Minsu Choi. Efficient online self-checking modulo  $2^n+1$  multiplier design. *IEEE Transactions on Computers*, 60(9):1354–1365, 2011.
- [50] Henrik Hulgaard, Steven M Burns, and Gaetano Borriello. Testing asynchronous circuits: A survey. *Integration, the VLSI journal, Elsevier*, 19(3):111–131, 1995.
- [51] Michael Huth and Mark Ryan. *Logic in Computer Science: Modelling and Reasoning About Systems*. Cambridge University Press, 2004.
- [52] S-W Jeong, Bernard Plessier, Gary D Hachtel, and Fabio Somenzi. Variable ordering and selection of fsm traversal. In *International Conference on Computer-Aided Design*, pages 476–479, 1991.
- [53] N.K. Jha and S.-J. Wang. Design and synthesis of self-checking VLSI circuits and systems. *IEEE Transactions on CAD of Integrated Circuits and Systems*, 12(6):878–887, 1993.
- [54] A Jutman, J Raik, and R Ubar. SSBDDs: Advantageous model and efficient algorithms for digital circuit modeling, simulation and test. In *proceedings of International Workshop on Boolean Problems*, pages 19–20, 2002.

## REFERENCES

---

- [55] A Jutman and R Ubar. Design error diagnosis in digital circuits with stuck-at fault model. *Microelectronics Reliability, Elsevier*, 40(2):307–320, 2000.
- [56] Anton Karputkin and Jaan Raik. A synthesis-agnostic behavioral fault model for high gate-level fault coverage. In *Design, Automation and Test in Europe Conference and Exhibition*, pages 1124–1127, 2016.
- [57] R Karri and Kaijie Wu. Algorithm level re-computing using implementation diversity: a register transfer level concurrent error detection technique. *IEEE Transactions on Very Large Scale Integration (VLSI) Systems*, 10(6):864–875, 2002.
- [58] Ramesh Karri and Balakrishnan Iyer. Introspection: A register transfer level technique for cocurrent error detection and diagnosis in data dominated designs. *ACM Transactions on Design Automation of Electronic Systems*, 6(4):501–515, 2001.
- [59] M. Karunaratne, A. Sagahayroon, and S. Prodhuturi. RTL fault modeling. In *Midwest Symposium on Circuits and Systems*, pages 1717–1720, 2005.
- [60] Natalja Kehl and Wolfgang Rosenstiel. Circuit level concurrent error detection in FSMs. *Journal of Electronic Testing, Springer*, 29(2):185–192, 2013.
- [61] Zvi Kohavi and Niraj K Jha. *Switching and finite automata theory*. Cambridge University Press, 2009.
- [62] Mattias Krysander and Erik Frisk. Sensor placement for fault diagnosis. *IEEE Transactions on Systems, Man, and Cybernetics-Part A: Systems and Humans*, 38(6):1398–1410, 2008.
- [63] A Anand Kumar. *Fundamentals of digital circuits*. PHI Learning Pvt. Ltd., 2014.
- [64] CY Lee. Representation of switching circuits by binary-decision programs. *The Bell System Technical Journal, Alcatel-Lucent*, 38(4):985–999, 1959.
- [65] David Lee and Mihalis Yannakakis. Principles and methods of testing finite state machines-a survey. *Proceedings of the IEEE*, 84(8):1090–1123, 1996.
- [66] R Leveugle and G Saucier. Concurrent checking in dedicated controllers. In *International Conference on Computer Design: VLSI in Computers and Processors*, pages 124–127, 1989.
- [67] R. Leveugle and G. Saucier. Optimized synthesis of concurrently checked controllers. *IEEE Transactions on Computers*, 39(4):419–425, 1990.

- 
- [68] Huawei Li, Yinghua Min, and Zhongcheng Li. An rt-level atpg based on clustering of circuit states. In *Test Symposium, 2001. Proceedings. 10th Asian*, pages 213–218, 2001.
- [69] C. N. Liu. A state variable assignment method for asynchronous sequential switching circuits. *Journal of the ACM*, 10(2):209–216, 1963.
- [70] Junxiu Liu, Jim Harkin, Yuhua Li, and Liam Maguire. Online fault detection for networks-on-chip interconnect. In *Conference on Adaptive Hardware and Systems*, pages 31–38, 2014.
- [71] D. Lu and C.Q. Tong. High level fault modeling of asynchronous circuits. In *Proceedings on VLSI Test Symposium*, pages 190–195, 1995.
- [72] Christoph Meinel and Thorsten Theobald. *Algorithms and Data Structures in VLSI Design: OBDD-foundations and applications*. Springer Science and Business Media, 2012.
- [73] C. Metra, M. Favalli, P. Olivio, and B. Ricco. On-line detection of bridging and delay faults in functional blocks of CMOS self-checking circuits. *IEEE Transactions on CAD of Integrated Circuits and Systems*, 16(7):770–776, 1997.
- [74] Mohammad Mirzaei, Mahmoud Tabandeh, Bijan Alizadeh, and Zainalabedin Navabi. A new approach for automatic test pattern generation in register transfer level circuits. *IEEE Design and Test*, 30(4):49–59, 2013.
- [75] S Mitra, N.R. Saxena, and E.J. McCluskey. Common-mode failures in redundant VLSI systems: a survey. *IEEE Transactions on Reliability*, 49(3):285–295, 2000.
- [76] S. Mitra, N.R. Saxena, and E.J. McCluskey. Fault escapes in duplex systems. In *VLSI Test Symposium*, pages 453–458, 2000.
- [77] M. Moreira, B. Oliveira, F. Moraes, and N. Calazans. Impact of C-elements in asynchronous circuits. In *International Symposium on Quality Electronic Design*, pages 437–443, 2012.
- [78] A Morozov, Va V Saposhnikov, Vl V Saposhnikov, and M Gossel. New self-checking circuits by use of berger-codes. In *On-Line Testing Workshop*, pages 141–146, 2000.
- [79] Luca Mostardini, Luca Bacciarelli, Luca Fanucci, Lorenzo Bertini, Marco Tonarelli, and Marco De Marinis. FPGA-based low-cost automatic test equipment for digital

## REFERENCES

---

- integrated circuits. In *International Workshop on Intelligent Data Acquisition and Advanced Computing Systems: Technology and Applications*, pages 32–37, 2009.
- [80] Chris J Myers. *Asynchronous circuit design*. John Wiley and Sons, 2004.
- [81] Zainalabedin Navabi. *Digital System Test and Testable Design*. Springer, 2011.
- [82] M. Nicolaidis. Self-exercising checkers for Unified Built-In-Self-Test (UBIST). *IEEE Transactions on Computers*, 38(3):203–218, 1989.
- [83] M Nicolaidis and L Anghel. Concurrent checking for VLSI. *Microelectronic Engineering, Elsevier*, 49(1):139–156, 1999.
- [84] Michael Nicolaidis and Yervant Zorian. On-line testing for VLSI– a compendium of approaches. *Journal of Electronic Testing, Springer*, 12(1-2):7–20, 1998.
- [85] Hongxia Pan and Xiuye Wei. Optimal placement of sensor in gearbox fault diagnosis based on vpso. In *International Conference on Natural Computation*, pages 3383–3387, 2010.
- [86] Antonis Paschalis, Dimitris Gizopoulos, and Nikolaos Gaitanis. Concurrent delay testing in totally self-checking systems. *Journal of Electronic Testing, Springer*, 12(1):55–61, 1998.
- [87] Philippe Perdu. Life issues, robustness consequences and reliability challenges for very deep sub micron technologies. In *Asia-Pacific International Symposium on Electromagnetic Compatibility*, pages 1014–1019, 2010.
- [88] I. Pomeranz and S. M. Reddy. A measure of quality for n-Detection test sets. *IEEE Transactions on Computers*, 53(11):1497–1503, 2004.
- [89] Andreas Prodromou, Andreas Panteli, Chrysostomos Nicopoulos, and Yiannakis Sazeides. NoCAAlert: An on-line and real-time fault detection mechanism for network-on-chip architectures. In *Annual International Symposium on Microarchitecture*, pages 60–71, 2012.
- [90] Mihaela Radu. Testing digital circuits using a mixed-signal automatic test equipment. In *International Conference on Automation, Quality and Testing, Robotics*, pages 1–4, 2014.

- 
- [91] Jaan Raik, Urmas Repinski, Raimund Ubar, Maksim Jenihhin, and Anton Chepurov. High-level design error diagnosis using backtrace on decision diagrams. In *Norchip Conference*, pages 1–4, 2010.
- [92] Jaan Raik and Raimund Ubar. Fast test pattern generation for sequential circuits using decision diagram representations. *Journal of Electronic Testing, Springer*, 16(3):213–226, 2000.
- [93] Jaan Raik, Raimund Ubar, and Taavi Viilukas. High-level decision diagram based fault models for targeting FSMs. In *Euromicro Conference on Digital System Design: Architectures, Methods and Tools*, pages 353–358, 2006.
- [94] Jaan Raik, Raimund Ubar, Taavi Viilukas, and Maksim Jenihhin. Mixed hierarchical-functional fault models for targeting sequential cores. *Journal of Systems Architecture, Elsevier*, 54(3):465–477, 2008.
- [95] Jutman Peder Raik, A. Jutman, A. Peder, J. Raik, M. Tombak, and R. Ubar. Structurally synthesized binary decision diagrams. In *International Workshop on Boolean Problems*, pages 271–278, 2004.
- [96] Ubar Raimund. Overview about low-level and high-level decision diagrams for diagnostic modeling of digital systems. *Facta universitatis - series: Electronics and Energetics*, 24(3):303–324, 2011.
- [97] Uljana Reinsalu, Jaan Raik, and Raimund Ubar. Register-transfer level deductive fault simulation using decision diagrams. In *Electronics Conference*, pages 193–196, 2010.
- [98] Uljana Reinsalu, Jaan Raik, Raimund Ubar, and Peeter Ellervee. Fast RTL fault simulation using decision diagrams and bitwise set operations. In *International Symposium on Defect and Fault Tolerance in VLSI and Nanotechnology Systems*, pages 164–170, 2011.
- [99] R Rinitha and R Ponni. Testing in VLSI: A survey. In *International Conference on Emerging Trends in Engineering, Technology and Science*, pages 1–6, 2016.
- [100] S.H. Robinson. *Finite State Machine Synthesis for Continuous, Concurrent Error Detection using Signature-Invariant monitoring*. Ph.D. Dissertation, Carnegie Mellon University, Pittsburgh, Pennsylvania, USA, 1992.

## REFERENCES

---

- [101] V. V. Saposhnikov, A. Morosov, Vl. V. Saposhnikov, and M. Gossel. Design of self-checking unidirectional combinational circuits with low area overhead. In *International On-Line Testing Workshop*, pages 280–286, 1996.
- [102] V. V. Saposhnikov, A. Morosov, Vl. V. Saposhnikov, and M. Gossel. A new design method for self-checking unidirectional combinational circuits. *Journal of Electronic Testing: Theory and Applications*, Springer, 12(1-2):41–53, 1998.
- [103] Bibhash Sen, Jyotirmoy Das, and Biplab K Sikdar. A DFT methodology targeting online testing of reversible circuit. In *International Conference on Devices, Circuits and Systems*, pages 689–693, 2012.
- [104] V. R. Ser-Dessai and D.M.H Walkar. Resistive bridge fault modelling, simulation and test generation. In *International Test Conference*, pages 596–605, 1999.
- [105] M. Shams, J.C. Ebergen, and M.I. Elmasry. A comparison of CMOS implementations of an asynchronous circuits primitive: the c-element. In *International Symposium on Low Power Electronics and Design*, pages 93–96, 1996.
- [106] M. Shams, J.C. Ebergen, and M.I. Elmasry. Modeling and comparing CMOS implementations of the c-element. *IEEE Transactions on Very Large Scale Integration Systems*, 6(4):563–567, 1998.
- [107] D. Shang, A. Bystrov, A. Yakovlev, and D. Koppad. On-line testing of globally asynchronous circuits. In *International On-Line Testing Symposium*, pages 135–140, 2005.
- [108] D Shang, F Xia, and A Yakovlev. Asynchronous circuit synthesis via direct translation. In *International Symposium on Circuits and Systems*, pages 369–372, 2002.
- [109] D. Shang, A. Yakovlev, F.P. Burnsand, F. Xia, and A. Bystrov. Low-cost online testing of asynchronous handshakes. In *European Test Symposium*, pages 225–232, 2006.
- [110] Detlef Sieling and Ingo Wegener. Graph driven BDDs – a new data structure for boolean functions. *Theoretical Computer Science*, Elsevier, 141(1):283–310, 1995.
- [111] Jens Sparso and Steve Furber. *Principles of Asynchronous Circuit Design: A Systems Perspective*. Springer Science and Business Media, 2013.
- [112] A.P. Stroele and S. Tarnick. Programmable embedded self-testing checkers for all-unidirectional error-detecting codes. In *VLSI Test Symposium*, pages 361–369, 1999.

- 
- [113] X. Sun and M. Serra. On-line and off-line testing with shared resources: a new BIST approach. *IEEE Transactions on CAD of Integrated Circuits and Systems*, 16(9):1045–1056, 1997.
- [114] Kyohichiro Tada, Syuhei Kawamoto, Noboru Yamada, Tetsuya Kimura, Masahiro Iwahashi, Toshiya Tadaumi, and Kazuhiko Kato. Sensor placement optimization in on-site photovoltaic module inspection robot for fast and robust failure detection. In *Photovoltaic Specialist Conference*, pages 1–3, 2015.
- [115] Lanfang Tan, Ying Tan, and Jianjun Xu. CFEDR: Control-flow error detection and recovery using encoded signatures monitoring. In *International Symposium on Defect and Fault Tolerance in VLSI and Nanotechnology Systems*, pages 25–32, 2013.
- [116] S. Tarnick. Controllable self-checking checkers for conditional concurrent checking. *IEEE Transactions on CAD of Integrated Circuits and Systems*, 14(5):547–553, 1995.
- [117] P.A. Thaker, V.D. Agrawal, and M.E. Zaghoul. Register-transfer level fault modeling and test evaluation techniques for vlsi circuits. In *Test Conference, 2000. Proceedings. International*, pages 940–949, 2000.
- [118] N. A. Touba and E. J. McCluskey. Logic synthesis techniques for reduced area implementation of multilevel circuits with concurrent error detection. In *International Conference on Computer-Aided Design*, pages 651–654, 1994.
- [119] N.A. Touba and E.J. McCluskey. Logic synthesis of multilevel circuits with concurrent error detection. *IEEE Transactions on CAD of Integrated Circuits and Systems*, 16(7):783–789, 1997.
- [120] M. Trevisan Moreira, F. Gehm Moraes, and N.L. Vilar Calazans. Beware the dynamic c-element. *IEEE Transactions on Very Large Scale Integration (VLSI) Systems*, 22(7):1644–1647, 2014.
- [121] Raimund Ubar. Test generation for digital systems based on alternative graphs. In *European Dependable Computing Conference*, pages 149–164, 1994.
- [122] Raimund Ubar. Test synthesis with alternative graphs. *IEEE Design and Test of Computers*, 13(1):48–57, 1996.
- [123] Raimund Ubar, Artur Jutman, and Zebo Peng. Timing simulation of digital circuits with binary decision diagrams. In *Proceedings of the conference on Design, automation and test in Europe*, pages 460–466, 2001.

## REFERENCES

---

- [124] Raimund Ubar, Jaan Raik, Eero Ivask, and Marina Brik. Multi-level fault simulation of digital systems on decision diagrams. In *proceedings of the International Workshop on Electronic Design, Test and Applications*, pages 86–91, 2002.
- [125] Raimund Ubar, Jaan Raik, Anton Karputkin, and Mati Tombak. Synthesis of high-level decision diagrams for functional test pattern generation. In *International Conference on Mixed Design of Integrated Circuits and Systems*, pages 519–524, 2009.
- [126] Frank Vahid. *Digital Design with RTL Design, Verilog and VHDL*. John Wiley and Sons, 2010.
- [127] K Vanitha and CA Sathiya Moorthy. Implementation of an integrated FPGA based automatic test equipment and test generation for digital circuits. In *International Conference on Information Communication and Embedded Systems*, pages 741–746, 2013.
- [128] Dilip P Vasudevan and Parag K Lala. A technique for modular design of self-checking carry-select adder. In *International Symposium on Defect and Fault Tolerance in VLSI Systems*, pages 325–333, 2005.
- [129] T. Verdel and M. Yiorgos. Duplication-based concurrent error detection in asynchronous circuits: Shortcomings and remedies. In *International Symposium on Defect and Fault-Tolerance in VLSI Systems*, pages 345–353, 2002.
- [130] I. Voyiatzis, A. Paschalis, D. Gizopoulos, C. Halatsis, F. S. Makri, and M. Hatzimihail. An input vector monitoring concurrent BIST architecture based on a precomputed test set. *IEEE Transactions on Computers*, 57(8):1012–1022, 2008.
- [131] Ioannis Voyiatzis, Costas Efstathiou, and Cleo Sgouropoulou. Symmetric transparent online bist for arrays of word-organized rams. In *International Conference on Design and Technology of Integrated Systems in Nanoscale Era*, pages 122–127, 2013.
- [132] Laung-Terng Wang, Charles E Stroud, and Nur A Touba. *System-on-chip test architectures: nanometer design for testability*. Morgan Kaufmann, 2010.
- [133] Laung-Terng Wang, Cheng-Wen Wu, and Xiaoqing Wen. *VLSI test principles and architectures: design for testability*. Academic Press, 2006.
- [134] Ingo Wegener. Efficient data structures for boolean functions. *Discrete Mathematics, Elsevier*, 136(1):347–372, 1994.

- [135] T.W. Williams and N.C. Brown. Defect level as a function of fault coverage. *IEEE Transactions on Computers*, 30(12):987–988, 1981.
- [136] Pengzhan Yan, Shixiong Jiang, and Ramalingam Sridhar. A novel fault-tolerant router architecture for network-on-chip reconfiguration. In *System-on-Chip Conference*, pages 292–297, 2015.



# Publications Related to Thesis

## Journals

1. **P. K. Biswal**, H.P. Sambho and S. Biswas, “*A Discrete Event System approach to On-line Testing of digital circuits with measurement limitation*”, Engineering Science and Technology, an International Journal, Elsevier, Volume 19, Number 3, Pages 1473-1487, 2016.
2. **P. K. Biswal** and S. Biswas, “*A Binary Decision Diagram based On-line Testing of Digital VLSI Circuits for Feedback Bridging Faults*”, Microelectronics Journal, Elsevier, Volume 46, Number 7, Pages 598-616, 2015.
3. **P. K. Biswal**, K. Mishra, S. Biswas and H. K. Kapoor, “*A Discrete Event System Approach to On-line Testing of Speed Independent asynchronous circuits*, VLSI Design Hindawi, Volume 2015, Article ID 651785, 16 pages, 2015.
4. **P. K. Biswal** and S. Biswas, “*On-Line Testing of Digital VLSI Circuits at Register Transfer Level Using High Level Decision Diagrams*”, Microelectronics Journal, Elsevier (Submitted after first revision).

## Conference

1. **Pradeep Kumar Biswal** and Santosh Biswas, “*Timed Discrete event system approach to on-line testing of asynchronous circuits*”, 23rd IEEE Mediterranean Conference on Control and Automation, Pages 341-348, 2015, Torremolinos, Spain.



# Brief Biography of the Author

**Name:** Pradeep Kumar Biswal  
**Father's Name:** Nanda Kishore Biswal  
**Mother's Name:** Janakilata Biswal  
**Date of Birth:** 28.02.1982  
**Address:** Department of Computer Science and Engineering,  
IIT Guwahati, Assam-781039, India  
**Email:** p.biswal@iitg.ernet.in

Pradeep Kumar Biswal received the B.E degree in Computer Science and Engineering from Dhaneswar Rath Institute of Engineering and Management Studies, Cuttack, Odisha (under Biju Patnaik University of Technology, Odisha), in the year of 2004. He has completed his M.Tech degree from the Department of Computer Science and Engineering, Indian Institute of Technology Guwahati, India in the year 2011. He is currently a Ph.D. student in the Department of Computer Science and Engineering of the same institute under the supervision of Dr. Santosh Biswas. His research interests include VLSI testing and design for testability, discrete event systems and system verifications. He has published about ten research papers.





Department of Computer Science and Engineering  
Indian Institute of Technology Guwahati  
Guwahati 781039, India